

NUMERICAL INVESTIGATION OF BRACES AND REPLACEABLE LINKS
FOR STEEL FRAMES

A THESIS SUBMITTED TO
THE GRADUATE SCHOOL OF NATURAL AND APPLIED SCIENCES
OF
MIDDLE EAST TECHNICAL UNIVERSITY

BY

SINA KAZEMZADEH AZAD

IN PARTIAL FULFILLMENT OF THE REQUIREMENTS
FOR
THE DEGREE OF DOCTOR OF PHILOSOPHY
IN
CIVIL ENGINEERING

FEBRUARY 2021

Approval of the thesis:

**NUMERICAL INVESTIGATION OF BRACES AND REPLACEABLE
LINKS FOR STEEL FRAMES**

submitted by **SINA KAZEMZADEH AZAD** in partial fulfillment of the requirements for the degree of **Doctor of Philosophy in Civil Engineering, Middle East Technical University** by,

Prof. Dr. Halil Kalıpçılar
Dean, Graduate School of **Natural and Applied Sciences**

Prof. Dr. Ahmet Türer
Head of the Department, **Civil Engineering**

Prof. Dr. Cem Topkaya
Supervisor, **Civil Engineering, METU**

Examining Committee Members:

Prof. Dr. Özgür Kurç
Civil Engineering, METU

Prof. Dr. Cem Topkaya
Civil Engineering, METU

Prof. Dr. Eray Baran
Civil Engineering, METU

Asst. Prof. Burcu Güldür Erkal
Civil Engineering, Hacettepe University

Asst. Prof. Halil Fırat Özel
Civil Engineering, Çankaya University

Date: 10.02.2021

I hereby declare that all information in this document has been obtained and presented in accordance with academic rules and ethical conduct. I also declare that, as required by these rules and conduct, I have fully cited and referenced all material and results that are not original to this work.

Name, Last name: Sina, Kazemzadeh Azad

Signature:

ABSTRACT

NUMERICAL INVESTIGATION OF BRACES AND REPLACEABLE LINKS FOR STEEL FRAMES

Kazemzadeh Azad, Sina
Doctor of Philosophy, Civil Engineering
Supervisor: Prof. Dr. Cem Topkaya

February 2021, 288 pages

Concentrically braced frames (CBFs) and eccentrically braced frames (EBFs) are among popular lateral load resisting systems for steel structures. The present study investigates different aspects of these systems. The part devoted to EBFs begins with a comprehensive review of research where 22 future research needs are identified and presented. This is followed by an experimental study on the low-cycle fatigue behavior of links, which are the most important members of an EBF. Results of the experimental study are then combined with a comprehensive database of previous experiments available in the literature and synthesized to calibrate a cumulative damage law for estimating the exhausted as well as the remaining life of a link during an earthquake. A simple 8-step algorithm was outlined which utilizes the developed damage law for estimating the accumulation of damage as well as the instant of link fracture in nonlinear time history analysis under earthquake-induced loading histories. The algorithm can also contribute significantly to the decision-making process of the post-earthquake replacement of EBF links.

In addition, in the EBF part of the thesis, a replaceable link detail with a mid-splice connection (referred to herein as the detachable replaceable link concept), recently

developed at METU, is numerically investigated. After reviewing the previous experiments conducted on the concept, a comprehensive parametric study is carried out and a design equation is developed for estimating the axial force that the mid-splice connection can experience due to large link deformations and end restraint effects. In order to further investigate the application of the proposed detail for larger (deeper) shear links than those previously tested, another set of sophisticated simulations is conducted. The analysis results further suggest the potential of the detachable concept for practical applications.

For the CBF part of the thesis, first, the seismic design rules recommended by American and European provisions are thoroughly reviewed and compared. A series of CBF archetypes are then designed based on American and European provisions and subjected to a large set of earthquakes in order to investigate and compare their seismic performances. Results of more than 800 nonlinear time-history analyses reveal that the differences which exist between these provisions can lead to significant differences in the observed seismic performances. The most notable difference is the occurrence of soft-story behavior at the top stories of the CBF archetypes designed according to European provisions. Possible reasons for this phenomenon are investigated and recommendations are provided.

In the last part of the thesis, the effect of rapid shortening of braces during earthquakes on the seismic behavior of CBFs is investigated. Axially loaded members might experience compressive forces above their static buckling capacity as a result of dynamic buckling under such rapid shortenings. A theoretical background on the topic is provided followed by a comprehensive parametric study considering several CBF configurations under a large set of earthquakes. Results of a total of 1600 nonlinear time-history analyses are utilized to demonstrate the frequency of occurrence and importance of this phenomenon particularly for the capacity design of columns, beams, and gusset plates of CBFs. The implications of these extra forces were discussed, and a simple formula was developed which can be

used for the estimation of the ultimate brace force (considering the dynamic buckling effect) during the capacity design of CBF systems.

Keywords: Eccentrically Braced Frames, Concentrically Braced Frames, Replaceable Links, Low-Cycle Fatigue, Dynamic Buckling

ÖZ

ÇELİK ÇERÇEVELİ SİSTEMLERDE KULLANILAN ÇAPRAZ VE DEĞİŞTİRİLEBİLİR BAĞ KIRIŞLARININ NÜMERİK İNCELENMESİ

Kazemzadeh Azad, Sina
Doktora, İnşaat Mühendisliği
Tez Yöneticisi: Prof. Dr. Cem Topkaya

Şubat 2021, 288 sayfa

Merkezi Çaprazlı Çerçeveler (MÇÇ'ler) ve Dışmerkez Çaprazlı Çerçeveler (DÇÇ'ler) çelik yapılar için kullanılan yatay yük taşıyıcı sistemler arasındadır. Bu çalışma, bahsi geçen sistemlerin farklı yönlerini araştırmaya yöneliktir. DÇÇ'lere ayrılan bölüm, gelecekteki 22 araştırma ihtiyacının belirlendiği ve sunulduğu kapsamlı bir araştırma incelemesi ile başlamaktadır. Bunu, DÇÇ'lerin en önemli elemanı olan bağ kirişlerinin düşük çevrimsel yorulma davranışı üzerine deneysel bir çalışma izlemektedir. Deneysel çalışmanın sonuçları literatürde mevcut olan deneysel sonuçlarla birleştirilerek bir veritabanı oluşturulmuştur. Veritabanı doneleri kullanılarak deprem sırasında bağ kirişlerinin tükenen ve kalan ömrünü tahmin etmek için kümülatif bir hasar yasası kalibre edilmiştir. Deprem kaynaklı yüklemeye geçmişleri altında doğrusal olmayan zaman tanım alanı analizinde hasar birikimini tahmin etmek için geliştirilmiş hasar yasasını ve bağ kirişinin göçme anını kullanan basit bir 8 aşamalı algoritma özetlenmiştir. Algoritma ayrıca deprem sonrası DÇÇ bağ kirişlerinin değiştirilmesinin karar verme sürecine önemli ölçüde katkıda bulunabilecek niteliktedir.

Ayrıca tezin DÇÇ bölümünde son zamanlarda ODTÜ'de geliştirilen orta ek bağlantılı değiştirilebilir bir bağ kiriş detayı numerik olarak incelenmiştir. Ayrılabilir değiştirilebilir bağ kirişleri üzerinde yapılan önceki deneyler gözden geçirildikten sonra, yüksek bağ kiriş deformasyonları ve uç kısıtlama etkileri nedeniyle orta ek bağlantısının maruz kalacağı eksenel kuvveti tahmin etmek için kapsamlı bir parametrik çalışma gerçekleştirilmiş ve bir tasarım denklemi geliştirilmiştir. Deneysel olarak incelenen bağ kirişlerinden daha derin kesme bağ kirişleri için önerilen detayın uygulanmasını araştırmak için numeric simülasyonlar yapılmıştır. Analiz sonuçları ayrılabilir değiştirilebilir bağ kirişi konseptinin pratik uygulamalar için potansiyelini ortaya koymaktadır.

Tezin MÇÇ kısmı için öncelikle Amerika ve Avrupa şartnameleri tarafından önerilen sismik tasarım kuralları iyice gözden geçirilmiş ve karşılaştırılmıştır. Daha sonra bir dizi MÇÇ modeli, Amerikan ve Avrupa şartnamelerine göre tasarlanmış ve sismik performanslarını araştırmak ve karşılaştırmak için geniş bir deprem setine tabi tutulmuştur. Sekizyüzden fazla doğrusal olmayan zaman tanım alanı analizinin sonuçları, bu şartnameler arasında var olan farklılıkların gözlemlenen sismik performanslarda önemli farklılıklara yol açabileceğini ortaya çıkartmıştır. En dikkate değer fark, Avrupa şartnamelerine göre tasarlanan MÇÇ modellerinin en üst katlarında yumuşak kat davranışının ortaya çıkmasıdır. Bu olayın olası nedenleri araştırılmıştır ve öneriler sunulmuştur.

Çalışmanın son bölümünde depremler sırasında çaprazların yükleme hızının MÇÇ'lerin sismik davranışına etkisi araştırılmıştır. Eksenel olarak yüklenmiş elemanlar, ani yüklemeler altında dinamik burkulmanın bir sonucu olarak statik burkulma kapasitesinin üzerinde basınç kuvvetlerine maruz kalabilirler. Konuyla ilgili teorik bir arka plan ve ardından geniş bir deprem dizisi altında çeşitli MÇÇ konfigürasyonlarını dikkate alan kapsamlı bir parametrik çalışma yapılmıştır. Toplam 1600 doğrusal olmayan zaman tanım alanı analizinin sonuçları, özellikle MÇÇ'lerin kolonlarının, kirişlerinin ve guse levhalarının kapasite tasarımı için bu durumun ortaya çıkma sıklığını ve önemini göstermek için kullanılmıştır. Bu ekstra

kuvvetlerin etkileri tartıřılmış ve MÇÇ sistemlerinin kapasite tasarımı sırasında, dinamik burkulma etkisi dikkate alınarak, nihai çapraz kuvvetinin tahmin edilmesi için kullanılabilir basit bir formül geliştirilmiştir.

Anahtar Kelimeler: Merkezi Çaprazlı Çerçevesel, Dışmerkez Çaprazlı Çerçevesel, Deęiřtirilebilir Baę Kiriři, Düşük Çevrimsel Yorulma, Dinamik Burkulma

I would like to dedicate this thesis to my wife Narges, for her endless love,
incredible support, and being the source of joy in my life

ACKNOWLEDGMENTS

I would like to express my sincere gratitude to my supervisor Prof. Dr. Cem Topkaya for his excellent guidance and support throughout my studies. He is a brilliant researcher, a fantastic teacher, a great engineer, a caring supervisor, and a humble and nice person. A combination of qualities which are indeed rare. I would also like to thank him for his tremendous support in advancing my academic career. I could have not wished for a better supervisor and mentor.

I would also like to thank the examining committee members for their time and constructive comments.

Tests carried out in the present study were conducted on a test setup previously designed and built by Dr. Mehmet Bakır Bozkurt. Professor Abolhassan Astaneh-Asl provided valuable input on Chapter 5 of the thesis. Professors Taichiro Okazaki, Mario D'Aniello, Benjamin V Fell, and Suhaib Salawdeh, provided test data which was used in the research. All these contributions are acknowledged and appreciated.

The financial support provided by the Scientific and Technological Council of Turkey, under grant number TUBİTAK 114M251, which supported the candidature of the author as well as the experimental program, is also gratefully acknowledged.

Lastly, but most importantly, I would like to thank my parents, Nasrin and Mehdi, for their continuous support and being the best role models in my life. A special thank you to my lovely wife Narges, whose love and support were instrumental in the completion of this thesis, and to her family Shahla and Niloufar, and the late Mr. Karim Nikmardan, who supported us in every possible way through the past year. A sincere thank you also to my brother, Assoc. Prof. Dr. Saeid Kazemzadeh Azad, who guided me in difficult times with his calm and objective analyses. Finally, I would like to thank my most brilliant friend Milad Bybordiani, for his help and our enjoyable discussions.

TABLE OF CONTENTS

ABSTRACT	v
ÖZ	viii
ACKNOWLEDGMENTS	xii
TABLE OF CONTENTS	xiii
LIST OF TABLES	xviii
LIST OF FIGURES	xix
LIST OF SYMBOLS	xxiv
CHAPTERS	
1 INTRODUCTION	1
1.1 General	1
1.2 Objectives and Scope	2
1.3 Thesis Organization	6
2 A REVIEW OF RESEARCH ON STEEL EBFs	9
2.1 Introduction	9
2.2 Characteristics of Links	10
2.2.1 Yield Behavior, Shear Capacity and Overstrength	10
2.2.2 Link Rotation Demand and Capacity	16
2.2.3 Effect of Axial Force	20
2.2.4 Effect of Concrete Slab	21
2.2.5 Effect of Loading History	23

2.3	Detailing of Links.....	24
2.3.1	Flange and Web Compactness	24
2.3.2	Web Stiffeners.....	26
2.3.3	Lateral Bracing.....	34
2.3.4	Connections.....	35
2.4	Numerical Modeling of Links.....	40
2.5	EBF Systems	43
2.5.1	Characteristics and Capacity Design Approach.....	43
2.5.2	Research on Seismic Performance	47
2.6	Special Topics	56
2.6.1	EBFs with Vertical Links.....	56
2.6.2	Tied Braced Frames and EBFs with Zipper Struts.....	59
2.6.3	Replaceable Links	60
2.6.4	Use of EBFs or links in Reinforced Concrete Structures	63
2.6.5	Progressive Collapse of EBFs.....	63
2.6.6	Fragility Functions for Links	64
2.6.7	Other Applications.....	64
2.7	Chapter Summary.....	65
3	LOW-CYCLE FATIGUE TESTING OF SHEAR LINKS AND CALIBRATION OF A DAMAGE LAW.....	71
3.1	Introduction.....	71
3.2	Experimental Program.....	73
3.2.1	Test Setup and Instrumentation.....	73
3.2.2	Details of Specimens	76

3.2.3	Loading Protocols for Reliability Assessment of the Damage Law	83
3.3	Experimental Results	86
3.4	Low-Cycle Fatigue Behavior of Specimens	91
3.5	Calibration of a Cumulative Damage Law for Specimens Tested as a Part of the Present Research Program	92
3.6	Verification of the Damage Law Using More Complicated Loading Histories	96
3.7	Development of a Generalized Damage Law for Shear Links	99
3.8	Algorithm for the Application of the Generalized Damage Law for Shear Links	105
3.9	Practical Application of the Generalized Damage Law to the Shear Links of Christchurch Hospital Garage	107
3.10	Evaluation of the ASCE41 Metrics for Link Performance	111
3.11	Evaluation of the AISC Loading Protocol from a Cumulative Damage Perspective	113
3.12	Chapter Summary	114
4	NUMERICAL ANALYSIS OF DETACHABLE REPLACEABLE LINKS	115
4.1	Introduction	115
4.2	Previous Experiments on Detachable Links	119
4.3	Numerical Study	123
4.3.1	General Modeling Details	124
4.3.2	Prediction of Design Axial Force	126
4.3.3	Investigation of Larger (Deeper) Mid-Spliced Links	132
4.4	Chapter Summary	138

5	SEISMIC BEHAVIOR OF CONCENTRICALLY BRACED FRAMES DESIGNED TO AISC341 AND EC8 PROVISIONS.....	139
5.1	Introduction.....	139
5.2	Comparison of Design Provisions in AISC341 and EC8.....	141
5.2.1	Definition and Geometries.....	141
5.2.2	Seismic Demands.....	143
5.2.3	Energy Dissipation and Response Modification Coefficients.....	145
5.2.4	Classification of Cross Sections for Local Buckling.....	147
5.2.5	Design of Bracing Members.....	147
5.2.6	Design of Columns.....	152
5.2.7	Design of Beams.....	155
5.2.8	Design of Brace Connections.....	157
5.2.9	System Requirements.....	158
5.3	Design of Archetypes.....	159
5.3.1	Selected Geometries, Materials, and Member Sizes.....	159
5.3.2	Split X-Braced System.....	163
5.3.3	X-Braced System.....	166
5.3.4	V-Braced System.....	167
5.4	Comparison of Seismic Behaviors.....	168
5.4.1	Details of Numerical Simulations.....	169
5.4.2	Split X-Braced System.....	173
5.4.3	X-Braced System.....	186
5.4.4	V-Braced System.....	189
5.5	Chapter Summary.....	194

6	DYNAMIC BUCKLING OF BRACES IN CONCENTRICALLY BRACED FRAMES.....	195
6.1	Introduction.....	195
6.2	Theoretical Background.....	197
6.3	Investigation of Recent Dynamic Tests.....	201
6.3.1	Dynamic Tests of Fell on a Brace Member	201
6.3.2	Shake Table Test of Goggins on a Single-Story CBF	205
6.3.3	Shake Table Test of Okazaki et al. on a Single-Story CBF.....	208
6.4	Effect of Dynamic Buckling of Braces on Seismic Behavior of CBFs..	212
6.4.1	Design and Analysis of Archetypes	212
6.4.2	Discussion of Results.....	216
6.4.3	Further Important Inferences.....	222
6.5	Estimation of Dynamic Overshoot in Brace Compressive Capacity.....	224
6.6	Chapter Summary	228
7	CONCLUSIONS	231
7.1	EBF-Related Conclusions.....	231
7.2	CBF-Related Conclusions.....	234
	REFERENCES.....	239
	CURRICULUM VITAE.....	287

LIST OF TABLES

TABLES

Table 3.1 Nominal and measured dimensions of the rolled HEA160 and built-up BU250 sections.....	79
Table 3.2 Material properties of the rolled HEA160 and built-up BU250 sections	79
Table 3.3 Details of the tested specimens.....	80
Table 3.4 Summary of experimental results.....	89
Table 4.1 Details of the specimens tested during the METU experimental program and considered herein for verification of FE modelling.....	121
Table 4.2 Material Properties of I-shaped links tested during the METU experimental program and considered herein for verification of FE modelling.....	121
Table 5.1 Brace overstrengths of the designed archetypes.....	161
Table 5.2 Comparison of steel weights of the designed archetypes.....	165
Table 5.3 Comparison of responses of the designed archetypes.....	175
Table 5.4 Percentage of yielded or buckled members of the designed archetypes	185
Table 6.1 Percentage of yielded or buckled members of the designed archetypes	226

LIST OF FIGURES

FIGURES

Figure 1.1. Typical CBF (a-c) and EBF (d-f) configurations	2
Figure 1.2. Some of the previously developed replaceable link details	3
Figure 1.3. Detachable replaceable link detail	4
Figure 1.4. Development of axial force in links.....	5
Figure 1.5. Dynamic buckling in an elastic steel rod	6
Figure 2.1. EBF configurations and their corresponding plastic mechanisms.....	10
Figure 2.2. Free-body diagram of an isolated link segment.....	11
Figure 2.3. Failure mechanisms of (a) short, (b) intermediate, and (c) long links (photo courtesy of T. Okazaki).....	11
Figure 2.4. Link overstrength factors reported in different experimental studies...	14
Figure 2.5. Inelastic link rotation capacity for a link specimen	17
Figure 2.6. Inelastic link rotation capacities reported in experimental studies.....	19
Figure 2.7. AISC 341-10 [11] link web stiffening requirements	29
Figure 2.8. New web stiffening schemes for short (a-d) and long (e-f) links.....	31
Figure 2.9. EBF link-to-column connections.....	36
Figure 2.10. Plan view of the use of duplicate floor beams in EBFs [181].....	53
Figure 2.11. Previously developed replaceable link details.....	60
Figure 2.12. Detachable replaceable link detail	62
Figure 3.1. Details of the test setup; Not all instrumentations are shown	74
Figure 3.2. Instrumentation used for monitoring link rotation angle	75
Figure 3.3. Typical stress-strain curves observed in the coupon tests.....	79
Figure 3.4. Details of the tested specimens.....	81
Figure 3.5. Utilized loading protocols in the experimental program.....	84
Figure 3.6. Hysteretic response of Specimens 1–6 of the present study and SP2 and SP1 from Bozkurt and Topkaya [8] (rolled HEA160 links)	87
Figure 3.7. Hysteretic response of Specimens 7–14 (built-up BU250 links)	88

Figure 3.8. Typical failure modes: (a) web fracture in HEA160 links; (b) severe flange buckling and fracture in HEA160 links; (c) web fracture in BU250 links...	90
Figure 3.9. Calibration of the damage laws based on (a) plastic cycle range and (b) cycle range (axes are in logarithmic scale)	95
Figure 3.10. Comparison of the test results with predictions of the calibrated damage laws	98
Figure 3.11. Values of normalized C determined based on the results reported in the present study as well as previous studies: (a) the entire data; (b) a close-up view of data points with normalized C values less than 14.....	104
Figure 3.12. The link fracture detection algorithm.....	107
Figure 3.13. LCF behavior of the N-S and E-W links predicted by CVGM and the proposed generalized damage law: (a) N-S and (b) E-W with EQ loading; (c) N-S and (d) E-W with Richard and Uang protocol	110
Figure 4.1. Typical moment and shear variations within an internal EBF link	117
Figure 4.2. Proposed detachable replaceable link detail: (a) replaceable link with gusseted brace attachments; (b) bolted extended end-plated link	117
Figure 4.3. Possible connection details for the mid-splice of the detachable link detail	118
Figure 4.4. Details of Specimens 2, 3, 5, 6 (residual drift of 0.5%) tested during the METU experimental program and considered herein for verification of FE modelling approach.....	120
Figure 4.5. Mid-splice connection detail for Specimens 2, 3, 5, and 6 tested during the METU experimental program and considered herein for verification of FE modelling approach.....	122
Figure 4.6. Hysteretic response of Specimens 2, 3, 5, and 6 tested during the METU experimental program and considered herein for verification of FE modelling approach.....	123
Figure 4.7. Stress-strain curve utilized in the FE analysis of Specimen 6.....	125
Figure 4.8. Bolt pretensioning in ABAQUS using the bolt load technique.....	126

Figure 4.9. Full models of Specimens 2, 3, 5, and 6 testing in the METU experimental program: (a) mesh; (b) PEEQ contours at the end of the analysis	127
Figure 4.10. Results of the parametric study on the design axial force for the mid-splice connection	132
Figure 4.11. Details of the studied deep mid-spliced links: (a) Case 2; (b) Case 3	134
Figure 4.12. The refined mesh used for the calculation of MRI in HEB500-Case2	135
Figure 4.13. MRI contours at the end of the analysis for (a) conventional HEA160, (b) mid-spliced HEA160, (c) conventional HEA220, (d) mid-spliced HEA220, (e) conventional HEB500-Case 1, (f) mid-spliced HEB500- Case 2, and (g) mid-spliced HEB500-Case 3	136
Figure 4.14. Variation of MRI along the critical path for the studied models.....	137
Figure 5.1. Single diagonal and X-braced systems	142
Figure 5.2. V-braced, Inverted V-braced, and K-braced systems	142
Figure 5.3. Comparison of design response spectra	144
Figure 5.4. Typical analysis models for diagonal bracings.....	149
Figure 5.5. Typical analysis models for the capacity design of columns in CBFs	153
Figure 5.6. Typical forces on beams of CBF systems	156
Figure 5.7. Floor plan and elevation view of the archetype building (all dimensions are in meters).....	160
Figure 5.8. Member sizes for the designed original split X-braced, X-braced, and V-braced archetypes	162
Figure 5.9. Comparison the finite element results with the test results of Black et al. [284]; Tension (+) Compression (-).....	173
Figure 5.10. Summary of analysis results for US-2X.....	174
Figure 5.11. Comparison of analysis results for US-2X and EU-2X	176
Figure 5.12. Deformation of brace-intersected beam and its effect on brace ductility demands	178

Figure 5.13. Distribution of PEEQ in EU-2X at the end of the analysis for record No. 30	179
Figure 5.14. Member sizes for the alternative designs as per EC8	182
Figure 5.15. Height-wise variation of brace overstrengths for the designed split X-braced archetypes.....	183
Figure 5.16. Median of drift responses for the designed split X-braced archetypes	184
Figure 5.17. Comparison of analysis results for US-X and EU-X	187
Figure 5.18. (a) and (b) Variation of brace overstrengths and (c) median of drifts for the designed X-braced archetypes	189
Figure 5.19. Comparison of analysis results for US-V and EU-V	191
Figure 5.20. (a) and (b) Variation of brace overstrengths and (c) median of drifts for the designed V-braced archetypes	191
Figure 6.1. Rod under a constant boundary velocity (a) deflected shape (b) an infinitesimal segment of the rod.....	198
Figure 6.2. Dynamic overshoot in the buckling load of an elastic rod (v in mm/s)	200
Figure 6.3. FE model of Fell's [329] HSS1-3 test (a) specimen details with dimensions in mm (b) meshed quarter model (c) von Mises stress contour in MPa at the end of the analysis.....	202
Figure 6.4. Loading history in the HSS1-3 test of Fell [329] (data courtesy of B. V. Fell); Tension (+) Compression (-).....	202
Figure 6.5. Fell's [329] HSS1-3 test results (data courtesy of B. V. Fell) versus FE results of the present study.....	204
Figure 6.6. FE model of the ST4 test of Goggins [378] (a) specimen details with dimensions in mm (b) meshed model.....	206
Figure 6.7. Goggins' [378] ST4 test results (data courtesy of S. Salawdeh) versus FE results of the present study.....	208
Figure 6.8. FE model of Okazaki et al.'s [306] test (a) specimen details with dimensions in mm (b) meshed model.....	209

Figure 6.9. Okazaki et al.'s [306] test results (data courtesy of T. Okazaki) versus FE results of the present study	210
Figure 6.10. FE results of re-analyzing the shake table test of Okazaki et al. [306] with an initial imperfection of $l/1000$	211
Figure 6.11. Plan dimensions and story heights (in meter) for the archetype buildings (a) 9-story (b) 3-story.....	213
Figure 6.12. Selected member sizes for the designed archetype CBFs	214
Figure 6.13. Results for 3-story archetype CBFs under near-field ground motions	218
Figure 6.14. Results for 9-story archetype CBFs under far-field ground motions	219
Figure 6.15. Summary of changes recorded for maximum base shears	221
Figure 6.16. Ratio of the recorded maximum compressive brace force divided by the static buckling capacity (i.e. α).....	224
Figure 6.17. Recorded maximum compressive brace loading rates (in mm/s).....	225
Figure 6.18. FE response of an HSS $4 \times 4 \times 1/4$ steel brace with $\lambda = 60$ to different loading rates	226

LIST OF SYMBOLS

SYMBOLS

A (or A_g)	Gross area
A^+	Areas of the horizontal projections of the cross sections of the tension diagonals when the horizontal seismic actions have positive direction
A^-	Areas of the horizontal projections of the cross sections of the tension diagonals when the horizontal seismic actions have negative direction
C (or \bar{C})	Structural performance parameters
\mathbf{C}	Damping matrix
C_d	Displacement amplification factor
C_{ult}	Expected brace compressive strength
D	Damage
DL	Dead loads
D_{max}	Seismic design category
E	Elastic modulus
E_{amp}	Amplified seismic loads
F	Applied force
F_{cre}	Critical stress calculated using column buckling equations
F_y	Yield stress
$F_{y,0.2}$	Yield stress at 0.2% permanent elongation
F_{yl}	Lower yield stress
F_{yu}	Upper yield stress
F_u	Ultimate stress
HL	Loads due to lateral earth pressure
I	Moment of inertia
K	Link elastic stiffness
\bar{K}	Effective length factor
K_s	Plate buckling coefficient
\mathbf{K}	Stiffness matrix

L	Length of the member
L_{bay}	Bay width
LL	Live loads
\mathbf{M}	Mass matrix
M_P	Plastic moment capacity
N_{amp}	Amplified seismic column axial force
N_{design}	Amplified axial demand of the column
N_E	Column axial force resulting from seismic actions
$N_{Ed,i}$	Design axial force in the brace i
N_f	Number of cycles to failure
N_G	Available non-seismic column axial force
$N_{pl,Rd,i}$	Design plastic resistance of the brace i ;
P	Axial force
P_{beam}	Maximum value of beam axial force
P_{br}	Brace axial force
P_{col}	Maximum value of column axial force
P_{cr}	Critical Euler buckling load
P_{design}	Design axial force of the mid-splice connection
P_{EQ}	Column axial force generated by the code-specified earthquake loads
P_n	Nominal compressive strength
P_{max}	Maximum link axial force
P_y	Axial yield strength
P_y^{flange}	Flange yield force
P_{fy}	Yield strength of both flanges
R	Response modification coefficient
R_y	Ratio of expected to nominal yield stress
SL	Snow loads
S_{DS}	Design spectral acceleration value at short period
SD_1	Design spectral acceleration value at 1 second period
S_{MS}	Modified spectral acceleration value at short period

S_{MI}	Modified spectral acceleration value at 1 second period
S_s	Spectral acceleration value at short period
S_l	Spectral acceleration value at 1 second period
T	Time
\hat{T}	Stress triaxiality
T_o	Fundamental period
T_{fr}	The time instant corresponding to the state of full damage
T_{ult}	Expected brace tensile strength
V	Links shear
V_b	Base shear
V_e	Expected (or actual) shear capacity
V_{max}	The maximum shear force that can develop in a link
V_n	Nominal shear capacity
V_n^{meas}	Measured link shear strength
V_P	Plastic shear capacity
Z	Section plastic modulus
a	Stiffener spacing
a_g	Design ground acceleration
b_f	Flange width
c (or \bar{c})	Structural performance parameter
d	Section depth
e	Length of a link segment
g	Standard acceleration due to gravity
h	Web depth
h_{col}	Distance between the column end pins
l	Effective buckling length
q	Behavior factor
r	Radius of gyration
t	Time

t_f	Flange thickness
t_s	Stiffener thickness
t_w	Web thickness
u_a	Axial shortening
u_b	Axial shortening due to lateral deflection
u_{br}	Brace elongation/shortening
v	Boundary velocity
v_{br}	Brace loading rate or velocity
v_{max}	Peak value of brace loading rate
y	Total deflection
y_m	Dimensionless deflection parameter
y_o	Deflection of the rod due to initial imperfections
$\%EL$	Percentage of elongation
Δ	Interstory drift ratio
Δ_P	Plastic story drift
ΔT	Time step
$\Delta\gamma$	Cycle range
$\Delta\gamma_P$	Plastic cycle range
Ω	Overstrength factor
$\hat{\Omega}$	Dynamic similarity number
Ω_a	Calibrated overstrength factor
Ω_i	Overstrength of the brace i
Ω_i^{max}	Maximum brace overstrength in a CBF
Ω_i^{min}	Minimum brace overstrength in a CBF
Ω_o	Structural overstrength factor
α	Dynamic overshoot amplification factor
$\hat{\alpha}$	Web panel aspect ratio
α_m	Proportionality factor for mass
α_y	Saturation value for α

β	A factor which takes into account the effect of link length ratio on the design axial load
$\hat{\beta}$	Web panel height to thickness ratio
β_k	Proportionality factors for stiffness
γ	Link rotation angle
$\bar{\gamma}_B$	Link rotation angle measured from the farthest point of zero shear to the point of buckling
γ_{ov}	Ratio of the expected yield stress to the specified minimum yield stress
γ_P	Inelastic (or plastic) link rotation angle
γ^{max}	Maximum total link rotation angle
γ_P^{max}	Maximum inelastic (or plastic) link rotation angle
γ_u	Rotation angle at which buckling is anticipated for the link web under cyclic loading
δ	Dimensionless imperfection parameter
δ_{bro}	Maximum brace out-of-plane deformation
$\dot{\epsilon}_{br}$	Brace axial strain rate
$\dot{\epsilon}^p$	Plastic strain rate tensor
λ	Non-dimensional slenderness
μ	Ductility
μ_{br}	Maximum brace ductility demand
ξ	Percentage of critical damping
ρ	Link length ratio
$\bar{\rho}$	Material density
ρ^{meas}	Measured link length ratio
ρ^{nom}	Nominal link length ratio
ρ^{theor}	Theoretical dividing link length ratio between shear dominated and flexure dominated behavior
σ_m	Hydrostatic stress
σ_v	Von Mises stress
τ	Dimensionless time

CHAPTER 1

INTRODUCTION

1.1 General

Steel frames are used in structures as gravity and lateral load resisting systems. Two of such lateral load resisting systems are *centrically braced frames* (CBFs) and *eccentrically braced frames* (EBFs). As shown in Figure 1.1, both systems utilize brace members, however, in EBFs the braces are placed in an eccentric configuration that creates small segments in the frame which are called *links* (shown with e in the figure).

CBFs have been quite popular since the 1960s mainly because of their economic advantages over moment resisting frames (MRFs) particularly in cases where the drift requirements govern the design. Furthermore, beam-to-column connections of MRFs suffered premature fractures in the 1995 Kobe and the 1994 Northridge earthquakes [1, 2]. In the aftermath of these earthquakes, considerable research and development projects were conducted in the US, Japan, Europe, and elsewhere to develop new moment connections that have sufficient strength, stiffness, and ductility to perform satisfactorily during future strong seismic events. However, the new MRF connections and the modifications made to then existing moment connections have caused their cost of construction and inspection to increase significantly, making the use of CBFs even more economical. In this structural system, the input earthquake energy is mainly dissipated by the braces through complicated cycles of yielding in tension and buckling in compression.

EBFs, on the other hand, were first introduced for seismic applications in the 1970s in Japan [3, 4] and are generally considered as a hybrid system integrating the

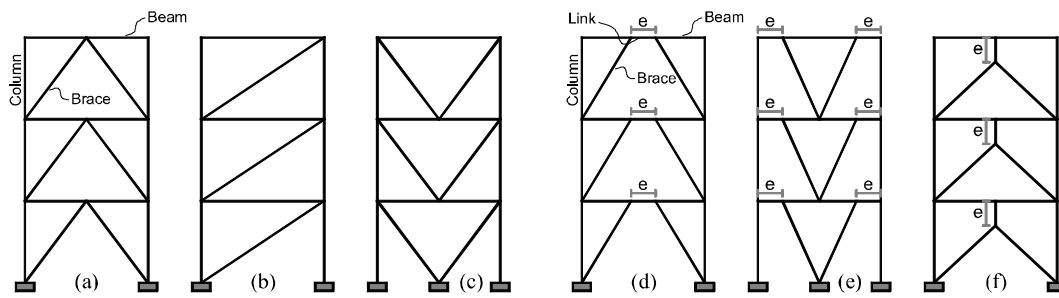


Figure 1.1. Typical CBF (a-c) and EBF (d-f) configurations

advantages of both MRF and CBF lateral load resisting systems into a single structural system. They typically have relatively high lateral stiffness (comparable to CBFs) and considerably high energy-dissipation capacities (comparable to MRFs). Unlike CBFs where brace buckling can create pinched hysteretic loops, in EBF systems yielding is concentrated only at links and all other members of the frame are proportioned to remain essentially elastic. Therefore, during severe earthquakes, links serve as structural fuses dissipating the seismic input energy through stable and controlled plastic deformations, resulting in relatively high energy dissipation. Furthermore, EBFs offer larger architectural openings compared to CBFs as schematically depicted in Figure 1.1.

While both CBF and EBF systems are typically well-recognized by researchers and practicing engineers, there remain many aspects of them that have not been fully explored. The present thesis is therefore an attempt to address a number of these less-studied aspects which were identified at the start of the project through a preliminary investigation. These are discussed in the following section.

1.2 Objectives and Scope

The first issue noticed during the preliminary investigation was the lack of a research review on the studies conducted on EBFs. The only comprehensive literature review on the topic was found to be published in the late 1980s [5] when researchers had just started to realize the potential of EBFs. Many more studies have been carried

out since then on EBFs. Consequently, it was deemed fruitful to first conduct a comprehensive review of research on eccentrically braced frames considering both component level and system level studies. Such a review study also helped identify other research gaps.

One of the major research gaps identified was the lack of low-cycle fatigue (LCF) tests and calibrated damage laws for EBF links. As mentioned earlier, links in EBFs are subjected to large inelastic cyclic actions during earthquakes. A major concern is the possibility of link fracture during such events which, for instance, was observed in the 2011 Christchurch earthquake in New Zealand [6]. Although this issue has been known to researchers and engineers, straight-forward methods for estimating the fracture life of a link have not been developed. In other words, for a given link rotation history under an earthquake, there are no practical methods for predicting whether the link would fracture or not; except highly sophisticated finite element analysis (FEA) methods considering extremely refined meshes (in the order of 0.1 mm) [7]. Therefore, a part of the present thesis was focused on conducting low-cycle fatigue tests and calibrating a damage law for predicting the fracture life of links.

An emerging topic in the field of EBFs is the concept of *replaceable links* where the link segments are designed and detailed in a way that they can be easily replaced after a severe earthquake. Several details have been proposed in the last decade, as depicted in Figure 1.2, including those developed at Middle East Technical University (METU) [8, 9].

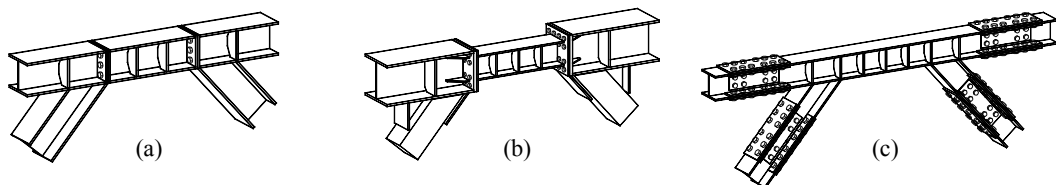


Figure 1.2. Some of the previously developed replaceable link details

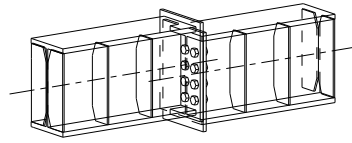


Figure 1.3. Detachable replaceable link detail

A special type of replaceable link, namely *detachable replaceable link*, is under development at METU which is based on splicing the link at its mid-length in order to facilitate the link replacement procedure after an earthquake where the structure will most probably have residual drifts. As shown in Figure 1.3, by adjusting the mid-splice detail, it is possible to replace the link under different levels of post-earthquake residual drifts. An issue not addressed in the experimental study at METU is the level of axial force required for the design of the splice connection. As schematically shown in Figure 1.4, large axial forces can develop in links experiencing high levels of link rotation angle (γ) [10]; i.e. the angle between the link and the beam outside of the link. This axial force is critical and shall be accounted for in the design of the splice connection of the detachable replaceable link detail (Figure 1.3). Another important issue was also observed during the experimental study at METU. The behavior of the proposed detail was mainly investigated by testing relatively shallow links with an HEA160 section. Only one deeper specimen with an HEA220 section was tested at METU, which exhibited a significantly lower rotation capacity than previously tested comparable links. This raised the question of whether the presence of the mid-splice connection was responsible for the premature fracture and whether the details can be employed in practical applications where deeper link sections are utilized. In line with this, another part of the present thesis investigates the two issues discussed above regarding the detachable replaceable link detail; i.e. (i) the level of design axial force and (ii) the behavior of deeper mid-spliced links.

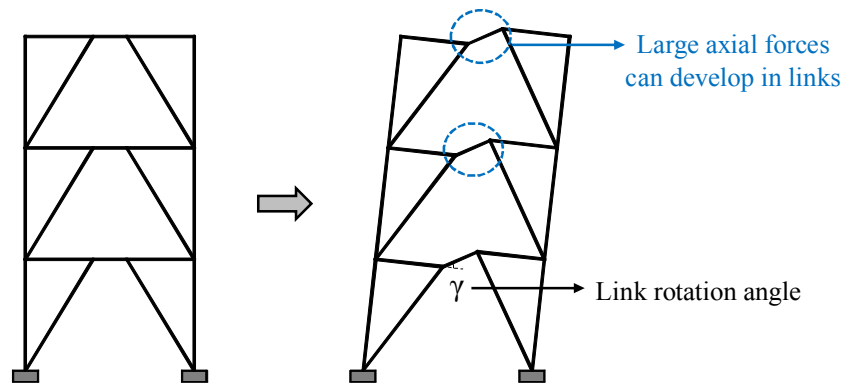


Figure 1.4. Development of axial force in links

As mentioned earlier, in addition to EBFs, some aspects of concentrically braced frames (CBFs) are also investigated in the present thesis. An issue which was noticed during the preliminary investigation is that the provisions used in the United States and Europe for the seismic design of CBFs are substantially different. While both design approaches are intended to result in structures with comparable performances during a major earthquake, there are, in some cases, stark differences between the design philosophies. Since there were no studies directly comparing these differences and their effects on the seismic behavior of CBFs, a part of the present thesis was focused on this issue.

Another interesting issue noticed during the preliminary investigation is the effect of *dynamic buckling* of braces on the seismic behavior of CBFs. Axially loaded members might experience compressive forces above their static buckling capacity as a result of dynamic buckling under rapid shortening. This is schematically shown in Figure 1.5 for an elastic steel rod where higher buckling loads are attained when the rod is subjected to faster shortenings. It should be emphasized that this phenomenon is because of the inertia effect of the mass of the rod and is *not* due to the strain rate effect which can increase the material strength. Although the subject is studied in the context of engineering mechanics, it has not been thoroughly investigated in the field of earthquake engineering. Such dynamic overshoots in the

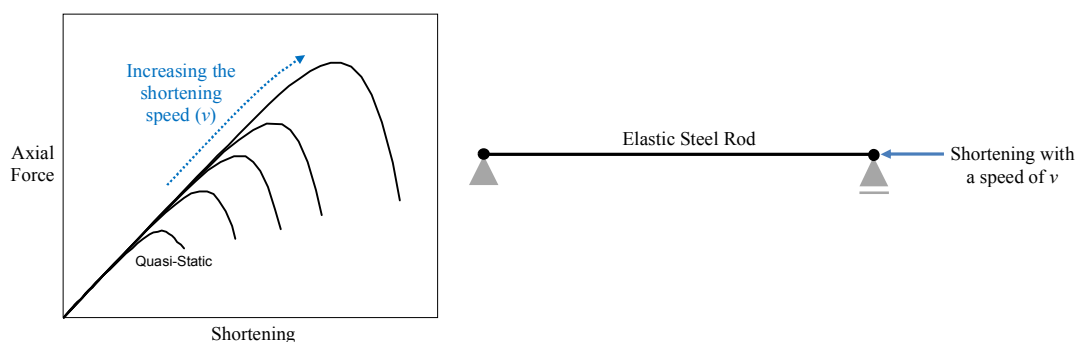


Figure 1.5. Dynamic buckling in an elastic steel rod

compressive capacity can also be observed for braces of CBFs during earthquakes which could, in turn, affect the seismic performance of these systems. Therefore, the final part of the present thesis is a comprehensive numerical investigation on the dynamic buckling of CBF braces.

1.3 Thesis Organization

In addition to the Introduction chapter, the present thesis contains six more chapters. EBF-related topics are studied in Chapters 2 to 4, while CBF-related topics are investigated in Chapters 5 and 6.

In Chapter 2, the above-discussed comprehensive review of research conducted on EBFs is presented which contains over 240 references.

Chapter 3 contains the results of a series of low-cycle fatigue tests on EBF links as well as calibration of a damage law for predicting the possibility of fracture in these members during an earthquake.

In Chapter 4, the results of the numerical investigation on the behavior of detachable replaceable links are presented where the axial design force for this link detail as well as the behavior of deeper mid-spliced links are studied.

The seismic behavior of CBFs designed following the American and European provisions are compared and investigated numerically in Chapter 5 using extensive nonlinear time history analyses.

In Chapter 6, the phenomenon of dynamic buckling of braces and its effect on the seismic performance and design of CBFs is studied numerically.

Finally, the conclusions of the study are summarized in Chapter 7.

CHAPTER 2

A REVIEW OF RESEARCH ON STEEL EBFs

As discussed in the previous chapter, a part of the study was allocated to conduct a comprehensive review of research on EBFs. Considering that the present thesis investigates a number of different topics on EBFs and CBFs, it was decided to include the comprehensive literature review on EBFs as a separate chapter (i.e. Chapter 2), whereas at the introduction of each following chapter a shorter, more focused, review is presented which summarizes the studies related more directly to the topic under investigation in that chapter.

2.1 Introduction

The main idea in the design of an eccentrically braced frame (EBF) is to integrate the advantages of both moment resisting frame (MRF) and concentrically braced frame (CBF) lateral load resisting systems into a single structural system. The EBF system originated from Japan in 1970s [3, 4] with the aim of achieving a structure with high elastic stiffness as well as high energy dissipation during severe earthquakes.

There are several configurations for an EBF system, some of which are depicted in Figure 2.1 along with their expected plastic mechanisms. Larger architectural openings can be used with EBF systems when compared to CBFs. The short segment of the frame generally designated by the length e (Figure 2.1) is called the link. In EBF systems, yielding is concentrated only at link segments and all other members of the frame are proportioned to remain essentially elastic. Therefore, during severe earthquakes, links can be considered as structural fuses which will dissipate the seismic input energy through stable and controlled plastic deformations.

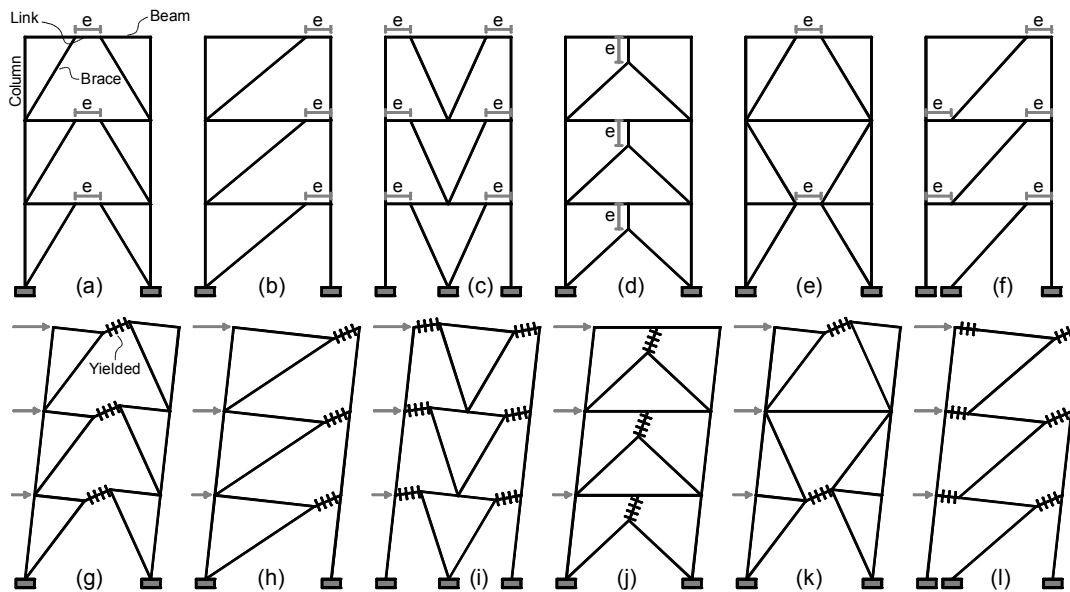


Figure 2.1. EBF configurations and their corresponding plastic mechanisms

A comprehensive review is provided in this chapter on the behavior and design of eccentrically braced frames. The review includes research conducted on links, as they comprise the most critical elements of an EBF. In addition, the research on EBF system response is elaborated. Areas of future research needs are also identified. The comparison of design provisions as presented in various design specifications is out of the scope of this investigation; however, the AISC Seismic Provisions for Structural Steel Buildings [11] are mentioned throughout the chapter to illustrate relationships between research findings and design rules.

2.2 Characteristics of Links

2.2.1 Yield Behavior, Shear Capacity and Overstrength

The length of a link segment (e) is one of the key parameters that controls the stiffness, strength, ductility, and behavior of an EBF system. The link length ratio, $\rho = e/(M_P/V_P)$, where M_P and V_P are the plastic moment and plastic shear capacities of

the link, provides a convenient measure for the yield behavior. The free-body diagram of an isolated link is shown in Figure 2.2. Based on equilibrium, considering equal end moments at the ultimate state, no moment-shear interaction, and an elastic-perfectly plastic material, the theoretical dividing link length ratio between shear dominated and flexure dominated behavior is $\rho^{\text{theor}} = 2.0$.

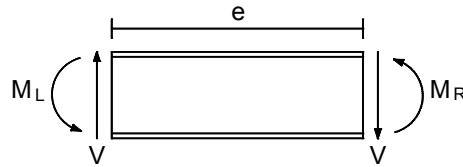


Figure 2.2. Free-body diagram of an isolated link segment

In short (or shear) links, shear yielding of the web is found to be predominant (Figure 2.3a). On the other hand, in long (or moment) links, flexural yielding controls the link behavior (Figure 2.3c). An intermediate link, however, would experience a combination of both shear and flexural yielding (Figure 2.3b).

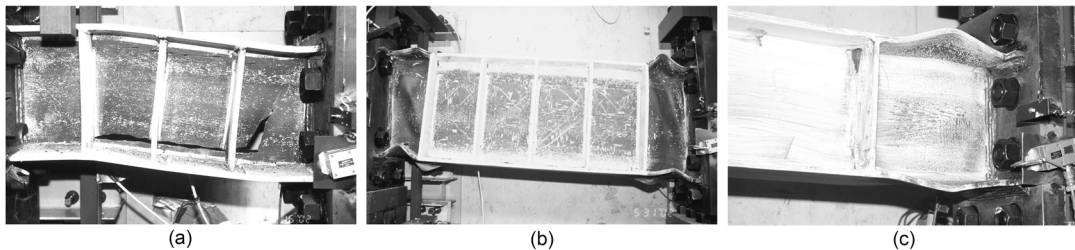


Figure 2.3. Failure mechanisms of (a) short, (b) intermediate, and (c) long links
(photo courtesy of T. Okazaki)

There are substantial differences between the behavior of short and long links. Although longer links provide more architectural freedom for openings, early experimental studies by Roeder and Popov [12, 13] and Hjelmstad and Popov [14, 15] showed that the performance of short links is considerably better than that of long links under severe cyclic loadings in terms of strength and ductility. Over the years Popov and his colleagues [14, 16-18] suggested different practical limiting

lengths for shear dominated behavior, finally arriving at the limit of $\rho < 1.6$, which is still in use in many design specifications including AISC 341-10 [11].

The first comprehensive study on the behavior of intermediate and long links ($\rho > 1.6$) was conducted by Engelhardt and Popov [19] in 1989. A total of 14 tests were conducted on 12 two-third scale subassemblage specimens with ρ ranging from 1.45 to 4.25. Based on the experimental results it was concluded that a gradual transition from the shear-dominant behavior to the flexure-dominant behavior occurs as ρ is increased from 1.6 up to 3. Despite this, in most of the previous and current specifications (e.g. [11, 20]), links with length ratios of $1.6 < \rho < 2.6$ are classified as intermediate links while links with $\rho > 2.6$ are generally referred to as long links. It is important to note that the presence of high axial force in a link may change this categorization, as discussed in Section 2.2.3. Engelhardt and Popov [19] also reported that moment-shear interaction has a notable effect on the behavior of intermediate links, while short and long links are generally unaffected.

Terms such as very short and very long links are also used in the literature. Although there are no explicit definitions, links with $\rho > 3 \sim 3.5$ are sometimes referred to as very long links [19, 21] while links with $\rho < 1$ as very short links [22]. In 2012, finite element (FE) analyses conducted by Daneshmand and Hashemi [21] demonstrated that the behavior of very long links can differ notably from that of long links in terms of failure mode and ductility, and thus, dividing the long link range in design codes into two or more sub-regions was suggested. Furthermore, recent studies (e.g. [22]) have proved that there are also other remarkable differences between the characteristics of very short links and short links, which will be discussed later.

The nominal shear capacity (V_n) of a link can be defined as follows [11]:

$$V_n = \text{Min} [V_p, 2M_p/e] \quad (2.1)$$

where the plastic capacities (i.e. V_p and M_p) are calculated based on the nominal yield stress, F_y . For links with length ratios less than 2.0 the first term will govern;

however, for longer links the second term is dominant. In order to meet the objectives of the capacity design approach, it is necessary to estimate the maximum shear force that can develop in a link during an intense loading, i.e. V_{max} . Consequently, other structural members shall be designed to remain essentially elastic and resist the loads developed by the fully yielded and strain-hardened link. Any underestimation of the maximum link force may lead to unfavorable failures in other members. To have a reliable estimate of V_{max} the link overstrength concept is generally utilized as follows:

$$V_{max} = \Omega (R_y V_n) = \Omega V_e \quad (2.2)$$

where R_y is the ratio of expected to nominal yield stress, considered for each steel grade based on statistical data, V_e is the expected (or actual) shear capacity of the link, and Ω is the overstrength factor due to strain hardening. Early experimental studies by Popov and his colleagues [12, 14, 19, 23, 24] suggested the value of $\Omega = 1.5$ for design purposes, which is still (implicitly) in use in most seismic design specifications (e.g. [11, 25]). The link overstrengths observed in the previous experimental studies on horizontal I-shaped links [14, 19, 22, 23, 26-47] are presented in Figure 2.4. The traditional line of $\Omega = 1.5$ is also depicted in this figure. It should be mentioned that the value of V_e for every data point is calculated using the measured properties reported in the original reference. Only cyclic test results for links with $F_y > 200$ MPa are included in the figure. A summary of the experiments conducted between 1983 and 2002 on EBF links is also presented by Richards [48] in his dissertation. Most of the links tested by Popov and his colleagues [14, 17, 19, 23, 27] were constructed from A36 steel, while links with higher strength steels such as A709 and A992 were tested later by other researchers such as McDaniel [32], Okazaki and his colleagues [39, 41], Mansour et al. [49], and Dusicka et al. [44]. Shear links constructed from low-yield-strength steels were also tested more recently by Dusicka et al. [44] and Ji et al. [22].

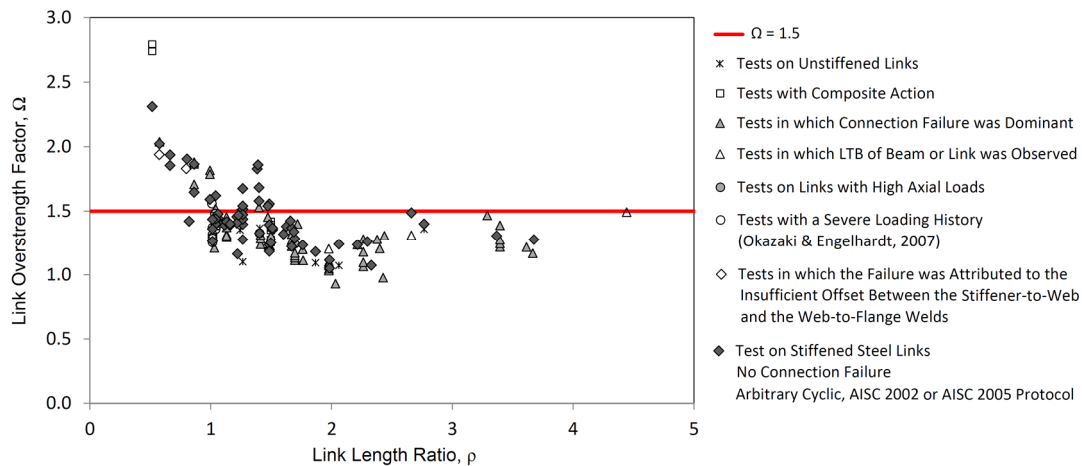


Figure 2.4. Link overstrength factors reported in different experimental studies

As can be seen in Figure 2.4, the value of $\Omega = 1.5$ seems like a reasonable upper-bound for links with $\rho > 1$. However, this overstrength value overestimates V_{max} for some intermediate links ($1.6 < \rho < 2.6$) and drastically underestimates V_{max} for very short links ($\rho < 1$). There are several reasons for these discrepancies, which can be summarized as follows.

Using a constant value of 1.5 for the overstrength factor neglects the effect of moment-shear (M-V) interaction. However, the study by Engelhardt and Popov [19] proved that this interaction can be important for intermediate links where Ω values lower than 1.5 were observed (Figure 2.4).

The nominal shear capacity of short links is generally calculated based on the web area, neglecting the contribution of the flanges [11]. However, as mentioned by McDaniel et al. [32], in short links with relatively thick flanges, there is a significant shear force carried by the flanges. Manheim and Popov [16] and Richards [48] have proposed methods for determining the link plastic shear capacity considering the flange effect. Through nonlinear FE analysis of isolated links, Richards [48] demonstrated that the overstrength factor of 1.5 is a reasonable limit even for very short links, provided that the flange effect is included in determining V_P . However, the same conclusion was not reached when previous test results on short and very

short built-up links [29, 30, 32, 50] were examined. The calculated overstrengths for these links decreased slightly by including the flange effect in determining V_P ; however, they were still significantly higher than 1.5 for most cases. Richards [48] attributed this discrepancy to the presence of other factors, besides the flange effect, in experimental studies. In 2007, Okazaki and Engelhardt [39] reported the test results for a total of 37 links constructed from ASTM A992 steel. Although not very short, some of the specimens had very high ratios of the flange to web area (A_f/A_w). These specimens however did not exhibit overstrengths substantially higher than 1.5. On the contrary, other recent results by Ji et al. [22] indicated that very short links with even lower flange to web area ratios could achieve remarkably high overstrengths, in some cases even over 2.0. A further numerical investigation by Ji et al. [22] revealed that for the tested specimens the shear contribution of flanges could be as much as $0.2V_P$. However, it was concluded that other factors in addition to the flange effect are influential in causing the observed high overstrengths. Thus, it can be deduced that the numerical and experimental studies are inconclusive about the contribution of flanges to the link overstrength.

If axial restraints are present at the link ends, tension can develop during shearing, due to nonlinear geometric effects, especially at high rotation angles [48] (Figure 1.4). In 2012, this crucial issue was investigated by Della Corte et al. [10] using detailed FE analyses considering both geometric and material nonlinearities. Based on the numerical results it was concluded that the presence of axial restraints can significantly increase the overstrength (up to 15% increase was reported in some models) especially for short links. In a more recent study, Ji et al. [22] also mentioned that restraining axial deformations of very short links by adjacent members can create non-negligible axial forces in these links and affect their behavior significantly.

Another possible cause for the very high overstrengths observed in some tests is the excessive cyclic hardening of steel due to very large plastic strains. This idea was introduced recently by Ji et al. [22] on the basis of an experiment conducted by Kasai et al. [51] on stocky short steel panels in which hardening continued to very large

shear angles. Based on this observation, Ji et al. [22] proposed that the very high overstrengths reported for very short links are related to their high rotation capacities. These links experience large plastic rotations (substantially higher than 0.08 rad) and consequently their webs are subjected to excessive shear strains which may lead to excessive cyclic hardening. A refined FE analysis by Ji et al. [22] on very short links revealed that for a link plastic rotation of the order of 0.15 rad the cyclic hardening effect can increase the shear strength by about 70%.

The combined effect of the above-mentioned factors should be considered for each link in order to have a reasonable estimate of its overstrength. Nonetheless, reasons behind some of the unusually high overstrengths reported in the literature still remain unclear. For instance, Dusicka et al. [44] observed overstrengths of about 5.0 in their experiments on very short links constructed from low-yield-strength steel ($F_y = 100$ MPa) without web stiffeners. Such cases require further investigation.

Based on the numerical and experimental works of Berman and Bruneau [52-56] the use of built-up box (or tubular) links is also permitted by AISC 341-10 [11]. A comparison between the test results reported by Berman and Bruneau [56] with the numerical data presented by Richards [48] revealed that the overstrength factor of built-up box links is typically higher than that of I-shaped links, by about 11%. It is worth noting that the use of hollow structural sections (HSS) as links is prohibited by AISC 341-10 [11] due to their questionable performance in terms of low cycle fatigue life under large strains [57]. In addition, as explained in Berman and Bruneau [54], the longest shear link that can be constructed from a common HSS is about 460 mm, which is rather short and will cause congested details as well as very high rotation demands at the code-specified drift level.

2.2.2 Link Rotation Demand and Capacity

The expected plastic mechanisms of EBF systems are depicted in Figure 2.1. The angle between the link and the beam outside of the link is termed as the total link

rotation angle (γ) and its inelastic part as the inelastic (or plastic) link rotation angle (γ_p). In general, the inelastic rotation capacity of a link, γ_p^{max} , is defined as the maximum inelastic rotation angle (i.e. excluding the elastic portion which is usually less than 0.01 rad) sustained by the link during a cyclic test, for at least one full cycle of loading, before the shear resisted by the link drops below a predefined limit. This limit can be quantified as 80% of the maximum link shear recorded during the cyclic test ($0.8V_{max}$), the plastic shear capacity (V_p), or the code-specified nominal shear strength of the link (V_n) [22, 38, 49, 58]. Figure 2.5 shows an example of using the first definition for determining the inelastic rotation capacity (γ_p^{max}) of a specimen tested by Okazaki et al. [37].

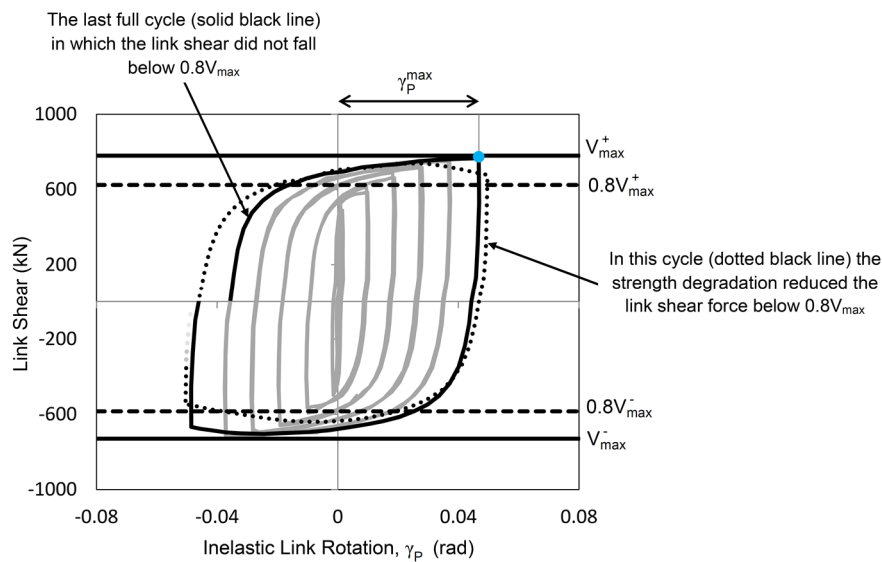


Figure 2.5. Inelastic link rotation capacity for a link specimen

Experimental studies have shown that the rotation capacity of links depends significantly upon several factors such as the link length ratio, loading history, compactness and web stiffening. A summary of findings from the experimental studies on horizontal I-shaped links [14, 19, 22, 23, 26-47] is given in Figure 2.6. The figure includes links with $F_y > 200$ MPa subjected to various cyclic loading histories. It should be mentioned that a few monotonic tests were also conducted on links [23, 26, 35, 36, 45, 59] which demonstrated rotation capacities between 0.19 ~

0.42 rad. Short links exhibit higher rotation capacities compared to intermediate and long links. As shown in Figure 2.6, AISC 341-10 [11] limits the inelastic rotation of short links to 0.08 rad and long links to 0.02 rad. For intermediate links, linear interpolation is utilized. The following issues should be borne in mind when examining the data shown in Figure 2.6. In a number of tests in which connection yielding or failure was reported (grey triangles in the figure), specifically those located in the range of $1 < \rho < 2$, high rotation capacities in excess of 0.10 rad were observed. It should be noted that in most of these tests the connection inelastic rotation also contributed to the total link rotation, and thus, the reported high γ_P^{max} values are not solely because of the inelastic action of the link. The results denoted by hollow circles indicate tests conducted by Galvez [33] and Ryu [36] and reported by Okazaki and Engelhardt [39], in which the observed rotation capacities fall significantly below the code-specified limit due to the use of a severe loading protocol. On the other hand, most of the γ_P^{max} values reported for very short links (i.e. $\rho < 1$) exceed the AISC limit by a wide margin. These results (particularly the ones reported in [22, 44]) revealed that the rotation capacity of very short links can be substantially higher than that of short links. Note that some of the tested very short links (shown by hollow diamonds) failed prematurely due to the brittle fracture of the link web, which was initiated as a result of the insufficient offset between the stiffener-to-web and the web-to-flange welds, as explained by McDaniel et al. [32]. Considering only the proper test data (grey diamonds in Figure 2.6), it can be deduced that the current AISC requirements provide a reasonable lower-bound for the inelastic rotation capacity of links with various length ratios.

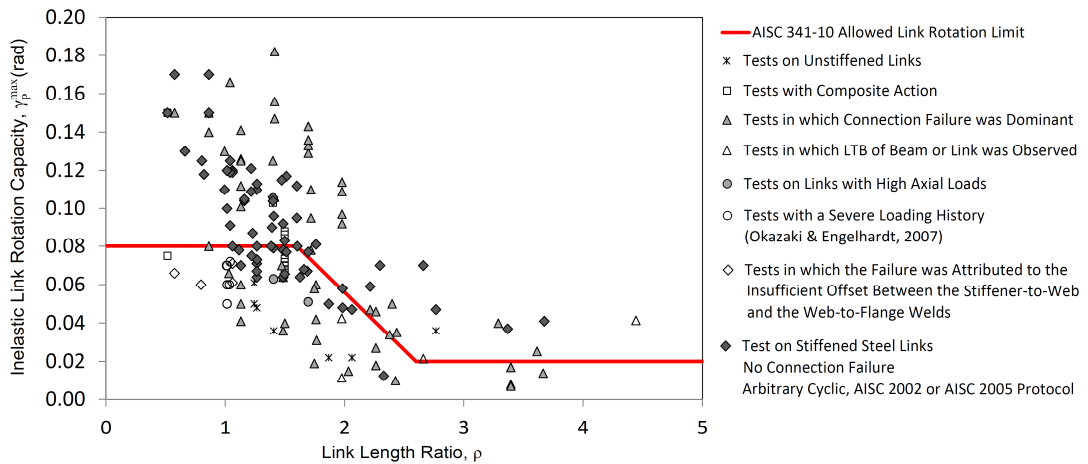


Figure 2.6. Inelastic link rotation capacities reported in experimental studies

It is difficult to predict the rotation capacity of all links by means of pure numerical simulation. For the case of long and some intermediate links, in which strength degradation is due to local buckling, γ_p^{max} can be estimated reasonably via nonlinear FE analysis. However, it is troublesome to estimate the rotation capacity of shorter links since strength degradation is generally due to low-cycle fatigue induced fractures, which are not commonly considered in FE simulations. Nonetheless, results of the numerical simulations [21, 58, 60-62] concurred with experimental observations that the inelastic rotation capacity of short links is considerably higher than that of intermediate and long links.

The inelastic link rotation demand must be estimated at the design stage. The most accurate way of determining this quantity is through inelastic dynamic analysis. Alternatively, a rigid plastic mechanism can be used to estimate the inelastic link rotation angle. In this method the inelastic link rotation angle, γ_p , is related to the plastic story drift, Δ_p , via geometrical relationships [11]. Extensive nonlinear time-history analyses conducted by Koboevic et al. [63, 64] on low-, mid-, and high-rise EBFs further confirmed the appropriateness of assuming such a relationship. However, it was noted by Koboevic et al. [63, 64] and other recent studies [65-67] that determining Δ_p based on the results of an elastic analysis using the codified

displacement amplification factors (C_d) or the equal-displacement rule may provide unconservative estimates of γ_p . This item is further discussed in Section 2.5.2.

2.2.3 Effect of Axial Force

Links can be subjected to axial loads due to the axial restraining effect of adjacent members (which was discussed in Section 2.2.1) and also the loading scheme and/or geometry of a structural system. For instance, in case of a seismic loading, the EBF configuration shown in Figure 2.1b will impose higher axial forces on link segments compared to the negligible link axial forces developed in the configuration shown in Figure 2.1a. A study by Kasai and Popov [18] revealed that the presence of axial force can have deteriorative effects on link behavior. These researchers proposed modified expressions for the plastic moment and shear capacities of links in the presence of axial force. In addition, a modified shear link length limit was defined. The modified capacities are in general related to the axial load ratio, defined by P/P_y , where P is the available axial force and P_y is the nominal axial yield strength. This study revealed that the plastic capacities should be reduced as a function of P/P_y when this ratio exceeds 0.15. These recommendations still form the basis of the AISC 341-10 [11] provisions for links under axial loads.

In 1990, Ghobarah and Ramadan [68] used nonlinear FE analysis to investigate the effect of axial force on the performance of EBF links. Numerical results demonstrated that the presence of axial force not only reduces the link plastic strength but also its plastic rotation capacity and energy dissipation. A maximum decrease of 37% in γ_p^{max} was reported. It was also noted that the effect of axial force is most pronounced in links with length ratios near 1.6.

In a study by Mansour et al. [49] in 2011, the behavior of replaceable shear links was investigated inside a frame system. In these tests the cyclic loading was applied to the floor beam from one end, and thus, half of the applied load was transferred axially through the link. The maximum value of P/P_y was reported to be 0.26 which

represented a relatively high axial force level. Mansour et al. [49] observed that the links experienced higher peak shear forces when subjected to tension rather than compression, with a maximum difference of 12%. Mansour [42] also demonstrated this issue numerically in his dissertation and proposed a simple equation for estimating the increase in the shear capacity due to axial tension.

In 2014, Dastmalchi [69] conducted nonlinear time-history analyses on a three-story prototype structure with eccentric braces, similar to the configuration shown in Figure 2.1b. Results revealed that the peak value of P/P_y recorded for the links exceeded 0.15 by a wide margin under most earthquake records, indicating the high probability of developing large axial forces in shear links with the selected configuration. Dastmalchi [69] also performed nonlinear FE analyses to examine the behavior of shear links under very high levels of axial force ($0.15 < P/P_y < 0.5$). The monotonic and cyclic shearing of short links under constant axial compression confirmed its detrimental effect on the shear strength and ductility of short links, especially when the length of the shear link was increased. It was also found that the shear capacity formula given in AISC 341-10 [11] underestimates this effect for $P/P_y > 0.2$, and therefore, a numerically calibrated modification factor was introduced for this formula.

It is worth noting that, as stated in the AISC 341-10 [11] commentary, the effect of high axial force on the behavior of long and intermediate links has not been investigated adequately. Therefore, the specification requires the use of shear links if high axial force is present in a link [11].

2.2.4 Effect of Concrete Slab

In 1989, Ricles and Popov [70] conducted research on the effect of a concrete slab, placed over the steel framing as a floor system, on EBF links. These researchers reported that the initial stiffness and strength of the composite links were higher than those of the steel links, however, the composite action deteriorated in later cycles.

The maximum shear forces resisted by the composite links were 1 to 13% higher than the corresponding steel links. Nevertheless, the general hysteretic behavior of the composite links resembled that of the bare steel links. The slab damage was localized in the vicinity of the link and no damage was observed in the concrete located away from the link segment. The test results also demonstrated that a concrete slab alone cannot provide sufficient lateral bracing for links. Engelhardt and Popov [19, 71] noted in their experimental study that if a diagonal brace is connected to the bottom flange of a link, the presence of a concrete slab can substantially enhance the stability of the link by restraining the top flange. A similar observation was also reported by Tsai et al. [72] during the tests on large EBF sub-assemblages conducted at the National Taiwan University in the early 1990s.

Mansour et al. [49] also investigated the effect of a concrete slab on link behavior. In the details studied, the replaceable link segment had a smaller depth than the floor beam. Therefore, there was no direct interaction between the link and the composite slab. Nevertheless, it was reported that the specimen with the concrete slab sustained a higher shear force, 14% more when compared to the bare steel specimen, without a notable change in the link rotation capacity. Mansour et al. [49] recommended using more shear studs away from the link region in order to guarantee the slab diaphragm action during major earthquakes.

Recently, Ciutina et al. [45] tested a single-story EBF setup with very short links with and without a concrete slab. In one case the shear studs were placed along the entire beam length, while in the other case they were suppressed in the link region. Tests by Ciutina et al. [45] confirmed that omitting shear studs only in the link region does not fully eliminate the composite action, since in both of the above cases the shear strength and stiffness were notably higher than those of the steel link. Therefore, it was recommended that the composite action be considered during the EBF design, even if shear studs are only available on the floor beams and not in the link regions. It is worth noting that link regions are protected zones per AISC 341-10 [11] in which the use of shear studs is prohibited. In addition to link behavior, the

presence of a concrete slab also affects the structural response of EBF systems, which is discussed further in Section 2.5.2.

2.2.5 Effect of Loading History

Popov and his colleagues (e.g. [14, 26]) noticed that the applied loading history (or protocol) during an experimental study has a major effect on the observed plastic rotation capacity of EBF links. A comprehensive study on this effect was, however, conducted recently by Richards and Uang [73, 74].

Okazaki et al. [37] reported unexpected link web fractures for a number of tested short links prior to reaching the code-specified 0.08 rad rotation limit. Richards and Uang [73, 74] attributed this issue mainly to the utilized loading history and stated that the loading protocol used by Okazaki et al. [37] (based on Appendix S of AISC 341-02 [75]) was significantly more severe than the loading sequences used in the 1980s tests on short links. Nonlinear time-history analyses were conducted by Richards and Uang [73, 74] on three prototype EBF structures subjected to 20 large-magnitude-small-distance Los Angeles ground motions. The obtained cumulative rotation demands were used to come up with a new protocol which was adopted by AISC 341-05 [76] for the cyclic testing of link-to-column connections. The proposed protocol has fewer cycles with large rotations compared to the old protocol.

Okazaki et al. [37] retested the specimens which failed to reach the code-specified plastic rotation limit under the AISC 341-02 [75] old protocol using the new (revised) loading protocol. All of the newly tested specimens exhibited rotation capacities higher than the code-specified limit, with an average increase of 52% in γ_P^{max} . Further studies by Okazaki and his colleagues [39, 41] also confirmed the conclusion that the old protocol is overly demanding compared to the revised protocol for shear links. It is worth noting that other loading protocols, for instance, random loading protocols, loading protocols available in specifications other than the U.S. standards, or more severe loading histories than the AISC 341-02 [75] old

protocol have also been used in some studies (e.g. [22, 39]) to demonstrate the sensitivity of the rotation capacity of shear links to the applied loading sequences.

As explained by Richards [48], if the revised protocol is used for testing intermediate or long links, a modest increase in γ_P^{max} for intermediate links and a modest decrease in γ_P^{max} for long links might be observed. Okazaki et al. [41] also noted that the cyclic demand imposed on flexural links by both protocols is somewhat similar. The revised protocol was used in a number of experimental and numerical studies on intermediate and long links (e.g. [21, 39, 77]). Daneshmand and Hashemi [21] demonstrated the sensitivity of the rotation capacity of intermediate links to the employed loading protocol. The value of γ_P^{max} obtained via nonlinear FE analysis for an intermediate link reduced by 18% when the link was loaded based on the old protocol instead of the revised protocol.

2.3 Detailing of Links

2.3.1 Flange and Web Compactness

The link flange slenderness limit is needed to prevent severe strength degradation due to flange local buckling during intense loadings. Kasai and Popov [18] calculated the link flange stress at the ultimate shear of $1.5V_P$ and its associated moment for 156 links with four different yield stresses and two length ratios, $\rho = 1.6$ (short) and $\rho = 2$ (intermediate), with and without axial force. The obtained maximum flange stresses were compared to a conservative critical plastic buckling stress determined based on Haaijer's method [78]. Kasai and Popov [18] did not detect flange buckling for the links with $\rho = 1.6$ with no axial force when the flange slenderness (i.e. $b_f/2t_f$) was limited to $0.38\sqrt{E/F_y}$, where b_f and t_f are the flange width and thickness respectively and E is the elastic modulus of the steel material. However, if these links were subjected to axial force, the stringent flange slenderness limit of $0.3\sqrt{E/F_y}$ was suggested to prevent flange buckling. On the other hand, some of the intermediate

links with $\rho = 2$, especially if subjected to axial force, were prone to flange buckling even if the flange slenderness was kept below the more stringent limit of $0.3\sqrt{E/F_y}$. Based on these, it was recommended to limit the flange slenderness of links to $0.3\sqrt{E/F_y}$. This limit was adopted by the early EBF specifications [20, 79, 80] and was in use prior to the 2005 edition of AISC 341 [76].

Adhering to the flange slenderness limit of $0.3\sqrt{E/F_y}$ disqualified several efficient wide-flange rolled sections constructed from A992 steel from being used as links. A992 steel has become the most widely used steel material in the U.S. and has replaced A36 steel after the 1994 Northridge earthquake [58]. Using heavier sections to satisfy this requirement would be the common approach in practice, but this is not fruitful from the capacity design point of view. Richards and Uang [58] conducted a comprehensive numerical study to further investigate this issue. After verifying the FE modeling procedure using the experimental data reported by Arce [31], a total of 112 isolated I-shaped link models were analyzed considering different flange slenderness values. The numerical results demonstrated that the flange slenderness limit can be relaxed from $0.3\sqrt{E/F_y}$ to $0.38\sqrt{E/F_y}$. Although some of the intermediate links could not achieve the code-specified rotation limit, this issue was related to the stiffener requirements and not the flange slenderness limit [58]. In addition to the numerical investigation of Richards and Uang [58], subsequent experimental studies by Okazaki and his colleagues [37, 39] on wide-flange links constructed from A992 steel confirmed that the above relaxation can be safely applied to short links. However, Okazaki et al. [37, 39] observed strength degradation due to flange buckling in some of the intermediate link specimens. Taking into account previous studies [18, 37, 39, 58] it was permitted as per AISC 341-05 [76] to use moderately ductile flanges for I-shaped links with the slenderness limit of $0.38\sqrt{E/F_y}$ only in short links ($\rho < 1.6$). It should be noted that in the numerical study of Richards and Uang [58] and also the recent tests of Okazaki and his colleagues [37, 39] no axial force was imposed on the links. Nevertheless, the above relaxation in the flange

slenderness requirements includes all shear yielding links regardless of the level of axial force.

Based on the results obtained from an exhaustive numerical parametric study containing more than 200 analyses as well as a subsequent experimental study, Berman and Bruneau [55, 56] concluded that the flange slenderness of built-up box links should be limited to $0.64\sqrt{E/F_y}$. Until 2005, this limit was the seismically compact limit for walls of rectangular HSS members as per AISC 341 [76]. However, in 2010 the more stringent limit of $0.55\sqrt{E/F_y}$ was adopted by AISC 341-10 [11] for flanges of highly ductile built-up box sections, which is the case for tubular links.

In general, compact webs are used in links to prevent or delay the deteriorative effect of web buckling [11]. Berman and Bruneau [55, 56] suggested that the web slenderness for built-up box shear links should be limited to $1.67\sqrt{E/F_y}$. However, this limit was reduced to $0.64\sqrt{E/F_y}$ for intermediate and long built-up box links in which local buckling of both webs and flanges can cause strength degradation [55, 56].

2.3.2 Web Stiffeners

The proper detailing of end and intermediate web stiffeners in links is a major parameter for achieving stable and controlled hysteresis behavior. End stiffeners are usually full-depth stiffeners provided for all link length ratios located on both sides of the web at link ends. In 1977, Roeder and Popov [12] provided the rationale for the necessity of using end stiffeners to ensure local stability at a brace-link-beam connection panel. In the previous and current EBF specifications (e.g. [20, 79-81]) the use of end stiffeners has always been mandatory with an aim of improving the link shear force transfer to reacting elements as well as preventing premature local buckling in links.

In the early experiments by Popov and his colleagues (e.g. [14, 82]) it was observed that in short links tearing of web and severe strength degradation usually occurred shortly after web buckling. Although in some tests (e.g. [14]) a considerable amount of energy was also dissipated by the link in the post-buckling phase, since post-buckling behavior and its subsequent failure are difficult to predict and more hazardous, web buckling is generally considered as the design ultimate state for short links [14, 15, 82]. Popov and his colleagues [14, 26, 82] demonstrated that providing intermediate stiffeners could substantially improve the strength and energy dissipation capacity of links. In 1983, Hjelmstad and Popov [15] proposed the first relation for determining the required intermediate stiffener spacing based on the expected energy dissipation of a link. However, later tests by Kasai and Popov [18] demonstrated that such a relation does not exist and instead, the required intermediate stiffener spacing is dependent upon the expected ultimate link rotation, γ_u . In 1986, Kasai and Popov [82] proposed a conservative spacing formula for intermediate stiffeners using a cyclic plastic theory and the experimental data obtained from tests [23] on short links constructed from A36 steel. The stiffener spacing was expressed as a function of the depth of the I-shaped link and its web thickness for three different ultimate rotations. The maximum spacing allowed for the intermediate stiffeners of short links per AISC 341-10 [11] is based on this proposal with slight modifications. It is worth noting that a number of recent studies [39, 42] have mentioned that the shear link stiffener spacing requirements of the AISC Seismic Provisions [11] are somewhat conservative and might be relaxed if justified by further experimental research.

Malley and Popov [17] investigated the required area and moment of inertia of link intermediate stiffeners using Basler's theory for plate girders [83] and the approach adopted by Bleich [84]. The requirements proposed by Malley and Popov [17] were not included in AISC 341 [11, 75, 76], and instead, the regular requirements of plate girder web stiffeners were recommended for determining the required moment of inertia of link stiffeners with the addition of a minimum thickness limit. Bruneau et al. [57] further discussed this issue and mentioned that the previous reasonable

performances of EBFs designed as per AISC 341 [11, 75, 76] indicate that the recommendations of Malley and Popov [17] were based on overly conservative assumptions.

Intermediate stiffeners are also required in links with flexure-dominant behavior. The comprehensive experimental study by Engelhardt and Popov [19, 71] on long links revealed that, unlike shear links, local buckling of flanges will not necessarily cause strength degradation in stiffened long links. It was concluded that placing stiffeners at a distance of $1.5b_f$ from each end of the link, while not preventing flange buckling, would limit the strength loss due to flange buckling [71]. The large scale pseudo-dynamic tests by Tsai et al. [72] indicated that such stiffeners may still be beneficial if substantial axial force is also available in the link. Engelhardt and Popov [71] also mentioned the beneficial effect of placing stiffeners outside the link region, in the brace-link-beam connection panel. Furthermore, it was concluded that intermediate links, which will experience both shear and flexural yielding, should have intermediate stiffeners at $1.5b_f$ from the link ends, and also equally spaced additional stiffeners through the link length based on the requirements of short links. These recommendations have generally been adopted by AISC 341-10 [11]. However, the provisions require no intermediate stiffeners when the link length ratio (ρ) is larger than 5.0.

Previous and recent experimental studies [17, 18, 37, 71] have demonstrated that, unlike end stiffeners, intermediate stiffeners can also be one-sided in links with various lengths. The numerical study of Daneshmand and Hashemi [21] revealed that using one-sided stiffeners can reduce the rotation capacity of intermediate and long links, however, this reduction rarely decreases γ_p^{max} below the code-specified rotation capacity. Furthermore, the reduction was reported to be more pronounced for links in the range of $1.8 < \rho < 2.2$. Nevertheless, AISC 341-10 [11] permits the use of one-sided intermediate stiffeners for links with a depth of less than 635 mm. Malley and Popov [17] demonstrated that partial depth intermediate stiffeners can also be used in shear links, provided that a concrete slab properly restrains the top

flange. However, as required by AISC 341-10 [11], it is more advisable to use full-depth intermediate stiffeners welded to the web and both flanges since these stiffeners can enhance the stability of the link against flange local buckling as well as against lateral torsional buckling [5, 15, 71]. A summary of AISC 341-10 [11] link web stiffening requirements is presented in Figure 2.7.

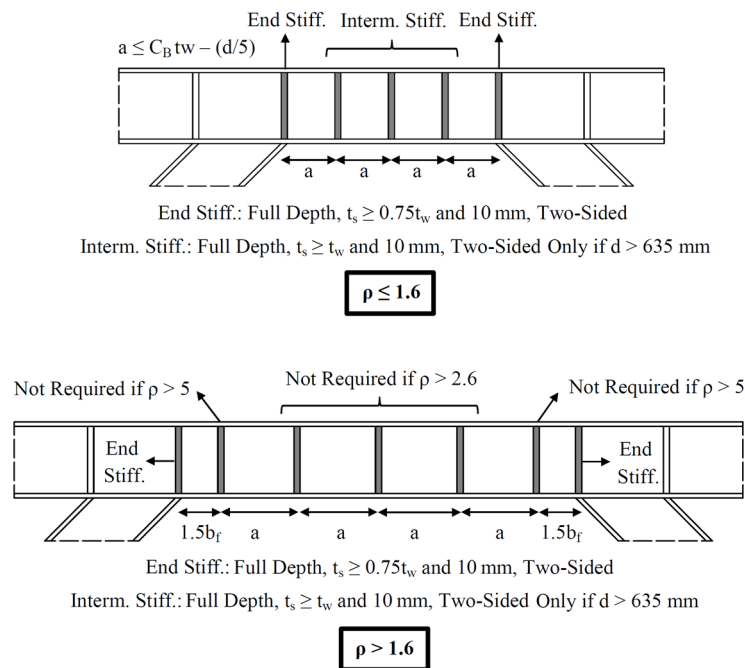


Figure 2.7. AISC 341-10 [11] link web stiffening requirements

Recent tests and the probabilistic analysis of Bulic et al. [59] suggested the use of at least two couples of properly designed web stiffeners in short I-shaped links to achieve enough reliability according to Eurocode 0 [85] for the mean recurrence interval of 50 years.

Richards and Uang [58] noticed during their numerical study that some of the intermediate links failed to achieve the rotation capacity predicted by the provisions, with a maximum difference of 11%. Similar observations were also reported by Arce [31]. Richards and Uang [58] attributed the issue to the intermediate stiffener spacing

requirements of the AISC Seismic Provisions [11]. As stated earlier, Kasai and Popov [82] proposed their stiffener spacing formula for short links; however, the provisions extended its use to intermediate links, without accounting for the significant moment-shear interaction that is present in the web panels of these links. Thus, it was concluded by Richards and Uang [58] that the direct use of stiffener spacing requirements of short links may be unconservative for intermediate links.

During a series of tests [31, 33, 34, 36] from 2002 to 2005 on A992 links, conducted at the University of Texas at Austin, another important issue was observed. Most of the specimens with $\rho < 1.7$ exhibited web fractures at the ends of the stiffener-to-web welds prior to any notable web buckling (Figure 2.3a). This was not consistent with the failure modes observed in the early studies of Popov and his colleagues (e.g. [14, 23, 26]) where web fracture occurred only after severe web buckling at locations of large deformations. The pre-buckling web fracture had also been reported previously by McDaniel et al. [32] during tests on large built-up links where it was attributed to the insufficient offset between the stiffener-to-web and the web-to-flange welds. It is also worth noting that in a number of more recent tests this type of failure mode has also been reported [22, 49]. Based on the test results, Okazaki and his colleagues [37, 39] have concluded that altering the applied loading history or the utilized stiffener detailing cannot change the link failure type from the web fracture mode. The test results however revealed that it is fruitful to terminate the stiffener-to-web weld at a distance not less than $5t_w$ from the k-line of the link section. A clear correlation between the reduced material toughness in the k-area and the occurrence of link web fracture was not established [39]. In addition to the above findings, a new stiffener detailing was also reported by Okazaki and Engelhardt [39] which can delay web fracture and provide enhanced cyclic performance. This detail consists of two-sided intermediate stiffeners which are welded only to the flanges that restrain the web by sandwiching it (Figure 2.8a). Additional research regarding this detail was deemed necessary by Okazaki and Engelhardt [39].

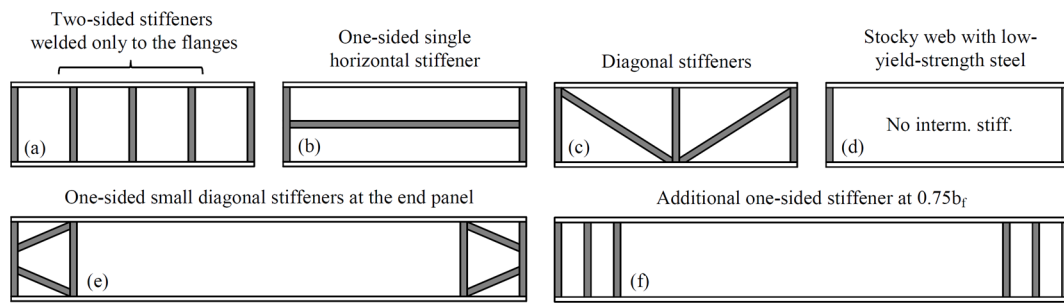


Figure 2.8. New web stiffening schemes for short (a-d) and long (e-f) links

In order to further investigate the cause of the recently observed pre-buckling web fracture failures, Chao et al. [86] conducted a detailed numerical study. Numerical results suggested that the web fractures are due to the high triaxial constraints that develop at the ends of the stiffener-to-web weld and the localized high plastic strains at these locations. Beneficial effects of welding stiffeners to both flanges, using two-sided intermediate stiffeners and avoiding large stiffener spacing were also mentioned. Similar observations were also reported in previous experimental studies [33, 39]. Chao et al. [86] also proposed a possible reason for the observed web fractures in the recent tests as opposed to the 1980s experiments. The new straightening process for structural shapes causes higher strength and reduced toughness in the k-area, along the full length of the rolled sections, unlike the old method which induced localized changes in the material properties due to work hardening. As explained by Chao et al. [86], the higher k-area strength in the new shapes prevents yielding in this region, and consequently, high plastic strains are developed in the adjacent web steel. These localized strains coupled with high stress triaxiality at the stiffener-to-web weld ends increase the possibility of ductile fracture initiation at the weld ends. Based on the numerical results, Chao et al. [86] proposed a single horizontal stiffener (Figure 2.8b) instead of multiple vertical stiffeners for short links and demonstrated its promising performance numerically. The sandwich stiffener detail (Figure 2.8a) proposed by Okazaki and Engelhardt [39] also performed well during the simulations [86].

Dusicka et al. [44] conducted experiments on isolated very short built-up I-shaped links with a different stiffener detailing in which the link web was constructed from low-yield-strength steel (with F_y of 100 MPa or 225 MPa) without any stiffeners (Figure 2.8d). The test results revealed that, unstiffened links with stocky webs constructed from low-yield-strength steel can sustain extremely high cyclic rotation angles, of the order of 0.2 rad. As a result of such detailing, the failure mode was altered from that controlled by fracture at the ends of the stiffener-to-web weld to web tearing at the link end corners accompanied by web out-of-plane deformations in some cases. Bahrampoor and Sabouri-Ghomi [87] also studied the effect of using very low-yield-strength steel with $F_y = 90$ MPa in EBF links. Comparison between the results of one-story one-bay FE models with links constructed from regular and low strength steels revealed that the energy dissipation characteristics of links can be enhanced using unstiffened stocky webs constructed from very low-yield-strength steel.

The use of diagonal web stiffeners for shear links (Figure 2.8c) was studied both experimentally and numerically by Yurisman et al. [88]. Based on the results reported by these researchers it appears that the diagonal web stiffeners may provide an alternative to the commonly used vertical stiffener arrangement for short links; however, further research is essential. Chegeni and Mohebkhah [77] proposed new stiffener details for improvement of the rotation capacity of long links. Two details were suggested: placing an additional one-sided stiffener at a distance of $0.75b_f$ from the link ends (Figure 2.8f); and using small one-sided diagonal stiffeners between the end stiffener and the intermediate stiffener in long links (Figure 2.8e). Results of the parametric study indicated that the latter detail is more effective in improving the rotation capacity and energy dissipation of long links. However, further experiments for validating the suggested details were deemed necessary [77].

Ohsaki and Nakajima [89] investigated the optimization of stiffeners in I-shaped EBF links. These researchers used the heuristic Tabu Search algorithm for optimizing the locations and thicknesses of link stiffeners.

Stiffener requirements for built-up box links were studied by Berman and Bruneau [52-56]. The use of end stiffeners for built-up box links was recommended similar to I-shaped links. However, results reported by Berman and Bruneau [55, 56] revealed that intermediate stiffeners are only required for shear links ($\rho \leq 1.6$) in which the web depth-to-thickness (h/t_w) ratio is greater than or equal to $0.64\sqrt{E/F_y}$. For shear links with lower h/t_w ratios, flange buckling is the controlling failure mode, for which the presence of intermediate stiffeners is not effective. Berman and Bruneau [55, 56] also demonstrated that intermediate stiffeners are not beneficial in intermediate and long links where compressive local buckling of both webs and flanges controls the link performance. The required intermediate stiffener spacing for shear links with $h/t_w \geq 0.64\sqrt{E/F_y}$ has been determined by Berman and Bruneau [52] using a methodology similar to that used by Kasai and Popov [82] for I-shaped links.

In the numerical and experimental investigations of Berman and Bruneau [55, 56] external stiffeners welded to webs and flanges were considered. However, as stated above, these stiffeners are not effective in controlling flange buckling. Thus, stiffeners welded to outsides of the link webs or located inside the box section and welded to the insides of the webs can be considered in practical applications.

During the 2011 earthquakes in Christchurch, New Zealand, the first documented field fractures of EBF short links were recorded at the Christchurch hospital garage [7]. In some of the fractured links, unlike the correct detailing, the end stiffeners were not aligned with the brace flanges. This misalignment was speculated to be a probable reason for the observed fractures in the link flange and connection panel. Kanvinde et al. [7] performed in-depth numerical analyses to investigate the issue. Numerical results revealed that the misalignment had an influential effect in triggering the fractures; however, other factors, such as the imposed ground acceleration which was several times higher than the expected design value, also played a major role. The use of field-welded stiffeners and gusset plates for brace connections was suggested by Kanvinde et al. [7] for better fit-up. Another recent

study by Imani and Bruneau [90] further confirmed that the severe stress concentration in the vicinity of the misalignment can initiate fracture and reduce the link rotation capacity significantly. The numerical results also demonstrated that correcting the misalignment by using a different brace section or, more conveniently, by relocating the end stiffeners can mitigate the problem [90].

2.3.3 Lateral Bracing

Lateral torsional buckling (LTB) can have deteriorative effects on the cyclic performance of links. The lateral bracing requirements are intended to restrain the link against out-of-plane displacement and twist to ensure stable inelastic response [11]. Although lateral bracing was provided in earlier tests [12], the importance of proper link lateral bracing was fully understood during the tests of Manheim [91] on three-story prototypes in 1982, where LTB occurred in some test specimens. As a result, lateral bracing of link ends was suggested by Manheim [91] with moment connections between the lateral braces and the link ends to increase the torsional stiffness of the link. In 1989, Hjelmstad and Lee [92] conducted a study to investigate the lateral buckling of beams in EBFs. Based on the experimental results of five tests on propped cantilever beams with different lateral bracing schemes at the link ends and a numerical parametric study, Hjelmstad and Lee [92] concluded that providing full rotational restraints at the link ends is essential. Furthermore, it was noted by these researchers that the forces imposed on the lateral braces were much higher than the traditionally used design load of 2% of the flange yield force, P_y^{flange} . During the experimental study of Engelhardt and Popov [19, 71] on long links, strength degradation due to LTB of the link or the beam outside the link was reported for some specimens. These observations further emphasized the importance of providing strong and stiff lateral bracing at link ends. Similar to Hjelmstad and Lee [92], Engelhardt and Popov [19, 71, 93] also mentioned that the demand on link lateral braces is several times higher than the minimum load of 1.5% of P_y^{flange} , considered in the 1980s design codes [20, 79]. A minimum load of 6% of P_y^{flange} was

suggested by these researchers for the design of lateral braces of short and long links. Furthermore, it was recommended that the lateral braces should frame into the link ends from only one side in order to prevent imposing excessive in-plane restraint to the link [19].

Based on the above research, the use of lateral braces at the link ends was required by the early EBF codes [20, 79, 80]. Similarly, AISC 341-10 [11] requires lateral bracing of both top and bottom flanges of I-shaped links at the link ends. The concrete slab may only provide restraint to the top flange [70, 71] and thus, explicit bracing of link ends is generally necessary.

The main advantage of built-up box links compared to I-shaped links is their significant resistance to LTB. Berman and Bruneau [54] demonstrated that lateral bracing at link ends is not necessary for typical built-up box links. This can be fruitful in cases where providing lateral bracing for links is not possible or not desired. For instance, lateral bracing of links adjacent to elevator cores or links used in bridge piers is generally cumbersome. Consequently, built-up box links are also referred to as self-stabilizing links [53].

2.3.4 Connections

In EBF systems, brace-to-beam and link-to-column connections attracted particular research attention due to the high level of demands on these joints. Gusset plate buckling at the brace-to-beam connection was observed in the full-scale tests of Roeder et al. [94] and Foutch [95]. Engelhardt and Popov [19, 71] proposed and tested modified gusseted and directly welded brace-to-beam connections. Satisfactory results were reported for all of the proposed connection details; however, the directly welded connections were found to be more advantageous in controlling LTB of the beam segment outside the link. Considering that the braces are expected to remain essentially elastic during severe loadings, most of the ductility

requirements which are required for braces of special CBFs are not mandatory for EBF braces and their connections, based on the AISC Seismic Provisions [11].

Tests by Hjelmstad and Popov [14, 15], and Malley and Popov [17, 26] in the 1980s suggested that fully welded link-to-column connections can exhibit satisfactory behavior during severe loading scenarios. In these tests, short links with different combinations of complete joint penetration (CJP) groove welds and fillet welds for the flanges and the web were considered. In contrast, details with welded flanges and bolted web connections tested by Malley and Popov [17, 26] showed significant bolt slippage which led to premature flange fractures.

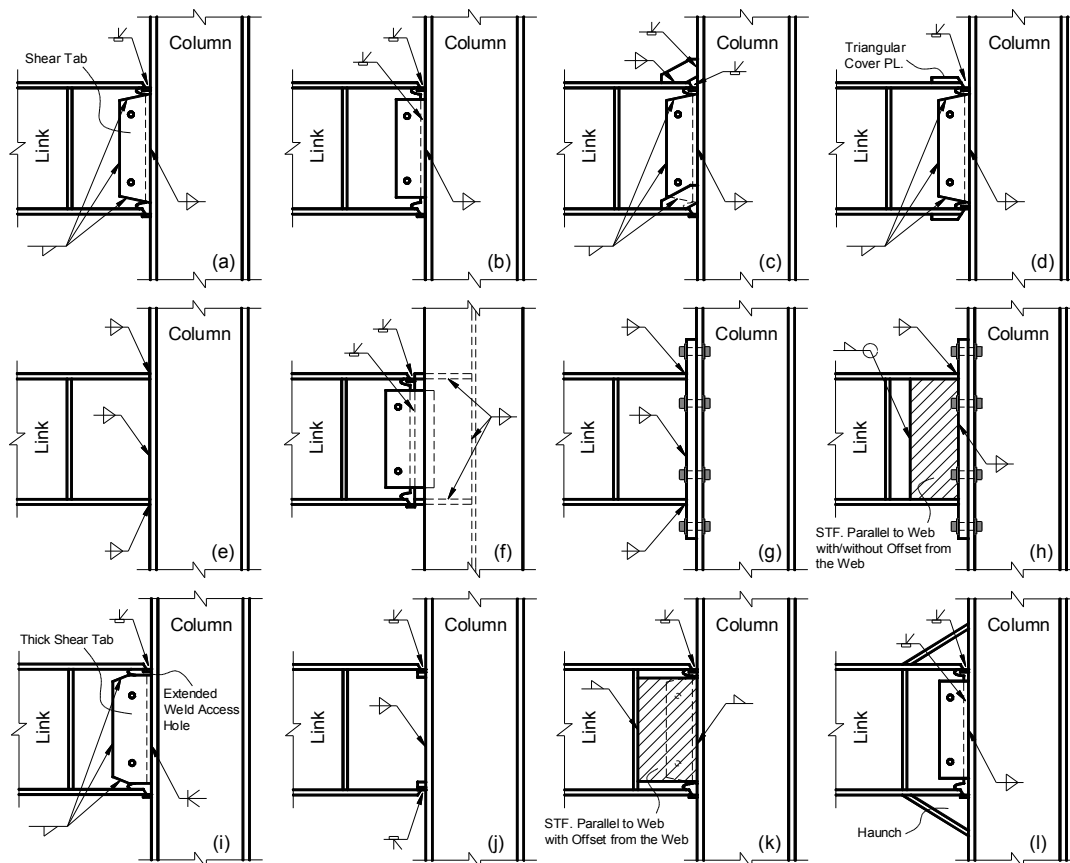


Figure 2.9. EBF link-to-column connections

Engelhardt and Popov [19, 71] investigated the behavior of link-to-column connections for the case of long links. Details employing CJP groove welds at the flanges and either a fully welded shear tab or a CJP groove weld at the link web (Figure 2.9a and b) were considered owing to their acceptable performances in previous tests on short links (e.g. [15, 17]). Premature link flange fracture was observed for these specimens at early stages of loading, and thus, modified details (e.g. Figure 2.9c and d) were proposed and tested by these researchers. Furthermore, a link-to-column connection with all-around fillet welds (Figure 2.9e) was also studied. Although some of the modified details sustained high rotations prior to failure (especially the cover plate (Figure 2.9d) and the all-around fillet weld (Figure 2.9e) details) due to the doubtful performance of the tested specimens as well as the observed brittle failure modes, it was concluded that the use of long links attached to a column should be avoided. Engelhardt and Popov [19, 71] also tested two short links which were connected to the web of an I-shaped column through continuity plates (Figure 2.9f). A similar detail was previously studied by Malley and Popov [17, 26] and acceptable results were reported with minor flaws compared to the link-to-column-flange connections. However, the tests of Engelhardt and Popov [19, 71] revealed that the link-to-column-web connection is prone to premature link flange fracture and should be avoided. Based on these studies, the 1992 AISC Seismic Provisions [96] limited the use of link-to-column connections to short links, recommending details such as Figure 2.9a and b.

In the experiments of Tsai et al. [72] CJP groove welds at the flanges and fillet weld at the web were used to connect short links to box columns. Premature fractures at very low link rotations (sometimes less than 0.005 rad) were observed in the link flange welds. Although a number of modified details performed remarkably better, the observed fractures gave cause for concern.

Ghobarah and Ramadan [28, 97] proposed an extended end-plate link-to-column connection (Figure 2.9g) in 1994. In this approach the link is shop-welded to the end-plate using all-around fillet welds and the end-plate is then field-bolted to the column flange. Although some of the specimens exhibited bolt or flange weld fractures, it

was concluded that properly designed extended end-plate link-to-column connections would remain elastic during severe loadings and demonstrate a similar performance to that of a fully welded connection. In a recent study by Dusicka and Lewis [43] on end-plate link-to-column connections, different stiffening details were investigated to reduce the demand on link flanges in the vicinity of the link-to-end-plate welds, which was found to be a potential region for brittle failure [28, 39, 97]. These details included using an additional pair of stiffeners in the first web panel which were either parallel to the web and connected to the web or within a small distance from it (Figure 2.9h), or angled from the link end towards the web, or curved stiffeners made from round HSS. Promising results were reported based on FE analyses for the first detail with stiffeners parallel to the web which shifted the failure mode from the link flange fracture to fracturing of the web. The results were further confirmed through a number of experiments on long links. In 2016, Pirmoz et al. [98] numerically studied the behavior of extended end-plate link-to-column connections, with rib stiffeners, in contrast to the suggestion of Ghobarah and Ramadan [28, 97]. Although the study did not address issues such as low-cycle fatigue or material fracture, the promising performance of this link-to-column connection was demonstrated.

An experimental study was undertaken by Tsai et al. [99] on the behavior of link-to-box column connections in 2000. In these tests, short links were connected to box columns using CJP groove welds at the flanges and either a fully welded shear tab or a CJP groove weld at the link web. Although some of the specimens used the improved weld access hole detail suggested by Mao et al. [100], premature fracture was observed in all connections at the link flange in the vicinity of the groove weld. The urgent need for research on this issue was emphasized. Consequently, an extensive study was initiated at the University of Texas at Austin in the early 2000s [34]. These tests along with those performed previously at the National Taiwan University by Tsai et al. [72, 99] were the first experiments on large-scale link-to-column connections with realistic details. Okazaki et al. [38] tested 12 welded link-to-column specimens considering short, intermediate, and long links with four

different connection details using the old loading protocol of AISC 341-02 [75]. Pre-Northridge as well as other moment connections which adhered to the recommendations of FEMA 350 [101] were considered. Recently developed welded moment connections with free flange [102] (Figure 2.9i) and no access hole (Figure 2.9j) [103] details were also tested. Except for one specimen, all of the tested connections failed due to abrupt fracture of the flange near the groove weld prior to developing the required level of plastic rotation. The performance was inferior for the pre-Northridge and FEMA 350 [101] details which only developed about half of the required γ_p . Results proved that the connections which are suitable for MRFs may not necessarily perform well as link-to-column connections. It was concluded that link-to-column connections are prone to brittle failure regardless of the link length ratio and should therefore be avoided until a satisfactory detail is developed.

In a subsequent study, Okazaki et al. [41] tested an additional 12 welded link-to-column specimens to investigate the effect of loading history and to study other details such as the all-around fillet weld detail (Figure 2.9e) and a new reinforced detail (Figure 2.9k) referred to as the supplemental web doubler connection. The test results seemed inconclusive as regards the effect of the loading protocol. On the other hand, an excellent performance was reported for most of the specimens with the fillet welded and the newly proposed supplemental web doubler details. A summary of the experimental results for these two connections reported by Okazaki et al. [46] indicates their high potential for practical applications. Several design and welding details for the all-around fillet weld connection were also outlined by these researchers. A step-by-step design procedure for the supplemental web doubler connection was developed by Hong et al. [104] through a series of nonlinear FE analyses and substantiated by experiments [46].

Two numerical studies were conducted recently to propose alternatives for reducing the demand in critical regions of welded link-to-column connections, i.e. at the link flanges in the vicinity of groove welds. Prinz and Richards [105] studied reduced web section links while Berman et al. [106] investigated reduced flange section links.

The reduced web section links with perforated webs did not perform well in the simulations while the reduced flange section links were found to be a potential solution, pending testing required for further validation.

The AISC Seismic Provisions [11] do not require qualification testing for the link-to-column connection of a short link, provided that the connection is reinforced with haunches or other proper details which prevent yielding in the reinforced segment adjacent to the column (e.g. Figure 2.9f). Although this approach is found to be effective in MRF connections, no research is available at the time which proves the reliable performance of such a reinforced detail specifically in EBF link-to-column connections. The commentary on AISC 341-10 [11] mentions the promising performance of the supplemental web doubler detail proposed by Okazaki et al. [41]; however, it encourages designers to configure EBFs to avoid link-to-column connections entirely. The use of built-up box links in EBFs with link-to-column connections has not been studied explicitly nor addressed by the specifications.

2.4 Numerical Modeling of Links

General FE techniques which model links using shell or solid elements can reasonably simulate the behavior of these members under monotonic and cyclic loadings (e.g. [7, 10, 21, 55, 58, 60, 62, 68, 86, 90, 98, 104-108]), specifically if the strength degradation related with low-cycle fatigue-induced fractures does not need to be captured. However, due to the complexity and computational burden of these methods, they are not typically used for nonlinear time-history analysis, and instead, simplified approaches are utilized which model a link through a combination of line elements, nodal constraints, springs, or plastic hinges. Although the detailed description and evaluation of the latter are out of the scope of this thesis, a brief outline of each method is provided here for the sake of completeness.

In 1977, Roeder and Popov [12] proposed a sandwich beam model for links where shear was resisted by the web and moment (through uniaxial stresses) by the flanges

with bilinear responses. The method was intended to be used for modeling shear yielding links with small end moments. A very simple model was later proposed by Yang [109] in which the shear link behavior was simulated using a truss member with calibrated uniaxial strength. In 1983, a finite element model based on a stress resultant formulation was developed by Hjelmstad and Popov [14] which utilized a moment-shear yield surface. The method was not suitable for link modeling since strain hardening effects were not incorporated. A simplified approach was proposed in 1987 by Whittaker et al. [24] for short links where regular flexural elements with moment hinges were calibrated to exhibit moment capacities corresponding to the nominal shear strength of the link.

Ricles and Popov [110, 111] developed an approach in which a link was represented by a linear elastic beam with a nonlinear zero-length hinge at each end. Although the numerical results obtained using this approach were fairly accurate, the calibration and programming of the method was quite complex [112].

A modeling procedure was developed by Ramadan and Ghobarah [112] on the basis of the theory proposed by Ricles and Popov [110, 111]; however, with simpler end hinges and the ability to be conveniently incorporated into regular analysis programs. The model was calibrated using the results of experiments conducted at the University of California at Berkeley in the 1980s on links constructed from A36 steel (e.g. [14, 23, 27]). The accuracy of the method was demonstrated through a comparison with test results. In 2003, Richards and Uang [74] modified the link model proposed by Ramadan and Ghobarah [112] in order to improve its accuracy in predicting the behavior of links constructed from A992 steel. The proposed element was later used in an extensive parametric study [73, 74].

A simplified approach was recently used by Khandelwal et al. [113] in which the behavior of short links was simulated using a rectangular truss system with vertical rigid bars and elastic horizontal bars and a nonlinear diagonal spring.

A three element link model consisting of a central beam element and concentrated hinges at the ends was introduced by Rossi and Lombardo [114] in 2007 and

extensively used in the numerical studies of Bosco and her colleagues [115-118]. Although suitable for initial analysis, the model was not able to properly capture the cyclic response of links. For instance, non-zero stiffness values were provided by this model even at very large deformations [119]. To overcome these deficiencies, an enhanced model of this element was recently developed by Bosco et al. [119] in which the responses of flexural and shear hinges were defined using the uniaxial material model of Zona and Dall'Asta [120]. The model was separately calibrated for short and long links using a large body of test data [14, 19, 33, 34, 40]. The effectiveness of the approach was demonstrated for short, intermediate, and long links by comparing numerical and test results. It is worth noting that in all of the above-mentioned models the effects of axial force and strength degradation on the nonlinear behavior were neglected.

In studies by Malakoutian et al. [121], O'Reilly and Sullivan [67], and Kanvinde et al. [7] the OpenSees [122] analysis platform was utilized where a beam-column element with distributed plasticity and additional independent nonlinear shear springs located at the element ends was used for link modeling. Various different material models were adopted in each of these studies. Moghaddasi B. and Zhang [123] used the beam element of OpenSees [122] with zero-length moment hinges at the ends as well as four parallel translational springs at each end for simulating the behavior of shear links. This method was also used in the numerical study of Dastmalchi [69].

Other more sophisticated elements have been developed for modeling steel members with dominant shear yielding behavior, that are also applicable to EBF links. On the basis of the method proposed by Ricles and Popov [110, 111], Kazemi and Erfani [124, 125] developed a model with a combined shear-flexural inner hinge and two rigid beams on its sides. Numerical results were compared to the test data reported by Kasai and Popov [18] to demonstrate the accuracy of the proposed approach. An improved version of this model with an axial-shear-flexural hinge was recently developed by Kazemi and Hoseinzadeh Asl [126]. A mixed-formulation (or force-based) element was proposed by Saritas and Filippou [127] with independent

displacement, stress, and strain fields, where the displacement field was based on Timoshenko's beam theory. As a result, shear locking was avoided and mesh refinement was deemed unnecessary. Since the axial-shear-flexural interaction was captured using material data only, the model did not need further calibration for different loading and boundary conditions, unlike most of the methods with concentrated hinges. Comparison between numerical and experimental results revealed the accuracy and robustness of the method. Papachristidis et al. [128] have also proposed a force-based element; however, considering a three-dimensional state of stress and taking into account the interaction of axial, shear, flexural, and torsional actions. The kinematics of the model were obtained through the natural-mode method. Fairly accurate results were reported using this element when compared with the results of previous tests and also accurate FE analyses.

2.5 EBF Systems

2.5.1 Characteristics and Capacity Design Approach

This section provides general insight into the behavior and design philosophy of EBF systems, while the subsequent section is devoted to more in-depth discussions about the research on the seismic performance of these structures. As mentioned by Popov and Engelhardt [5], the use of eccentric bracing for resisting wind loads was well recognized even in the 1930s [129]; however, the use of this system for seismic applications was proposed in the 1970s in Japan [3, 4]. The studies of Roeder and Popov [12, 13, 130] in the late 1970s pioneered the research on EBFs in the United States. The cyclic loading tests of Roeder and Popov [12, 130] and Manheim [91] on a reduced-scale three-story one-bay EBF, the pseudo-dynamic tests on a full-scale six-story two-bay EBF as a part of the U.S.-Japan Cooperative Program in Earthquake Engineering reported by Roeder et al. [94] and Foutch [95], the shaking table tests of Whittaker et al. [24, 131, 132] on a scaled replica of the same six-story EBF, and the pseudo-dynamic tests of Balendra et al. [133] as well as the early

analytical studies of Hjelmstad and Popov [134], Ricles and Popov [110], and Popov et al. [135] on EBF systems, all confirmed that this system could be effectively used for seismic applications. The EBF system was utilized in several major applications (e.g. [136-138]) shortly after these studies. Short links in EBF systems are preferred since they will provide higher stiffness, strength, and ductility over intermediate and long links [5, 135]. Nevertheless, Popov and Engelhardt [5] demonstrated that using links that are too short will impose unmanageably high rotation demands on links. It was also noted by these researchers that the stiffness and consequently the fundamental period of EBF systems can be adjusted simply by altering the link length.

The capacity design approach [5, 135] is utilized in the EBF design to ensure concentration of yielding in links while keeping other members essentially elastic. First, the links are sized and then, other members are designed to resist the loads generated by the yielded and strain hardened links. Plastic design methods for EBF systems were initially proposed by Roeder and Popov [12], Manheim [91], and Kasai and Popov [23] in the 1970s and 1980s. An allowable stress design method was also developed by Teal [139] in the late 1970s. In the current practice, an elastic analysis is typically conducted during the design of EBF systems. Design examples for EBF systems can be found, for instance, in Bruneau et al. [57], the AISC Seismic Design Manual [140], Popov et al. [135] and Becker and Ishler [141].

The overstrength of links (Ω) must be considered in the design of members other than the links to estimate the maximum loads that might be imposed on these members by the fully yielded and strain-hardened links. Design specifications (e.g. [11, 142]) provide overstrength values which may be different for beams, braces, and columns. The AISC Seismic Provisions [11] suggest a value of $\Omega = 1.25$ for I-shaped links during the capacity design of EBF braces, which is lower than the traditional value of 1.5 (Section 2.2.1), mainly for considerations of economy. It is worth noting that a recent numerical study by Yiğitsoy et al. [108] demonstrated the adequacy of the current overstrength provisions for braces.

The design of a beam in an EBF system is often problematic since it is generally under high axial force and high bending moment. Increasing the size of the beam will not benefit the design, since the link-induced forces will also increase. Several methods such as using short links and braces with moment connections possessing inclination angles above 40° can reduce the demand on beams [5, 57, 93, 135, 143]. In addition, an EBF configuration proposed by Engelhardt and Popov [93] (Figure 2.1e) can minimize the beam axial force at the cost of using larger links and reducing the system redundancy. A similar EBF configuration was tested by Yang [109] in the early 1980s. In order to aid this design difficulty, a lower overstrength factor is used in AISC 341-10 [11] for the capacity design of beams when compared to that of braces. This is justified by considering the positive effect of the composite floor on beam performance as well as the fact that limited yielding of a beam will not negatively affect the behavior of an EBF system, as long as the stability of the beam is assured [19, 71, 144]. Based on extensive FE analyses on EBF sub-assemblages, Yiğitsoy et al. [108] suggested that the overstrength value recommended in AISC 341-10 [11] could be reduced even further in the design of an EBF beam with I-shaped links, provided that the demand-to-capacity ratio of the beam is kept below unity. For other cases a maximum unbraced length recommendation was developed. The FE analyses demonstrated that the probable yielding of the beam due to the above relaxation would not be detrimental and would only affect the brace end moment.

Early analytical and experimental studies [24, 110] demonstrated that all of the links above the level of the column under consideration would not develop their maximum shear forces simultaneously. Based on this observation a lower overstrength factor was suggested by AISC 341-10 [11] for the capacity design of columns in EBFs of three or more stories of bracing, when compared with the Ω value used in the design of brace members. Columns also need to be checked for the amplified seismic axial force of $\Omega_o P_{EQ}$, where Ω_o is the structural overstrength factor taken as 2.0 per ASCE 7-10 [145] and P_{EQ} is the column axial force generated by the code-specified

earthquake loads. It is important to note that drift-induced flexural forces are generally neglected in the design of columns as permitted by AISC 341-10 [11].

During the design process, it is necessary to estimate link end moments in order to determine the internal force distribution after formation of the expected plastic mechanism. For links located in the middle portion of floor beams (internal links) the end moments will almost be equal throughout a seismic loading. On the other hand, for links connected to columns (external links) the end moments will not be identical in the elastic range. However, early studies of Kasai and Popov [18, 23] proved that for most cases these moments would equalize as the link goes through large plastic rotations. Thus, in both cases, the link end moments can be readily estimated using equilibrium. The only exception reported by Kasai and Popov [18, 23] was the case of external links with $\rho \leq 1.3$, for which the end moments did not equalize at the ultimate state. For such cases, recommendations for moment distribution were developed by these researchers. Kasai and Popov [23] also demonstrated that it is advantageous to avoid EBF configurations with inactive links (e.g. Figure 2.1f) in which only one of the links located at one end of a brace would dissipate most of the energy (and thus become active) while the other would not contribute notably to the energy dissipation of the system (and thus remain inactive).

It is worth mentioning that early multi-story tests [24, 94, 95] demonstrated that, in some cases, the plastic behavior could be concentrated in the first story links leading to the development of a soft-story mechanism. Popov et al. [146] attributed this issue to the incorrect proportioning of the links along the height of the EBFs in the above-mentioned tests. The static pushover and dynamic time-history analyses of Kasai and Popov [23], Ricles and Popov [110], Ricles and Bolin [147, 148], and Popov et al. [146] revealed that in order to achieve a reasonable distribution of link inelastic action throughout an EBF height, all of the links need to have uniform capacity-to-demand ratios.

2.5.2 Research on Seismic Performance

An enormous amount of research on the seismic performance and design of EBF systems has been conducted in the past decades and important aspects of this research are briefly discussed in this section.

In a series of studies by Koboovic and her colleagues [63, 64, 143, 149] in late 1990s and 2010s the seismic behavior of low-, mid-, and high-rise EBF systems was investigated under several earthquake records via nonlinear time-history analysis. Similar to previous findings [19, 71, 144], limited yielding in EBF beams was found acceptable provided that braces were capable of resisting the additional moments. The use of a higher overstrength factor in the capacity design of upper tier columns was recommended, which is the approach used in CSA S16-14 [25]. The importance of drift-induced column flexural forces was also demonstrated in the above studies. The last observation was reported previously by Kasai and Han [150] as well. An iterative design methodology based on selecting appropriate earthquake records and performing time-history analyses was also outlined by these researchers [143, 149]. Although all of the links in the studied EBFs had similar capacity-to-demand ratios, the numerical results [63, 64] revealed that the energy dissipation might be non-uniform along the EBF height and more concentrated in the first and last story links.

The seismic behavior of six-story one-bay EBFs with long links under several earthquake records was studied by Tirca and Gioncu [151] in 1999. It was concluded that long links should be used with caution and avoided as much as possible due to their poor performance as observed in some of the studied cases.

The effect of shear-moment interaction in the plastic design of EBFs was studied by Mastrandrea et al. [152, 153], where a procedure for determining the ultimate link shear force and link end moments was proposed for a given collapse mechanism. In companion studies [154, 155], a design methodology for EBFs was developed which ensures formation of a global mechanism and prevents partial or local collapse mechanisms. The behavior of EBFs designed with this method was compared to that

of EBFs designed using a simplified method proposed by Kasai and Han [150] and satisfactory results were reported [154]. Further nonlinear static and dynamic analyses were conducted to demonstrate the effectiveness of the proposed method in distributing the inelastic link action through an EBF height while preventing the occurrence of undesirable failure modes [155]. The method was also verified via incremental dynamic analysis (IDA) in a study by Mastrandrea et al. [156] in 2013. The above-mentioned plastic mechanism control theory was recently implemented in the design of dual EBFs (i.e. systems composed of EBFs and MRFs) by Montuori et al. [157].

In 2006, Köber and Ștefănescu [158] compared the seismic behavior of EBFs designed on the basis of four different specifications including AISC 341-02 [75] and Eurocode 8-2002 [159] using nonlinear time-history analysis. It was reported that AISC 341-02 [75] required heavier sections for columns, beams, and braces. In a companion study by these researchers [160] the positive and negative aspects of placing webs of I-shaped braces normal or parallel to the plane of EBFs were investigated. Recommendations regarding each configuration were given considering seismic performance and required amounts of steel. In 2009, Köber and Ștefănescu [161] investigated the effects of using different structural details at the plastic hinge locations near the bottom of the first story columns in EBFs. Numerical results pointed to the advantages of utilizing a detail with reduced column flanges at these locations.

The effects of frame geometry on the seismic behavior and weight of chevron EBFs were investigated in 2008 by Özhendekci and Özhendekci [162]. It was concluded that EBFs with shear links performed better than those with intermediate and moment links. Furthermore, the use of longer shear links and shorter intermediate links was found to be advantageous in terms of seismic performance. However, it was demonstrated that for shear links, the frame weight would also increase along with the link length.

A novel performance-based plastic design (PBPD) methodology for EBFs was proposed by Chao and Goel [163, 164] in 2005. The method, which uses an energy-balance criterion and provides a design base shear for a given hazard level, global yield pattern, and target drift, is a direct method in the sense that it does not require any assessment after the initial design. A procedure for the height-wise distribution of this lateral force was also proposed based on the results of extensive nonlinear dynamic analyses. The results revealed that the EBFs designed using the new approach can satisfy expected performance objectives and perform better than those designed using conventional methods, without any notable increase in material usage. It is worth noting that an application of a performance-based approach for the design of a 97.6m-tall EBF system located in the United States was reported by Sabol and Nishi [165] in 2011.

In 2013, Sullivan [166] developed a direct displacement-based design (DDBD) method for EBFs with the aim of overcoming the deficiencies generally attributed to the force-based design approach. The method replaces a multi-degree-of-freedom (MDOF) system with an equivalent single-degree-of-freedom (SDOF) structure. A flow chart of this iterative design process as well as a design example were also provided. Sullivan [166] and O'Reilly and Sullivan [67] demonstrated the effectiveness of the method through time-history analyses of EBFs designed using DDBD. The studied EBFs exhibited lower-than-expected ductilities ($\mu < 3$), and thus it was noted that the codified response modification factors (i.e. R factors) are generally unconservative. Furthermore, using a unique R factor and a single displacement amplification factor (C_d) factor for all EBFs was found to be inappropriate since the ductility (μ) would tend to reduce as the EBF height increases. The use of longer shear links was recommended by Sullivan [166] similar to Özhendekci and Özhendekci [162].

The effect of height-wise distribution of the demand-to-capacity ratio of links was studied by Rossi and Lombardo [114] in 2007 using IDA. Partial collapse mechanisms, especially in the upper stories, were observed in all of the cases which had scattered height-wise link demand-to-capacity ratios. Furthermore, the R factors

for mid- and high-rise EBFs as well as EBFs with long links were found to be considerably lower than those proposed by different building codes [75, 167]. A subsequent study was undertaken by Bosco and Rossi [116] in 2009. The results of extensive nonlinear incremental dynamic analyses revealed that the traditional method of designing EBFs considering capacity design principles as well as providing uniform demand-to-capacity ratios for links would not necessarily ensure proper distribution of link inelastic action through the height, especially for mid- and high-rise EBFs. To have a better prediction of the seismic performance of EBFs, a new parameter, called the damage distribution capacity factor, was introduced by Bosco and Rossi [116]. It was demonstrated that, considering both of the demand-to-capacity ratio and the damage distribution capacity factor, it is possible to accurately predict the collapse mechanism of an EBF system.

In 2013, Bosco and Rossi [117] proposed a design procedure for dual EBFs to overcome the deficiencies observed in their previous studies regarding regular EBFs. In this approach, EBF links are the main energy dissipating mechanisms while MRFs provide lateral stiffness during inelastic behavior. Nevertheless, to have a more cost-efficient design, limited yielding was also permitted in MRFs at beam ends, bottom ends of the first story columns, and top ends of upper story columns. In a companion numerical study by Bosco and Rossi [118] it was demonstrated that dual EBF structures designed based on the proposed methodology perform better than those designed according to conventional methods. In addition, an expression for determining the R factor for dual EBFs was proposed which was dependent upon the link rotation capacity, γ_p^{max} , and gave R factors ranging from 4.0 (for long links) to 7.5 (for short links). A similar formula for the R factor of EBFs, ranging from 3.5 (for long links) to 5.0 (for short links), was suggested more recently by Bosco et al. [115]. Furthermore, the use of modal response spectrum analysis instead of equivalent lateral load methods for the design of mid- and high-rise EBFs was emphasized by Bosco et al. [115]. In a very recent study by Bosco et al. [168] the Eurocode 8 [159] EBF design procedure has been thoroughly reviewed and the important drawbacks and discrepancies are highlighted.

The seismic column demands of EBFs were studied by Richards [169] in 2009. The demands from nonlinear dynamic analyses were compared to the amplified seismic axial force ($\Omega_o P_{EQ}$) according to IBC 2006 [170] or ASCE 7-10 [145] considering the amplification factor (or structural overstrength) of 2.0. The numerical results revealed that designing EBF columns solely using the amplified seismic axial force can be quite unconservative for upper tier columns of tall EBFs while overly conservative for columns at the base of these structures. A similar conclusion was reported by Kuşyılmaz and Topkaya [171] in 2013. An average value of 3.25 was reported by these researchers for the structural overstrength factor which is well above the codified value of 2.0. The results reported by both studies may indicate some concern regarding the EBF column design; however, as noted by Kuşyılmaz and Topkaya [171], recalling that the capacity design principles should also be considered in the EBF column design it is anticipated that the use of $\Omega_o = 2$ would not yield substantial underestimations in the EBF column design process.

The appropriateness of using the displacement amplification factor, C_d , equal to 4.0 per ASCE 7-10 [145], which is directly used for estimating the plastic link rotation angle, γ_p , was studied by Richards and Thompson [65] in 2009. Nonlinear dynamic analyses of a large set of EBFs revealed that a factor of $C_d = 4$ can underestimate γ_p for links of low-rise EBFs while overestimating the plastic rotations of links in mid- and high-rise EBFs. Although calibrated C_d factors were proposed, the researchers pointed out that the study was inadequate to recommend factors for general design. To further investigate this design deficiency, a numerical study was undertaken by Kuşyılmaz and Topkaya [66] in 2015 and it was demonstrated that the C_d factor of 4.0 may result in significantly unconservative estimates of γ_p in low-, mid-, and high-rise EBFs. Results of the inelastic time-history analyses were used to develop a nonlinear relation which provides C_d values ranging from 8.0 (in the lower stories) to 5.0 (in the upper stories). In a subsequent study by Kuşyılmaz and Topkaya [172] nonsimulated collapse analyses revealed that EBFs designed in accordance with the U.S. provisions [11, 145], considering an R factor of 8.0, have higher collapse probabilities than expected. Consequently, two distinct design modifications were

proposed to reduce this probability. The first one was a modification to the C_d value based on [66] and the second one was a modification to the R factor, where a value of 4.0 was recommended.

In a recent study by Speicher and Harris [173] the seismic performance of six EBFs designed using IBC 2012 [174] were assessed based on ASCE 41-06 [175] using static and dynamic, linear and nonlinear analyses. The correlation between ASCE 7-10 [145] and ASCE 41-06 [175] in terms of the anticipated performance level was also studied. Numerical results once again indicated the possibility of concentration of inelastic action in a limited number of links in a properly designed EBF system. In addition, it was observed that the linear assessment methods given in ASCE 41-06 [175] are less conservative than the nonlinear assessment procedures. However, it was unclear which of these procedures is more representative of the actual behavior, since the code does not consider the effect of loading history in the assessment process and acceptance criteria. Speicher and Harris [173] mentioned that the responses of links under earthquake loadings were mostly one-sided with a ratcheting approach towards large rotations, and thus, higher rotation capacities might be anticipated for links compared to the codified limits. Consequently, the need for link assessment criteria which are based on cumulative demands was highlighted.

Studies have also been undertaken recently to provide simple relations for estimating the fundamental period as well as the stiffness of EBF systems. In 2010, Richards [176] derived a simple relation for predicting the lateral stiffness of an EBF story based on the design story shear, frame geometry, and beam depth. A comprehensive study was conducted in 2015 by Kuşyılmaz and Topkaya [177] to improve the accuracy of the formula available in ASCE 7-10 [145] for estimating the fundamental period (T_o) of EBFs, which first appeared in UBC 88 [79] and has not been calibrated since then. A hand-method for estimating T_o was first formulated and its accuracy was demonstrated by comparing the results with data obtained through an extensive parametric study and also with data available in the literature. A simple period-height relation for EBFs was then developed. The results obtained by this expression were

compared to the apparent (measured) periods of actual EBF buildings, reported by Kwon and Kim [178], and acceptable conformity was reported. In a similar study, Young and Adeli [179] studied the effect of building irregularities on the fundamental period of EBFs. It was demonstrated that the formula given in ASCE 7-10 [145] can yield overly conservative estimates of T_o for these systems. The results from analyses of 12 properly designed EBFs as well as the data available in the literature were combined to propose a three-variable power expression for predicting T_o , which included the effects of EBF building irregularities. The study also confirmed that regular EBF buildings tend to have a longer fundamental period compared to EBF buildings with irregularities. The accuracy of the proposed formula was demonstrated using the analytical periods compiled by Tremblay [180] and the apparent periods reported by Kwon and Kim [178].

The effect of the variability of steel material in the seismic performance of EBFs was studied by Badalassi et al. [181] in 2013. The numerical results revealed that the variability of the steel material did not have a major effect on the failure probability of the studied structures. In addition, the capacity design requirements of Eurocode 8 [182] were found to be appropriate. It is worth mentioning that in some of the studied EBFs by Badalassi et al. [181] two floor beams were used in each level of the EBFs to avoid interaction between the floor deck and the link. The coupled beam sustained the gravity loads while the main beam contained the link and carried the seismic loads (Figure 2.10). This approach is generally attributed to Perretti [183].

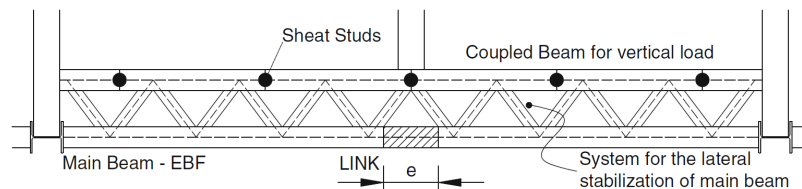


Figure 2.10. Plan view of the use of duplicate floor beams in EBFs [181]

The seismic reliability of EBFs was investigated recently by Lin et al. [184] by means of nonlinear dynamic analyses, considering far-fault and near-fault earthquakes, based on the guidelines of FEMA 356 [185]. It was concluded that EBFs (particularly low-rise EBFs) have lower failure probabilities than MRFs. The reduction was more pronounced when far-fault ground motions were considered. The behavior of EBFs under near-fault earthquakes was also studied by Eskandari and Vafaei [186] In 2015. Even though near-fault earthquakes were found to be somewhat more destructive, the probability of low-cycle fatigue-induced premature web fractures were observed to be higher for the case of far-fault ground motions. Nevertheless, it was also concluded that EBFs are suitable systems to be used in near-fault regions owing to the fact that the γ_p values recorded for all links were in the acceptable range based on FEMA 356 [185] requirements for the life safety performance level.

The application of the reduced beam section (RBS) connection in dual EBFs with long external links was investigated in 2011 by Naghipour et al. [187]. Results of nonlinear static (pushover) analyses on four-, seven-, and ten-story dual EBFs revealed that the RBS connection can increase the ductility of the system (by about 10%) and reduce the demand on link-to-column connections by moving the hinge location away from the column face. The RBS connection was however recommended only for long links with shallow sections.

The seismic performance of a special type of EBF, hereafter referred to as HS-EBF, in which links are constructed from conventional steel while other members are made from high strength (HS) steels with F_y in excess of 345 MPa, was investigated by Lian et al. [47] in 2015. Results of a cyclic test on a scaled one-story one-bay chevron HS-EBF conducted by these researchers were used to validate their numerical modeling approach. The results of the subsequent analyses under cyclic loading and three ground excitations revealed a general similarity between the performances of HS-EBFs and equivalent conventional EBFs. However, better load carrying capacity and lower material consumption was reported for the HS-EBFs while slightly higher

ductility and energy dissipation was indicated for the EBFs. The inter-story drifts and plastic link rotations were also found to be lower in the studied EBFs. Furthermore, a maximum height limit of sixteen stories was recommended for HS-EBFs in order to achieve better seismic performance.

A number of recent studies have focused on the optimization of EBF systems. In 2013, Gong et al. [188] presented a genetic algorithm based structural optimization technique for EBFs. A successful application of this optimization method was demonstrated for a hypothetical three-story EBF building; however, this came with the cost of an excessive computational burden (of the order of days). In a more recent study, Karami Mohammadi and Sharghi [189] developed an optimum design technique for EBFs based on the concept of uniform deformation theory. These researchers applied the method to three-, five-, and ten-story EBFs and demonstrated that the optimized EBFs have lower weights and better seismic performances compared to those of regularly designed EBFs.

There are also a limited number of studies regarding the effect of concrete slabs on the structural response of EBF systems. In 2013, Danku et al. [190] investigated the issue in three EBFs and three dual EBFs with four, eight, and twelve stories through nonlinear static (pushover) analyses as well as IDA considering seven earthquake records. The models were calibrated using the outcomes of a companion experimental study [45]. The numerical results revealed that composite action can increase the system stiffness and reduce the structural drifts and rotation demands on links and lead to a more optimum EBF design. For the case of dual EBFs, inelastic action was reported to be mainly concentrated in the links. Furthermore, the R factor for the steel EBFs and the steel dual EBFs was found to be about 6.0 (similar to Eurocode 8 [142]); however, a lower R factor (between 3.5 to 6.0) was reported when composite action was incorporated in the models. Prinz and de Castro-e-Sousa [191] also investigated the effect of concrete slabs on the EBF behavior in 2014. Two three-story EBFs with and without concrete slabs were modeled via FE method. The results of dynamic analyses under two earthquake accelerations confirmed the findings of Danku et al. [190] regarding the effects of concrete slabs on stiffness,

inter-story drifts, and rotation demands of EBFs, especially for the case with long links, where a reduction of 35% was reported in the residual drifts because of composite action. Although the link rotation demands were lower in the composite models, Prinz and de Castro-e-Sousa [191] observed that the link damage accumulation was rather independent of the presence of concrete slabs. This increase of plastic demand in the composite models was attributed to the shift in the neutral axis which in turn produced higher strains in the bottom flanges of the links.

2.6 Special Topics

Beside the topics covered in the previous sections, some special and emerging topics related with EBF systems are also available in the literature, and these are briefly discussed here.

2.6.1 EBFs with Vertical Links

Although one of the earliest experimental studies on EBFs was conducted on frames with vertical links (also known as inverted Y-braced EBFs; Figure 2.1d) by Tanabashi et al. [4] in 1974, the use of horizontal links in EBFs has become more popular through the years. Compared to their horizontal counterpart, vertical links have an easier post-earthquake repair process. In addition, they can be conveniently used for the seismic rehabilitation of existing structures. Furthermore, their use can be advantageous in cases where the floor girders are required to remain elastic due to the presence of very large gravity loads. On the other hand, proper lateral bracing of vertical links can be difficult in certain cases. Early static, cyclic, and dynamic loading experiments by Seki et al. [192] and Vetr [193] on single- and multi-story EBFs with vertical shear links revealed that this system can exhibit a very ductile and stable behavior during an intense loading, provided that proper lateral bracing for the link ends is available. The results of a numerical study by Fehling et al. [194] in 1992 further emphasized the importance of lateral bracing for vertical links. A

force equal to 1/50 of the link shear force was deemed adequate for the design of these lateral braces. In a subsequent study by Bouwkamp and Vetr [195] a relation for limiting the length ratio of short (or shear) vertical links was proposed which was dependent upon the ratio of the link end moments.

The advantages of hybrid vertical links with low strength web and high strength flanges were demonstrated by Shinabe and Takahashi [196] in 1995. Similarly, the FE analyses of Saedi Daryan et al. [197] revealed that utilizing vertical links constructed from very low-yield-strength steel with F_y of about 100 MPa could increase the energy dissipation of an EBF notably while reducing the probability of local buckling.

The concept of EBFs with double vertical links, originally mentioned by Fehling et al. [194], was recently investigated numerically as well as experimentally by Shayanfar et al. [198, 199] and promising results were reported. This concept can be advantageous in cases where the dimensional limitations of the floor beam in an existing structure do not allow the use of a single large-size vertical link for seismic rehabilitation.

Through extensive nonlinear static and dynamic analyses, Dicleli and Mehta [200, 201] investigated the behavior of EBFs with vertical shear links built from compact HP sections. Results revealed that such systems can combine the advantages of MRFs and CBFs during an earthquake while experiencing less damage and eliminating the negative aspects of each system.

In 2012, Shayanfar et al. [202] tested a composite vertical shear link in which a steel link was partially encased in reinforced concrete. Results revealed that the concrete in these links can delay the web buckling and increase the shear strength and energy dissipation of the specimens significantly. Nevertheless, the behavior of the composite link coincided with that of the bare steel link when the concrete portion was fully damaged at later stages of the loading.

A novel two-stage seismic load resisting system was developed by Zahrai and Vosooq [203] in 2013 which combined an EBF system with vertical shear links with a knee braced frame. During a moderate earthquake, only the vertical links dissipate energy while in the case of a strong ground motion, the plastic deformations in the vertical links are limited to a certain extent using a mechanical stopper device and further frame drift causes yielding in the knee elements.

Shayanfar et al. [204] developed a performance-based plastic design (PBPD) methodology for EBFs with vertical links similar to the design methodology proposed previously by Chao and Goel [163, 164] for EBFs with horizontal links. Based on the approach developed by Mastrandrea et al. [152-155], a rigid-plastic analysis and design approach for EBFs with vertical links was developed by Montuori et al. [205, 206] in 2014 which included moment-shear interaction and aimed to prevent local and partial mechanisms while ensuring formation of a desired global collapse mechanism.

In a recent numerical study by Massah and Dorvar [207], the analysis and design of EBFs with vertical shear links and shape memory alloy (SMA) devices were investigated. The SMA material can recover its original shape even after very large strains through the shape memory effect (which requires heating) and the superelasticity effect (which requires unloading). In this study, SMA devices were mounted on sides of the vertical links to obtain a reversible system with reduced residual deformations.

In 2016, Wang et al. [208] conducted an experimental study on a three-story one-bay by one-bay EBF system with vertical links in which the links were constructed from conventional steel while other members were made from high strength steel, similar to the concept studied for EBFs with horizontal links by Lian et al. [47]. Although excellent cyclic performance was reported, significant out-of-plane deformation was observed at the conjunction of the vertical link and the braces (which was not laterally supported) leading to failure due to fracture in the link-to-beam connection at the first story.

Although the current AISC Seismic Provisions [11] are intended for designing EBFs with horizontal links, the commentary on the code emphasizes the importance of lateral bracing at the intersection of a vertical link and braces, if inverted Y-braced EBFs are utilized.

2.6.2 Tied Braced Frames and EBFs with Zipper Struts

To prevent the formation of a soft-story mechanism in an EBF [24, 94, 95], Martini et al. [209] proposed a modified EBF configuration in 1990, known as the tied braced frame (TBF), in which the link ends are vertically connected to each other over the entire height of the structure. Although a number of early studies indicated some advantages for using TBFs [148, 209], the nonlinear static and dynamic analyses of Popov et al. [146] in 1992 demonstrated that properly designed EBF systems can have well-distributed inelastic action throughout the building height without the need for ties. In a number of recent studies, however, unsatisfactory seismic behavior was reported, particularly for high-rise EBFs [114, 116]. As a result, design methodologies for TBFs were developed by Ghersi et al. [210] and Rossi [211] on the assumption that these systems are more prone to form a global collapse mechanism. A promising performance was reported by Rossi [211] for TBFs designed according to the proposed methodology.

In a similar approach, Zahrai et al. [212] proposed and numerically investigated the behavior of EBFs with zipper struts, which vertically connect the mid-points of shear links throughout the height. Results of the extensive pushover, cyclic loading, and time-history analyses revealed that the zipper struts not only help in having coincident yielding of the links but also increase the ductility and energy dissipation of the system.

2.6.3 Replaceable Links

Although the concept of replaceable links was previously mentioned in a number of studies (e.g. [32, 109, 192]), the first research specifically on EBFs with horizontal links that can be easily dismantled and replaced after an earthquake was conducted by Stratan and Dubina [35, 213] in the early 2000s. A link-to-beam connection with bolted end-plates, which were flush with the floor beam, was studied (Figure 2.11a). Pinched behavior due to the end-plate bending and bolt thread stripping was observed in some cases and it was concluded that the link length ratio (ρ) should be limited to 0.8 to have proper cyclic behavior. Further numerical and experimental studies of Dubina et al. [214, 215] confirmed the applicability of the concept and demonstrated that dual EBFs have a notable re-centering capability which significantly facilitates the post-damage replacement. To further investigate this, a comprehensive full-scale test program, known as the DUAREM project [216, 217], was recently conducted at the European Laboratory for Structural Assessment (ELSA) of the Joint Research Centre (JRC) in Ispra, Italy in which a three-story three-bay to one-bay dual EBF system with end-plated replaceable links was tested pseudo-dynamically under three earthquake levels and link replacement was performed after each ground motion simulation. It was concluded that the dual EBF system with replaceable links is a promising lateral load resisting system that provides the desired seismic performance as well as an economic post-earthquake repair procedure.

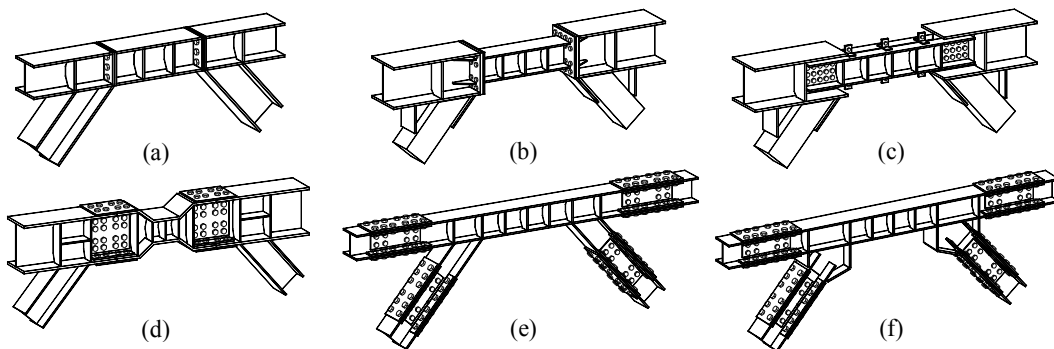


Figure 2.11. Previously developed replaceable link details

Two other replaceable shear link details were recently studied by Mansour et al. [42, 49] through isolated link tests as well as frame tests. The first detail was again a bolted end-plate link-to-beam connection; however, it had a link segment that was smaller than the floor beam, making it possible to use bolts above the top flange and below the bottom flange of the link (Figure 2.11b). Excellent ductility and stable behavior were reported for this detail proving its ability for practical applications. Further numerical studies of Mago [218] in 2013, which are summarized in the HERA R4-145 report, confirmed the reliability of the connection. In a recent study by Dusicka and Lewis [43] on a similar replaceable link connection, the use of an additional pair of stiffeners was proposed to reduce the probability of flange fracture in the vicinity of the link-to-end-plate welds. These additional stiffeners were placed parallel to the link web and located in the first web panel (similar to the detail shown in Figure 2.9h). In addition to the numerical analyses, the detail was verified experimentally for the case of replaceable long links by Dusicka and Lewis [43].

Another detail developed by Mansour et al. [42, 49] for replaceable shear links (originally proposed by Balut and Gioncu [219] for MRFs) was a bolted web connection where two back-to-back channel sections, considered as the link segment, were bolted to the web of the floor beam (Figure 2.11c). Although larger γ_P^{max} values were obtained compared to the tested end-plate connections, the bolted web connection experienced a pinched behavior due to the repeated cycles of bolt-slip, bolt bearing against the link web, and bolt hole ovalization. The larger rotation capacities of these links were attributed to the inelastic rotation of the connection itself which, in average, was about 16% of the total inelastic link rotation. Modified and reinforced details were proposed to overcome the pinched behavior observed for the web bolted connection. The replaceability of the damaged links was also studied in the frame tests.

Recently a replaceable link detail (Figure 2.11d), originally proposed by Mansour [42], was investigated by Ashikov et al. [220, 221] through experimental testing and numerical analysis.

A multi-phase experimental and numerical research program has been undertaken at Middle East Technical University (METU) to develop new replaceable EBF links which can potentially enhance the existing details. The first and the second phases of the research program concentrated on developing replaceable links which are based on splicing the braces and the collector beams as shown in Figure 2.11 e-f. This concept is well suited for EBFs with directly connected braces or gusseted brace attachments. The potential of these replaceable links was investigated through experimental testing [8, 9]. The results revealed that these links behave similar to ordinary links and the gaps provided at the splices of the braces and the collector beam facilitate easy replacement. Another type of replicable link detail, namely *detachable replaceable link*, is under development at METU which is based on splicing the link at its mid-length in order to facilitate the link replacement procedure after an earthquake. As shown in Figure 2.12, by adjusting the splice eccentricity, it is possible to replace the link under different levels of post-earthquake residual drifts. This detail is further investigated in Chapter 4 of the present thesis.

It is also worth mentioning that there are also a limited number of practical applications of replaceable links in New Zealand which are summarized by Fussel et al. [222], Ramsay et al. [223], and Gardiner et al. [224]. Furthermore, design guidelines for replaceable links are given in the specifications of New Zealand and Canada [25, 225].

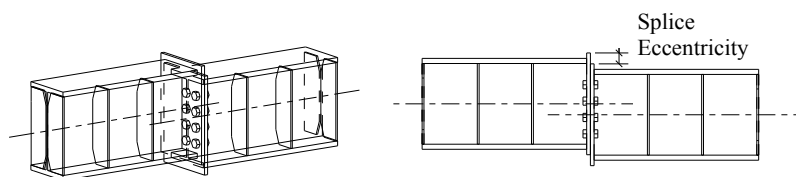


Figure 2.12. Detachable replaceable link detail

2.6.4 Use of EBFs or links in Reinforced Concrete Structures

Providing a thorough review of this topic is out of the scope of the present thesis; however, the main applications of EBF configurations in reinforced concrete (RC) structures are mentioned here for the sake of completeness. Steel eccentric braces with or without vertical links can be connected to existing RC frames for seismic rehabilitation. This concept was numerically and experimentally studied by Bouadi and Engelhardt [226], Ghobarah and Abou Elfath [227], Bouwkamp et al. [228], Perera et al. [229], D'Aniello [230], Mazzolani et al. [231], Pina et al. [232], Durucan and Dicleli [233], Özel and Güneyisi [234], Varum et al. [235], and Wang and Yu [236] in the past few decades. Steel links are also utilized as energy dissipating coupling beams between adjacent RC wall piers in hybrid coupled wall (HCW) systems. A comprehensive review of the research on the behavior, analysis, and design of these systems as well as particular topics such as link-to-wall connections can be found in El-Tawil et al. [237].

2.6.5 Progressive Collapse of EBFs

In 2009, the gravity-induced progressive collapse of EBFs was studied by Khandelwal et al. [113] utilizing validated numerical analyses. To this end, the alternate path method (APM) was used, i.e. critical columns and adjacent braces were instantaneously removed from a ten-story EBF, properly designed based on the U.S. specifications [76, 238] for high seismic risk. The limited numerical results demonstrated that EBFs are less vulnerable to progressive collapse compared to special CBFs, mainly because of their improved system layout. The beneficial effect of locating EBFs at the perimeter of the structure was also noted.

2.6.6 Fragility Functions for Links

The damage states and fragility functions for EBF links were developed recently by Gulec et al. [239]. Based on a precise evaluation of the test data of 82 links (reported previously in the literature) a total of 9 damage states, such as web yielding, flange local buckling, flange fracture, damage to concrete slab, etc., were indicated. Furthermore, the methods of repair (MoR) were categorized into 4 groups (i.e. cosmetic repair, concrete replacement, heat straightening, and link replacement) and each damage state was related to a certain MoR. Fragility functions were also developed for short and long links based on statistical analyses to specify the probability that a specific MoR will be required as a function of γ_P .

2.6.7 Other Applications

In a number of studies by Bruneau and his colleagues [240-244], the concept of EBFs with horizontal or vertical links has been used in steel bridge superstructures in order to introduce energy dissipation in end-diaphragms instead of the common approach which relies on the energy dissipation of the substructure. This can be fruitful for instance in cases where stable and ductile behavior of the substructure is doubtful. Results of the extensive numerical and experimental studies as well as design procedures are presented by these researchers.

The applicability of stainless steel in EBFs was studied by DiSarno et al. [245] in 2008. The results of nonlinear pushover and time-history analyses of a sample structure revealed that using members made from stainless steel can enhance the energy dissipation and structural overstrength of the system compared to regular EBFs while reducing the roof drift and the probability of local buckling in members.

In addition to EBFs, HCWs, and bridges, the concept of dissipative link segments has also been utilized in other structural systems. For instance, Moghaddasi B. and Zhang [123] studied the seismic behavior of diagrid structural frames with replaceable shear links, in 2013. In another recent study, the concept of linked

column frames (LCF) was proposed and numerically studied by Malakoutian et al. [121]. The use of buckling-restrained braces (BRB) in eccentric configuration was studied by Prinz and Richards [246, 247]. The energy dissipation mechanism in this system is however substantially different from that of EBFs since yielding is concentrated in the braces rather than in the links.

2.7 Chapter Summary

A comprehensive review of the research conducted on the behavior and design of eccentrically braced frames was presented in this chapter which covered both component level and system level responses. Experimental and numerical studies that address the main characteristics of links as well as link detailing were presented. Different numerical techniques for link modeling were discussed. Furthermore, studies which focused on the seismic behavior and design of EBF systems were summarized with an emphasis on the capacity design approach. Finally, special applications of EBF systems or link segments were discussed. For the improvement of EBF design and applications, the following items were identified in the course of this review process as important research needs:

1. Further research on the behavior of very short links ($\rho < 1$) is required in order to take advantage of their excessive inelastic rotation capacity in EBF systems. In contrast, considering the doubtful performance of very long links ($\rho > 3 \sim 3.5$) reported in some numerical studies, additional research for identifying their deficiencies and limitations would appear to be beneficial.
2. The use of a single link overstrength factor (Ω) for all link length ratios in the EBF design process can lead to significant underestimations of internal forces developed in other members due to the yielded and strain hardened links, especially when very short links are utilized. Thus, further research is needed to develop simple methods for estimating the actual link overstrength factor for different link length ratios considering the effects of moment-shear interaction, link flange shear resistance, axial restraint provided by the

adjacent members, and excessive cyclic hardening. A similar concern is also valid for the case of built-up tubular links. Furthermore, the unusually high overstrengths (of the order of 5.0) which have been reported recently for some unstiffened very short links also need further attention.

3. There is a substantial research need for investigating the effect of high axial load on the behavior of intermediate and long links. In addition, the effect of tensile axial force on increasing the link overstrength requires further attention, as mentioned in a number of recent studies.
4. The increase in the link overstrength due to the presence of a concrete slab has not been adequately investigated. This effect can be hazardous particularly from the capacity design point of view. Methods for estimating this increase are required which can be conveniently applied in practice.
5. Additional investigation is required to validate whether the recent relaxation in the flange slenderness requirements of shear links by the AISC Seismic Provisions [11] can also be considered for shear links subject to high axial loads.
6. Several issues have recently been reported for the spacing requirements of links per AISC 341-10 [11] which need further consideration. Research is required to investigate the possibility of any relaxation in the stiffener spacing requirements of I-shaped shear links. On the contrary, the observed poor performance of some intermediate links, which is attributed mostly to their stiffener spacing requirements, should be studied carefully to come up with appropriate solutions.
7. Many novel web stiffening details for reducing the probability of premature fracture and improving the link rotation capacity including, but not restricted to, the sandwich, horizontal stiffener, and diagonal stiffeners details have been proposed which require further research. In addition, the feasibility of other approaches, such as links without intermediate stiffeners, should be studied. Furthermore, if approved, the development of design guidelines for employing these details is essential.

8. The relation between the reduced material toughness in the k-area of I-shaped links and the recently observed link web fractures is still unclear and necessitates additional experiments.
9. The deteriorative effect of misalignment between the link end stiffeners and brace flanges in triggering fracture was observed during recent earthquakes, and thus, providing practical methods for reducing the probability of this misalignment in field applications would be fruitful.
10. The current intermediate stiffener spacing requirements of built-up box shear links are not dependent upon the required level of γ_p . Further experimental research is needed to validate such a relation.
11. Although the crucial importance of link lateral bracing is well understood, there exist only a handful of studies which have explicitly investigated the effect of lateral bracing on link behavior, considering realistic loading and boundary conditions. Additional research on this topic would be beneficial since the current codified lateral bracing requirements for links are in fact based on studies which focused mainly on the plastic hinge locations of MRFs.
12. There is a significant research need in the field of link-to-column connections considering the fact that most of the connections suitable for MRFs exhibit poor performance when used as link-to-column connections. Promising details such as the all-around fillet weld and the supplemental web doubler connections require further experimental verification, especially for long links, with the aim of developing prequalified link-to-column connections. In addition, other less studied link-to-column connections such as the end-plate connection with and without rib stiffeners as well as the connection reinforced by haunches need additional investigation and development of design procedures. There are also details such as the reduced flange section link connection, which have not been studied experimentally at all.
13. There is almost no study which specifically investigates the behavior and design of the column panel zones of EBFs with link-to-column connections.

Research on this issue is indispensable. The current AISC Seismic Provisions [11] use the requirements of special MRFs for EBF column panel zone design without the necessary research background.

14. The amount of reduction in Ω for the capacity design of columns in EBFs is typically limited since there are no methods for predicting the actual number of simultaneously yielded links above the column under consideration except for complicated nonlinear analysis. Thus, developing simple and reliable methods for estimating the reduced column forces can be advantageous, especially for high-rise EBFs, where a potential cost saving might be achieved.
15. There is an urgent need for the reevaluation of the response modification factors (R) of EBFs that are in use by most of the design specifications, since they can significantly overestimate the ductility of these structures. In a similar manner, previous studies have proven that the codified displacement amplification factors (C_d) for EBFs are not capable of predicting the actual inter-story drifts and inelastic link rotations based on the results of linear analysis, and thus, reevaluation again appears to be necessary. Although several studies have been undertaken regarding these issues, further research is essential in order to confirm such alterations.
16. The problem of the concentration of yielding in a limited number of stories is reported even for some properly designed mid- and high-rise EBFs. New methodologies have been proposed recently to overcome this issue, which require further verification (and in some cases simplification) so as to be considered as reliable and practical methods for the design of EBFs.
17. The codified assessment procedures for EBFs typically do not consider the effect of the loading history on the acceptance criteria and link failure detection. As noted in recent studies, this deficiency can be overcome by introducing measures based on cumulative demands. Further monotonic tests or experiments with other more suitable loading histories might be fruitful

for developing these cumulative criteria, which can be used for predicting the actual link rotation capacities during an earthquake.

18. The research on EBFs with vertical links is limited when compared to their horizontal counterparts. There is a significant need for research on the behavior and design of these structures to address issues such as stability and the detailing of vertical links. There is also a notable gap in the design specifications regarding EBFs with vertical links, which can only be closed with additional studies.
19. The promising performance of tied braced frames (TBFs) as well as EBFs upgraded with zipper struts in terms of the proper distribution of yielding over the structure height necessitates further confirmation through extensive numerical simulations as well as experimental studies. Practical procedures for the design of these systems are also required.
20. There has been a considerable improvement in the field of replaceable links in the past decade; however, there is still a need for additional research to develop codified design and detailing rules for link-to-beam connections with the final goal of proposing prequalified connection types for replaceable links. Furthermore, studies on intermediate and long replaceable links as well as external replaceable links located between a brace and a column are few in number.
21. Research on the progressive collapse of EBFs is very limited. Future research on this topic is essential, particularly for improving the behavior of these structures under probable blast loading scenarios.
22. Newly proposed concepts such as composite links, EBFs with shape memory alloy (SMA) devices, EBFs made of high strength or stainless steel, and the use of energy-dissipating steel links in other structural systems such as diagrids and linked column frames (LCF) are also potential areas for future studies.

CHAPTER 3

LOW-CYCLE FATIGUE TESTING OF SHEAR LINKS AND CALIBRATION OF A DAMAGE LAW

The low-cycle fatigue (LCF) behavior of shear links in eccentrically braced frames (EBFs) is experimentally studied in this chapter with the aim of calibrating a convenient damage law for estimating the exhausted as well as remaining fracture life of these members under any loading history.

3.1 Introduction

As discussed extensively in the previous chapter, during strong earthquakes links act as structural fuses and dissipate the seismic input energy through repeated inelastic cycles. In short or shear links (i.e. $\rho = e/(M_P/V_P) \leq 1.6$) shear yielding of the web is predominant while in longer links, flexural yielding or a combination of shear and flexural yielding is typically observed. It should be noted that, ρ is the link length ratio, e is the link length, and $M_P = ZF_y$ and $V_P = 0.6F_y(d-2t_f)t_w$ are the plastic moment and plastic shear capacities of the I-shaped link, respectively, as per the AISC Seismic Provisions [248] where Z is the section plastic modulus, F_y is the yield stress, d is the section depth, t_f is the flange thickness, and t_w is the web thickness. Although long links provide more architectural freedom for openings, shear links are structurally preferred since they perform substantially better under severe cyclic loadings in terms of strength and ductility [13, 15]. In the current design practice, the plastic link rotation angle (γ_p) is estimated based on the anticipated interstory drift level and checked against codified limits, which can be as high as 0.08 rad for shear links [248]. Despite its deficiencies [64, 66], this approach is commonly utilized in the design as a simple and convenient method for reducing the possibility of link fractures during earthquakes.

A similar method is followed during the performance evaluation of an EBF building. The ASCE 41-13 [249] standard, which is also used in some cases by engineers for the performance-based design of new buildings, provides four analysis procedures for the seismic evaluation of existing EBF systems: linear static, linear dynamic, nonlinear static, and nonlinear dynamic. In the nonlinear procedures, the estimated γ_p for a link shall not exceed a predefined limit so that it would satisfy the requirements of a certain performance level (e.g. $\gamma_p \leq 0.14$ rad for shear links considering the Life Safety performance level). Although experimental studies such as [37] have substantiated the strong dependency of the rotation capacity of a link to the applied loading history, the acceptance criteria used by ASCE 41-13 [249] do not fully consider this effect when assessing EBF links. Speicher and Harris [173] recently demonstrated that this shortcoming of ASCE 41-13 [249] can result in excessive link failures when nonlinear dynamic procedure is used. The reason is that the standard detects failure for links subjected to symmetric large cycles using the same approach that it does for links subjected to one-sided large cycles. Reliable methods for damage estimation of EBF links are also required to study seismic performance of EBF systems. The FEMA P695 [250] procedure requires collapse assessment of archetype buildings to quantify the response factors to be used for this lateral load resisting system. In its present form, the FEMA P695 procedure relies on the assessment metrics given by ASCE 41-13 [249] which depend solely on the maximum amount of link rotation and disregard cumulative effects. These issues were also emphasized in the literature review of Chapter 2 of the present thesis where the need for developing measures based on cumulative demands was further highlighted.

Such measures can also significantly contribute to the decision-making process of the post-earthquake replacement of EBF links. The last decade has witnessed significant improvements in the development of replaceable links for EBFs, as summarized Section 2.6.3. The 2010-2011 series of Christchurch earthquakes in New Zealand resulted in yielding and fracture of links in EBFs. As discussed by Gardiner et al. [224], the identification and replacement of damaged links in such

cases is a challenging and complicated task. In such cases, damage laws based on cumulative measures can significantly assist the process of identifying damaged links after an earthquake, particularly if signs of fracture or severe low-cycle fatigue (LCF) damage are not encountered in field observations.

Consequently, the main objective in this chapter is to calibrate a damage law to estimate the fracture life of shear links used in EBFs. Pursuant to this goal, low-cycle fatigue testing of shear links was conducted. A damage law was then calibrated based on the findings of low-cycle fatigue tests. The damage law was further generalized based on a comprehensive data compilation of test results reported in literature. Finally, a systematic procedure for the application of the damage law on earthquake-induced loading histories was developed. For further validation, the procedure was applied to the practical case of links fractured at the Christchurch hospital garage during the Christchurch earthquakes. The metrics given by ASCE 41-13 [249] and the loading protocol currently in use by the AISC Seismic Provisions [248] were also investigated based on the results of the LCF testing program. Details and findings of the study are presented in the subsequent sections.

3.2 Experimental Program

3.2.1 Test Setup and Instrumentation

The experimental program was conducted at the Structural Mechanics Laboratory of Middle East Technical University. The utilized test setup (Figure 3.1), designed and previously used by Bozkurt [251], consisted of a reaction wall, a rigid floor, a lateral restraining system, a 1500 kN capacity hydraulic actuator, and a nearly full-scale one-story one-bay EBF with a width of 5 m and a height of 3.5 m (2.7 m between the column pin supports). With the help of a loading beam, the applied force from the actuator was distributed almost uniformly to the columns which were pin-connected at both ends. All other connections of the EBF were moment connections.

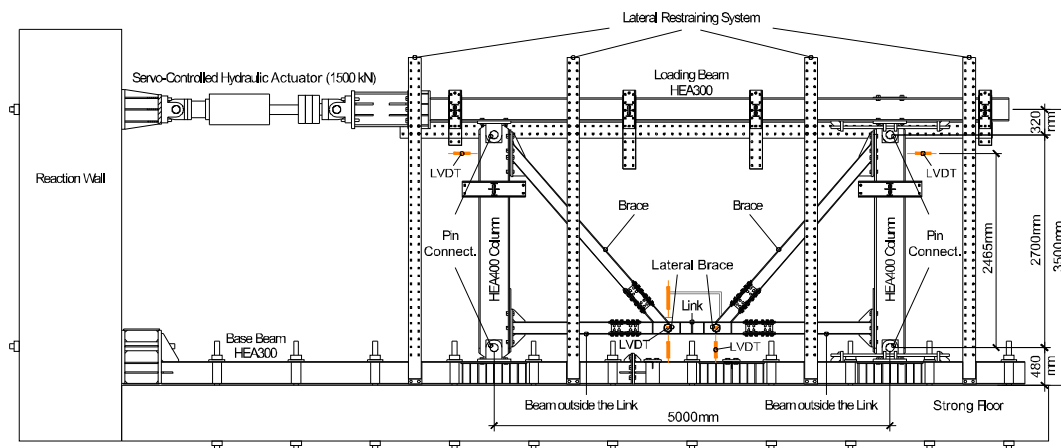


Figure 3.1. Details of the test setup; Not all instrumentations are shown

Following the capacity design procedure outlined in the AISC Seismic Provisions [248], the EBF columns, beams, and braces were designed to remain elastic through the tests whereas the yielded and fractured link segment was replaced after each test. Further details on the design of the EBF frame can be found in Bozkurt [251]. As will be discussed later, three replaceable link schemes were considered in the test program, however, Figure 3.1 shows only the scheme with direct brace attachments as a representative case. The EBF was tested in a V configuration in order to facilitate the replacement procedure, monitoring, and lateral bracing of links. The out-of-plane displacements of the loading beam, columns, and more importantly link ends were controlled using the lateral restraining system and lateral braces depicted in Figure 3.1. As shown in this figure, the horizontal displacement of columns (at a height of 2465 mm from the bottom pin support) was measured during each test using Linear Variable Differential Transformers (LVDTs).

Vertical displacement of the link ends was monitored with respect to the stationary strong floor using LVDTs (Figure 3.2). The differences between these individual measurements were used to calculate the link rotation angle. Furthermore, an LVDT was attached to an L-shaped frame (Figure 3.2) which was welded to one of the brace-to-link joints. This LVDT measured the tangential deviation of one of the link ends with respect to the other and provided a control measurement. Both the

approaches are affected by the deformations that take place in members outside of the link. The individual link end measurements are influenced by the global rotation of the test frame due to the flexibility at the pins and also by the slip that takes place in splice connections. These influences are eliminated when the tangential displacements are measured, however, the tangential measurements are adversely affected due to the rotation at link ends which in turn creates a rotation of the L-shaped frame. The link rotation angles monitored by making use of the two aforementioned techniques differ for low values of link rotation angles that correspond to elastic behavior. For larger values of link rotation angles, however, the measured values by these two methods are very close to each other. Earlier tests reported by Bozkurt and Topkaya [8] revealed that estimating link rotation angles by using individual link end measurements is suitable for cases where minimal slip takes place in the splice connections. Since slip critical bolted type connections are utilized in the present study, link rotation angles calculated based on individual link end measurements were used during the experiments.

Strain gauges were placed at the mid-length of braces and beams outside the link for monitoring the axial forces in these members.

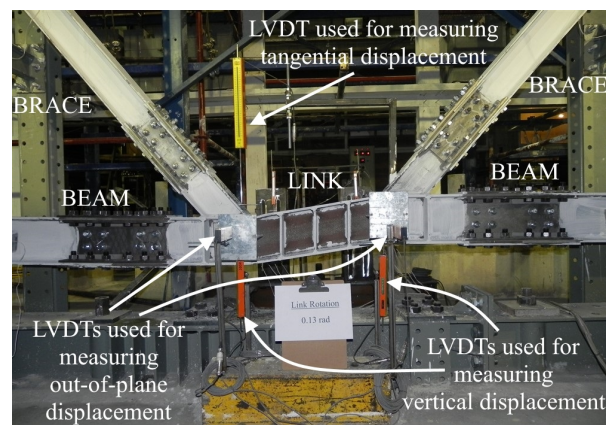


Figure 3.2. Instrumentation used for monitoring link rotation angle

3.2.2 Details of Specimens

Based on an initial investigation and considering the objectives of the study as well as the limitations of the testing facility, it was decided to test a total of 14 link specimens. It should be clarified that six of these specimens were tested by another PhD student (Bozkurt [251]) whereas the remaining eight specimens were tested by the author. All the results were however analyzed and synthesized herein.

Hysteretic behavior of shear links depends significantly on the stiffening of the link and web slenderness [82]. Consequently, these two factors were considered as the prime variables during the specimen selection. The AISC Seismic Provisions [248] provide stiffener spacing requirements for a given amount of plastic link rotation angle (γ_p). Properly stiffened links with stocky webs are expected to experience large inelastic deformations without experiencing severe shear buckling of the web. On the other hand, links with slender webs having widely spaced stiffeners are expected to experience severe shear buckling of the web during inelastic excursions. Furthermore, rolled and built-up members can behave differently because welds used for connecting the web to the flanges can adversely affect the LCF behavior. Based on this discussion, it was decided to test two different link cross sections that represent two of the extremes. A data compiled during the literature review of Chapter 2 demonstrated that the previous tests conducted on shear links have mostly employed h/t_w values in the range of 15 to 55, where h is the web height as defined per AISC 341-16 [248]. A link made from European rolled HEA160 section with a nominal h/t_w of 17 was selected to represent the stocky web case without additional welding. For this cross section, the required stiffener spacing (a) is equal to 149.6 mm for a γ_p of 0.08 radians according to the AISC Seismic Provisions [248]. A link length of 600 mm was considered for HEA160 links except for one specimen where the link length was 800 mm. Equally spaced single-sided stiffeners were provided with a spacing of 150 mm for the 600 mm long specimens and 133 mm for the 800 mm long specimens. On the other hand, a built-up link, designated as BU250 hereafter, with a nominal h/t_w of 46 was selected to represent a slender web case

which requires welding. A link length of 640 mm was considered for BU250 links. Although, the required stiffener spacing (a) for this link is equal to 100 mm for a γ_p of 0.08 radians according to the AISC Seismic Provisions [248], it was decided to use single-sided stiffeners with a spacing of 128 mm due to the following reasons. A larger spacing would promote shear buckling of the web plate and its influence on low-cycle fatigue can be investigated. Furthermore, not all links are stiffened for $\gamma_p = 0.08$ rad in practice and the stiffener spacing is determined based on the link rotation demand calculated at the design stage. The plastic link rotation capacity, according to the AISC Seismic Provisions [248], is equal to 0.065 rad for BU250 specimens based on the provided stiffener spacing. It is worth noting that, based on the recommendation of Okazaki et al. [37], stiffener welds were terminated at a distance of $5t_w$ from the k-line of each link section.

The rolled links were cut from two different heats of HEA160 I-sections whereas the built-up BU250 links were fabricated from two plates of 5 mm and 10 mm nominal thickness. All specimens were nominally made of the commonest European S275 steel with a yield stress of 275 MPa and ultimate stress of 430 MPa. Although, the selected material type is expected to have an influence on the LCF behavior, the same type of material was selected for both the rolled and built-up specimens to observe the variation in the behavior of such links by keeping the material properties the same. That way, the influence of geometrical properties on the response can be directly studied. Further elaboration of the issue and the extension of findings to links made from other steel materials are presented later.

The selected link sections satisfy the compactness limits given in the AISC Seismic Provisions [248] for shear links. In general, links should satisfy the requirements of highly ductile members. The only exceptions are the flanges of shear links which are allowed to satisfy the requirements of moderately ductile members. The flange slenderness for the HEA160 is 8.90 which is less than the slenderness limit of 10.24 for sections made of S275 steel according to the AISC Seismic Provisions [248]. Similarly, HEA160 sections are classified as Class 1 cross sections according to

Eurocode 3 [252] and are allowed to be used for Ductility Class High (DCH) systems according to Eurocode 8 [142]. No distinction is made between shear and intermediate links in Eurocode 8 [142] in terms of the required section classification. Therefore, HEA160 is well suited for use in EBFs as links. The same observations are valid for BU250 sections.

Archetype designs conducted by various research teams were considered by Bozkurt and Topkaya [8] to identify the range of nominal shear capacities possessed by shear links used in practical applications. A survey consisting of 19 archetypes with 3 to 12 stories revealed that the nominal capacity changes between 90 kN and 1324 kN with an average of 502 kN. The specimens selected in the present study belong to the lower portion of this range since the specimen selection was also limited by the available equipment capacity. Although the HEA160 link is relatively small in size when compared with typical links used in practice, it is considered as a reasonable section for studying the LCF behavior of links with stocky webs. The BU250 link section is, however, among the sections that can be used in practice for the upper stories in multistory EBFs. It is worth mentioning that, previous experimental studies such as [18, 28, 35, 45] have also used sections with similar nominal capacities to those used in the present paper.

The nominal and measured dimensions of the rolled and built-up sections as well as the material properties obtained from tensile coupon tests are summarized in Table 3.1 and Table 3.2, respectively. The coupons were extracted and tested according to EN 10002 [253] and the values reported in Table 3.2 are the average of two coupon test results. The material test results were all reasonable considering the nominal properties of S275 steel, except those found for flanges of the BU250 links. According to Table 3.2 as well as Figure 3.3, which depicts the typical stress-strain curves obtained from the coupon tests, the measured yield stress for flanges of the BU250 specimens was notably higher than the nominal value of 275 MPa. It should be emphasized that, the issue was in contrast to the mill certificate provided by the fabricator and was noticed only after the fabrication of the specimens and during the

coupon tests. Since the web material has the dominant role in the behavior of short links, the issue was considered to have a minor effect on the obtained results.

Table 3.1 Nominal and measured dimensions of the rolled HEA160 and built-up BU250 sections

Section	Heat	d (mm)		b_f (mm)		t_w (mm)		t_f (mm)	
		Nom.	Meas.	Nom.	Meas.	Nom.	Meas.	Nom.	Meas.
HEA160	1	152	153.04	160	160.05	6	6.37	9	8.85
HEA160	2	152	152.74	160	159.87	6	6.64	9	8.84
BU250	-	250	248.93	120	120.37	5	4.91	10	9.99

d = section depth; b_f = flange width; t_w = web thickness; t_f = flange thickness

Table 3.2 Material properties of the rolled HEA160 and built-up BU250 sections

Section	Heat	Web					Flanges				
		F_{yl}	F_{yu}	$F_{y,0.2}$	F_u	%EL	F_{yl}	F_{yu}	$F_{y,0.2}$	F_u	%EL
HEA160	1	283	298	289	426	32	278	294	285	421	35
HEA160	2	275	291	278	421	33	281	300	290	426	32
BU250	-	269	281	278	378	35	-	-	354	519	29

F_{yl} = lower yield stress (MPa); F_{yu} = upper yield stress (MPa); $F_{y,0.2}$ = yield stress at 0.2% permanent elongation (MPa); F_u = ultimate stress (MPa); %EL = percentage of elongation

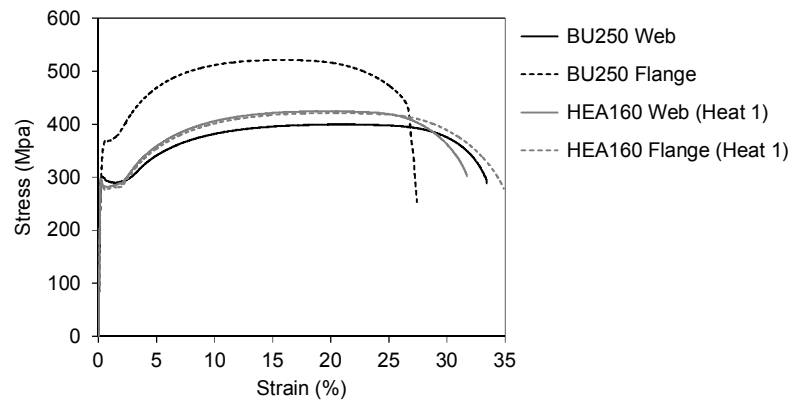


Figure 3.3. Typical stress-strain curves observed in the coupon tests

Table 3.3 Details of the tested specimens

#	Section	Heat	Connection Type	e (mm)	ρ		V_n (kN)		Loading Protocol
					Nom.	Meas.	Nom.	Meas.	
1	HEA160	1	Direct	600	1.19	1.28	133	146	0.03 rad ^a
2	HEA160	1	Direct	600	1.19	1.28	133	146	0.06 rad ^a
3	HEA160	2	Direct	600	1.19	1.29	133	148	0.09 rad ^a
4	HEA160	1	Direct	600	1.19	1.28	133	146	0.12 rad ^a
5	HEA160	2	Gusset-PL	600	1.19	1.29	133	148	0.15 rad ^a
6	HEA160	2	Gusset-PL	800	1.59	1.72	133	148	0.20 rad ^a
7	BU250	-	End-PL	640	1.25	0.98	190	182	0.03 rad ^a
8	BU250	-	End-PL	640	1.25	0.98	190	182	0.09 rad ^a
9	BU250	-	End-PL	640	1.25	0.98	190	182	0.15 rad ^a
10	BU250	-	End-PL	640	1.25	0.98	190	182	0.09 rad (s) ^b
11	BU250	-	End-PL	640	1.25	0.98	190	182	AISC 341-16
12	BU250	-	End-PL	640	1.25	0.98	190	182	Arbitrary 1
13	BU250	-	End-PL	640	1.25	0.98	190	182	Arbitrary 2
14	BU250	-	End-PL	640	1.25	0.98	190	182	Arbitrary 3

^a Constant-amplitude cycles

^b Single-sided constant-amplitude cycles

Further details regarding the specimens are summarized in Table 3.3 and Figure 3.4. It is worth reiterating that the testing of the HEA160 specimens (specimens 1 to 6) was done by another PhD student (Bozkurt [251]) whereas the remaining eight BU250 specimens were tested by the author. In the table, V_n corresponds to the link shear strength determined as per the AISC Seismic Provisions [248]. The link lengths were selected to ensure that all specimens qualified as shear yielding links ($\rho^{nom} < 1.6$). Despite this, Specimen 6 qualified as an intermediate link because the measured web thickness was higher than the nominal thickness resulting in a measured link

length ratio (ρ^{meas}) of 1.72. The reclassification of Specimen 6 resulted in the violation of flange slenderness limits according to the AISC Seismic Provisions (AISC 2016a) but created no adverse effects according to Eurocode 8 [142]. Designers should bear in mind that such unintended changes in the link categorization can also occur in practical cases.

As shown in Figure 3.4, three different replaceable link details were considered in the experimental program. The first two are identical to the detail proposed by Bozkurt and Topkaya [8] where splice connections are utilized for the braces and the beam outside the link. The braces were connected to the beam by either direct attachment or by making use of gusset plates. The third detail is identical to the bolted extended end-plated replaceable link proposed by Mansour et al. [49]. The spliced replaceable link details were used for the HAE160 specimens whereas the bolted extended end-plated replaceable link detail was used for BU250 specimens. It should be emphasized that the focus of the study was on the LCF behavior of the links and the replaceable details did not have a main role in the experiments.

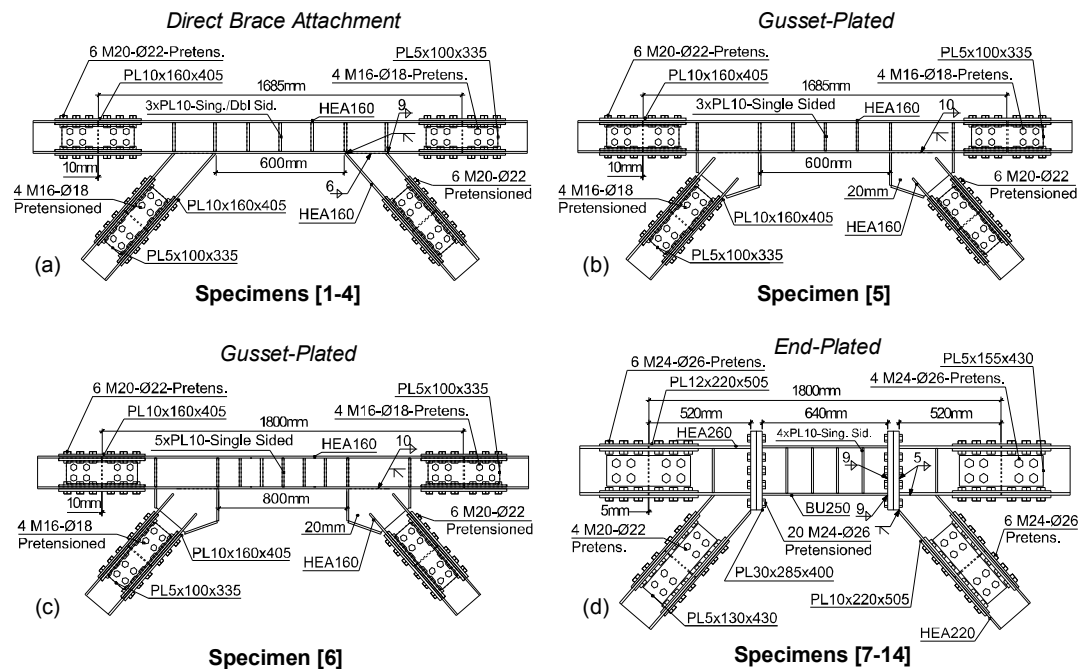


Figure 3.4. Details of the tested specimens

The specimens can be broadly classified into two categories. The first category (Specimens 1 to 10) belongs to specimens tested to study LCF life of shear links and the second category (Specimens 11 to 14) belongs to specimens tested to assess the reliability of the damage laws developed using the results of the LCF tests. As summarized in Table 3.3, Specimens 1 to 5 were nominally identical HEA160 links of length 600 mm and ρ^{meas} of 1.28 and 1.29. Specimens 1 to 5 were subjected to constant-amplitude cycles of $\gamma = \pm 0.03, \pm 0.06, \pm 0.09, \pm 0.12,$ and ± 0.15 rad. Specimens 1 to 4 utilized direct brace attachment detail (Figure 3.4a) whereas Specimen 5 utilized gusset-plated attachment detail (Figure 3.4b). On the other hand, Specimen 6 was a longer link with a length of 800 mm (Figure 3.4c) and a ρ^{meas} of 1.72 which was subjected to the largest constant-amplitude cycles of $\gamma = \pm 0.20$ rad.

Specimens 7 to 14 were identical built-up shear links with a ρ^{meas} of 0.98 which all utilized the end-plated replacement scheme (Figure 3.4d). It should be emphasized that the splices located in beams and braces of the end-plated detail (Figure 3.4d) were mandatorily included in the system due to changes which were made to the test setup. No sign of detrimental behavior was recorded during the tests for these splices, and therefore, the focus was on the LCF life of the link specimens. The only difference among Specimens 7 to 10 was the utilized loading protocol. Specimens 7 to 9 were tested under constant-amplitude cycles of $\gamma = \pm 0.03, \pm 0.09,$ and ± 0.15 rad whereas Specimen 10 was subjected to single-sided constant-amplitude cycles of $\gamma = +0.09$ rad. Specimens 11 to 14, on the other hand, were tested under more complicated loadings to assess the reliability of the developed damage laws. Details of the applied loading protocols are given in the following sections.

In all specimens, slip-critical type bolted connections, designed for forces corresponding to the fully yielded web or flange plates, were employed. The AISC Seismic Provisions [248] recommend bolts to be fully pre-tensioned and faying surfaces to have slip coefficients (μ) equal to or greater than 0.3 given for Class A surfaces as per AISC 360-16 [254]. Consequently, Grade 8.8 high-strength bolts, which conformed to ISO 898-1 [255], were utilized in the connections and fully pre-tensioned by making use of a calibrated torque wrench. Furthermore, all faying

surfaces were manually sand blasted to achieve Sa2.5 surface conditions, as per ISO 8501-1 [256], with a reported coefficient of friction in the range of 0.47 to 0.5 [257].

Welding details for all connections are indicated in Figure 3.4. In all welded connections Gas Metal Arc Welding was utilized with SG2 electrodes (similar to ER70S-6 electrodes) with a nominal tensile strength of 540 MPa. It should be noted that, in the built-up BU250 sections, the web was attached to the flanges using fillet welds of size 5 mm. The AISC Seismic Provisions [248] require complete-joint-penetration (CJP) groove welds for such connections, however, the fabricator recommended using fillet welds considering the rather thin web of the built-up section and the difficulty associated with its beveling. As shown Figure 3.4d, fillet welds were utilized to connect the built-up links to the end plates. In cases where a link connects to a column, the AISC Seismic Provisions [248] classify welds attaching link flanges to the column as demand critical. According to the Commentary of the AISC Seismic Provisions [248], demand critical welds are generally (CJP) groove welds so designated because they are subjected to yield level or higher stress demands. Development of satisfactory link-to-column connection details is the subject of ongoing research [38] and the Commentary recommends avoiding EBF configurations with links attached to columns. Recent tests on links connected to end plates with fillet welds [37] and link-to-column connections with all around fillet welds [41] showed acceptable performance. Based on these observations and the recommendations of the fabricator, it was decided to use fillet welds to connect BU250 links to the end plates. No detrimental behavior was observed due to the use of such welds as opposed to the use of CJP groove welds.

3.2.3 Loading Protocols for Reliability Assessment of the Damage Law

As stated in the previous section and summarized in Table 3.3, various loading protocols were utilized in the present study which are all depicted in Figure 3.5. The loading protocols were defined based on the total link rotation angle (γ). As discussed earlier, the difference between the vertical displacements recorded by the LVDTs

placed at the link ends (Figure 3.2) was divided by the link length (e) to obtain γ . Consequently, in each test, the displacement applied by the hydraulic actuator was monitored carefully and adjusted accordingly in order to follow the selected loading protocol appropriately.

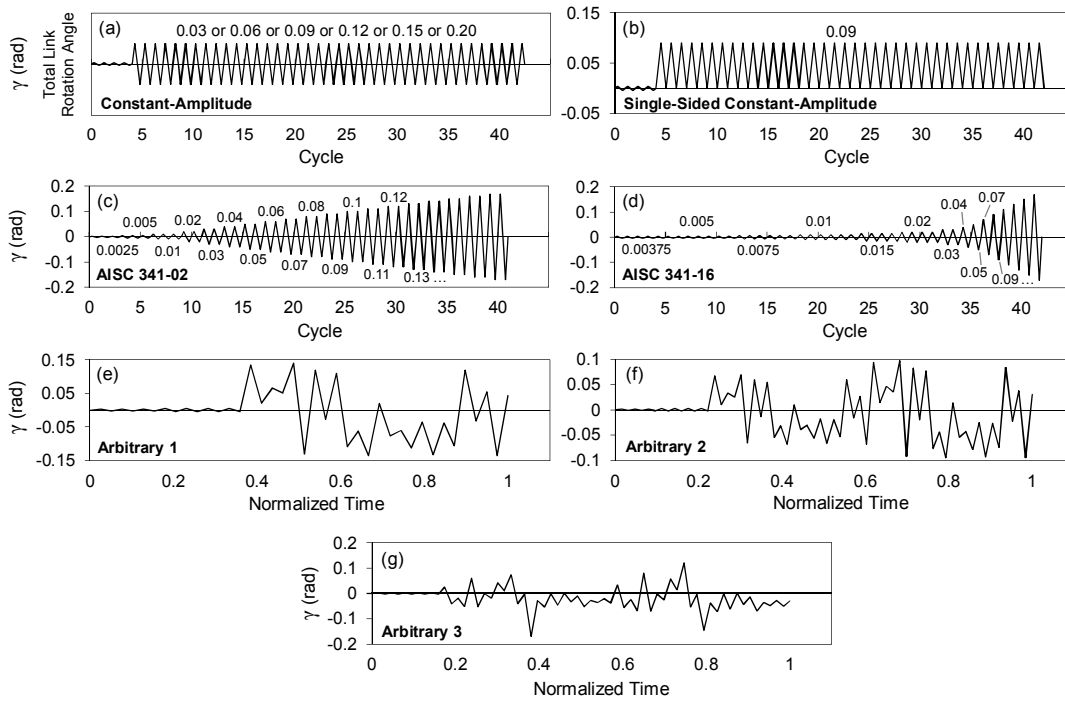


Figure 3.5. Utilized loading protocols in the experimental program

Based on Figure 3.5a, the loading protocol with constant-amplitude cycles, utilized for Specimens 1 to 9, contains four initial elastic cycles for checking the proper response of the test setup as well as the instrumentations. A similar procedure was followed for the loading protocol of Specimen 10 which is composed of single-sided constant-amplitude cycles of $\gamma = +0.09$ rad, as shown in Figure 3.5b.

In order to assess the reliability of the calibrated damage laws for each link section type (HEA160 and BU250), more complex loading protocols with proportional and non-proportional loadings were considered. No additional tests were conducted for the reliability assessment of the damage law calibrated for HEA160 links, and

instead, results from two experiments conducted by Bozkurt and Topkaya [8] were considered where HEA160 links with similar strength and a length of 600 mm were tested under proportional loading protocols. The first of these specimens was subjected to the loading protocol of AISC 341-02 [75], and the second one was subjected to the loading protocol of AISC 341-16 [248], which are shown in Figure 3.5c and Figure 3.5d, respectively. These protocols (generally referred to as the *old* and *revised* protocols) are originally intended to be used for qualifying the cyclic behavior of link-to-column connections in EBFs, however, they have been frequently used in previous studies for investigating the behavior of isolated links as well as EBFs with internal links (i.e. links located in the middle portion of floor beams).

For reliability assessment of the damage law for BU250 links, Specimen 11 was subjected to the revised protocol whereas Specimens 12 to 14 were respectively subjected to the three arbitrary loading protocols depicted in Figure 3.5e to Figure 3.5g. The loading protocol designated as Arbitrary 1 (Figure 3.5e) is identical to the random loading protocol proposed and previously used by Okazaki and Engelhardt [39] which imposes relatively large excursions during early cycles. The loading protocol shown in Figure 3.5f, i.e. Arbitrary 2, is in fact a combination of two consecutive loading scenarios: (i) the random loading protocol of Okazaki and Engelhardt [39] amplified by 0.50 followed by (ii) the same random loading protocol amplified, this time, by 0.70. The last loading protocol, i.e. Arbitrary 3 (Figure 3.5g), was, on the other hand, generated in the course of the present study to represent a more realistic loading similar to an earthquake-induced one. Therefore, the protocol was proposed based on a history of link rotation angle reported by Richards [48] from a nonlinear time-history analysis of a 3-story EBF with short links. The history was first simplified and then applied two times consecutively during the Arbitrary 3 loading protocol: (i) once with an amplification factor of 1.5 followed by (ii) a second time with an amplification factor of 2.0. The idea behind amplifying the response was to observe failure of the specimen under the applied loading history. The arbitrary loading protocols were experimented after the LCF tests were

completed and the damage law was calibrated. Based on this calibration, the expected damage to the link by applying the original form of the link rotation history of Richards [48] was estimated to remain well below the link fracture level. Therefore, several different alternatives were considered and finally it was decided to amplify the loading history by 1.5 and 2.0 and subsequently apply it to Specimen 14. It is worth noting that, effects of special phenomena such as ratcheting were not included in the arbitrary loading protocols investigated in the present study. EBF structures can in some cases exhibit ratcheting behavior under strong earthquakes [173]. Numerical studies should be conducted to determine the amount of residual deformations in such cases, which have a paramount impact on decisions for demolition and repair.

3.3 Experimental Results

The hysteretic response of the tested rolled HEA160 as well as built-up BU250 specimens is presented in Figure 3.6 and Figure 3.7, respectively, in terms of link shear (V) versus total link rotation angle (γ). The method utilized for obtaining γ from the measurements was discussed earlier. The link shear, on the other hand, was determined as $V = Fh_{col}/L_{bay}$, where F is the force applied by the actuator, h_{col} is the distance between the column end pins (i.e. 2700 mm), and L_{bay} is the bay width which is equal to 5000 mm according to Figure 3.1. A summary of experimental results is also presented in Table 3.4.

The maximum total and plastic link rotation angles (γ^{max} and γ_p^{max}) experienced by the link are reported in Table 3.4. For all specimens except Specimen 11 these values are in fact equal to the maximum applied rotations. On the other hand, for Specimens 11 which was tested under the revised protocol, the γ^{max} and γ_p^{max} values were determined according to AISC 341-16 [248]. It should be noted that, the γ values recorded in the tests were converted to γ_p using $\gamma_p = \gamma - V/K$, where K is the link elastic stiffness which was determined as 21000 kN/rad for the HEA160 links and as 67600 kN/rad for the BU250 links. Further details regarding the determination of K

can be found in Bozkurt and Topkaya [8]. For tests conducted under constant-amplitude cycles (i.e. Specimens 1 to 10) the *number of cycles to failure* (N_f) is also reported in Table 3.4 considering two criteria: (i) the instant at which V dropped below the measured link shear strength (i.e. V_n^{meas} based on Table 3.3) and (ii) the instant at which fracture was observed during the test. These two criteria offer very similar results for most of the specimens because, as shown in Figure 3.6 and Figure 3.7, the loss of shear strength was very sudden and no gradual reduction in strength was observed after the initiation of fracture. Only in Specimen 1 the fracture was observed after the 113th cycle and the capacity dropped below the measured link strength after the 117th cycle.

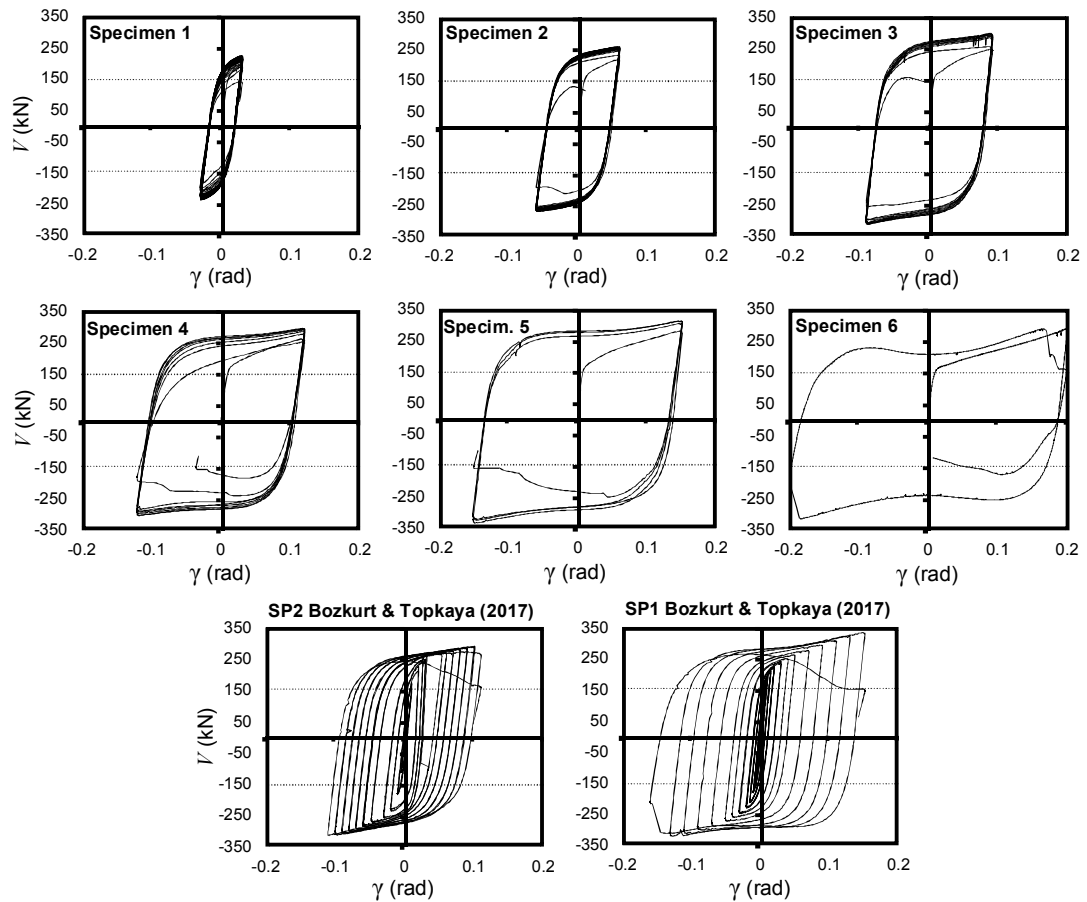


Figure 3.6. Hysteretic response of Specimens 1–6 of the present study and SP2 and SP1 from Bozkurt and Topkaya [8] (rolled HEA160 links)

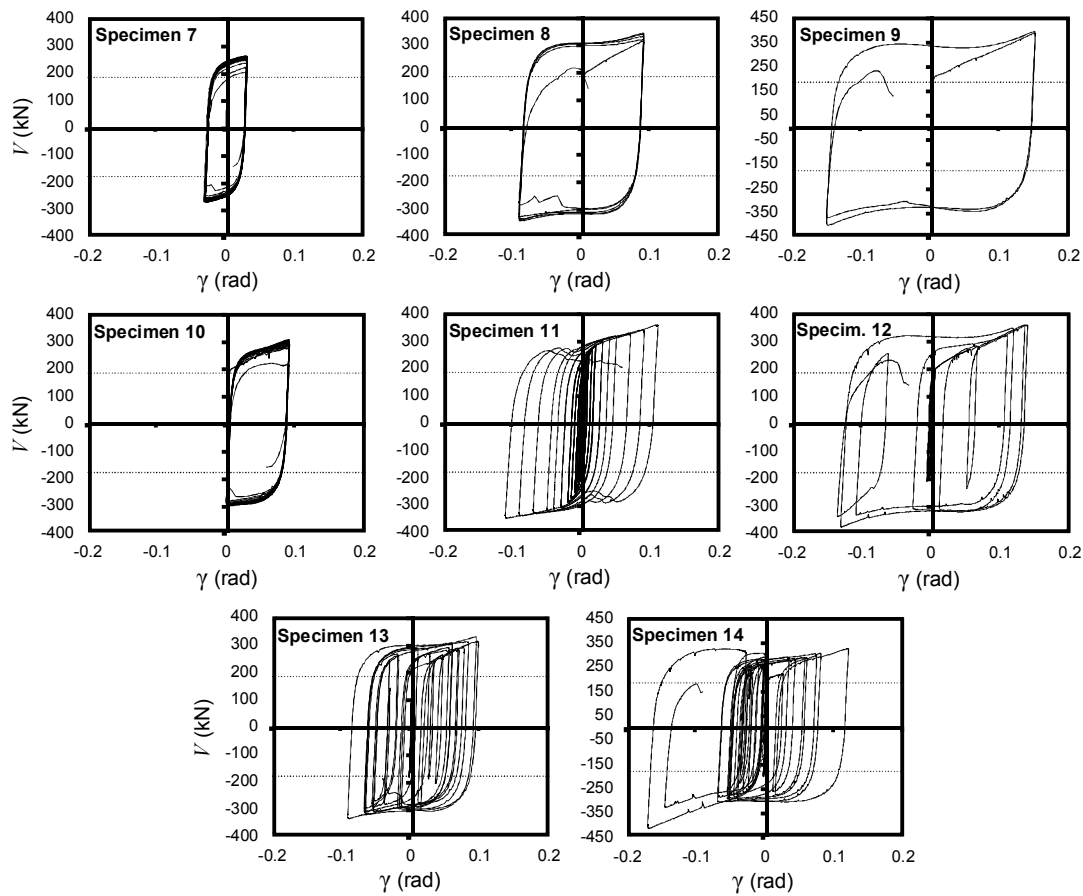


Figure 3.7. Hysteretic response of Specimens 7–14 (built-up BU250 links)

The observed failure modes are summarized in Table 3.4 and depicted in Figure 3.8. In general, two distinct failure modes were observed, namely web fracture and flange fracture. For Specimens 1-3, which were HEA160 links subjected to 0.03 rad, 0.06 rad, and 0.09 rad constant-amplitude cycles, web fracture (Figure 3.8a) was dominantly observed. Specimens 4-5 which were very similar to Specimens 1-3, however, subjected to larger rotations, exhibited severe flange buckling followed by flange fracture (Figure 3.8b). The only intermediate link (Specimen 6) which was tested under the largest link rotation angle of 0.20 rad also exhibited severe flange buckling and fracture. No signs of web buckling were observed for HEA160 links which had a low h/t_w ratio. These specimens were provided with stiffeners with a spacing calculated based on a plastic link rotation capacity of 0.08 rad. Although

Specimens 4 to 6 were subjected to larger plastic rotation angles, the webs of these links exhibited stable behavior without shear buckling. Flange buckling observed in HEA160 links is due to the relatively high flange slenderness of these members. Although the flanges satisfied the slenderness limits for shear links as per the AISC Seismic Provisions [248] and Eurocode 8 [142], flange buckling was observed at large link rotation angles that eventually lead to fracture of these flanges. The intermediate link (Specimen 6) did not satisfy the flange slenderness limit given in the AISC Seismic Provisions [248], however, qualified as a Class 1 cross section that can be used for DCH systems according to Eurocode 8 [142]. Nevertheless, this specimen also experienced severe flange buckling leading to fracture of the flange.

Table 3.4 Summary of experimental results

#	γ^{max} (rad)	γ_P^{max} (rad)	N_f		Failure Mode
			$V < V_n^{meas}$	Fracture	
1	0.030	0.020	117	113	Web Fracture at Edges ^a <i>a, b, c</i>
2	0.060	0.048	22.5	22	Web Fracture at Edges <i>a, b, c</i>
3	0.090	0.076	10	9	Web Fracture at Edges <i>a, c</i>
4	0.120	0.110	7.5	6.5	Severe Flange Buckling and Fracture
5	0.150	0.135	4	3.5	Severe Flange Buckling and Fracture
6	0.200	0.187	1	0.5	Severe Flange Buckling and Fracture
7	0.030	0.026	36.5	36	Web Fracture at Edge <i>d</i>
8	0.090	0.084	5	4.5	Web Fracture at Edges <i>c, d</i>
9	0.150	0.145	1.5	1.5	Web Fracture at Edges <i>c, d</i>
10	0.090	0.086	16	15.5	Web Fracture at Edges <i>a, d</i>
11	0.110	0.105	-	-	Web Fracture at Edges <i>a, d</i>
12	0.140	0.134	-	-	Web Fracture at Edges <i>a, d</i>
13	0.095	0.090	-	-	Web Fracture at Edges <i>a, b</i>
14	0.170	0.164	-	-	Web Fracture at Edges <i>b, d</i>

^a In each web panel, the top edge is designated as *a*, right edge as *b*, bottom edge as *c*, and left edge as *d*.



Figure 3.8. Typical failure modes: (a) web fracture in HEA160 links; (b) severe flange buckling and fracture in HEA160 links; (c) web fracture in BU250 links

For the built-up BU250 links (i.e. Specimens 7 to 14), the only dominant failure mode was web fracture (Figure 3.8c). It is worth noting that, in Table 3.4, pattern of the observed web fractures is also presented by reporting the torn edges of the fractured web panel. Edges of each web panel are designated with *a*, *b*, *c*, and *d* as defined in this table. For instance, Figure 3.8c depicts a web fracture where Edges *c* and *d* were ruptured. The results summarized in Table 3.4 demonstrate that in most cases at least one line of fracture occurred in the vicinity of the stiffener-to-web welds provided that the failure mode was web fracture.

Due to the high h/t_w and the rather large stiffener spacing in the BU250 links, unlike the shallow HEA160 links, web buckling was clearly observed in Specimens 7 to 14. Signs of such web buckles are visible in Figure 3.8c. The codified plastic rotation angle capacity of BU250 links is 0.065 rad as per AISC 341-16 [248] for the provided stiffener spacing. The test results revealed that web buckles formed at relatively low values of plastic rotation ($\gamma_p \approx 0.02$ rad), however, the effect of web buckling on the link shear strength became more pronounced at larger plastic rotations. For instance, although buckles formed at very early stages of loading in Specimen 11 which was subjected to the revised protocol, strength degradation initiated at the cycle of 0.062 rad of plastic rotation, which is close to the rotation capacity predicted by the AISC Seismic Provisions [248] for this specimen.

Experiments were conducted by other researchers in the past to investigate the implications of having fewer number of stiffeners than required for a plastic link

rotation capacity of 0.08 rad. Tests conducted by Okazaki and Engelhardt [39] and Ji et al. [258] showed that specimens with fewer stiffeners experienced web buckling at low levels of link rotation, however, these links were deemed to have an acceptable performance by sustaining plastic rotations in excess of 0.08 rad. A similar observation can be made based on the findings from Specimen 11. This specimen sustained 0.105 rad of plastic rotation before failure although fewer number of stiffeners were employed. The implications of having less number of stiffeners from a LCF standpoint are discussed in the following sections.

3.4 Low-Cycle Fatigue Behavior of Specimens

Specimens 1 to 6 (HEA160 links) as well as Specimens 7 to 10 (BU250 links) were experimented under constant-amplitude cycles (Figure 3.5a-b) to have a direct investigation on the LCF behavior of links. The N_f values reported in Table 3.4 clearly demonstrate that increasing the *cycle range* will result in a significant decrease in the number of cycles to failure. Cycle range ($\Delta\gamma$) is the difference between the maximum and minimum rotation angles experienced by a link during a cycle. It is worth noting that, *plastic cycle range* ($\Delta\gamma_p$) can also be defined similarly as the difference between the maximum and minimum plastic rotation angles (e.g. for Specimen 3, tested under constant-amplitude cycles of $\gamma = \pm 0.09$ rad, the cycle range is $\Delta\gamma = 0.18$ rad and the plastic cycle range is $\Delta\gamma_p = 0.152$ rad). According to Table 3.4, for instance, Specimen 1 sustained 113 cycles of range 0.06 rad prior to fracture whereas the almost identical Specimen 5 endured only 3.5 cycles of range 0.30 rad before fracture. Results for Specimen 6 demonstrated an extreme case in which the link was not even able to sustain one full cycle prior to fracture.

Another important issue deduced from the experimental results is the effect of web buckling on the LCF behavior of shear links. As it can be seen in Table 3.4, the HEA160 links have sustained significantly more number of cycles prior to failure compared to the BU250 links when subjected to identical loading protocols. For

instance, Specimen 3 (HEA160) endured 9 cycles of range 0.18 rad while Specimen 8 (BU250) failed during the 5th cycle of the same range.

The constant-amplitude test results substantiate the fact that, LCF-induced fracture is not solely dependent upon the maximum rotation experienced by a link and is rather a matter of the accumulation of damage. Thus, during a strong earthquake, an EBF link might fail by experiencing a number of cycles of moderate rotations or by experiencing a very few number of large cycles. On the other hand, a link might remain fully intact if it experiences, for instance, only one cycle of rather large rotation or a few numbers of one-sided large rotations. Therefore, assessing the performance of an EBF system solely based on the maximum rotation exhibited by its links might not be fully accurate. It is worth noting that, a similar approach is currently in use by a number of codes and standards such as ASCE 41-13 [249]. Consequently, in the following sections, a cumulative measure for assessing the performance of shear links is presented. The measure in fact provides an estimate on the exhausted and remaining LCF life of a shear link under any loading scenario.

3.5 Calibration of a Cumulative Damage Law for Specimens Tested as a Part of the Present Research Program

Based on the experimental results and the previous discussions, a damage law is calibrated in this section for the HEA160 and BU250 specimens tested as a part of the research program. Various damage models are available in the literature, however, in this study, the following well-known cumulative damage law is considered [259]:

$$D = C \sum_{i=1}^N (\Delta\gamma_{pi})^c \quad (3.1)$$

where D is the amount of damage which lies in the range of 0 (undamaged) to 1.0 (failed), N is the number of inelastic cycles, $\Delta\gamma_{pi}$ is the plastic range of the i^{th} cycle,

and C and c are the structural performance parameters. The Coffin-Manson relation and the Palmgren-Miner rule form the basis of the damage law. The former suggests that:

$$N_f = C^{-1} (\Delta\gamma_p)^{-c} \quad (3.2)$$

which indicates if identical steel components are tested under constant-amplitude cycles, however, each one under a different plastic cycle range of $\Delta\gamma_p$, the relation between N_f and $\Delta\gamma_p$ will be a power function (i.e. linear on a log-log plot). The Palmgren-Miner rule, on the other hand, suggests that the damage from different cycles can be summed linearly. Thus, it can be deduced that in Equation (3.1) the power term $C(\Delta\gamma_{pi})^c$ represents the damage due to the i^{th} cycle which can be linearly summed for all inelastic cycles ($i = 1, 2, 3, \dots, N$) to obtain the total damage, D , under a full loading history.

Based on the damage law, if the structural performance parameters are calibrated properly and provided that the above-stated hypotheses are accurate, a shear link shall fail exactly when D approaches to unity. Although the limit of $D = 1.0$ cannot precisely pinpoint the instant of failure in reality, experiments conducted by Krawinkler et al. [259] demonstrated that the damage law is capable of providing good predictions for steel specimens failed under different modes. Furthermore, the damage law has been utilized extensively in the literature [260, 261] and is found to be a convenient tool for investigating the LCF behavior of steel members and accumulation of damage under non-uniform strain histories.

Given that working with total link rotations instead of plastic link rotations can be more convenient in practical cases, the damage law and Coffin-Manson relation presented in Equations (3.1) and (3.2) can also be written in terms of cycle range as follows:

$$D = \bar{C} \sum_{i=1}^{\bar{N}} (\Delta\gamma_i)^{\bar{c}} \quad (3.3)$$

$$N_f = \bar{C}^{-1} (\Delta\gamma)^{-\bar{c}} \quad (3.4)$$

where \bar{N} is the number of *damaging* cycles, $\Delta\gamma_i$ is the range of the i^{th} cycle, and \bar{C} and \bar{c} are the structural performance parameters calibrated based on cycle range instead of plastic cycle range. A similar approach was utilized previously by Richards and Uang [73] in the process of proposing the revised loading protocol. It should be emphasized that, when working with $\Delta\gamma$ instead of $\Delta\gamma_p$, a lower bound shall at least be defined to filter out small elastic cycles which will not induce any damage to the link. Richards and Uang [73] suggested this lower bound limit as 0.0075 rad and, therefore, termed any cycle with $\Delta\gamma > 0.0075$ rad a damaging cycle. The same approach is used in the present thesis.

According to Krawinkler [262], in order to calibrate the damage law, at least three constant-amplitude cyclic tests shall be performed. The results of these tests (i.e. the applied $\Delta\gamma_p$ or $\Delta\gamma$ of each test and the corresponding N_f) along with the Coffin-Manson relation (Equation (3.2) or (3.4)) can then be used for the calibration of C and c or \bar{C} and \bar{c} . The same procedure was followed in this chapter using the results found for Specimens 1-5 and 7-10. It is worth noting that, although Specimen 6 was also tested under constant-amplitude cycles, it was not included in the calibration process mainly due to the fact that it qualified as an intermediate link when measured properties were considered.

The calibration results are summarized in Figure 3.9. In this figure, each circle corresponds to one of the experimental results. The dashed lines, on the other hand, are power functions (see Coffin-Manson relation in Equation (3.2) or (3.4)) fitted to the test results. It should be emphasized that the N_f values used in this figure are those reported in Table 3.4 based on the criterion of fracture initiation. According to the table, the N_f values are mostly similar considering both criteria, however, the fracture

criterion was selected for the calibration since it was presumed to be more consistent with the theoretical basis of the damage law. Figure 3.9a depicts the dependency of N_f to the applied plastic cycle range ($\Delta\gamma_p$) which, as anticipated, is almost linear when the axes are in logarithmic scale. Figure 3.9b, on the other hand, presents the dependency of N_f to the applied cycle range ($\Delta\gamma$) which is also found to be linear in a log-log plot. This further confirms that the damage (D) can also be related to the cycle range, as in Equation (3.3), to be used more conveniently in practice.

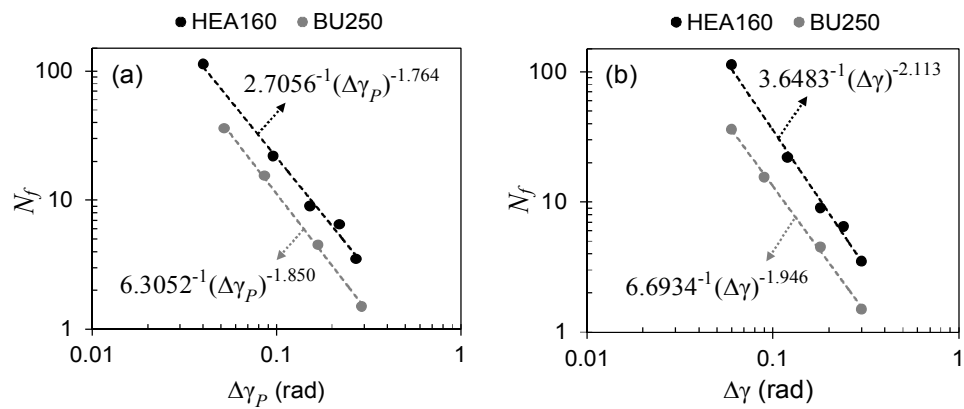


Figure 3.9. Calibration of the damage laws based on (a) plastic cycle range and (b) cycle range (axes are in logarithmic scale)

In each subplot of Figure 3.9, two sets of data are presented which correspond to the experimental results found for the rolled HEA160 links and built-up BU250 links. The markedly different behavior of HEA160 and BU250 links can be attributed to the cyclic web buckling observed in BU250 links which had a profound effect on the LCF life. It is worth noting that, although in the HEA160 tests Specimens 1-3 failed due to web fracture while Specimens 4-5 due to flange fracture (Table 3.4), the linearity of N_f versus $\Delta\gamma_p$ (or $\Delta\gamma$) was not affected notably as shown in Figure 3.9.

The equation corresponding to each of the fitted power functions is also reported in Figure 3.9. Comparing these fitted functions with Equations (3.2) and (3.4) will yield

the calibrated values of C and c as well as \bar{C} and \bar{c} for the HEA160 and BU250 links. The *calibrated damage laws* can consequently be summarized as follows:

$$D = \begin{cases} 2.7056 \sum_{i=1}^N (\Delta\gamma_{Pi})^{1.764} \\ 3.6483 \sum_{i=1}^{\bar{N}} (\Delta\gamma_i)^{2.113} \end{cases} \quad \text{for HEA160} \quad (3.5)$$

$$D = \begin{cases} 6.3052 \sum_{i=1}^N (\Delta\gamma_{Pi})^{1.850} \\ 6.6934 \sum_{i=1}^{\bar{N}} (\Delta\gamma_i)^{1.946} \end{cases} \quad \text{for BU250} \quad (3.6)$$

By knowing the number of inelastic cycles (N) or damaging cycles (\bar{N}) and inputting the associated plastic cycle ranges ($\Delta\gamma_{Pi}$) or cycle ranges ($\Delta\gamma_i$) into Equation (3.5) or (3.6), the LCF damage ($0 \leq D \leq 1.0$) experienced by an HEA160 or a BU250 shear link can readily be estimated. The calibrated powers in these equations are all above 1.0 indicating that the damage induced by a large cycle to a shear link is significantly more than that of a small cycle. It should be mentioned that, the calibrated damage laws are further generalized in next sections for practical use.

3.6 Verification of the Damage Law Using More Complicated Loading Histories

The calibration process was conducted based on the results of constant-amplitude cyclic tests. However, the main objective is to use the damage law for estimating the fracture life of an EBF shear link under any loading history. As discussed earlier, the reliability of the calibrated damage laws for HEA160 links (Equation (3.5)) was assessed based on the results reported by Bozkurt and Topkaya [8] for two HEA160 links, namely SP2 and SP1, with $e = 600$ mm. These links, which had similar strengths to those of Specimens 1 to 5 of the present study, failed at γ_p^{max} of 0.095 rad

and 0.135 rad (corresponding to γ^{max} of 0.11 rad and 0.15 rad) under the old and revised protocols of AISC, respectively (Figure 3.6). This was an expected outcome since previous studies have clearly demonstrated that the old protocol is overly severe for testing short links and would result in lower rotation capacities compared to the revised protocol [37, 73]. The reliability of the calibrated damage laws for BU250 links was, on the other hand, assessed by making use of the results for Specimens 11-14 which were tested under the revised and arbitrary loading protocols.

The loading protocol associated with each of these specimens is depicted in Figure 3.10 along with the instant of fracture observed in the test against the excursion at which the value of calibrated damage (found via Equation (3.5) or (3.6)) exceeds unity (i.e. $D > 1.0$). In other words, the figure compares the failure point observed in the test with that predicted by the calibrated damage laws. Furthermore, the accumulation of damage (D) is also plotted in the figure with grey dashed lines which start from zero (based on the secondary vertical axis on the right side of each subplot) and gradually increase along the loading history. The excursion at which this grey line hits the horizontal axis of $D = 1.0$ indicates fracture based on the calibrated damage laws. It should be emphasized that, for Figure 3.10, D is calculated based on cycle ranges ($\Delta\gamma_i$), however, almost identical results would have been found if plastic cycle ranges ($\Delta\gamma_{Pl}$) were utilized in the damage laws. Since cycle ranges are not obvious for Specimens 12-14 (tested under arbitrary loading histories) an algorithm was utilized for determining the damage which is thoroughly discussed in the following sections.

Results summarized in Figure 3.10 reveal that, the damage laws calibrated based on results of constant-amplitude cyclic tests are reliable and are able to predict the instant of fracture during proportional and arbitrary loading histories as well with a reasonable accuracy.

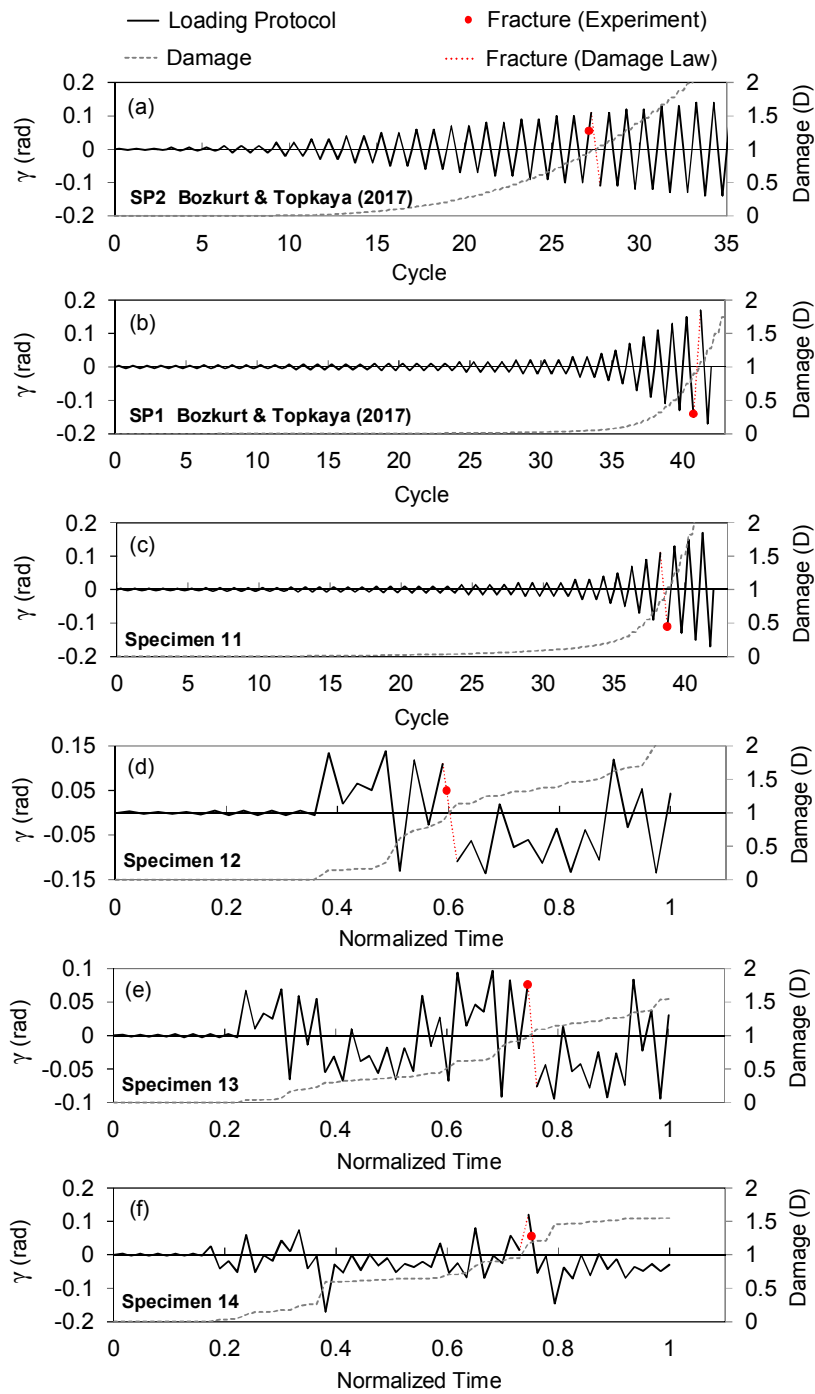


Figure 3.10. Comparison of the test results with predictions of the calibrated damage laws

3.7 Development of a Generalized Damage Law for Shear Links

Although the damage laws calibrated in the previous sections (Equations (3.5) and (3.6)) are reasonably accurate, they should be modified to be used in practical cases due to the fact that a number of limitations are associated with them. For instance, the link length ratios and geometrical as well as material properties of the specimens used in their calibration process limit their range of direct applicability. In order to propose a more comprehensive damage law for shear links, indeed many more number of specimens shall be tested. Nevertheless, having these limitations in mind, an attempt has been made in this section to expand the applicability range of the calibrated damage laws.

A comprehensive database compiled during the literature review of Chapter 2 revealed that the number of tests conducted previously on short links using constant-amplitude cycles is very limited. Therefore, the results obtained through these tests cannot be directly used for the calibration of both the power and the coefficient of the damage law. However, assuming the value of either of these unknowns, the other value can readily be determined. According to Equations (3.5) and (3.6), the calibrated powers (i.e. c and \bar{c}) for HEA160 and BU250 links are very similar despite the drastically different LCF lifespans observed for these two sets of specimens during the constant-amplitude tests (Table 3.4). On the other hand, the calibrated coefficients (C and \bar{C}) differ significantly for the two test sets. These are in line with the experimental observations of Krawinkler et al. [259] which suggest that the power is rather stable (between 1.5 and 2.0 for steel members under inelastic cyclic deformations) whereas the coefficient typically exhibits a considerable scatter.

The idea behind selecting the same grade of steel for HEA160 and BU250 links was to observe the difference in calibrated powers for these sets of specimens. The test results revealed that, although the calibrated powers are close to each other, there is still a variation in values even for the same material type. Furthermore, in general, the power is expected to be influenced by the selected grade of steel. While many more LCF tests on shear links with different grades of steel are required for an

accurate assessment, a decision on a representative power value can be made based on test data available in the literature. Dusicka et al. [263] studied the LCF behavior of plate steels through cyclic tension and compression testing of coupons. Apart from low yield strength materials, three different grades of steel were considered namely GR345, HPS485, and HT440 which conform to ASTM A709M, ASTM A709M HPS, and BT-HT440C standards, respectively. The measured yield strengths of GR345, HPS485, and HT440 were 353 MPa, 503 MPa, and 501 MPa, respectively. The calibrated powers (\bar{c}), determined based on applying the damage law presented in the present paper, are 1.78, 1.81, and 2.00 for GR345, HPS485, and HT440 specimens, respectively. The findings are in line with those of the present paper that HPS485 and HT440 specimens were found to have somewhat different powers although the yield strengths were similar. Kasai et al. [51] studied the LCF behavior of thick shear panels fabricated without welding. In addition to cyclic shear tests, these researchers also studied the LCF behavior under axial loading for Japanese steel grades SN400B and SM490A with yield strengths of 273 MPa and 332 MPa. The test results revealed that the calibrated powers (\bar{c}) are 1.82 and 1.81 for SN400B and SM490A, respectively, when the plates are subjected to cyclic shear whereas they are equal to 1.98 and 1.96 under axial loading. These results suggest that the direction of loading is also important in determining the value of the power. Salem Milani and Dicleli [264] studied the LCF performance of solid cylindrical components subjected to torsion. The calibrated power was equal to 1.65 for S355J2+AR steel rods having a yield strength of 404 MPa. Furthermore, results from these experiments on material response show that the power ranges mostly between 1.5 and 2.0. Considering the scarcity of the LCF data for EBF shear links and based on the experimental results presented in this chapter as well as those reported in the aforementioned tests on bare materials, mean powers of $c_m = 1.8$ and $\bar{c}_m = 2.0$ are conservatively suggested for practical use.

In the next step, to recommend a reasonable value for the coefficient of the damage law, appropriate tests conducted previously by other researchers on shear links were carefully examined. It should be emphasized that, due to the difficulties associated

with working with plastic link rotations, only the coefficient \bar{C} was investigated. To this end, first, the instant of fracture (T_{fr}) was determined in each test as the point of a notable drop in the load carrying capacity of the link. The determined instant was also checked to comply with the reported experimental observations. Afterward, it was assumed that the time $T = T_{fr}$ corresponds to the state of full damage, i.e. $D = 1.0$. Finally, using Equation (3.3), assuming $D = 1.0$, $\bar{c} = \bar{c}_m$, and determining the number of damaging cycles (\bar{N}) corresponding to the timespan of $T = 0$ to T_{fr} , the value of \bar{C} was back-calculated for each of the investigated specimens.

Although the original dataset compiled during the literature review of Chapter 2 contained 218 specimens, a total of 59 links were considered in this section which were all short steel links ($\rho \leq 1.6$) tested cyclically. The selected specimens did not exhibit any premature fractures as a result of issues such as connection failure or low weld quality. Specimens that were stiffened for a plastic link rotation capacity of 0.08 rad according to the AISC Seismic Provisions [248] as well as the ones with fewer number of stiffeners were both considered.

The data set consists of specimens 4, 7, 9 from Hjelmstad and Popov [15], specimens 17, 23 from Malley and Popov [17], specimens 3 and 7 from Kasai and Popov [18], specimens D1 and D2 from Ricles and Popov [70], specimens 4C, 8, 10, 4A-RLP, 4C-RLP, 8-RLP, 10-RLP, 12, 12-RLP, 12-SLP from Okazaki et al. [37], specimens S1, S2, S3, S4, S10 from Okazaki and Engelhardt [39], specimens NAS, AISC-5, AISC-6 from Okazaki et al. [41], specimen H485 from Dusicka et al. [44], specimens L11C, L11D, L12, L13, L22, Q13, Q21, Q22 from Ji et al. [258], specimens RSL-2, RSL-3, RSL-4, RSL-5, RSL-6-2, RSL-6-3, RSL-7, RSL-8, RSL-9, RSL-10 from Liu et al. [265], specimen EPM-11B from Mansour et al. [49], specimens SP1, SP2 from Bozkurt and Topkaya [8], and specimens 1 to 11 (except Specimen 6) tested as a part of the present thesis. It should be noted that the specimens S6 and S9 from Okazaki and Engelhardt [39] were excluded from the data set because these specimens were identical to the S4 specimen except the welding process used for connecting the stiffeners to the link. The S4 specimen showed a much better performance as

compared to S6 and S9. Shielded metal arc welding (SMAW) was used for specimen S4 while self-shielded flux cored arc welding (FCAW) was used for specimens S6 and S9. The lower fracture toughness and higher heat input of the FCAW process was considered responsible for poorer performance of specimens S6 and S9 by Okazaki and Engelhardt [39]. Furthermore, specimens AISC-4 and AISC-7 from Okazaki et al. [41] were also excluded from the data set because these specimens were identical to the AISC-6 specimen of Okazaki et al. [41] except the details adopted for connecting the link to the column. AISC-4 utilized all around fillet welds while AISC-7 utilized supplemental web doubler stiffeners. The specimen AISC-6 performed substantially better than these two specimens and the poorer behavior of AISC-4 and AISC-7 can be attributed to the problems particular to the link-to-column connection detailing.

The back-calculated \bar{C} values for the specimens were recorded which ranged approximately from 2.0 to 50. Many factors are known to influence the link LCF behavior. These include but are not limited to the dimensions of the link section, material properties, mode of failure, stiffener detailing, link length ratio, type of connection at end of the link, and quality of workmanship. A careful examination of the data revealed that the calculated \bar{C} values are significantly influenced by the material properties of the link web and the web buckling behavior. A mechanical model proposed by Kasai and Popov [82] was adopted to represent the calculated \bar{C} values. The following expression was developed by Kasai and Popov [82] to calculate the link rotation angle at buckling:

$$2\gamma_u \approx \bar{\gamma}_B = 8.7K_s(\hat{\alpha}) \frac{1}{\hat{\beta}^2} \quad (3.7)$$

where γ_u , is the rotation angle at which buckling is anticipated for the link web under cyclic loading and, as discussed by Kasai and Popov [82], is the rotation capacity that should be considered for the ultimate design of a link, $\bar{\gamma}_B$ is the link rotation angle measured from the farthest point of zero shear to the point of buckling, K_s is

the plate buckling coefficient, $\hat{\alpha}$ is the web panel aspect ratio (a/h , where a is the stiffener spacing), and $\hat{\beta}$ is the web panel height to thickness ratio or, in other words, web slenderness (h/tw).

It is worth noting that, as discussed by Kasai and Popov [82], $2\gamma_u$ is only about 5 to 10 percent larger than $\bar{\gamma}_B$. The plate buckling coefficient, K_s , can be determined as follows considering clamped-end conditions for the link web:

$$K_s(\hat{\alpha}) = \begin{cases} 8.98 + \frac{5.60}{\hat{\alpha}^2} & \text{if } \hat{\alpha} \geq 1 \\ 5.60 + \frac{8.98}{\hat{\alpha}^2} & \text{if } \hat{\alpha} \leq 1 \end{cases} \quad (3.8)$$

The calculated \bar{C} values were normalized by $(1000F_y/E)$ where E is the elastic modulus of steel material and the measured yield strength of the web was used as F_y . The normalized values are plotted with respect to γ_u in Figure 3.11. In Figure 3.11a the entire data is presented while in Figure 3.11b a close-up view is provided which focuses on data points with normalized \bar{C} values less than 14. As shown in this figure the adopted mechanical model can successfully capture the trend of the data provided that the calculated \bar{C} values are normalized by the yield stress of the web material. Two ranges of behavior are identified from Figure 3.11. For the range of γ_u between 0.035 rad and 0.11 rad there is a drastic decrease in the \bar{C} values with an increase in γ_u . For values of γ_u larger than 0.11 rad, however, the \bar{C} values approach a plateau which can be represented by a single constant. The threshold of $\gamma_u = 0.11$ rad can also be justified by examining the behavior of links during the experiments. A detailed investigation of the literature revealed that the specimens with $\gamma_u < 0.11$ rad typically experienced severe web buckling during the tests whereas specimens with $\gamma_u \geq 0.11$ rad generally exhibited stable web behavior until fracture. In other words, the data presented in Figure 3.11 suggests that for webs that behave in a stable manner the most influential factor on the LCF life is the material of the web whereas for webs that experience severe buckling, the LCF life is influenced not only by the

material of the web, but also by γ_u which depends on the web panel aspect ratio and web slenderness.

The behavior shown in Figure 3.11 further substantiates the selection of two different link sections for studying LCF of shear links in the present study. The HEA160 specimens with proper stiffening and stocky webs have γ_u values in the range of 0.13 to 0.15 radians and behaved in a stable manner during the experiments. The differences in γ_u values are due to the differences in measured dimensions between the specimens. On the other hand, the BU250 specimens with wider stiffener spacing and slender webs have a γ_u value equal to 0.069 radians and experienced significant web buckling during the experiments.

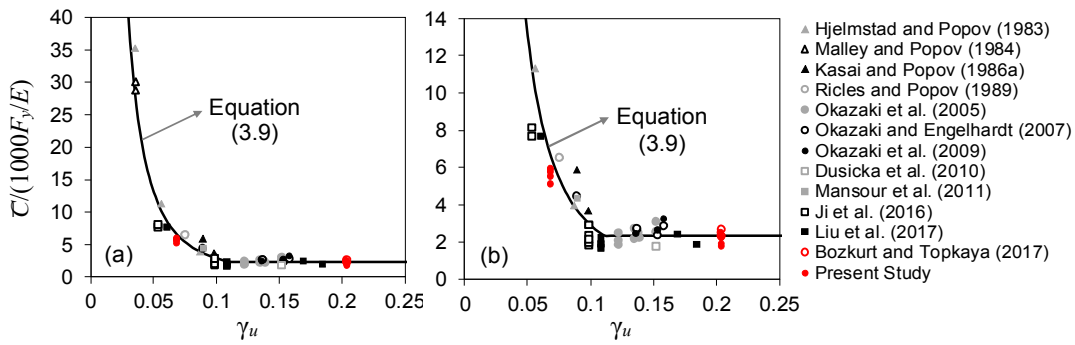


Figure 3.11. Values of normalized \bar{C} determined based on the results reported in the present study as well as previous studies: (a) the entire data; (b) a close-up view of data points with normalized \bar{C} values less than 14

On the basis of the above discussions, the following equation was developed to represent the data presented in Figure 3.11:

$$\bar{C} = \begin{cases} \left(\frac{F_y}{E} \right) (20\gamma_u^{-2.16}) & \text{if } 0.035 \leq \gamma_u < 0.11 \\ \left(\frac{F_y}{E} \right) (2350) & \text{if } \gamma_u \geq 0.11 \end{cases} \quad (3.9)$$

The predictions offered by this equation are also plotted in Figure 3.11 with a solid line. As it can be seen, the proposed equation provides predictions with a reasonable accuracy for a wide range of γ_u . The ratios of calculated to predicted \bar{C} values have an average, standard deviation, maximum, and minimum equal to 0.98, 0.20, 1.59, and 0.61, respectively. It should be noted that, the statistical measures are not significantly affected by including specimens S6 and S9 from Okazaki and Engelhardt [39] and specimens AISC-4 and AISC-7 from Okazaki et al. [41]. When these specimens are included in the data set, the average, standard deviation, maximum, and minimum of the ratios become 1.02, 0.25, 1.66, and 0.61 respectively. It is also worth noting that the applicability of Equation (3.9) is limited to $0.035 \leq \gamma_u$ since there are no experimental results in the literature below this level. Furthermore, for practical links, the γ_u angle is typically above 0.035 rad.

Consequently, based on the original form of the damage law (Equation (3.3)), the following *generalized damage law* can be recommended considering the mean power of $\bar{c}_m = 2.0$ and the coefficient of \bar{C} which can be estimated using Equation (3.9):

$$D = \bar{C} \sum_{i=1}^{\bar{N}} (\Delta\gamma_i)^{2.0} \quad (3.10)$$

3.8 Algorithm for the Application of the Generalized Damage Law for Shear Links

The presented generalized damage law is a convenient tool for estimating the exhausted as well as remaining LCF life of internal shear links. The damage law can be used as a guide for investigating the occurrence of link fracture during an earthquake, however, the range of cycles, which is required as an input for the generalized damage law, is typically not obvious in the output of nonlinear time

history analysis. In such cases, the link rotation history is first transformed into a series of symmetric cycles taking advantage of special techniques (e.g. *rainflow counting*), broadly known as cycle counting methods [266]. On the basis of these methods, the following steps can be taken to detect the occurrence of link fracture:

1. From the results of a nonlinear analysis extract the time history of link rotation for the link under investigation.
2. Set $n = n + 1$, where n is a counter with an initial value of zero at Step 1.
3. Crop part of the link rotation history which is from $T = 0$ to $T = n\Delta T$, where ΔT is the time step size at which the results of the analysis are saved.
4. Perform a legitimate cycle counting technique on the cropped part of the link rotation history (obtained in Step 3) to determine the corresponding symmetric cycles. For instance, follow the rainflow counting algorithm explained by Richards [48].
5. Calculate the damage (D) exhibited by the link under the symmetric cycles (obtained in Step 4) using Equation (3.10). Only consider the damaging cycles in this step, i.e. cycles with ranges larger than 0.0075 rad. Save the current pair of $[n\Delta T, D]$ as a data point.
6. Return to Step 2 and repeat the process until the end of the link rotation history is reached.
7. Plot the link rotation history. In the same figure, also plot the saved pairs of $[n\Delta T, D]$ (obtained in Step 5) using a secondary vertical axis. The final plot will, for instance, look similar to Figure 3.10d-f.
8. The fracture can be considered as the instant at which the accumulation of damage reaches to unity (i.e. $D = 1.0$).

These steps are also illustrated for a sample case in Figure 3.12. As shown in this figure, consecutive cycle counting algorithms are performed to determine the accumulation of damage and initiation of fracture through the link rotation history.

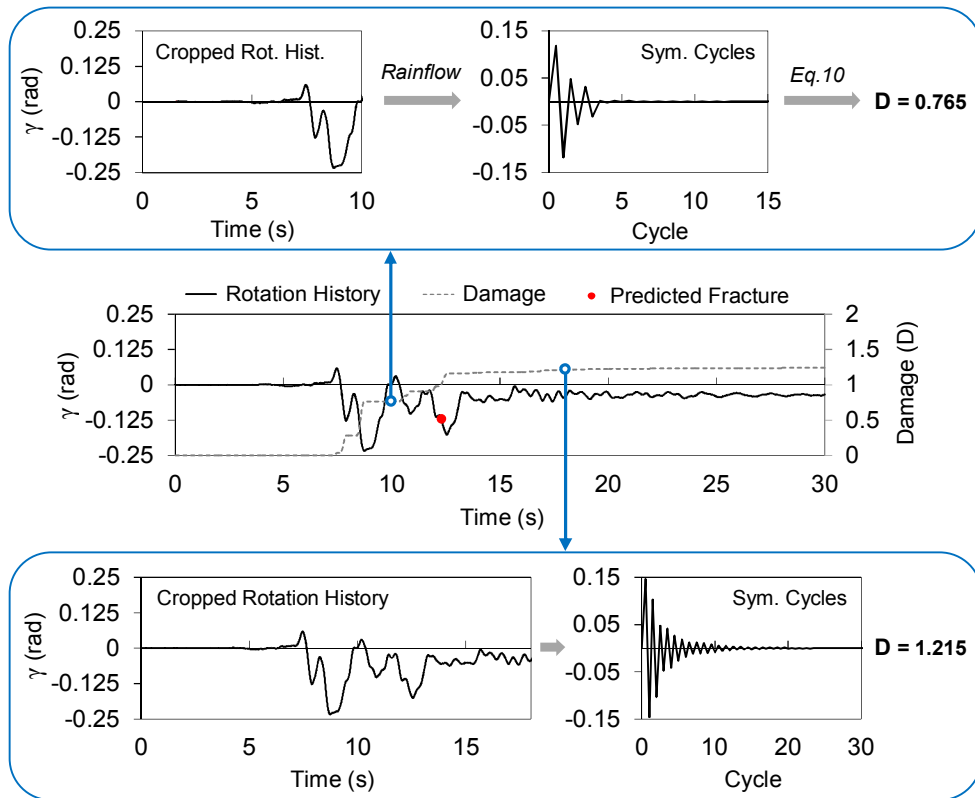


Figure 3.12. The link fracture detection algorithm

3.9 Practical Application of the Generalized Damage Law to the Shear Links of Christchurch Hospital Garage

The first documented field fractures of links in EBFs was after the earthquake on February 22, 2011, in Christchurch, New Zealand. Large fractures were found in two of the links of the parking garage of Christchurch hospital. The structure employed a group of EBFs as a lateral force-resisting system. There are 8 EBFs in each principle direction and link fractures did not result in structural collapse due to this high level of redundancy. Preliminary assessments suggested that the cause of the fractures was due to the misalignment of stiffeners with the brace flange [6]. For the two links that fractured, no fractures were observed on the other end of the links where there was no misalignment. Furthermore, other links of EBFs which did not have any misalignment did not fracture either.

A comprehensive multi-scale forensic analysis of the Christchurch hospital garage fractures was conducted by Kanvinde et al. [7]. The study consisted of material testing, nonlinear time history analysis of the structure, and detailed finite element analysis of the fractured links. The studied links were named N-S and E-W links according to the position of these members with respect to the building plan layout. The recorded ground motion history was applied to a numerical model employing line elements to obtain the link rotation (γ) history for these fractured links. Two different values of maximum link rotation were reported by Kanvinde et al. [7] depending on whether the deformations of the members other than the links were considered or not. The maximum values of link rotation were reported as 0.075 rad and 0.25 rad for N-S and E-W links, respectively when the deformations of other members were considered. These values amplified to 0.13 rad and 0.38 rad for N-S and E-W links, respectively, when other members were considered as rigid. The high levels of link rotation were attributed to two reasons the first being the intensity of shaking and the other being the large values of bay width to link length ratio employed in the framing system.

The link rotation histories obtained from nonlinear time history analysis were used by Kanvinde et al. [7] in finite element simulations that employed the Cyclic Void Growth Model (CVGM) for Ultra Low Cycle Fatigue (ULCF) analysis. In this approach, a fracture index (FI) is calculated at critical points and $FI > 1.0$ indicates fracture at a particular location. The links were analyzed for link rotations obtained using the actual ground motion record and two cases were considered. In the first case, stiffener misalignment based on field measurements was modeled, and in the second case, as-specified (i.e. no stiffener misalignment) condition was assumed in the modeling. The results confirmed the assessments by Clifton et al. [6] that the misalignment was a key factor for link fractures, particularly for the E-W link where the FI index stayed below unity for the as-specified case. On the other hand, some of the results were counterintuitive as the finite element simulations showed FI values slightly above unity for the N-S link even when as-specified conditions were modeled. The results for the N-S link were not in line with the field observations

because no fractures were observed in the links where the stiffeners were properly positioned. The CVGM is a comprehensive and very powerful approach for studying ULCF effects under different conditions, however, the method is computationally very expensive and is not suited for a design office. The N-S and E-W link models used by Kanvinde et al. [7] employed 630,000 and 430,000 hexahedral finite elements, respectively. These observations strengthen the need for alternative approaches to be developed to detect link fractures for properly fabricated links. The generalized damage law developed as a part of the present thesis can be conveniently used for this purpose.

The applicability of the generalized damage law is assessed by making use of the results provided by Kanvinde et al. [7]. N-S and E-W were properly stiffened 500 mm links which employed 460UB67 and 410UB60 sections [267] with measured yield strengths of 382 MPa and 349.4 MPa, respectively. Based on these properties, the coefficient (\bar{C}) according to Equation (3.9) is 4.49 and 4.10 for the N-S and E-W links, respectively. A summary of the results is presented in Figure 3.13. In each sub-figure, in addition to the applied link rotation history, the evolution of the fracture index (FI) based on CVGM (reported by Kanvinde et al. [7]) as well as the accumulation of damage (D) according to the generalized damage law proposed in the present thesis are plotted. It should be emphasized that all the results presented in Figure 3.13 are for the case of as-specified condition with no misalignment. Figure 3.13a and b summarize the predicted LCF behavior of the N-S and E-W links under the earthquake loading. Kanvinde et al. [7] also reported the evolution of FI under the loading protocol proposed by Richards and Uang [73] which forms the basis for the revised protocol of AISC 341-16 [248]. Therefore, in Figure 3.13c and d, a summary of the LCF behavior of the links predicted by CVGM (reported by Kanvinde et al. [7]) and the proposed generalized damage law under this loading protocol is also presented.

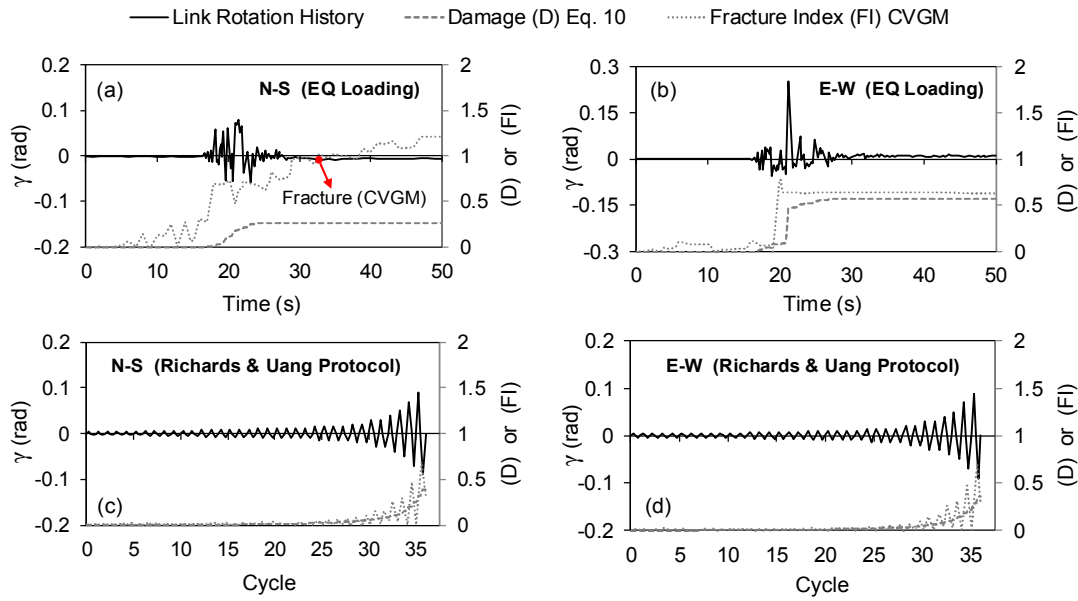


Figure 3.13. LCF behavior of the N-S and E-W links predicted by CVGM and the proposed generalized damage law: (a) N-S and (b) E-W with EQ loading; (c) N-S and (d) E-W with Richard and Uang protocol

Based on Figure 3.13, for the studied links, both CVGM and the proposed generalized damage law provide very similar results in most cases. For the E-W link (Figure 3.13b and d), no fracture is detected by either method under the earthquake loading as well as the cyclic protocol of Richards and Uang [73]. Furthermore, the predicted level of exhausted LCF life by both approaches is very close (of the order of 50%). Similarly, both methods give consistent results for the case of the N-S link under the cyclic protocol of Richards and Uang [73] (Figure 3.13c). The only notable difference between the results is for the case of the N-S link under the earthquake loading (Figure 3.13a) where CVGM predicts fracture at about $T = 35$ s while the damage (D) calculated based on the proposed generalized damage law does not exceed 0.3 throughout the loading history. In other words, the proposed generalized damage law indicates that no fractures would have been observed for the N-S link if it had been constructed without any misalignment. This is in line with the field observations where properly constructed links experienced yielding without fracture. In addition, based on Figure 3.13c, both CVGM and the proposed generalized

damage law predict that the rotation capacity of the N-S link is well above 0.10 rad in the as-specified condition, further substantiating the findings of the generalized damage law. Despite the general similarity between the results of the two approaches, the reasons for the discrepancy observed in Figure 3.13a are unclear, particularly during the first and last 15 seconds of the earthquake where the fracture index (FI) of CVGM (reported by Kanvinde et al. [7]) shows drastic increases without any notable rotations being imposed to the link.

The results discussed above demonstrate that the proposed generalized damage law can yield accurate solutions when applied to a practical case. The proposed method does not require sophisticated calculations and can be programmed conveniently into a spreadsheet to provide reasonable predictions.

3.10 Evaluation of the ASCE41 Metrics for Link Performance

As discussed earlier, one of the main motives for the present study was the lack of cumulative measures which can be used as acceptance criteria in the performance-based evaluation and design of EBFs. The experimental results of the present study further demonstrated that the maximum rotation angle experienced by a link is not a proper measure for accepting its performance. For instance, as shown in Figure 3.10e, the whole history of γ was below 0.10 rad (or $\gamma_p \leq 0.093$ rad) for Specimen 13, however, fracture occurred during the test regardless of the fact that, based on ASCE 41-13 [249], the acceptance criterion for shear links is $\gamma_p \leq 0.14$ rad for the Life Safety performance level and $\gamma_p \leq 0.16$ rad for the Collapse Prevention performance level. On the other hand, Specimen 14 (Figure 3.10f), underwent an extreme rotation of $\gamma = 0.17$ rad (or $\gamma_p = 0.164$ rad) at an initial stage of loading, however, did not show any sign of strength degradation until many cycles later.

Evaluation of the Christchurch hospital garage structure resulted in a similar conclusion. The maximum amount of rotation angle reported for the E-W link by Kanvinde et al. [7] is equal to 0.25 rad which is well above the limits provided in

ASCE 41-13 [249]. Nevertheless, CVGM and the proposed generalized damage law both predicted no fracture for this link if it had been constructed without any misalignment. An evaluation of the response of the Christchurch hospital garage structure based on ASCE 41-13 [249] would suggest that the structure should have experienced rotations in excess of the Collapse Prevention performance limit and significant amount of damage in a number of links including E-W and potentially collapsed. Nevertheless, the structure performed well during the Christchurch earthquake and remained intact except the fractures attributed to the misalignment of stiffeners introduced during the construction.

The limits provided in the ASCE 41-13 [249] standard are also accepted by the FEMA P695 [250] procedure which is used to develop response factors for structural systems. The use of these limits in collapse simulation and assessment of EBF buildings can result in erroneous conclusions because the effect of link rotation history is not taken into account. Assessments based on the maximum link rotation angle are not reliable and this study demonstrated through experimental testing and evaluation of an existing structure that cumulative measures should be adopted in the evaluation process. The proposed generalized damage law not only provides an assessment method for link fractures, but also information on the remaining life of a shear link which cannot be judged solely on the maximum link rotation angle.

Another important issue recently argued by Speicher and Harris [173] is that the effect of loading history should also be reflected in the link modeling approach used for the analysis of EBFs in the nonlinear dynamic procedure of ASCE 41-13 [249]. It is inferred from the study of Speicher and Harris [173] that strength degradation in the hysteretic behavior of frame elements used for link modeling shall be initiated based on criteria which rely on cumulative demands. This is an important issue which can have drastic effects on the performance evaluation of the response of an EBF system. The proposed generalized damage law and the 8-step algorithm discussed earlier can readily be incorporated into the formulation of a proper frame element, yielding an efficient tool with the capability of link fracture detection. Strength degradation in the hysteretic shear versus rotation behavior of the link element can

then be initiated during the nonlinear analysis based on the level of damage accumulation.

3.11 Evaluation of the AISC Loading Protocol from a Cumulative Damage Perspective

The revised loading protocol of AISC Seismic Provisions [248] is based on a comprehensive study by Richards and Uang [73]. Nonlinear time-history analyses were conducted by these researchers on three prototype EBF structures considering a set of twenty ground motions. The numerical results were then synthesized to come up with a loading protocol that had a reasonable similarity to the target values observed in the analyses in terms of factors such as the number of inelastic cycles and their distribution, sum of cycle ranges, and maximum rotation angle.

The experimental results of the present study along with the subsequent discussions on the damage law revealed that the accumulation of damage in a shear link under the revised protocol is extremely low at the initial cycles. As shown in Figure 3.10b and c for SP1 from Bozkurt and Topkaya [8] and Specimen 11 of the present study which were tested under the revised protocol, the damage is almost negligible until the 25th cycle (i.e. $\gamma = 0.015$ rad) and grows rapidly afterwards.

The AISC loading protocol can be re-evaluated based on the findings of the present study. The current protocol results in a sum of cycle ranges ($\Sigma(\Delta\gamma)$) equal to 1.24 rad at a link rotation of 0.09 rad which is the target rotation capacity for most shear links. The findings of the present study reveal that the linear addition of cycle ranges is not the most accurate way of representing cumulative effects since the damage induced by large cycles to a link is drastically higher than that of small cycles. The LCF tests conducted as a part of this study and the power of 2.0 recommended in the generalized damage law suggest that using the *sum of square of cycle ranges* ($\Sigma(\Delta\gamma)^2$) can be a more accurate measure for determining the target cumulative demand for shear links. The time history analyses used to derive the current loading protocol of

AISC 341-16 [248] can be reused to arrive at a revised target value based on the sum of square of cycle ranges ($\Sigma(\Delta\gamma)^2$).

3.12 Chapter Summary

A series of shear links were tested utilizing a nearly full-scale test setup in order to study their low-cycle fatigue behavior. The results of the LCF experiments were used to calibrate damage laws to estimate the instant of fracture initiation of the shear links. The reliability of the calibrated damage laws was assessed by using experimental results of links subjected to proportional and non-proportional loadings. A generalized damage law was then developed in light of the experimental results reported herein and in the literature to cover a wider range of shear links.

A simple 8-step algorithm was outlined which utilizes the generalized damage law for estimating the accumulation of damage as well as the instant of link fracture in nonlinear time history analysis under earthquake-induced loading histories. The algorithm can also contribute significantly to the decision-making process of the post-earthquake replacement of EBF links.

The generalized damage law was applied to the practical case of the fractured EBF links of the Christchurch hospital garage. The metrics provided in the ASCE 41-13 [249] standard and the loading protocol of AISC 341-16 [248] were also evaluated based on the results of the study.

All the conclusions drawn based on studies of this chapter are summarized in detail in Chapter 7.

CHAPTER 4

NUMERICAL ANALYSIS OF DETACHABLE REPLACEABLE LINKS

This is a short chapter where two issues related with the detachable replaceable link detail, which is being developed at METU, are numerically investigated. The first aim is to estimate the design axial force in this detail and the second aim is to investigate the applicability of this novel detail in larger (deeper) replaceable EBF shear links.

4.1 Introduction

The seismic resilience of a system is directly influenced by the time and effort required for recovery after a major earthquake [268]. Steel eccentrically braced frames (EBFs) offer the advantage of quick repair and retrofit when compared to other lateral load resisting systems since replacing the links should be sufficient for an EBF to restore its expected level of functional performance.

Repair and retrofit of EBF systems gained importance after the 2010 and 2011 New Zealand earthquakes where fractured links were replaced with new ones [6, 223, 224]. The links which were damaged during the New Zealand earthquakes were not originally designed as replaceable links. The existing links were removed by cutting out the braces and the collector beams and fabricating the new link segment with braces based on a template obtained after removal of the link. Both the welded and bolted connection details were employed to attach the new links to the existing frame system.

Link replacement procedure is not a straightforward task where the type of link and residual frame deformations play an important role in this process. Research works undertaken in the past decade concentrated on developing replaceable link details.

The primary focus was to develop links that behave similar to ordinary links and that can facilitate replacement. The replaceable link details developed in recent years were summarized in Section 2.6.3 (see Figure 2.11). Among these details, only the web connected links (Figure 2.11c) are well suited for replacement under residual drift conditions and Mansour et al. [49] demonstrated that installation of the link and repair of concrete slab are possible for a case with 0.5% residual drift. Among the other details proposed to date, the flush end-plated replaceable links (Figure 2.11a) were installed under a maximum residual drift of 0.15% [214, 215] which is below the construction tolerance of 0.2% given in AISC 303 [269] and EN 1090 [270]. Replacement of other proposed details has not been demonstrated for residual drifts in excess of 0.15%. Residual drifts result in a misalignment of the collector beams and the ends of the two collector beams will not be in the same vertical position when measured from the base of the story. This mismatch cannot be easily tolerated by the end connection details of most of the replaceable links except the web connected links. It is generally considered that replacement can be possible as long as the amount of residual drift is kept below the codified 0.2% limit. This stringent limit may require the use of dual systems with re-centering capability. For the cases where there is a significant mismatch, an option is to fabricate the new links based on a template obtained from the site after removal of the damaged link. This option, however, has negative impacts on the resilience of the system in terms of the time it takes for site measurements and fabrication of the links. Furthermore, considering the sensitivity of the residual frame deformations at each link location to the sequence of installation of the new links, the process might become even more cumbersome and time-consuming.

Consequently, a research program was undertaken at METU focused on developing replaceable links that can be installed under residual frame deformations. Pursuant to this goal, a *detachable replaceable link* concept was developed, and the proposed detail was studied through experimental testing. The detail is based on splicing the link at its mid-length. As shown in Figure 4.1, the link is subjected to a constant shear force and a variable bending moment along its length for the configurations

where braces are attached to both ends of the link. Standard end-plated details can be employed at the mid-splice connection. According to the bending moment variation shown in Figure 4.1, the bending moment at the mid-splice connection is theoretically zero. The low level of bending moment transfer enables to provide an end-plated connection which can be designed for shear and axial forces developed in the link. The end-plated connection enables a joint where the two parts of the link are connected to each other with an offset that can be present due to residual frame drifts. The detachable link detail can be utilized in combination with previously developed replaceable link details such as the gusseted replaceable link detail (Figure 4.2a) or the bolted extended end-plated replaceable link detail (Figure 4.2b)

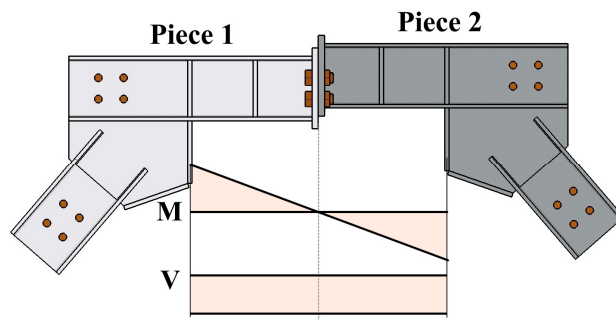


Figure 4.1. Typical moment and shear variations within an internal EBF link

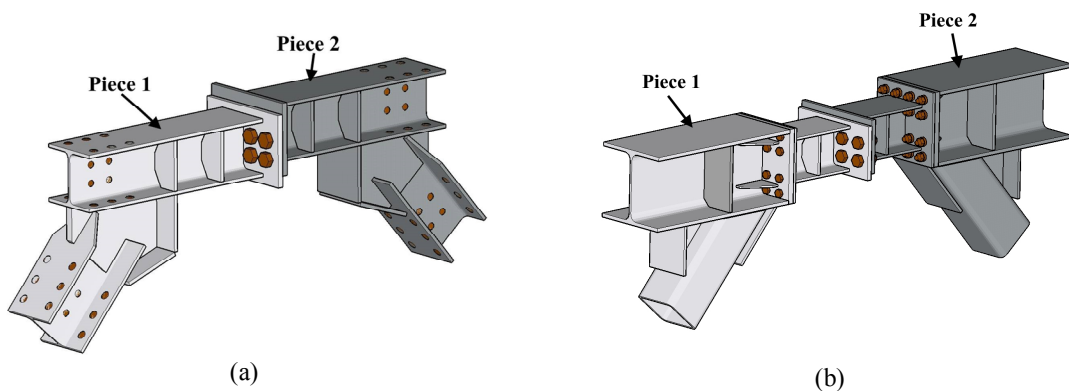


Figure 4.2. Proposed detachable replaceable link detail: (a) replaceable link with gusseted brace attachments; (b) bolted extended end-plated link

Different end-plated connection details can be employed for the mid-splice connection of the proposed detachable link detail. Flush end plates or extended end plates can be utilized. Alternatives developed for flush end plates are shown in Figure 4.3 where the splice connection can be bolted or welded. In this figure, the end plates used for the two different pieces are depicted. Slotted holes can be used as shown in Figure 4.3a when the shear transfer between the two pieces is accomplished by a frictional connection. Similarly, one of the side plates can be slotted and the other one can employ standard bolt holes as shown in Figure 4.3b. The slotted holes can be sized in these cases such that erection under various residual frame drift levels is possible. In cases where transfer of shear forces with friction cannot be considered reliable due to the uncertainties in the application of slip critical connections, the other alternative which is the bearing type connection can be used. As shown in Figure 4.3c one of the end plates should be provided with bolt holes and the other plates should be fabricated without any holes. The holes of the second plate can be drilled on site after the two pieces are installed. That way the holes are post drilled to match the geometric configuration of the holes which are present on the adjoining plate. The final alternative is to use a welded detail as shown in Figure 4.3d. All around fillet welds can be employed to connect the neighboring end plates. In all the details given in Figure 4.3, the height and width of the end plates can be changed to accommodate various levels of residual drift and number of bolts.

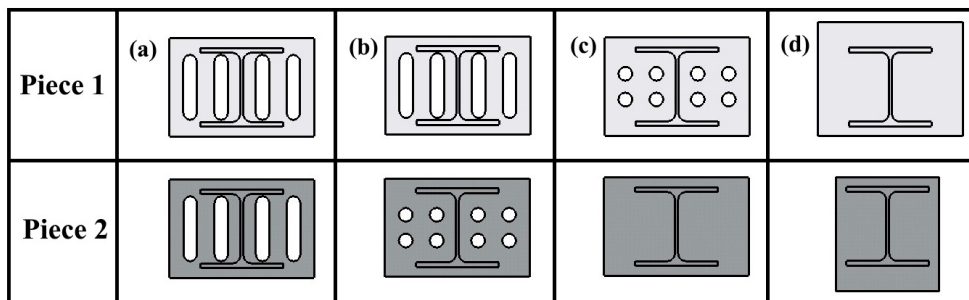


Figure 4.3. Possible connection details for the mid-splice of the detachable link detail

One important advantage of detachable links is the decreased weight and length requirements for the pieces that should be erected at the site. While typical link lengths and weights for links are not problematic for new construction, the requirements become much more stringent for existing buildings. It is quite difficult to install links to existing structures because transportation and maneuver inside the building is an onerous task. Therefore, reducing the length and the weight is a significant advantage for replaceable links. From this perspective, employing detachable links reduces the weight and length of pieces by almost a half when compared to the continuous replaceable links.

4.2 Previous Experiments on Detachable Links

As noted earlier, an experimental program was carried out at METU to develop and investigate the behavior of the proposed detachable replaceable link detail. The experiments were initiated during the PhD studies of Bozkurt [251] and are summarized in [271]. While the full details of the experiments are not repeated in the present thesis, some of the main results are provided herein in order to be used for the verification of the finite element (FE) modeling approach.

A total of six specimens were tested during the experimental program at METU using the same setup depicted in Figure 3.1. The main difference was that, depending on the level of residual frame drift, the column tops were displaced laterally which caused an offset (*eccentricity*) between the member axes of the collector beams. While the free end of one of the collector beams moved upwards, the free end of the other collector beam moved downwards by the same amount due to symmetry, creating an eccentric connection in the mid-splice of the detachable link detail as illustrated in Figure 4.1.

Four specimens (namely Specimens 2, 3, 5, and 6 following the same naming convention utilized in the METU experimental program) were considered for the verification process in this chapter and their details are summarized in Figure 4.4

and Table 4.1. It should be mentioned that the splices in the brace-to-link and beam-to-link joints were included mandatorily considering the configuration of the test setup. They were designed conservatively and did not have a detrimental effect on the focus of the study; i.e. the mid-splice connection of the detachable link detail. All specimens used HEA160 section as the link segment except one specimen which utilized HEA220. The link sections were ordered to match the European steel grade S275 with a nominal yield strength (F_y) of 275 MPa and an ultimate strength (F_u) of 430 MPa. The measured material properties of I-shaped links are summarized in Table 4.2 based on averaging the values from two coupon tests. As discussed thoroughly in Chapter 2, short or shear links ($\rho \leq 1.6$) are generally preferred in practice due to their high energy dissipation capacity when compared with intermediate and long links. In addition, short links should be preferred for replaceable links to reduce the length and weight of the part that requires replacement. Therefore, shear links were the focus of the METU experimental program. All specimens, except Specimen 3, were subjected to the loading protocol of AISC 341 [248] (Figure 3.5d). Specimen 3 was, on the other hand, subjected to a link rotation history where the amplitudes of rotations given in AISC 341 loading protocol were amplified by 4/3.

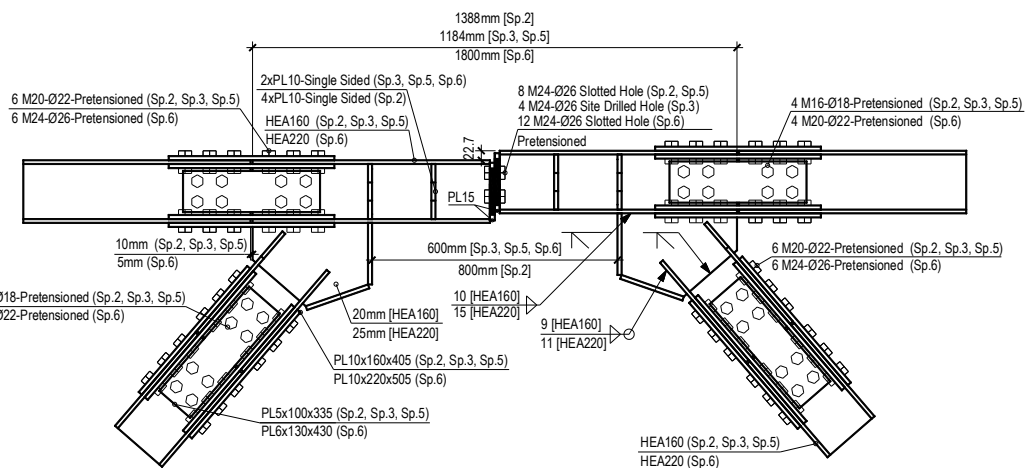


Figure 4.4. Details of Specimens 2, 3, 5, 6 (residual drift of 0.5%) tested during the METU experimental program and considered herein for verification of FE modelling approach

Table 4.1 Details of the specimens tested during the METU experimental program and considered herein for verification of FE modelling

#	Link Section	Brace Section	Link Length (mm)	ρ Nm.	ρ Me.	Mid-splice Connection Type	Res. Drift	Mid-Splice Bolts
2	HEA160	HEA160	800	1.59	1.68	Slotted	0.5%	8 M24
3	HEA160	HEA160	600	1.19	1.26	Site Drilled	0.5%	4 M24
5	HEA160	HEA160	600	1.19	1.26	Slotted	0.5%	8 M24
6	HEA220	HEA220	600	0.84	0.86	Slotted	0.5%	12 M24

Nm.: Nominal, Me.: Measured.

Table 4.2 Material Properties of I-shaped links tested during the METU experimental program and considered herein for verification of FE modelling

Section	Web					Flanges				
	F_{yL} (MPa)	F_{yu} (MPa)	$F_{y,0.2}$ (MPa)	F_u (MPa)	%EL	F_{yL} (MPa)	F_{yu} (MPa)	$F_{y,0.2}$ (MPa)	F_u (MPa)	%EL
HEA160	283	298	289	426	32	278	294	285	421	35
HEA220	343	353	349	487	30	-	-	357	497	26

F_{yL} = lower yield stress, F_{yu} = upper yield stress, $F_{y,0.2}$ = yield stress at 0.2% permanent elongation, F_u = ultimate strength, %EL = percentage of elongation.

McCormick et al. [272] conducted a detailed study on the permissible residual deformation levels. This study revealed that 0.5% is an important engineering index in terms of permissible residual drift levels. There are two important consequences of having residual drifts in excess of 0.5%. Larger residual drifts cause dizziness and nausea in occupants. Another important issue is the cost associated with repair. It was demonstrated that in Japan, it was less expensive to rebuild the structure when compared to repair if the residual drifts exceed 0.5%. Based on these studies a residual frame drift of 0.5% was considered in the METU experimental program. As explained earlier, the residual drift was applied to the testing frame and resulted in an offset of 22.7 mm in the mid-splice connection of the detachable link (Figure 4.4).

Based on Table 4.1, different types of mid-splice connection were used in the studied specimens, details of which are depicted in Figure 4.5. Specimens 2, 5, and 6 employed slotted holes with slip critical connections with M24 Grade 8.8 bolts. Specimen 3, on the other hand, utilized bearing type connections with site drilled holes as shown in Figure 4.5. All the mid-splice connections for the detachable links were designed for 2 times the link shear strength where the coefficient of 2.0 represents the anticipated overstrength factor. The design shear force was also combined with an axial force of $0.5P_y$ which was half of the axial yield strength of the link. The $0.5P_y$ force level was selected based on engineering judgment and is scrutinized as a part of the present thesis in the next sections.

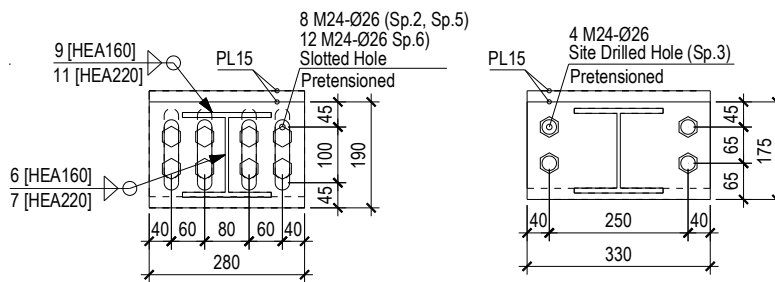


Figure 4.5. Mid-splice connection detail for Specimens 2, 3, 5, and 6 tested during the METU experimental program and considered herein for verification of FE modelling approach

The link rotation versus link shear responses of the specimens, reported in the METU experimental program, are presented in Figure 4.6. The results are used in the present thesis for the verification of the FE modelling approach in the next sections. In this figure, the shear strengths calculated based on measured properties are also shown with dashed horizontal lines. In essence it was reported that the proposed mid-splice connection for the detachable detail performed satisfactorily. No failures were reported in the mid-splice connection and it was demonstrated that the proposed detail can be a reliable option for replacing EBF shear links under residual drifts. Further details regarding the experimental program can be found in [271].

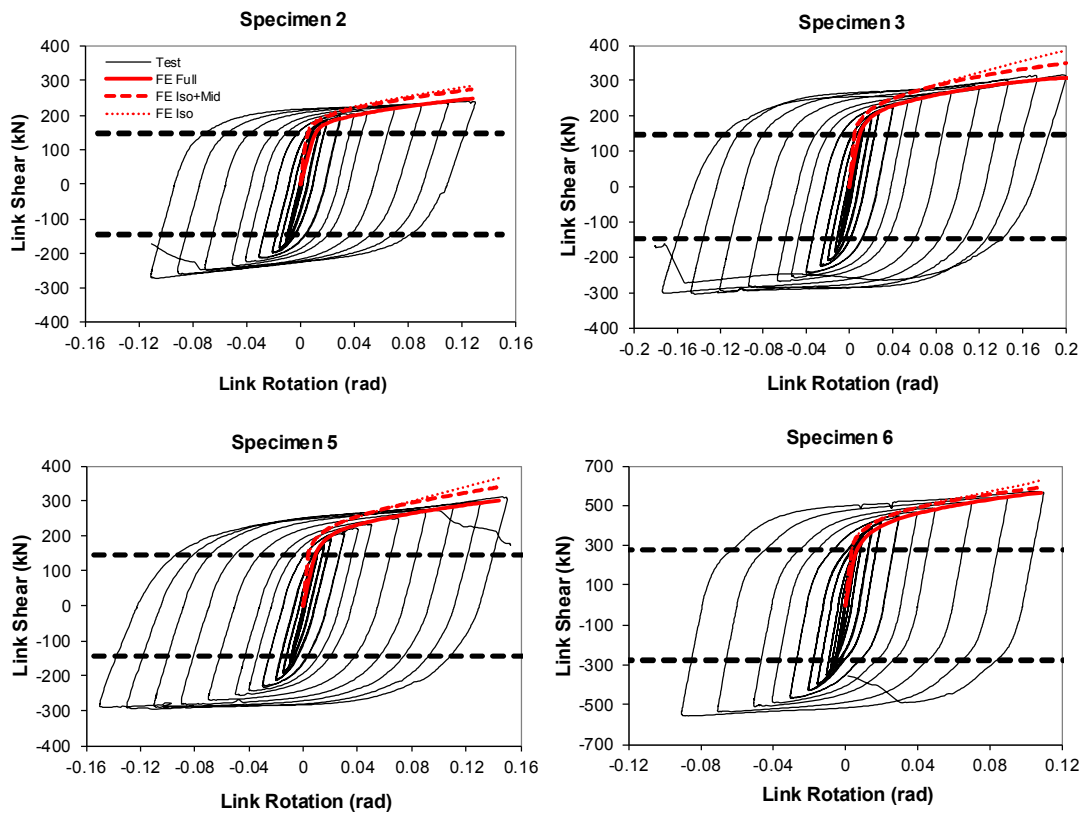


Figure 4.6. Hysteretic response of Specimens 2, 3, 5, and 6 tested during the METU experimental program and considered herein for verification of FE modelling approach

4.3 Numerical Study

A detailed numerical investigation was conducted as a part of the present thesis on the mid-splice connection proposed at METU for the concept of detachable replaceable links. The aim of the analyses was twofold. The first objective was to quantify the level of axial force which should be used for the design of the mid-splice connection. As discussed in the previous section, a value of $0.5P_y$ was utilized for this purpose during the design of specimens at METU based solely on engineering judgment. This issue is further scrutinized in this section.

The second objective was to investigate the effect of the mid-splice connection on links larger (deeper) than those tested in the METU experimental program. This was deemed necessary due to an issue reported during the experimental program. The

proposed mid-spliced HEA160 links tested at METU (Specimens 2, 3, 5) performed very similar to and exhibited comparable rotation capacities to the conventional HEA160 links tested previously by Bozkurt and Topkaya [8]. On the contrary, the only mid-spliced HEA220 link tested at METU (Specimen 6) exhibited a much lower inelastic rotation capacity (0.08 rad) compared to its conventional counterpart tested previously by Bozkurt and Topkaya [8] (which showed an inelastic rotation capacity of 0.141 rad). This raised the question of whether the presence of the proposed mid-splice connection was the main reason for the observed inferior performance of the tested HEA220 links. Advanced numerical modelling techniques are used in this section to investigate this issue.

4.3.1 General Modeling Details

All the analyses were conducted using the finite element package ABAQUS 6.12-1 [273] considering both geometrical and material nonlinearities. *Full models* of the test setup as well as *isolated models* of the links were considered in the simulations, details of which are discussed later. A von Mises plasticity constitutive model was utilized in the models considering different uniaxial stress-strain curves for links and other members. The number of degrees-of-freedom (DOFs) was extremely large in the full models of Section 4.3.2 (+3,000,000 DOFs) and the refined isolated link models of Section 4.3.3 (+10,000,000 DOFs). On the other hand, for the case of smaller isolated link models of Section 4.3.2, the number of analyses was large as they were used in a parametric study. Consequently, it was decided to conduct monotonic simulations, instead of cyclic analyses, in the FE models, considering the enormous computational cost of the latter. In order to obtain reasonable results through monotonic simulations, a stabilized cyclic stress-strain curve was utilized for links (instead of that obtained directly from tensile coupons) since only the links were subjected to cyclic hardening during the tests. The stabilized cyclic curve was obtained using the relations of Kaufmann et al. [274] which were calibrated up to 4% strain. Above this strain level, the curve was smoothly extrapolated to reach the

ultimate stress level recorded during the tensile coupon tests of the present study. A similar approach was used previously by Della Corte et al. [10]. For all other members, a generic multilinear stress-strain curve (considering S275 steel) was used, although they remained mostly elastic during the analyses. As a representative case, the stabilized cyclic curve utilized in the simulation of Specimen 6 is depicted in Figure 4.7.

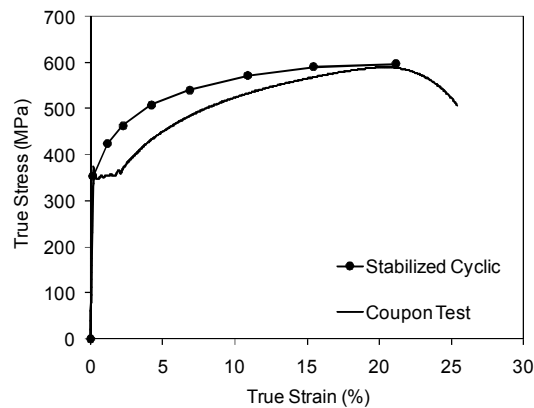


Figure 4.7. Stress-strain curve utilized in the FE analysis of Specimen 6

The contact phenomenon plays a vital role in the studied models, and therefore, 3D continuum elements were utilized in the simulations to accurately capture the contact behavior. Eight-node linear brick elements with reduced integration (C3D8R) were used in all FE models of this chapter. A *surface-to-surface* interaction was used to define contact between different parts. To this end, the penalty method with a predefined coefficient of friction of 0.5 was considered for the tangential behavior and the hard contact approach for the normal.

There exist several methods for modeling bolts in numerical studies. These methods include using simple node-to-node connector elements or even using tie constraints instead of bolts, at one end of the spectrum, to detailed 3D continuum models at the other end. The accuracy and computational cost of these methods are quite different and several studies have been conducted for comparing them (Korolija [275] and Tanlak et al. [276]). The choice of the method used for modeling bolts in an EBF

system with replaceable links is crucial and may alter the results significantly. Rudimentary bolt models may generate inaccurate results, whereas using unnecessarily detailed bolt models might lead to unmanageable computational demands. In this chapter, 3D continuum elements were used for bolt modeling. In order to accurately capture the connection behavior.

Another important issue in the modeling of bolts is the application of the bolt pretensioning load. The *bolt load* feature of ABAQUS is recommended in the software documentation [273] for bolt pretensioning, particularly in cases that the bolt is modeled with 3D continuum elements. Using this feature, pretensioning is simulated more realistically in ABAQUS by defining a cutting surface in the bolt shank, as shown in Figure 4.8, and subjecting it to a tensile load.

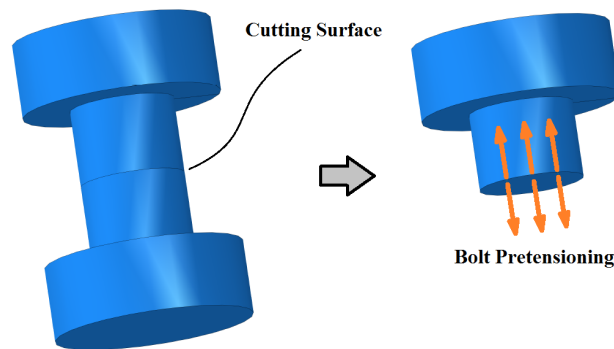


Figure 4.8. Bolt pretensioning in ABAQUS using the bolt load technique

4.3.2 Prediction of Design Axial Force

As discussed in Section 2.2.3, significant tensile forces can develop in a link, as a result of the axial restraining effect of the connecting members, when it undergoes large rotations. One of the main objectives of the numerical simulations was to understand the level of these tensile forces which would also develop in the proposed mid-splice connection for the detachable replaceable link concept. During the METU experimental program, the mid-splice connections were designed considering an axial load $0.5P_y$ based on engineering judgment. Although the performance of the

mid-splice connections was satisfactory during the tests, it was deemed necessary to provide a more accurate and reliable axial force level to be used in the design of the mid-splice connection. To provide such a design recommendation, the analyses were conducted in several steps. The simulations first started from the most sophisticated form and were simplified in two steps until a reliable model was achieved which was suitable for a parametric study.

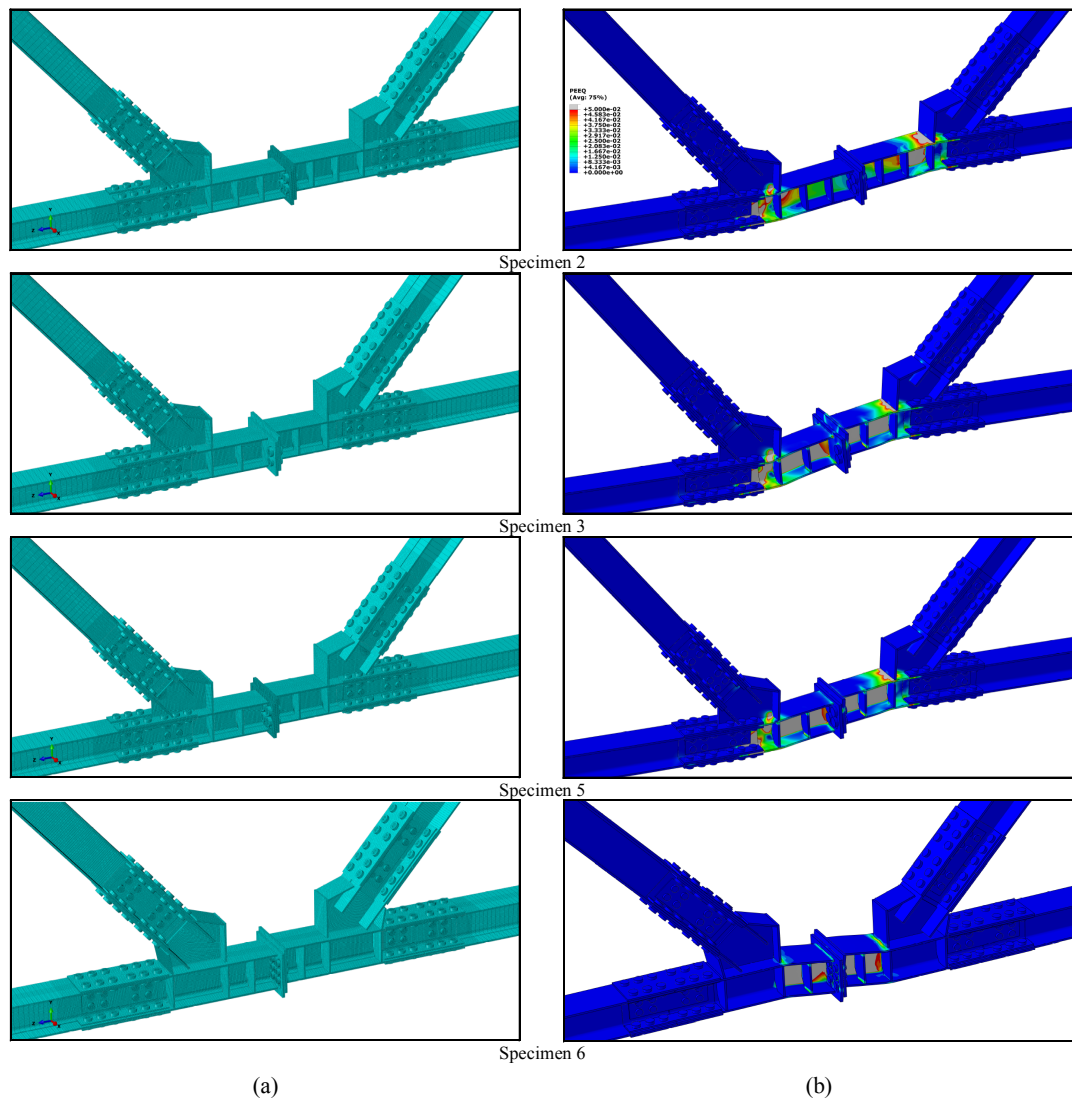


Figure 4.9. Full models of Specimens 2, 3, 5, and 6 testing in the METU experimental program: (a) mesh; (b) PEEQ contours at the end of the analysis

In the first step, the full models of Specimens 2, 3, 5, and 6 (detailed in Section 4.2) were developed in order to verify the accuracy and applicability of the FE modeling approach. A rather detailed model of each test was developed considering all the components including the link, beams, columns, braces, mid-splice connection, stiffeners, gusset plates, and bolts. Since linear C3D8R elements were used, four elements were used through the thickness of each plate in order to properly capture the stress gradient. A rather refined mesh was used in the critical regions of each model with dimensions of the order of 5 mm. The developed full models of Specimens 2, 3, 5, and 6 are depicted in Figure 4.9a. Each model was subjected to the maximum displacement level recorded during the test and analyzed with the help of a computer cluster.

Results of the full model analyses (FE Full) are compared with the experimental results in Figure 4.6. A good agreement is observed between the test and FE results in terms of the stiffness and link shear-rotation trend. The results suggest that, by using the stabilized cyclic stress-strain curve for link modeling, results of the monotonic simulations resembled those of the cyclic tests with a reasonable accuracy. The deformed shapes as well as the equivalent plastic strain contours (designated as PEEQ in ABAQUS) at the end of each analysis are also depicted in Figure 4.9b. PEEQ is defined as follows:

$$PEEQ = \int_0^t \sqrt{\frac{2}{3} \dot{\epsilon}_{ij}^p \dot{\epsilon}_{ij}^p} dt \quad (4.1)$$

Where $\dot{\epsilon}^p$ is the plastic strain rate tensor. The plastic strain concentration was found in the simulations to be more significant in the flanges of HEA160 links whereas more notable in the web of the HEA220 model. This is in line with the failure modes reported during the METU experimental program [271].

The first step towards simplification of the FE model was to repeat the analyses this time considering only the link segment and the mid-splice connection. Fully fixed boundary conditions were considered at the link ends with the exception of the

vertical displacement of one end which was used to apply link rotation. Considering the notable axial force levels recorded during the METU experimental program [271], the links were axially restrained. Results of the analyses of isolated links with mid-splice connection (FE Iso+Mid) are also plotted in Figure 4.6 along with the experimental and FE full model results. As expected, there is an increase in the stiffness and shear strength of the link in the “FE Iso+Mid” results. The reason is that the flexibility associated with the connecting members of the tested EBFs is eliminated in the models with isolated link and mid-splice connection. In contrast to the full models, any imposed displacement now translates directly into shear strain in the link web, increasing its strain hardening and the observed shear level.

In order to reach to FE models which would be suitable for a comprehensive parametric study, a second step of simplification was done. To this end, the mid-splice connection was also removed from the model, leaving only an isolated link model. The two link pieces were merged together, and a web stiffener was added at the middle of the link. Results of the isolated link models (FE Iso) are compared to the previous results in Figure 4.6. As it can be seen, the isolated models provide mostly similar predictions to the isolated models with mid-splice connection. The most notable difference is observed for Specimen 3 which utilized bearing type mid-splice connection with low number of bolts and, therefore, the flexibility of the connection played a more pronounced role in its behavior which was not captured by the isolated models. Nevertheless, results summarized in Figure 4.6 suggest that the isolated link models can provide reasonably accurate and conservative results with a fraction of the computational cost of full models. The close similarity of the results of the isolated link models with those of the tests as well as full FE models also suggests that the addition of the mid-splice connection did not have a notable detrimental effect on the behavior of the studied shear links.

The maximum level of axial tension, in terms of P/P_y , exhibited by Specimens 2, 3, 5, and 6 in the full models (i.e. “FE Full” models) was 0.20, 0.17, 0.19, and 0.18 respectively. These are comparable with those reported during the METU experimental program [271]. It should be emphasized that the experimental axial

forces were back-calculated using strain gauge readings combined with an assumed equilibrium condition and, thus, high precision should not be expected for these forces. The recorded axial forces were also affected by details of the test setup. When isolated models with mid-splice connection are considered, the P/P_y values for the specimens increases to 0.30, 0.22, 0.27, and 0.19 respectively. This is expected, since the axial stiffness of the isolated links with mid-splice connection (i.e. “FE Iso+Mid” models) is higher than that of the links in the full models. For isolated link models (i.e. “FE Iso” models), however, the tensile P/P_y values for the studied specimens reached to values of the order of 0.4 to 0.5 due to the higher axial stiffness of these models compared to the previous cases. Although the isolated link models produced high levels of axial force compared to the full models, they were selected for the parametric study on the basis of the following issues. Firstly, the computational cost of the full models as well as isolated models with mid-splice connections was rather high, making them unsuitable for the parametric study. On the other hand, supplementary analyses (not reported here for brevity) revealed that, changing the number of bolt rows and their locations in the mid-splice connection, using welded mid-splice detail (Figure 4.3d), and/or reducing the amount of offset in the mid-splice connection can drastically increase the level of axial tension exhibited by the link in the full models as well as isolated models with mid-splice connection. Consequently, since the amount of offset in the mid-splice connection is not known *a priori* (which can be very small due to small post-earthquake residual drift levels) and considering the fact that the design should consider the most conservative case, it was decided to use isolated link models in the following parametric study. It is also worth noting that, the axial-shear interaction of a typical bolt obeys a parabolic strength curve, and therefore, a conservative increase in the design axial force level does not lead to a linear increase in the required number of bolts.

Based on the above discussions, a parametric study using isolated link models was conducted to recommend a practical relation for estimating the design axial load of the mid-splice connection. Seven hot-rolled sections, namely IPE240, IPE500, HEA220, HEB500, HEM300, HEM500, and W27×84 were included in the study

considering five link length ratios $\rho = 0.5, 0.75, 1.0, 1.3, \text{ and } 1.6$. The sections were selected such that they would represent a wide range of practical shear links. Each link was stiffened as per AISC 341 [248] for a plastic link rotation angle of 0.08 rad. The stabilized cyclic stress-strain curve of Figure 4.7 was utilized in the parametric study. Consequently, a total of 35 links were modeled and subjected to a plastic rotation angle of 0.16 rad which corresponds to the Collapse Prevention performance level of ASCE 41-13 [249]. Results of the analyses are summarized in Figure 4.10 where P_{max} is the maximum link axial force recorded during the analysis. Investigation of the results revealed that the scatter in the data could be reduced and the general trend in the data could be represented more clearly if the link axial forces are normalized with respect to the total yield strength of both flanges ($P_{fy} = 2b_f t_f F_y$ as shown in Figure 4.10) suggesting that the major share of axial force in a yielded shear link would be carried by the flanges. The following simple formula was then calibrated based on the FE results as the design axial force of the mid-splice connection:

$$P_{design} = \Omega_a \beta P_{fy} \quad (4.2)$$

where Ω_a is an overstrength factor calibrated as 1.30 and β is a factor which takes into account the effect of link length ratio on the design axial load as follows:

$$\beta = 1.15 - 0.3\rho \quad (4.3)$$

where $\rho \leq 1.6$ for a shear link. Predictions of Equation (4.2) are compared with the FE results of the parametric study in Figure 4.10 where a reasonable agreement can be observed. As discussed earlier, the isolated models used in the parametric study provide conservative design axial forces compared to the axial force which would develop in comparable links with a mid-splice connection. Thus, it can be concluded that the mid-splice connection proposed at METU for the detachable replaceable link concept can be safely designed for a shear force of $2R_y V_n$ (where V_n is the nominal

shear capacity of the link and R_y is the ratio of expected to nominal yield stress of the material) and an axial force of P_{design} determined via Equation (4.2).

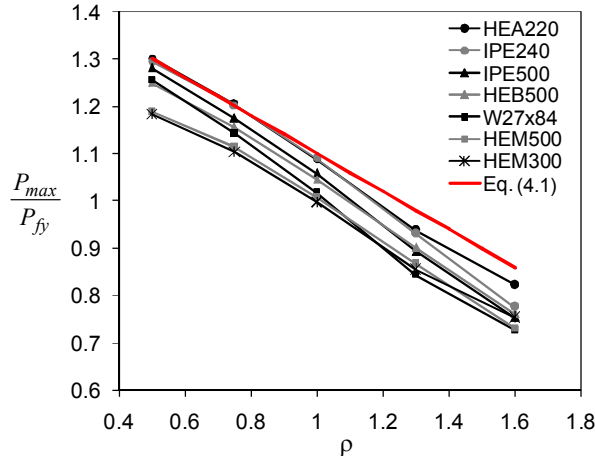


Figure 4.10. Results of the parametric study on the design axial force for the mid-splice connection

4.3.3 Investigation of Larger (Deeper) Mid-Spliced Links

As explained earlier, the second aim of the numerical investigation was to observe the effect of the mid-splice connection on the behavior of links larger than those tested in the METU experimental program [271]. An accurate prediction of the instant of fracture in a shear link can be obtained after calibrating a micro-mechanics based models with their required material parameters [277]. In this section, it aimed to investigate the fracture propensity of mid-spliced links *when compared* with the conventional links rather than determining the instant of fracture. Pursuant to this goal, a simple, yet reliable, method was utilized which was developed by Chao et al. [86] and El-Tawil et al. [278]. Based on this approach, a *modified rupture index* (MRI) can be defined as follows:

$$\text{MRI} = \frac{PEEQ}{\exp(-1.5 \times \max[\hat{T}])} \quad (4.4)$$

where PEEQ is the equivalent plastic strain reported by ABAQUS and $\max[T]$ represents the maximum *stress triaxiality* (\hat{T}) achieved during the loading history, with \hat{T} defined as the ratio between the hydrostatic and von Mises stresses, i.e. σ_m/σ_v . Two issues regarding the approach should be emphasized. First, calculation of MRI is a post-processing task and does not change the course of an analysis nor the obtained stress/strain pattern. Second, MRI is not calibrated to be used as a criterion for fracture initiation; it is only an indicator of the propensity for fracture at a particular location and is used in this respect to distinguish between alternative structural details [86]. The method was applied to EBF shear links by Chao et al. [86] in order to study web fracture initiation. Although links are typically subjected to cyclic loading, Chao et al. [86] conducted finite element analyses considering monotonic loading and it was assumed that conclusions drawn are qualitatively applicable to cyclic conditions. Due to the presence of very large finite element models a similar approach is adopted herein.

In order to investigate a larger (deeper) mid-spliced link, an HEB500 link with a length of 1250 mm ($\rho = 1.0$) was modeled considering three cases:

- Case 1: Isolated link with no mid-splice connection
- Case 2: Isolated link with mid-splice connection and an offset of 60 mm
- Case 3: Similar to Case 2 however with a different bolt pattern

The offset of 60 mm was selected by considering an EBF with 12 meter bay width subjected to 0.5% residual drift. For Case 2 and Case 3, the mid-splice was designed following the recommendations of Section 4.3.2. Each link was stiffened as per AISC 341 [248] for a plastic link rotation angle of 0.08 rad. Full details of these cases are depicted in Figure 4.11. The idea of analyzing these three cases was to see if the addition of the mid-splice connection and altering its bolt pattern would have any notable effect on the behavior of a deep shear link. In addition, Specimen 5 (HEA160) and Specimen 6 (HEA220), tested as a part of the METU experimental program (outlined in Section 4.2), were reanalyzed considering the MRI approach for comparison purposes.

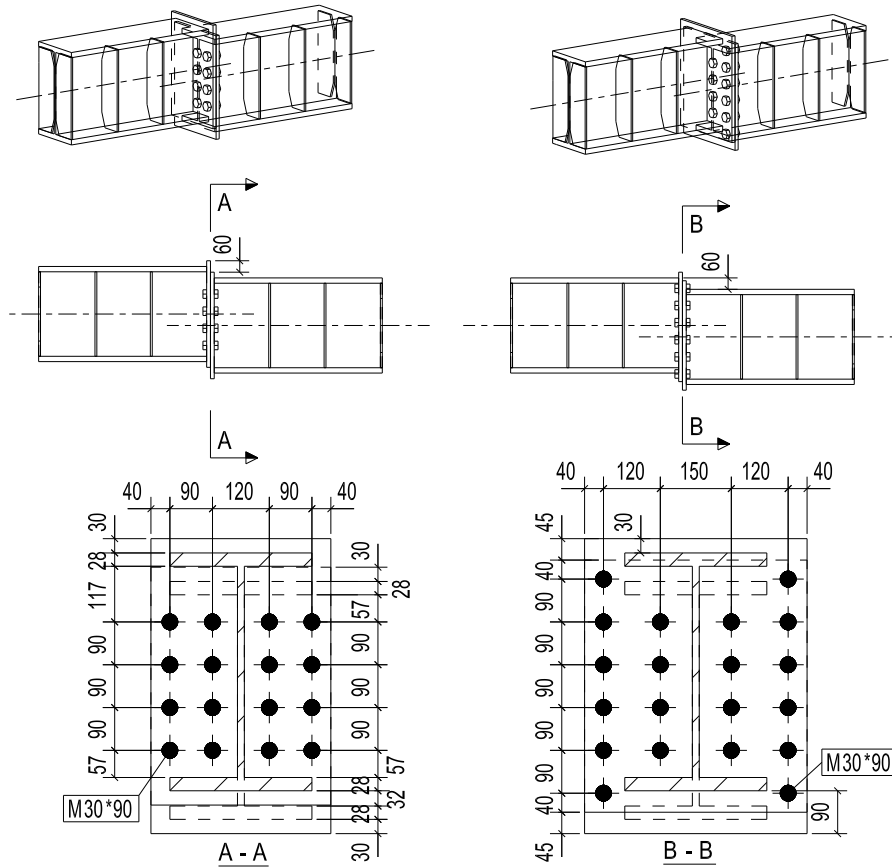


Figure 4.11. Details of the studied deep mid-spliced links: (a) Case 2; (b) Case 3

Each case was modeled following the main details explained in Section 4.3.1. The material was considered as S355 and a generic stress-strain curve for this grade was transformed into a stabilized cyclic curve using the calibrated formulae of Kaufmann et al. [274] as explained in Section 4.3.1. The most reliable evaluations with the MRI approach can be obtained if the element size in an FE model is set equal to the *characteristic length* of the material which is of the order of 0.1 to 0.3 mm for different steels [279]. Considering the limitations of the available computational facilities, it was not possible to refine the mesh down to these limits. After several trials, it was finally decided to use a mesh size of 2 mm for all three cases studied in this section which resulted in models with more than 10,000,000 DOFs. Reasonable

results were obtained in other studies using a similar approach [105, 280, 281]. As a representative, the refined mesh of HEB500-Case2 is shown in Figure 4.12.

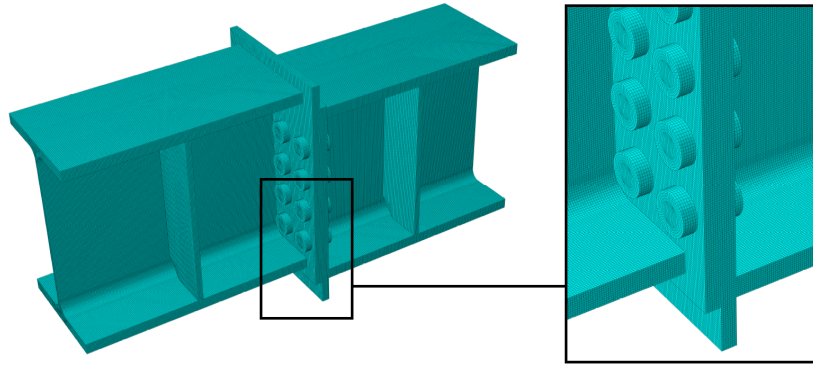


Figure 4.12. The refined mesh used for the calculation of MRI in HEB500-Case2

Each case was monotonically subjected to a plastic rotation angle of 0.16 rad which is the Collapse Prevention performance level of ASCE 41-13 [249]. The models were analyzed with the help of a computer cluster and the analysis time was approximately four days per cases with mid-splice connection. The MRI contours at the end of the analyses are summarized in Figure 4.13 where the results for the conventional links and mid-spliced links are reported. Based on the figure, MRI varied mostly between zero and 0.20 in the web of the studied links. Higher MRI values exceeding 0.3 were observed for some cases in small regions in the vicinity of the link-to-end-plate connection, however, it is considered that these would have been significantly reduced if the all-around fillet welds were modeled. Furthermore, recent experiments on links connected to end-plates or columns with proper all-around fillet welds demonstrated satisfactory behavior with no sign of premature fracture at the connection region [37, 41, 282]. Considering the observed early web fracture in Specimen 6 (HEA220) tested as a part of the METU experimental program (outlined in Section 4.2) compared to its conventional counterpart tested previously by Bozkurt and Topkaya [8], the investigation was focused on the change in the MRI values in the web of the analyzed cases.

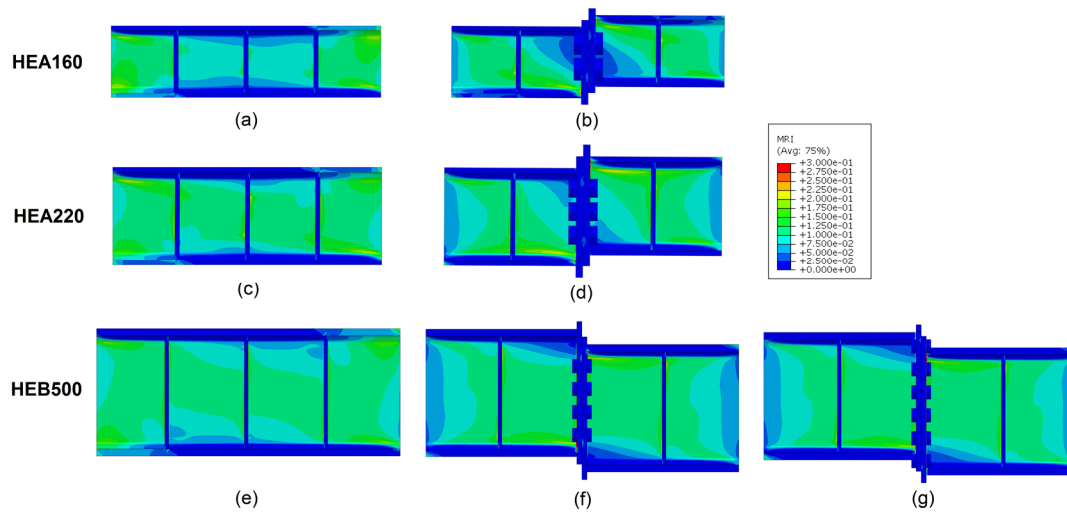


Figure 4.13. MRI contours at the end of the analysis for (a) conventional HEA160, (b) mid-spliced HEA160, (c) conventional HEA220, (d) mid-spliced HEA220, (e) conventional HEB500-Case 1, (f) mid-spliced HEB500- Case 2, and (g) mid-spliced HEB500-Case 3

As shown in Figure 4.13, the maximum MRI value was determined as 0.156, 0.180, and 0.168 in the web of the conventional HEA160, HEA220, and HEB500 links, respectively. These values increased to 0.194, 0.222, 0.212, and 0.188 for mid-spliced HEA160, HEA220, HEB500-Case2, and HEB500-Case3 links, respectively. The results show that introducing a mid-splice results in similar increases in the level of the maximum MRI for all cases. The exception was HEB500-Case3 where additional bolts were provided close to link flanges to reduce the amount of local bending. Therefore, the results summarized in Figure 4.13 suggest that the addition of a mid-splice connection to a shear link with a deep section (such as HEB500) does not lead to a notable increase in the propensity of its web for fracture, compared to the case where a mid-splice is added to a shallow section (such as HEA160).

The MRI contours given in Figure 4.13 show that the part of the web that experiences an increase in the MRI value is not identical for all specimens. In order to investigate this issue further, the MRI values are plotted along a path which has a length equal

to the panel width and is parallel to the link flange. The path was considered to pass through the maximum MRI point in each model. The variation of $[MRI/MRI_{max}^{conv}]$ as a function of the normalized panel width is reported in Figure 4.14 for the web of all the studied mid-spliced models, where MRI_{max}^{conv} is the maximum MRI value recorded for the web of the corresponding conventional link model. In the figure, any part of each curve that falls above the (red) horizontal line indicates a region in the mid-spliced link where the recorded MRI value is higher than the maximum MRI recorded for the corresponding conventional link model. The results indicate that the region that experiences an increase in MRI due to the addition of a mid-splice is larger for the HE220 link when compared with the other links. This observation strengthens the experimental results for the HEA220 specimen where lower link rotation capacities than expected were obtained when a mid-splice was introduced during the METU experimental program. It is also worth noting that the rotation capacity is also influenced by higher yield strength possessed by this specimen. Bozkurt et al. [282] demonstrated that the low-cycle fatigue life of a shear link is inversely proportional to its yield strength. While Specimen 6 (HEA220) of the METU experimental program had a yield strength of 343 MPa, the counterpart conventional link tested previously by Bozkurt and Topkaya [8] had a yield strength of 299 MPa.

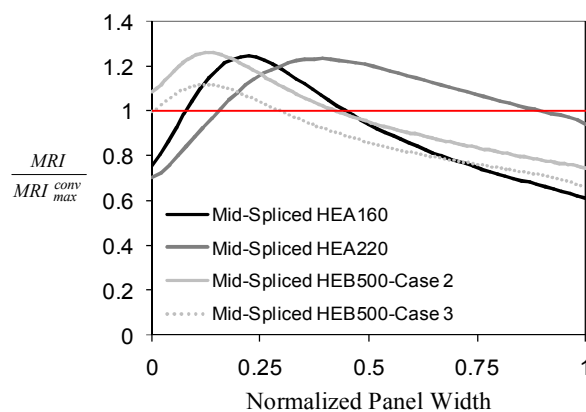


Figure 4.14. Variation of MRI along the critical path for the studied models

In essence, results of the numerical analysis of this section suggest that the mid-spliced detail developed at METU for detachable replaceable link concept can be adopted for larger (deeper) links as well. Considering the increase in the maximum MRI of the web, the addition of a mid-splice seems to have comparable effects on shallow links and deep links. The region with an increased MRI, however, can be local or more widespread based on the geometry of the link and the arrangement of bolts in the mid-splice. Consequently, future research should concentrate on a parametric study to investigate the fracture propensity of mid-spliced links with different geometrical properties. Other micro-mechanics-based models can also be adopted to further investigate the conclusions derived herein based on the MRI approach.

4.4 Chapter Summary

The detachable replaceable link concept which is under development at METU was numerically investigated in this chapter. The concept allows for post-earthquake link replacement under residual frame drifts of the order of 0.5% and even higher. After reviewing the previous experiments conducted on the proposed detail, finite element analyses were carried out to develop design recommendations for the end-plated mid-splice detail and to provide further validation. The axial force developed in the mid-splice connection (due to large link deformations and end restraint effects) was determined based on a comprehensive parametric study and a simple design expression (Equation (4.2)) was developed. In order to further investigate the application of the proposed detail for larger (deeper) shear links, another set of sophisticated numerical simulations was conducted. Comparison of modified rapture index (MRI) values revealed that the addition of a mid-splice connection has comparable effects on shallow links and deep links in terms of the fracture propensity, further suggesting its potential for practical applications.

All the conclusions drawn based on studies of this chapter are summarized in detail in Chapter 7.

CHAPTER 5

SEISMIC BEHAVIOR OF CONCENTRICALLY BRACED FRAMES DESIGNED TO AISC341 AND EC8 PROVISIONS

As outlined earlier, both EBF-related and CBF-related topics are investigated in this thesis. This chapter as well as the next chapter focus on CBF-related topics. In this chapter, the seismic behavior of concentrically braced frames designed following the provisions of American and European specifications is compared using extensive numerical simulations with over 800 nonlinear time history analyses. It should be mentioned that CBFs are used extensively to resist earthquake and wind loads, however, the focus here is on high seismic applications where the brace members dissipate energy through repeated cycles of buckling and yielding. Consequently, the conclusions might be different if wind load applications are considered.

5.1 Introduction

Currently, moment resisting frames, concentrically braced frames, eccentrically braced frames, special truss moment frames, steel plate shear walls, and buckling restrained braced frames are being commonly used as lateral force resisting systems for steel structures. While new systems such as buckling restrained braced frames are gaining popularity, moment resisting frames (MRFs) and concentrically braced frames (CBFs) are considered as two of the most popular systems among these alternatives. Although MRFs provide more architectural freedom, compared to the CBFs, they are expensive. CBFs have been quite popular since the 1960s mainly because of their economic advantages over MRFs particularly in cases where the drift requirements govern the design. Furthermore, beam-to-column connections of MRFs suffered premature fractures in the 1995 Kobe and the 1994 Northridge earthquakes [1, 2]. In the aftermath of these earthquakes, considerable research and

development projects were conducted in the US, Japan, Europe and elsewhere to develop new moment connections that have sufficient strength, stiffness, and ductility to perform satisfactorily during future strong seismic events. However, the new MRF connections and the modifications made to then existing moment connections have caused their cost of construction and inspection to increase significantly, making the use of CBFs even more economical. More recently, the 2011 Christchurch earthquake in New Zealand resulted in fracture of several eccentrically braced frames (EBFs), further adding to the popularity of CBFs. The CBF system is currently one of the most widely used seismic load resisting systems in steel structures; it is easy to design and the most efficient especially in controlling lateral drifts of buildings.

In recent decades, a significant amount of research has been conducted on the seismic behavior and design of CBFs. A major portion of these studies has focused mainly on the response of bracing members and their connections [283-298]. Extensive experimental [94, 299-309] and numerical [113, 261, 310-315] investigations have also been undertaken to study the behavior of single-story and multi-story CBFs under severe loading scenarios, assessing both the system level and component level responses.

In the United States, steel CBFs are designed according to the AISC Specification for Structural Steel Buildings [81], hereafter referred to as AISC360, as well as the special seismic design rules of the AISC Seismic Provisions for Structural Steel Buildings [11], which is referred to here as AISC341. In Europe, the CBFs are designed according to the regulations of the Eurocode 3: Design of Steel Structures – Part 1-1: General Rules and Rules for Buildings [252], hereafter referred to as EC3, as well as the seismic provisions of the Eurocode 8: Design of Structures for Earthquake Resistance – Part 1: General Rules, Seismic Actions and Rules for Buildings [142], which is referred to here as EC8.

Due to rapid globalization, engineers are now faced with the challenge of being competent with several design provisions. Owners may require the use of widely

accepted design codes regardless of the location of the structure. While both design approaches are intended to result in structures with comparable performances during a major earthquake, in some cases, there can be substantial dissimilarities between the regulations of different provisions which might significantly affect the behavior of the designed structure. Seismic design provisions in AISC341 and EC8 on MRFs and EBFs are quite similar. However, the rules on the seismic design of CBFs in these provisions have evolved separately and have some significant philosophical as well as procedural differences.

Consequently, the main objective in this chapter is to study the similarities and differences between the practices in the United States and Europe regarding the seismic design of CBFs. Under this goal, first, the provisions given in AISC341 and EC8 for steel CBFs are compared and studied thoroughly. CBF archetypes are then designed according to these provisions and subjected to a large set of ground motions to investigate and compare their seismic performances.

5.2 Comparison of Design Provisions in AISC341 and EC8

5.2.1 Definition and Geometries

AISC341 and EC8 provisions both define CBFs as systems where horizontal forces are mainly resisted by members subjected to axial forces. The centerlines of adjoining columns, beams and braces should be concentric. However, the AISC341 provisions allow eccentricities less than the beam depth if the resulting member and connection forces are addressed in the design. No information is provided in EC8 related to the acceptable level of eccentricities of members. Although presumably no such eccentricities are allowed as per EC8, Astaneh-Asl [316] has shown that such relatively small amount of eccentricity, if introduced correctly, can improve the ductility of the gusset-plated connection without increasing the size of the gusset plate or the beam.

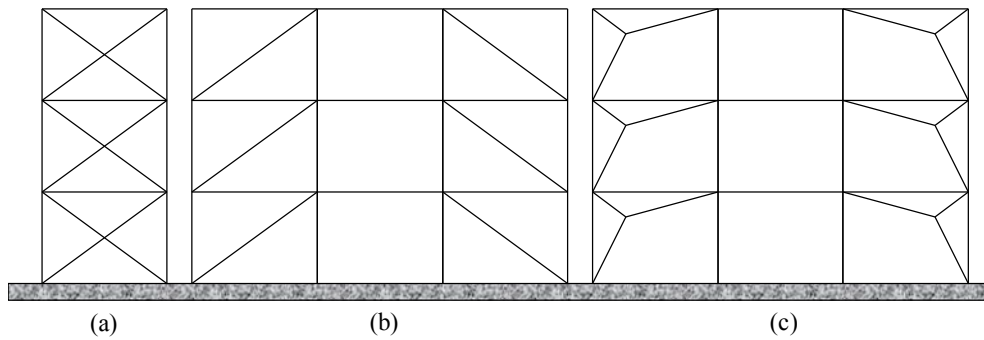


Figure 5.1. Single diagonal and X-braced systems

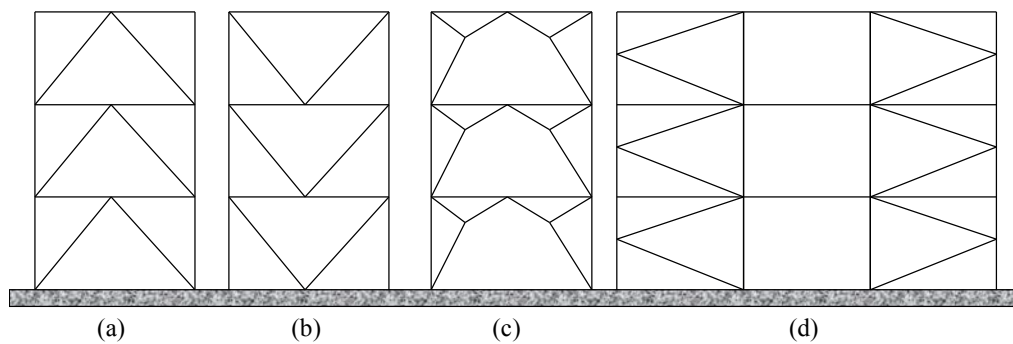


Figure 5.2. V-braced, Inverted V-braced, and K-braced systems

In both provisions, three broad geometries are defined for CBFs, namely, single diagonal or X-bracing (Figure 5.1), V-bracing or inverted V-bracing (Figure 5.2a-c), and K-bracing (Figure 5.2d). The K-braced system is forbidden in both provisions for structures designed for seismic loading due to the possible column plastic hinging at the mid-height as a result of unbalanced brace forces. Among the diagonally-braced and V-braced systems, EC8 presents special cases (Figure 5.1c and Figure 5.2c) where the diagonals can be discontinuous. This type of a bracing is referred to as the y-bracing [317] which allows for larger openings. While EC8 recognizes this system as a viable option, no specific design requirements are given in the European provisions.

5.2.2 Seismic Demands

To make a fair comparison, the seismic demands (i.e. the load effects) should also be considered. In the United States, seismic demands on structures are calculated based on the regulations of the Minimum Design Loads for Buildings and Other Structures [145], hereafter referred to as ASCE7-10. In Europe, on the other hand, EC8 provisions are used for seismic loading. Both provisions define a design response spectrum to be used for determining the design base shear force.

In ASCE7-10, two spectral acceleration values, S_s and S_l , are considered which are established using acceleration maps and depend on the location of the structure. The S_s and S_l parameters are based on risk targeted maximum considered earthquake (MCE_R) ground motions and are defined as mapped MCE_R , 5% damped, spectral response acceleration parameter at short periods and at a period of one second, respectively. These acceleration values are modified to arrive at S_{MS} and S_{MI} which are the MCE_R spectral response acceleration parameters adjusted for site class effects. These parameters are finally multiplied by a factor of 2/3 to arrive at S_{DS} and S_{DI} , which represent design spectral response acceleration parameters.

In EC8, the design response spectrum depends on a single acceleration parameter, a_g , which is the design ground acceleration on type A ground. This parameter together with the soil factor, S , are directly used in defining the design response spectrum. In this approach two types of response spectra are defined, namely, Type 1 and Type 2. National Annexes can provide detailed information on which spectrum should be used. A comparison of the response spectra given by the American and European provisions for a high seismic region is given in Figure 5.3. For the case of ASCE7-10, the values of S_s and S_l are considered to be equal to 1.5g and 0.6g, respectively. Also, for a site class D (stiff soil), the design spectral accelerations, S_{DS} and S_{DI} , are equal to 1.0g and 0.6g, respectively. For the EC8 spectrum, the value of a_g is considered equal to 0.35g and Type 1 spectrum is developed using ground type C. Figure 5.3 shows that the response spectra developed based on ASCE7-10 and EC8 for a high seismic region with stiff soil are very close to each other.

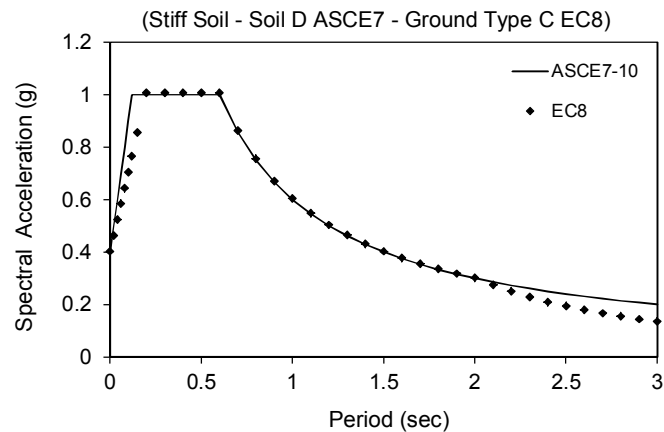


Figure 5.3. Comparison of design response spectra

In general, various methods are recommended in ASCE7-10 and EC8 for determining the earthquake-induced base shear and its height-wise distribution. The two most widely used methods are the equivalent lateral force procedure and the modal response spectrum analysis. Pushover and time history analysis procedures are also available, however, these are less frequently used in practice when compared to the former methods. Although the general principles are the same, there are differences between ASCE7-10 and EC8 in the application of these methods. The most significant difference affecting the CBF design is the use of different structural periods. In ASCE7-10 the fundamental period of vibration used for determining the base shear during the strength design cannot exceed a certain upper bound. This upper bound is however not applied in checking drifts, and instead, the period value obtained from an eigenvalue analysis can be directly used. In EC8, on the other hand, no such upper limit exists, and the period obtained from an eigenvalue analysis can be used for both strength and drift checks. More detailed information on this issue can be found in Günaydın and Topkaya [318].

In the US approach, only the dead load is considered as the reactive seismic mass with no live load considerations. However, in the European design, a portion of the live load (15% to 80% depending on the building category type) is added to the dead load and is used as the reactive mass of the structure.

5.2.3 Energy Dissipation and Response Modification Coefficients

In the United States and Europe, steel CBFs are classified into various categories and the seismic load reduction factor (i.e. the response modification coefficient (R factor) in the US approach and the behavior factor (q factor) in the EU method) changes depending on this category. According to AISC341, CBFs are classified into three categories depending on their expected energy dissipation capabilities. The first category belongs to CBFs which are not specifically detailed for seismic resistance and their expected level of energy dissipation is very low. ASCE7-10 assigns an R factor of 3.0 to these frames and notes that they can only be utilized for “wind and low seismic” applications. Therefore, these frames are designed to only satisfy the provisions of AISC360 and need not to comply with the additional seismic provisions of AISC341. The second category is the Ordinary Concentrically Braced Frame (OCBF) for which an R factor of 3.25 is given as per ASCE7-10. OCBFs are expected to withstand limited inelastic deformations in their members and connections when subjected to forces resulting from motions of the design earthquake. The third category is the Special Concentrically Braced Frame (SCBF) for which an R factor of 6 is considered by ASCE7-10. SCBFs are expected to sustain significant inelastic cyclic deformations in their members and connections in the form of yielding of steel before fracture. Unlike the first category (with $R=3$), the special rules given in AISC341 shall be applied in the seismic design of OCBFs as well as SCBFs.

The ASCE7-10 document regulates the use of different types of CBFs according to their ductility and energy dissipation capabilities. In general, a structure is assigned to a seismic design category which depends on the seismic hazard at the site and the importance of the structure. Two broad categories can be defined for structures with normal importance according to the seismic hazard. If $S_{DS} < 0.5g$ and $S_{DI} < 0.1g$, then the structure can be designed using any of the three categories of CBFs without a height limit being applied. If $S_{DS} > 0.5g$ or $S_{DI} > 0.1g$, then the structure must be designed as a Special CBF. In this particular case, Ordinary CBFs are allowed only

for seismic design categories D and E with a height limit of 10 meters. The spectral accelerations that define the boundary ($S_{DS}=0.5g$ and $S_{DI}=0.1g$) correspond to Type A ground with $a_g < 0.2g$ in the EC8 provisions.

Based on EC8, CBFs are classified into three categories as well. Two broad categories are defined first as low dissipative structural behavior and dissipative structural behavior. Low dissipative structural behavior corresponds to Ductility Class Low (DCL) where the recommended q factor is equal to 1.5. DCL is recommended only for low seismicity areas where a_g on Type A ground is less than 0.08g. No specific rules are given in EC8 for the seismic design of Ductility Class Low CBFs. Dissipative structural behavior is sub-divided into two categories, namely, Ductility Class Medium (DCM) and Ductility Class High (DCH). The recommended value of the q factor changes according to the ductility class. In addition to this, in EC8, frames with X- or diagonal bracings and V-bracings are treated separately. For frames with X- or diagonal bracings, the recommended value of q is 4.0 regardless of the ductility class. However, for V-braced frames, the recommended values of q are 2.0 for DCM and 2.5 for DCH cases. As discussed by Mazzolani and Piluso [319], in a V-braced CBF, during load reversals, it is possible that a previously buckled brace cannot become fully stretched and yield when subjected to a subsequent tension loading. Thus, in some instances, both braces might be in a buckled condition. This can be considered as a justification for assigning lower q factors for V-braced CBFs in the European design [319].

From the above discussion it is apparent that systems not specifically designed for seismic resistance in the United States (with $R=3$) correspond to DCL systems in Europe. Similarly, OCBFs and SCBFs of AISC341 correspond to DCM and DCH systems of EC8 respectively. Major differences exist between the response modification coefficients (behavior factors) proposed by the American and European provisions for the design of systems with similar expected performances. In general, the factors used for the reduction of earthquake forces found from an elastic analysis, are much less in EC8 when compared with their counterparts in ASCE7-10.

5.2.4 Classification of Cross Sections for Local Buckling

Members of seismic force resisting systems must exhibit stable behavior under cyclic loading without experiencing significant local buckling leading to possible fracture. In the United States and Europe, local buckling provisions are regulated by imposing width-to-thickness ratios on compression elements of a cross section. In the US, AISC360 classifies cross sections into three categories, namely, compact, non-compact, and slender. For structures which have to comply with the special seismic rules of AISC341, two other cross section classes are also defined as *highly ductile* members and *moderately ductile* members. In general, AISC341 requirements for moderately ductile members are similar to those given in AISC360 for compact sections with minor differences. However, the requirements for highly ductile members are typically more stringent. It is worth noting that the term seismically compact was in use in the previous versions of AISC341 instead of the term highly ductile.

In Europe, concerning local buckling, cross sections are grouped into four classes as per EC3, namely, Class 1, Class 2, Class 3, and Class 4. Comparison of EC3 and AISC341/AISC360 compactness requirements reveals that highly ductile members, moderately ductile members, non-compact sections and slender sections in the US provisions can be regarded as Class 1, Class 2, Class 3, and Class 4 cross sections, respectively, in the European provisions. For most cases, only minor differences exist between the two provisions in the classification of cross sections, however, for some cross section types (e.g. hollow structural sections) the differences can be significant. The reader can find more detailed information about this issue in Topkaya and Şahin [320].

5.2.5 Design of Bracing Members

Brace members are the primary source of energy dissipation in CBFs. Under an earthquake loading, braces dissipate energy by buckling in compression and yielding

in tension. Brace behavior is complex as it includes various cycles of compression and tension loadings. The most important difference between AISC341 and EC8 in the CBF seismic design stems from the design philosophy used for brace members. Under lateral loads, some braces are subjected to compression while others to tension. As will be explained in the following sections, for a properly designed CBF, there is usually a healthy balance between the loads resisted by tension braces and compression braces. When compression braces buckle, the load carrying capacity of the braces reduces significantly and the forces are redistributed to braces in tension. Thus, the lateral load resistance of a CBF has a history which is quite complex due to the behavior of its braces.

Two distinct approaches can be adopted for the design of CBFs depending on the instant at which the internal forces are calculated. Before brace buckling, both the compression and tension braces are active and a structural analysis model which takes into account all braces can be considered as representative of the true behavior. On the contrary, after buckling occurs in some braces, buckled members only provide a low residual resistance and almost no stiffness, and therefore, a structural analysis model which takes into account these effects can be considered as representative of the true behavior. The US and EU provisions differ in this aspect since AISC341 considers mostly the pre-buckled stage of brace members in the analysis while EC8 considers for some cases the pre-buckled stage and for other cases the post-buckled stage of these members.

Both the compression and tension braces are included in the structural analysis model for cases where the design is based on the pre-buckled stage. In contrast to this, only the braces in tension are represented in the structural analysis model and designed if the post-buckled stage is to be considered, and the compression braces are conservatively omitted. The latter approach is usually termed as the *tension-only bracing*. Both of these methods are schematically depicted in Figure 5.4. It should be mentioned that the tension-only bracing approach results in analysis models with significantly lower lateral stiffnesses and higher periods of vibrations when compared with models that include the axial stiffness of all braces.

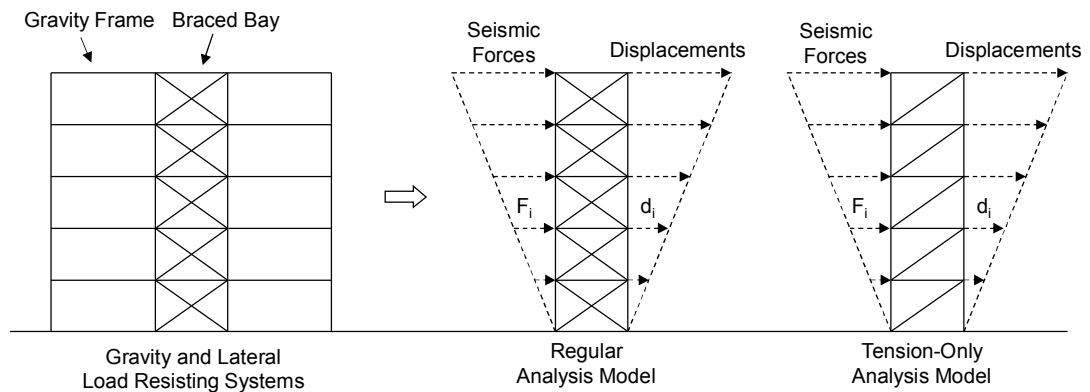


Figure 5.4. Typical analysis models for diagonal bracings

According to AISC341, both the compression and tension braces shall be represented in SCBFs regardless of the type of bracing configuration adopted, and the tension-only bracing is not allowed. On the other hand, OCBFs can be designed either using the tension-only approach or an approach similar to that described for SCBFs. Special rules are given in EC8 for frames with X- or diagonal bracings (Figure 5.1) and frames with V-bracings (Figure 5.2a-c). In frames with X- or diagonal bracings, only the tension diagonals shall be taken into account indicating a tension-only design. In the frames with V-bracings, however, both the tension and compression braces are to be taken into account, which is similar to the AISC341 approach for SCBFs.

In general, the concept of non-dimensional slenderness is used for imposing limits on the slenderness of brace members. The non-dimensional slenderness is a measure of the elastic buckling strength of a brace relative to its yield strength and is expressed as follows:

$$\lambda = \frac{\bar{K}L}{\pi r} \sqrt{\frac{F_y}{E}} \quad (5.1)$$

where \bar{K} : effective length factor; L : length of the brace member; r : radius of gyration of the brace member; F_y : yield strength of the brace material; and E : modulus of

elasticity of the structural steel. The AISC341 provisions impose a limit of $\lambda < 1.27$ for braces in V or inverted-V configurations used in OCBFs. This restriction intends to limit the unbalanced forces that are applied to beams of V-braced frames after brace buckling has occurred, as will be discussed later. For SCBFs, braces shall satisfy $KL/r < 200$ which converts to $\lambda < 2.65$ for a steel with a yield strength of 345 MPa. This upper limit is imposed to prevent dynamic shock effects during earthquakes which are observed for CBFs with very slender braces [11].

In EC8, for frames with X- or diagonal bracings (Figure 5.1a) the non-dimensional slenderness should be limited to $1.3 < \lambda \leq 2.0$. As discussed earlier, EC8 uses a tension-only approach for the design of CBFs with X- or diagonal braces by neglecting the contribution of compression braces. Therefore, the lower limit of 1.3 is defined to avoid using stocky braces with a high compressive strength which may lead to overloading of columns in the pre-buckled stage when both the compression and tension diagonals are active. It is worth noting that, although the tension-only approach is allowed for OCBFs as per AISC341, no such lower bound is imposed on the slenderness of brace members in the US code. On the other hand, the upper limit on non-dimensional slenderness is placed to reduce the shock effects [321] similar to the AISC341 approach for SCBFs. Also, such an upper limit is considered to be beneficial in controlling the out-of-plane deformations of gusset plates during the post-buckling response of braces, which might lead to undesirable premature failures [322]. In EC8, for frames with decoupled diagonal braces (Figure 5.1b) or V-braces (Figure 5.2a-c) the imposed limit is $\lambda \leq 2.0$. The lower bound of 1.3 is omitted for decoupled diagonal braces since twice as many columns are involved in the bracing system when compared with the X-braced system. The omission of the lower bound on λ for the case of V-braced frames is justified by the fact that these frames are not designed using a tension-only approach as per EC8. In structures of up to two stories no limitation applies to λ in the European design which means that rods or cables can be used as diagonals in such buildings.

A special rule (hereafter referred to as the *Omega Rule*) is presented in EC8 to ensure homogeneous dissipative behavior of braces along the height of a structure whereas

no such rule is given in AISC341. According to EC8, the overstrength of a brace member is calculated as follows:

$$\Omega_i = \frac{N_{pl,Rd,i}}{N_{Ed,i}} \quad (5.2)$$

where Ω_i : overstrength of the brace i ; $N_{pl,Rd,i}$: design plastic resistance of the brace i ; and $N_{Ed,i}$: design axial force in the brace i in the seismic design situation. The overstrength is the ratio of the available strength to the seismic demand. EC8 mandates that the maximum overstrength shall not differ from the minimum by more than 25%; i.e. $\Omega_i^{max} \leq 1.25\Omega_i^{min}$. This means that braces in some stories cannot be significantly over-designed while the members in other stories are designed for forces close to the demands produced under the seismic action. This rule on the overstrength produces additional design efforts and possible practical difficulties in proportioning of brace members as explained by Elghazouli [323].

There are also compactness requirements for brace members in both provisions. According to AISC341, braces in OCBFs should satisfy the requirements of moderately ductile members (equivalent to Class 2 in EC8) whereas braces in SCBFs should satisfy the requirements of highly ductile members (equivalent to Class 1 in EC8). On the other hand, EC8 provides cross section classification requirements based on the ductility class and the behavior factor adopted for the design. For DCM with $2 < q \leq 4$ Class 1 or Class 2 cross sections are suggested while for DCH with $q > 4$ Class 1 cross sections are recommended for dissipative members. As discussed in Section 5.2.3, the codified values of q range between 2 and 4 for CBFs designed according to EC8. Thus, it can be deduced that cross section classes 1 or 2 are required for braces of CBFs, qualifying them as either highly or moderately ductile members in the European design procedure.

5.2.6 Design of Columns

An elastic analysis is typically conducted for the design of CBFs which is inherently unable to predict the internal forces in columns when the framing goes into the inelastic range. As discussed earlier, compression braces reach their buckling capacity and can exhibit post-buckling behavior while tension braces yield and strain harden. Thus, following the principles of the *capacity design* approach, it is necessary to design columns of CBFs for the actual expected forces that braces can exert on them and not using those found directly from an elastic analysis. Therefore, both AISC341 and EC8 require that columns of braced bays be designed for additional special load combinations. In the US, ASCE7-10 gives these special seismic load combinations, which can be represented in the following general forms:

$$\underbrace{E_{amp} + 0.2S_{DS}DL}_{\text{seismic}} + \underbrace{1.2DL + 1.0LL + 0.2SL}_{\text{non-seismic}} \quad (5.3)$$

$$\underbrace{E_{amp} - 0.2S_{DS}DL}_{\text{seismic}} + \underbrace{0.9DL + 1.6HL}_{\text{non-seismic}} \quad (5.4)$$

where E_{amp} : amplified seismic loads; DL : dead loads; LL : live loads; SL : snow loads; and HL : loads due to lateral earth pressure. In this chapter, the emphasis is on the seismic part of the above load combinations. In Equations (5.3) and (5.4) the term $0.2S_{DS}DL$ represents the vertical seismic load effects. According to AISC341, for OCBFs, E_{amp} shall be determined by amplifying the lateral seismic loads with a structural overstrength factor of Ω_o . The recommended value of Ω_o in ASCE7-10 is 2.0 for OCBFs. For checking these special load combinations, AISC341 permits designing columns under the action of axial force only and without considering flexural actions. While earlier versions of AISC341 also recommended the use of Ω_o for the design of columns in SCBFs, the provisions of the current version recommend a different approach. In this approach, E_{amp} is determined using a plastic collapse mechanism type of analysis, as shown in Figure 5.5, where all braces are assumed to

resist forces corresponding to their expected strengths in compression and tension. As shown in this figure, the braces in tension carry forces denoted by T while the braces in compression carry forces denoted by C . The expected tensile (T_{ult}) and compressive (C_{ult}) strengths can be determined as follows:

$$T_{ult} = R_y F_y A_g \quad (5.5)$$

$$C_{ult} = \begin{cases} 1.14 F_{cre} A_g \leq T_{ult} \\ \text{or} \\ 0.3 \times (1.14 F_{cre} A_g) \leq 0.3 T_{ult} \end{cases} \quad (\text{whichever creates a larger demand}) \quad (5.6)$$

where R_y : ratio of the expected yield stress to the specified minimum yield stress of the brace material; A_g : gross area of the brace; F_{cre} : critical stress calculated using the column buckling equations of AISC360 considering the expected yield stress, i.e. $R_y F_y$, instead of F_y . The expression which yields the higher demand should be used in Equation (5.6). It is worth noting that the column axial force obtained using this approach does not need to exceed the force obtained through the approach explained for OCBFs (i.e. using the structural overstrength factor of $\Omega_o=2.0$), however, considering a tension-only bracing model.

It is worth noting that in the recent edition of AISC341 [248], it is permitted to use nonlinear dynamic analysis to determine the column forces in SCBFs.

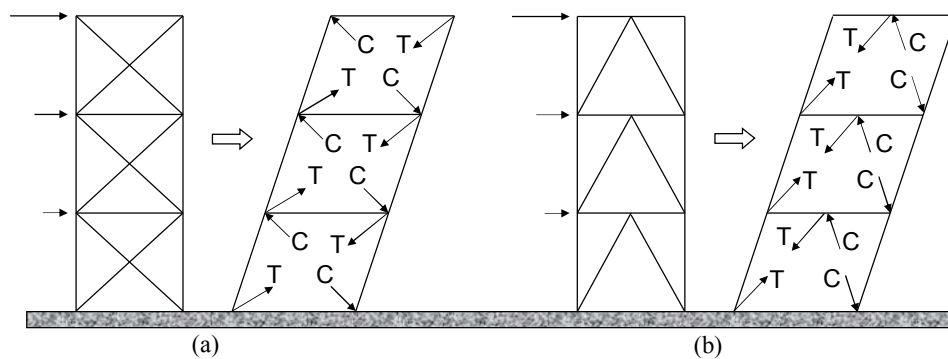


Figure 5.5. Typical analysis models for the capacity design of columns in CBFs

In EC8 no distinction is made between DCM and DCH for the design of CBF columns. In both cases the column axial force obtained from an elastic analysis for any load combination that involves earthquake loads is increased as follows:

$$N_{design} = N_G + N_{amp} \quad (5.7)$$

where N_{design} : amplified axial demand of the column; N_G : available column axial force due to the non-seismic part of the considered load combination; N_{amp} : amplified column axial force due to the seismic action, taken as $1.1\gamma_{ov}\Omega_{i,min}N_E$; with γ_{ov} : ratio of the expected yield stress to the specified minimum yield stress of the brace material, which is identical to R_y in AISC341; $\Omega_{i,min}$: the minimum value of brace overstrength (Ω_i) calculated using Equation (5.2); and N_E : column axial force resulting from the seismic actions according to EC8, which should include the vertical seismic load effects if required by the EU provisions. Consequently, the column axial resistance considering the effect of the available flexural moment due to the seismic loads shall be higher than N_{design} . This approach is somewhat similar to AISC341 approach for OCBFs, however, requires more parameters since N_{amp} is a function of the selected steel grade and the selected brace sizes throughout the building height. The amplification in the European approach is more pronounced for frames with higher γ_{ov} (or R_y) and for cases where the selected braces have strengths that are significantly higher than the applied actions. It should be emphasized that the minimum of the brace overstrengths across the stories shall be used in determining N_{amp} . Although the EU provisions (and partly the US provisions) allow the use of the amplified load approach, it is a well-known fact that this method might fail to properly estimate the expected column demands for some bracing configurations (e.g. see [57]). It is also worth noting that, during the design of columns of CBFs using both provisions, generally the contribution of braces in resisting gravity loads should be conservatively neglected.

AISC341 states that the columns of SCBFs shall satisfy the compactness requirements of highly ductile members (equivalent to Class 1 in EC8) while no such

requirement is given for OCBFs. The cross sectional class requirements of EC8, discussed in Section 5.2.5, are only postulated for energy dissipating members of a system. Thus, it is inferred that EC8 is silent regarding the cross section class level of columns in CBFs, which are not considered as energy dissipating members of this framing system.

5.2.7 Design of Beams

Both provisions have special clauses for the design of beams in CBFs. For OCBFs, AISC341 provides a special requirement for V-braced and inverted V-braced systems. In these structural configurations, the brace in tension reaches its yield capacity while the brace in compression buckles and provides a post-buckling resistance. Therefore, as shown in Figure 5.6a for *Beam A*, unbalanced forces can exist on beams of these systems. For this reason, AISC341 requires beams of Ordinary CBFs to be checked for a special condition where the earthquake loads in standard load combinations are replaced by the case where the tension braces are assumed to reach their expected tensile capacity (i.e. $R_y F_y A_g$) while the compression braces are assumed to carry $0.3P_n$, where P_n is the compressive strength according to AISC360. Note that the forces in the tension braces can also be obtained by replacing the earthquake loads in standard load combinations with E_{amp} , as discussed in Section 5.2.6, using a structural overstrength factor of $\Omega_o=2.0$.

A slightly different approach is considered for beams of Special CBFs in AISC341. For this case, regardless of the CBF configuration, the beams are checked for the special seismic load combinations given in Equations (5.3) and (5.4), where E_{amp} is determined assuming that the tension and compression braces have reached their ultimate capacities as defined by Equations (5.5) and (5.6). This approach results in unbalanced forces on beams of V-braced systems (e.g. *Beam A* in Figure 5.6a) as well as beams of other configurations (e.g. *Beam B* of the X-braced system shown in Figure 5.6b).

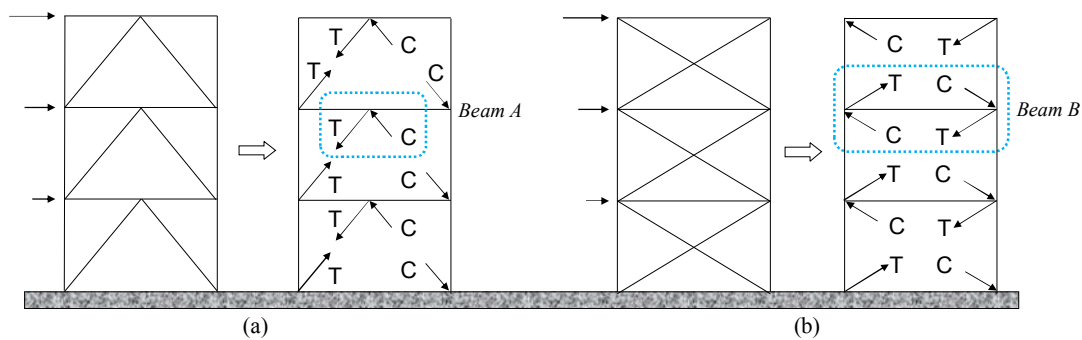


Figure 5.6. Typical forces on beams of CBF systems

In the European approach, no distinctions are made for DCM and DCH ductility class levels and all of the requirements are applied to both classes. Based on EC8, for beams of V-braced and inverted V-braced systems a similar approach to that of AISC341 is considered with the difference that the earthquake loads in standard load combinations are this time replaced by the case where the tension braces are assumed to reach their nominal tensile capacity (i.e. $F_y A_g$) while the compression braces are assumed to carry $0.3F_y A_g$. The main differences compared to the American approach are the omission of the R_y (or γ_{ov}) factor and the fact that the plastic resistance is used for determining the post-buckling strength of compression braces instead of their buckling strength. In addition to the above requirement, another rule is available in EC8 for the seismic design of CBF beams. To this end, the beam axial force obtained from an elastic analysis for any load combination that involves earthquake loads is increased using Equation (5.7), in the same manner explained for columns in Section 5.2.6. As discussed in Section 5.2.5, EC8 recommends a tension-only approach for the analysis of frames with X- or diagonal bracings (Figure 5.1), and thus, beams can have large axial forces based on an elastic analysis (e.g. *Beam B* of the X-braced system shown in Figure 5.6b, assuming $C=0$). For such cases, the latter requirement of EC8 will be influential. Note that, according to both provisions, during the design of CBF beams, the support that the braces can provide for gravity loads are neglected. Similar to columns, AISC341 also provides section compactness requirements for beams of CBFs, while EC8 is silent in this regard. The US provisions require that

beams of Special CBFs at least satisfy the compactness requirements of moderately ductile members (equivalent to Class 2 in EC8) while no such requirement is given for Ordinary CBFs.

5.2.8 Design of Brace Connections

According to AISC341, the brace effective net area shall not be less than the brace gross area for braces of Special CBFs. No such requirement is however given for Ordinary CBFs. This requirement ensures gross section yielding of braces by precluding net section fracture failure modes. In cases where a brace member has a reduced cross section at its connection regions, this requirement is not satisfied, and the brace must be reinforced in these regions. The rules for such reinforcing are also given in the AISC341 provisions. In EC8, no direct rule is presented to address the net area fracture issue. Instead, general design principles are laid out which indirectly take the net section fracture failure into account. According to EC8, if dissipative zones are located in structural members, non-dissipative parts and connections of the dissipative parts to the rest of the structure shall have sufficient overstrength to allow the development of cyclic yielding in the dissipative parts.

The diagonal brace connections in Ordinary CBFs are designed for load effects based on the amplified seismic load (i.e. E_{amp} of Section 5.2.6 using a structural overstrength factor of $\Omega_o = 2.0$) according to AISC341. Nevertheless, the design tension and compression loads of the connection need not be greater than T_{ult} and C_{ult} , respectively, as given by Equations (5.5) and (5.6). For Special CBFs, however, the amplified seismic load procedure is not recommended, and instead, three strength and ductility related provisions are provided. Under tensile actions, the connection must be designed for T_{ult} (Equation (5.5)) while under compressive actions for $1.1C_{ult}$ (Equation (5.6)). Also, rules on the required flexural strength and rotation capacity of brace connections are given for accommodating brace buckling.

EC8 has a less elaborate treatment for the design of brace connections. For fillet welded or bolted connections the following expression should be satisfied:

$$R_d \geq 1.1\gamma_{ov} R_{fy} \quad (5.8)$$

where R_d : resistance of the connection in accordance to EC3; and R_{fy} : plastic resistance of the connected dissipative member based on the design yield stress of the material. This expression is similar to the AISC341 expected tensile strength of the brace, T_{ult} given in Equation (5.5), however, the demand is further amplified by 1.1 which potentially takes into account the strain hardening effect. In EC8 no separate rules are given regarding the flexural strength or rotation capacity.

5.2.9 System Requirements

According to EC8, diagonal elements of bracings shall be placed in such a way that the structure exhibits similar load deflection characteristics at each story in opposite senses of the same braced direction under load reversals. This is ensured by satisfying the following inequality:

$$\frac{|A^+ - A^-|}{A^+ + A^-} \leq 0.05 \quad (5.9)$$

where A^+ and A^- : areas of the horizontal projections of the cross sections of the tension diagonals, when the horizontal seismic actions have positive or negative directions, respectively.

A somewhat similar requirement is provided in AISC341 for Special CBFs only. According to the American provisions, along any line of bracing, the braces shall be deployed in alternate directions such that, for either direction of the force parallel to the braces, at least 30% but no more than 70% of the total horizontal force along that line is resisted by the braces in tension.

5.3 Design of Archetypes

A series of CBF archetypes are design in this section following the American and European provisions. These archetypes are then subjected to a large set of ground motions in the next section to study and compare their seismic performances.

5.3.1 Selected Geometries, Materials, and Member Sizes

A total of six 9-story CBF archetypes were designed considering the following configurations:

- Two-story X-braced; referred to hereafter as the split X-braced configuration
- Single-story X-braced; referred to hereafter as the X-braced configuration
- Inverted V-braced; referred to hereafter as the V-braced configuration

Each configuration was designed using the US and EU provisions to explore the practical differences between the design philosophies as well as seismic performances of these frames. The US frames were designed as Special CBFs while the EU frames as DCH CBFs. The designs assumed the plan geometry of the SAC 9-story building [324], with X- or split X-braced frames in one direction, and V-braced frames in the other direction. In all cases, the braced frames were placed at the perimeter of the building as shown in Figure 5.7. The elevation view depicted in this figure shows the split X-bracing system as a representative. The studied building consists of a basement and nine stories above the ground level. The heights of the basement and the first story are 3.6 m and 5.4 m, respectively, while other stories are 3.9 m high.

Dimensions of the floor plan are 45 m by 45 m and the bay widths are 9 m. The mass values used in the SAC building [324] were directly used in the designs. For the US designs, the building was assumed to belong to the seismic design category D_{max} according to FEMA P695 [250], which represents the highest seismic hazard level with $S_{DS}=1.0g$ and $S_{D1}=0.6g$. To make a fair comparison, $a_g=0.35g$ with Type C

ground was considered as the seismic hazard in the European design. Consequently, the utilized design spectra are identical to those shown in Figure 5.3.

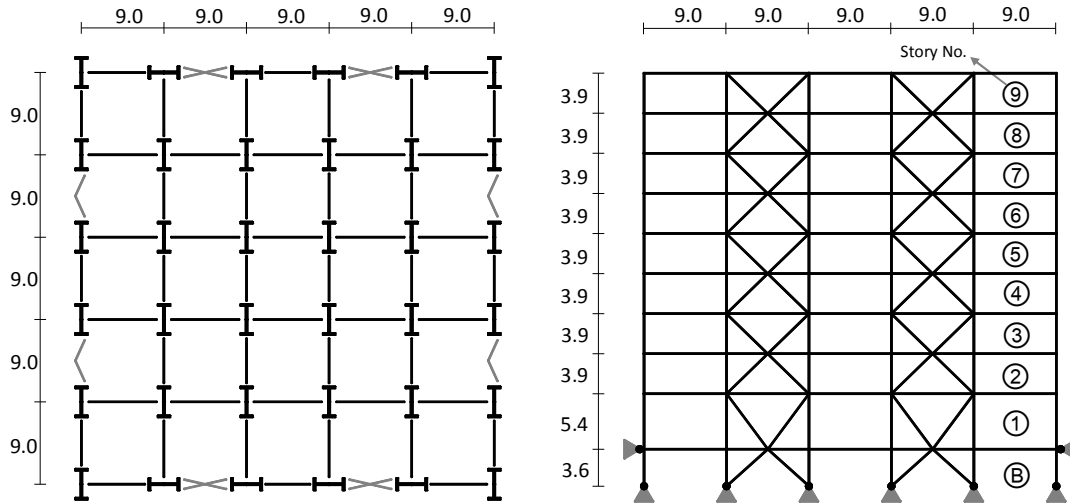


Figure 5.7. Floor plan and elevation view of the archetype building (all dimensions are in meters)

Since the current study was focused on the seismic design and performance of CBFs, only the braced bays were designed considering their share from gravity and earthquake loads. For the US designs, ASCE7-10, AISC360, and AISC341 documents were utilized while the regulations of EC8 and EC3 were considered for the EU designs. Beams and columns were selected from American wide flange sections while hollow structural sections (HSS) were considered for braces. Braces were assumed to be from ASTM A500 Grade B steel with a yield strength of 317 MPa. On the other hand, beams and columns were assumed to be from ASTM A992 steel with a yield strength of 345 MPa. The equivalent lateral force procedure was used in the design of plane CBFs and the interstory drift ratios were limited to 0.02 in all cases. Second-order effects were also incorporated in the design considering a leaner column concept. As noted in Section 5.2, EC8 does not have an explicit requirement regarding the cross sectional class of beams and columns in CBFs. However, to have a fair comparison between the US and EU designs, the beams were selected from Class 1 or Class 2 sections and columns from Class 1 sections in the

European designs. The selected member sizes of the designed split X-braced, X-braced, and V-braced archetypes are depicted in Figure 5.8. The designed archetypes are designated with two-parted names with the first part specifying that the utilized design provisions and the second part showing the structural configuration (2X for split X-braced, X for X-braced, and V for V-braced frame). For instance, the “EU-V” frame is designed as per EC8 and has a V-braced configuration. The height-wise variation of the brace overstrengths (i.e. Ω_i defined in Equation (5.2)) is also presented in Table 5.1 for the designed archetypes. It should be emphasized that the brace overstrengths are calculated only for the tension braces, as defined in EC8.

Table 5.1 Brace overstrengths of the designed archetypes

Story	Brace Overstrength (Ω_i)					
	US-2X	EU-2X	US-X	EU-X	US-V	EU-V
9	6.12	2.10	7.51	2.78	5.06	2.11
8	3.54	1.96	5.29	2.36	3.47	1.94
7	2.91	2.13	5.24	2.52	2.92	1.81
6	2.42	2.12	4.14	2.48	2.42	1.76
5	2.55	1.98	3.64	2.43	2.52	1.73
4	2.31	1.97	3.68	2.41	2.35	1.73
3	2.54	1.74	3.48	2.24	2.50	1.88
2	2.27	1.73	3.36	2.27	2.41	1.80
1	2.21	2.14	3.22	2.44	2.36	1.91

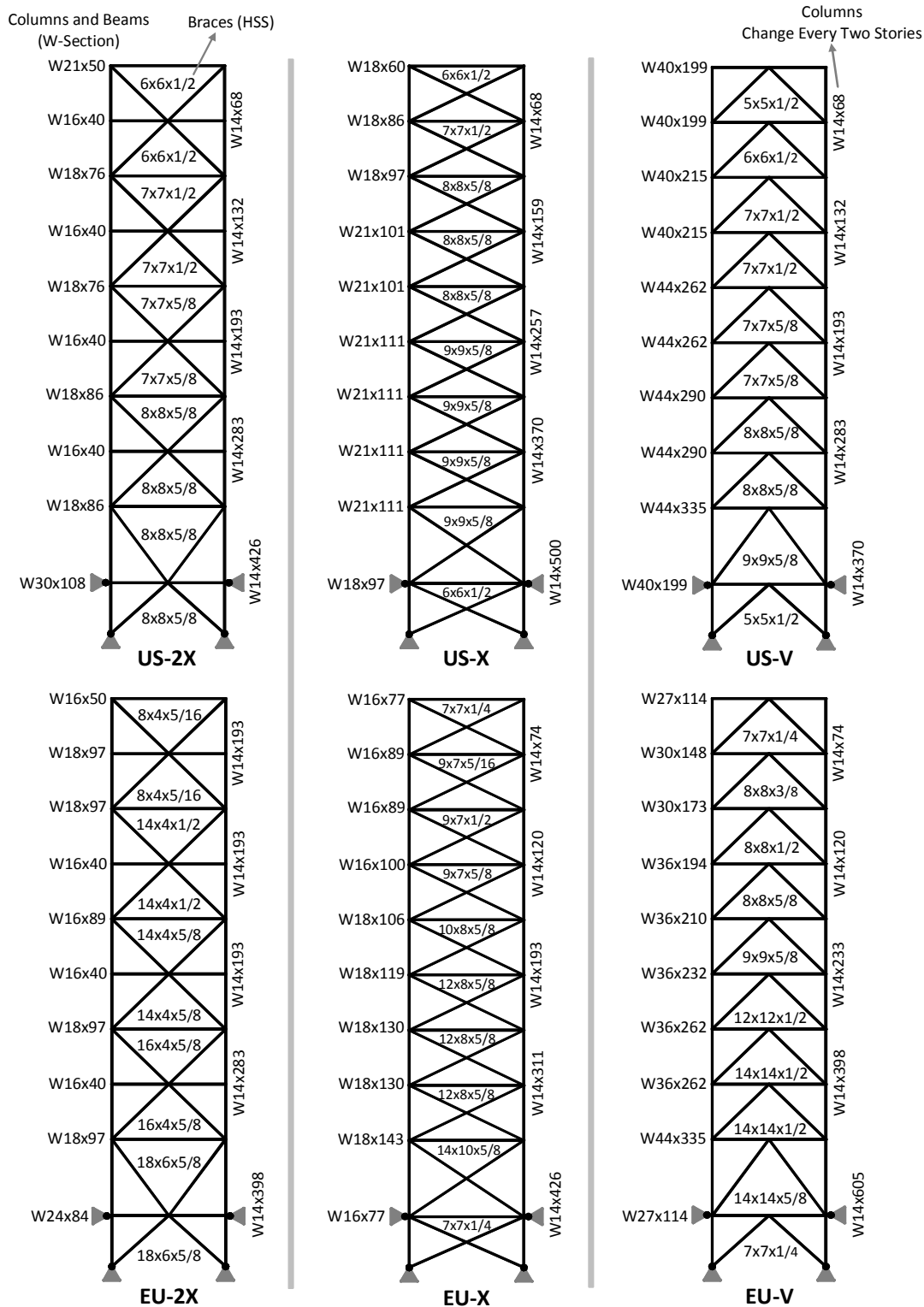


Figure 5.8. Member sizes for the designed original split X-braced, X-braced, and V-braced archetypes

5.3.2 Split X-Braced System

The US design for the split X-braced frame (designated as US-2X in Figure 5.8) has a fundamental period of 1.63 seconds according to an eigenvalue analysis. This value is, however, higher than the upper bound on the fundamental period, as per ASCE7-10, which is 1.02 seconds. Therefore, the base shear (for one braced bay) was determined as 2176 kN considering this upper bound which corresponds to 9.8% of the reactive weight.

In the EC8 provisions, the design methodology for frames with diagonal or X-bracings is notably different than that of V-braced frames, as discussed in Section 5.2. On the other hand, there is still no common consensus on whether frames with two-story split X-bracings shall be designed as frames with X-bracings or as frames with V-bracings, according to EC8. It was finally decided to design the original EU-2X frame using the provisions of EC8 for frames with X-bracings, as suggested in other well-known European references (e.g. [325]). However, for the sake of completeness, the EU-2X frame is also designed using the provisions of EC8 for frames with V-bracings, as an alternative design in a subsequent section. It should be emphasized that, all of the results presented under the name EU-2X correspond to the original design and not to the alternative one.

The EU-2X frame has a fundamental period of 2.00 seconds. This period value is significantly higher than that of the US-2X frame mainly because compression braces were removed from the analysis model of EU-2X, as discussed in Section 5.2.5. Since there is no upper bound for the period in EC8, this value is directly used in calculations, resulting in a base shear of 1728 kN (for one braced bay) which corresponds to 7.6% of the reactive weight. As it can be seen, although there are significant differences between the US and EU provisions regarding response modification coefficients (behavior factors), the definition of reactive mass, calculation of period, modeling approaches, etc. the design base shears for US-2X and EU-2X came out to be somewhat comparable to each other. In the design of US-2X, the drift constraints were not actively involved. However, these requirements

significantly affected the design of EU-2X in which the compression braces were neglected, and the system had a relatively lower lateral stiffness.

There are pronounced differences between the selected brace members, as shown in Figure 5.8. In the US-2X frame, stocky braces have been employed while in EU-2X, braces are relatively slender, mostly having slenderness ratios (i.e. KL/r) above 100. This is mainly because the braces in EU-2X are designed only for tension while satisfying the non-dimensional slenderness limit of $1.3 < \lambda \leq 2.0$. As a result, these braces are rectangular HSS with sufficient area to resist the applied tension while having low buckling capacities about one of the principal axes to satisfy $1.3 < \lambda$. On the other hand, braces in US-2X are square HSS since they have been designed for both tension and compression loadings. In addition to this, the section compactness requirements (i.e. b/t limit where b is the width of the HSS and t is its thickness) are significantly different in the US and EU designs for HSS braces. Based on AISC341, the b/t should be limited to 14 for $F_y=317$ MPa considering highly ductile members, while EC8 limits this ratio to 28 for Class 1 sections. Thus, the US design employed HSS braces with considerably lower b/t ratios compared to the EU design.

A weight-wise comparison between US-2X and EU-2X is presented in Table 5.2. Similar to the design base shears, the total weights are also comparable. The weight of the EU design is about 15% higher than that of the US design. Most of this difference stems from the fact that the weight of brace members is 28% more in EU-2X. Also, the total weight of beams and columns is about 14% heavier in the European design in which heavier sections are used in top floors to control the drift. The weights of braces, columns, and beams are also given in Table 5.2 as a percentage of the total weight inside parentheses. Although the total weights are not identical, the distribution of the steel material is very similar in the US-2X and EU-2X frames.

Table 5.2 Comparison of steel weights of the designed archetypes

Archetype	Steel Weight* (kN)			
	Braces	Columns	Beams	Total
US-2X	82 (19%)**	266 (62%)	84 (19%)	432
EU-2X	105 (21%)	301 (60%)	96 (19%)	502
US-X	152 (25%)	320 (53%)	130 (22%)	602
EU-X	153 (27%)	281 (50%)	133 (23%)	567
US-V	78 (12%)	251 (38%)	325 (50%)	654
EU-V	102 (14%)	350 (49%)	269 (37%)	721

* For one braced bay only

** As a percentage of the total weight

Based on Table 5.1 it is observed that the brace overstrengths are not changing notably through the height in the EU-2X frame, due to the Omega Rule of $\Omega_i^{max} \leq 1.25\Omega_i^{min}$, discussed in Section 5.2.5. For US-2X, on the other hand, the brace plastic overstrengths are higher than EU-2X (especially at the upper stories), with an increasing trend towards the top stories.

Another important issue observed in the course of this study was the difficulty of the design process associated with the European approach. As explained earlier, EC8 dictates many inter-related provisions for the design of braces in CBFs which significantly complicates the design procedures. For instance, during the design of EU-2X, it was deemed necessary to increase the brace sizes of the top two stories to control the interstory drifts of the 8th and 9th stories. However, the Omega Rule, necessitated that these brace sizes not be increased unless the braces of some of other stories are also increased in size. On the other hand, the brace size in the 2nd and 3rd stories could not be increased since the chosen section (i.e. HSS 16×4×5/8) was the heaviest available section in the HSS profile list which had the required area and satisfied the non-dimensional slenderness limit of $1.3 < \lambda$. Consequently, to comply with the drift requirements at the top two stories, instead of increasing the brace sizes, the less preferred method of increasing the column and beam sizes was employed in these stories.

It should be emphasized that the US approach for the design of CBF braces is much simpler compared to the European design and does not have many inter-related provisions. The numerical simulations of Section 5.4 will investigate how these complexities and simplifications associated with each design code can affect the seismic performance of the designed CBFs.

5.3.3 X-Braced System

For the X-braced configuration, the US design (designated as US-X in Figure 5.8) has a fundamental period of 1.41 sec which is again higher than the upper bound defined by ASCE7-10, resulting in a base shear of 2176 kN for one braced bay, which is 9.8% of its reactive weight. A higher fundamental period of vibration (i.e. 1.93 sec) was found for EU-X mainly due to the use of the tension-only approach, which corresponded to a base shear of 1784 kN (i.e. 7.8% of the reactive weight) for one braced bay.

Similar to the split X-braced frames, the design base shears for US-X and EU-X came out to be comparable to each other despite the many differences that exist in their design procedures. As reported in Table 5.2, the total steel weights are also close to each other, with the US design being 6% heavier this time, mainly due to the use of heavier columns. Also, the distribution of the steel material among the members is very similar in the two designs. Furthermore, similar to the previous section, rectangular HSS were employed in EU-X while square braces were utilized in US-X. Based on Table 5.1, it can be seen that the brace overstrengths are notably higher in US-X and increase significantly towards the top stories while the Ω_i values for EU-X are lower and have a uniform height-wise distribution. It is worth noting that the design of EU-X was significantly affected by the Omega Rule. The HSS section chosen for the top brace (i.e. HSS 7×7×1/4) is the smallest section which satisfies all the requirements. Nevertheless, the overstrength for this brace came out to be 2.78, as reported in Table 5.1. Thus, the braces at the lower stories were selected as the smallest feasible sections with Ω_i values above $(2.78/1.25=) 2.22$.

5.3.4 V-Braced System

The fundamental period of the US design for the V-braced frame (designated as US-V in Figure 5.8) is 1.58 seconds which is once more higher than the upper bound defined by ASCE7-10. Therefore, the base shear for one braced bay of US-V was again found to be 2176 kN (i.e. 9.8% of the reactive weight). On the other hand, the EU design for the V-braced frame (designated as EU-V in Figure 5.8) has a fundamental period of 1.30 seconds which is lower than that of US-V. Due to the use of a lower fundamental period and also a considerably lower behavior factor (i.e. $q=2.5$, as explained in Section 5.2.3) the base shear for one braced bay came out to be 4260 kN which is equal to 18.6% of the reactive weight. Unlike the US and EU designs for the X- and split X-braced frames which had somewhat similar base shears, the design base shear of EU-V is significantly higher than that of US-V.

The drift requirements were not actively involved in the design of V-braced archetypes. Similar to EU-X, the design process of EU-V was dominated by the Omega Rule. As reported in Table 5.1, the top braces have the highest overstrength in EU-V and the other braces are selected accordingly to comply with the Omega Rule. Similar to X- and split X-braced archetypes, the brace overstrengths are higher in US-V compared to EU-V, particularly at the top stories.

For the brace members in both US-V and EU-V stocky square HSS are employed, because in both frames the braces were designed for compression as well as tension loading. The weight-wise comparison presented in Table 5.2 shows that, although EU-V is designed for almost twice the base shear of US-V, the total weights of the frames are close to each other, with the European design being only 10% heavier. One of the key reasons for this is the difference that exist between the compactness requirements of AISC341 and EC8 for HSS braces. As discussed earlier, EC8 permits using HSS with higher b/t ratios compared to AISC341, and thus, in the European approach the designer can use HSS members with a relatively high radius of gyrations without increasing the thickness of the section significantly. In contrast, due to the stringent compactness requirement of the HSS braces in AISC341, the

designer is forced to use sections with relatively thick walls. This is clearly observed in Figure 5.8 where almost all of the brace members in EU-V have higher b/t ratios compared to their counterparts in US-V. It is important to note that the above discussion is limited to HSS braces since the compactness requirements for other types of sections are different in EC8 and AISC341 provisions.

Similar to what was observed for the X- and split X-braced archetypes, the total weights of US-V and EU-V are close, however, examining Table 5.2 reveals that, unlike the previous cases, there are significant differences in the distribution of the steel material between members of the two frames. As reported in this table, the highest share (about 50%) of the total steel is used in beams of US-V while the highest share (about 49%) is used in columns of EU-V. This is due to the use of different capacity design approaches by the US and EU provisions. As discussed in Section 5.2.6, EC8 requires columns to be designed for an amplified seismic load while AISC341 replaces braces with their expected tensile and compressive strengths to obtain the design loads of columns. Furthermore, as discussed in Section 5.2.7, there are differences between the codes in the definition of unbalanced loads which are used for the design of beams in V-braced frames. The American approach assumes that the forces in the tension and compression braces will reach $R_y F_y A_g$ and $0.3 \times 1.14 F_{cre} A_g$ while the European approach assumes these forces to be $F_y A_g$ and $0.3 F_y A_g$, respectively. It can readily be shown that the US method will result in significantly higher unbalanced loads (and consequently heavier beams) compared to the EU approach, provided that identical brace members are used. The effects of using different capacity design approaches in V-braced CBFs are further investigated in the nonlinear time history analyses of Section 5.4 that follows.

5.4 Comparison of Seismic Behaviors

A comprehensive study was undertaken to investigate the seismic behavior of the archetypes designed according to AISC341 and EC8. Numerical models of these structures were subjected to a large set of ground motions and the simulation results

of a total of 880 analyses were examined to highlight the similarities and differences between the responses.

5.4.1 Details of Numerical Simulations

All of the analyses were conducted using the FE package, ABAQUS 6.12-1 [273], considering two-dimensional models of the structures. Both material and geometric nonlinear effects were included in the analyses. Since the study is focused on the seismic performance of CBFs, only one braced bay was modeled, however, to properly capture the second-order effects, an elastic leaner column was also included.

A von Mises plasticity constitutive model with kinematic hardening considering bilinear material behavior was used in the numerical simulations. All members of the frame and the leaner column were modeled using B21 two-node linear beam elements, each having one integration point at the mid-length and five integration points through the height of the section. A rather small mesh size was employed with 12 elements in each brace, 18 elements in each beam, and 8 elements in each column. All of the beam-to-column, brace-to-column, and brace-to-beam connections were pinned and were modeled in the finite element models using the *pin-type multi-point constraint* (MPC Pin) technique available in ABAQUS [273]. Furthermore, at each story level, the horizontal displacement of the leaner column was constrained to that of the CBF column using the *equation* technique of ABAQUS [273].

Based on the recommendation of FEMA P695 [250], the reactive seismic mass of each floor was determined as $1.05DL+0.25LL$ using the dead and live load values reported for the original SAC building [324]. It is worth noting that 25% of this mass was considered in the models since the braced bay under investigation will only receive one-fourth of the base shear. The vertical loads on the leaner column were also calculated in a similar manner.

To properly capture the buckling behavior of braces in CBFs, it is necessary to include initial imperfection in these members. The comprehensive studies of D’Aniello et al. [326, 327] have shown that the introduced amount of imperfection can affect the seismic response of the CBF structure under consideration. Furthermore, it is suggested by these researchers to use theoretical formulations instead of empirical methods for estimating the proper level of imperfection, since the former depends not only on the brace length, but also on the flexural strength interaction of the brace cross section. Nevertheless, considering the comparative nature of the current study, it was finally decided to use an initial imperfection equal to 0.1% of the brace length (i.e. $L/1000$) in all models. This amount of imperfection has been previously reported as a reasonable estimate by Deierlein et al. [328] and also used successfully in numerical simulations of many other studies such as Fell [329] and Okazaki et al. [306]. In any case, more advanced and accurate methods for estimating the initial imperfection can also be employed, as thoroughly discussed by D’Aniello et al. [326, 327].

The imperfection can be incorporated in the finite element model via different approaches. For instance, an initial deformation can be superimposed on the brace members at the start of the analysis without altering the zero-stress field, or the braces can be modeled explicitly with imperfection. Nevertheless, the preliminary analyses using these methods revealed that, during a number of the investigated earthquakes, some of the braces became stretched significantly in tension and lost their imperfection to an extent that they failed to capture buckling in the next load cycles. Consequently, some of the brace members yielded both in tension and in compression during the earthquake. It should be emphasized that the problem was not seen in all braces and during all earthquakes, however, was observed sporadically, affecting the results notably. After investigating different approaches, it was finally concluded to introduce initial imperfection by applying out-of-plane distributed loads on brace members. This way the source of imperfection remained on the brace members, forcing them to buckle under compressive loads even after braces had experienced significant yielding and stretching. The method was found

to be a reliable approach which guaranteed brace buckling during the several hundred analyses conducted in the course of this study. It is important to note that the initial stress in the brace members due to this imperfection load was relatively low (below $0.07F_y$ in all models except EU-V where $0.12F_y$ was observed in braces of lower stories), and thus, did not have a detrimental effect on the analyses.

Another important issue in nonlinear time history analysis is damping. Although the equivalent viscous damping approach using Rayleigh formulation is commonly adopted, great care should be taken while using this method. Based on this approach, the damping matrix, \mathbf{C} , is determined as follows:

$$\mathbf{C} = \alpha_m \mathbf{M} + \beta_k \mathbf{K} \quad (5.10)$$

where \mathbf{M} and \mathbf{K} are the mass, and stiffness matrices, respectively, and α_m and β_k are proportionality factors which are calibrated to result in a predefined percentage of critical damping (ξ) at two desired vibration periods. Many researchers such as Hall [330], D’Aniello et al. [326], and Charney [331] have illustrated that using this method can produce unrealistically large damping forces and unconservative displacement demands in nonlinear analyses. This issue was also clearly observed in the present study during initial analyses. Brace members experienced very high velocities when yielded which in turn created large damping forces in these members, sometimes even comparable to their plastic capacities. As discussed by Deierlein et al. [328], there is no solid consensus on a solution scheme for this problem. Many approaches have been proposed such as using a capped viscous damping formulation or using the tangent stiffness matrix instead of the initial (or elastic) stiffness matrix as \mathbf{K} . However, most of these methods cannot be readily implemented in most commercial finite element software. A more convenient approach was consequently chosen in this study, as described by Deierlein et al. [328], where the stiffness proportional part of damping is minimized, and damping is mostly represented by the mass proportional part. This approach reflects the fact that the stiffness proportional part of damping is considered to have a more

pronounced effect in producing unrealistic damping forces. To this end, $\alpha_m=0.3$ and $\beta_k=0.00005$ were used in all models. The value of β_k was found to be sufficient enough to reduce high-frequency noises in the response while minimizing the stiffness proportional part of damping. Free vibration analyses of the designed archetypes revealed that the used factors correspond to a ξ of about 5% in the 1st mode of vibration and 2% in the 2nd mode.

To verify the adopted modeling approach regarding imperfection, material behavior, element type, mesh size, and other issues, the finite element results were compared to the test results of specimen No. 17 tested by Black et al. [284]. The specimen was an HSS 4×4×1/4 brace with a length of 2428 mm and yield stress of 407 MPa. The comparative results are depicted in Figure 5.9. An acceptable level of conformity can be observed between the results. It is worth noting that the numerical results are almost identical to those previously reported by D’Aniello et al. [326] considering a similar material model. Any discrepancy in Figure 5.9 can be attributed to the fact that the beam elements are unable to capture the additional imperfections caused by local buckling. Also, using more advanced material models (e.g. Menegotto-Pinto) instead of the utilized bilinear material model can enhance the results, as noted by D’Aniello et al. [326]. Nevertheless, considering the aims of this comparative study, the accuracy of the adopted modeling approach was deemed to be sufficient.

The developed finite element models were finally subjected to a set of 44 ground motion records presented in FEMA P695 [250]. This document provides two sets of records which are designated as “far-field” and “near-field” sets by FEMA. In the present thesis, the far-field set was utilized. It should be mentioned that these ground motions are first normalized based on their peak ground velocities and then, considering the fundamental period of the designed archetypes, are scaled by a factor of 2.59 during the analysis to reach the MCE_R spectral demand of the seismic design category D_{max} .

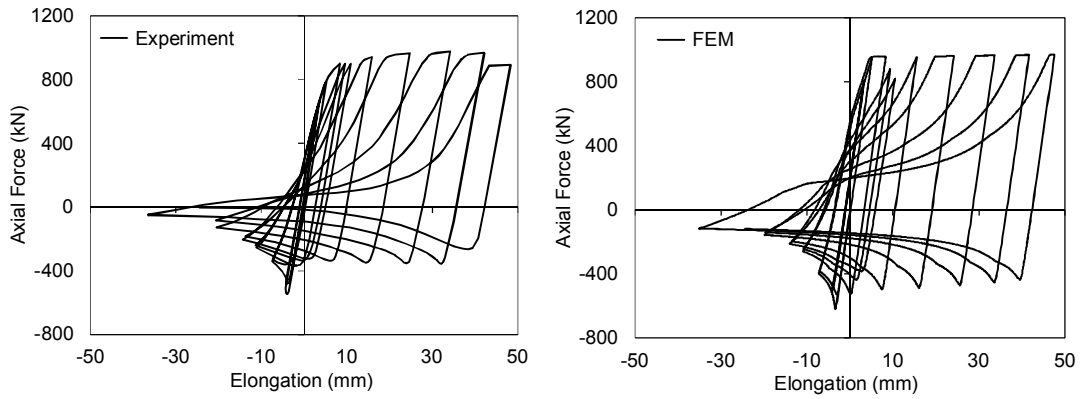


Figure 5.9. Comparison the finite element results with the test results of Black et al. [284]; Tension (+) Compression (-)

5.4.2 Split X-Braced System

For the sake of brevity only representative results of the nonlinear time history analyses for US-2X are presented in Figure 5.10, and for other cases, only the median of the recorded values is reported. In this figure, the gray lines represent the response values obtained for the whole record set and the solid black line is the median of the results. Interstory drifts, residual displacements, floor velocities, and floor accelerations are reported as global indicators while quantities such as the brace out-of-plane deformation and ductility as local performance indicators. It should be emphasized that floor velocities are reported relative to the ground so that they can be related to damping, while accelerations are reported as total floor accelerations so that they can be related to the seismic forces exerted on non-structural components [332, 333]. Figure 5.10g reports the brace accumulated equivalent plastic strain (designated as PEEQ in ABAQUS [273]), defined as follows:

$$PEEQ = \int_0^t \sqrt{\frac{2}{3} \dot{\epsilon}_{ij}^p \dot{\epsilon}_{ij}^p} dt \quad (5.11)$$

Where $\dot{\epsilon}^p$ is the plastic strain rate tensor. It should be noted that PEEQ is reported at the most critical point of each brace member which is located typically at its mid-length. The ductility demands for braces (i.e. brace elongation divided by brace yield

elongation) are also presented in Figure 5.10h in which positive values on the horizontal axis correspond to the ductility demand in tension and negative values to the ductility demand in compression.

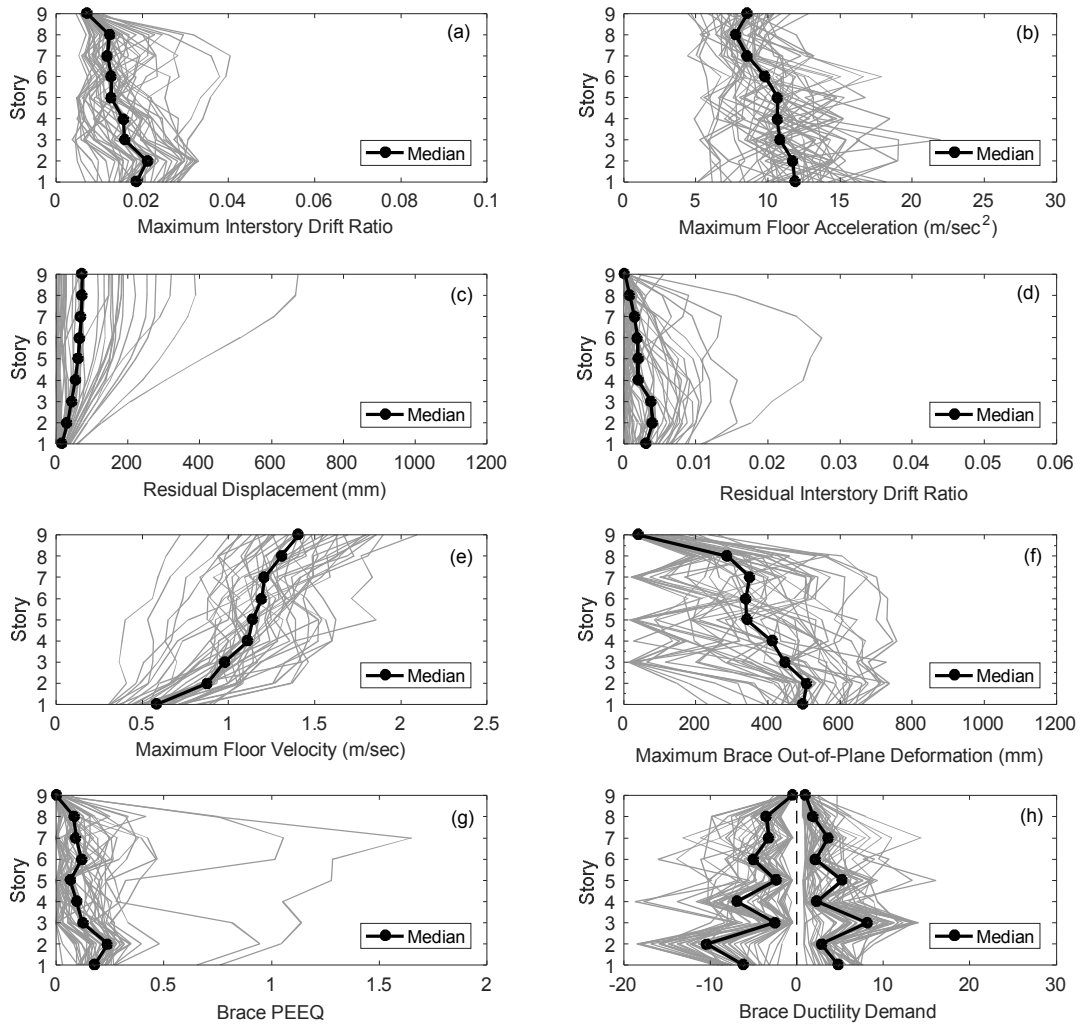


Figure 5.10. Summary of analysis results for US-2X

A clear comparison between the median responses of US-2X and EU-2X is given in Figure 5.11 as well as

Table 5.3. Based on this table, US-2X and EU-2X have experienced comparable base shears and column axial forces during the earthquakes. The difference is about 16%

between the median values, with US-2X exhibiting lower forces. This is in contrary to the results of the design phase, where the US frame had a slightly higher design base shear. The frame responses shown in Figure 5.11 are similar in some cases while quite distinct in others. Braces in EU-2X were significantly more slender than those of US-2X, however, Figure 5.11e shows that the medians of the recorded maximum floor velocities are very similar for both designs. Thus, it appears that the floor velocity is not too sensitive to the slenderness of the brace members in properly designed CBFs. On the other hand, as shown in Figure 5.11b, floor accelerations are generally higher in the EU design, indicating that higher inertial forces will be exerted on non-structural components of EU-2X compared to US-2X during earthquakes.

The medians of the recorded residual drift ratios are presented in Figure 5.11d which did not exceed 0.5% for both archetypes. McCormick et al. [272] suggest this limit as a permissible residual drift ratio above which repair of the structure might become uneconomical. The main difference is that the US frame exhibited higher residual drifts in the lower stories while the EU design had higher residual drifts in the upper stories.

Table 5.3 Comparison of responses of the designed archetypes

Archetype	Median of Results (kN)	
	Maximum Base Shear	Maximum Column Axial Force
US-2X	4966	11500
EU-2X	5969	13730
US-X	6235	14320
EU-X	7385	14420
US-V	5113	10640
EU-V	8380	15930

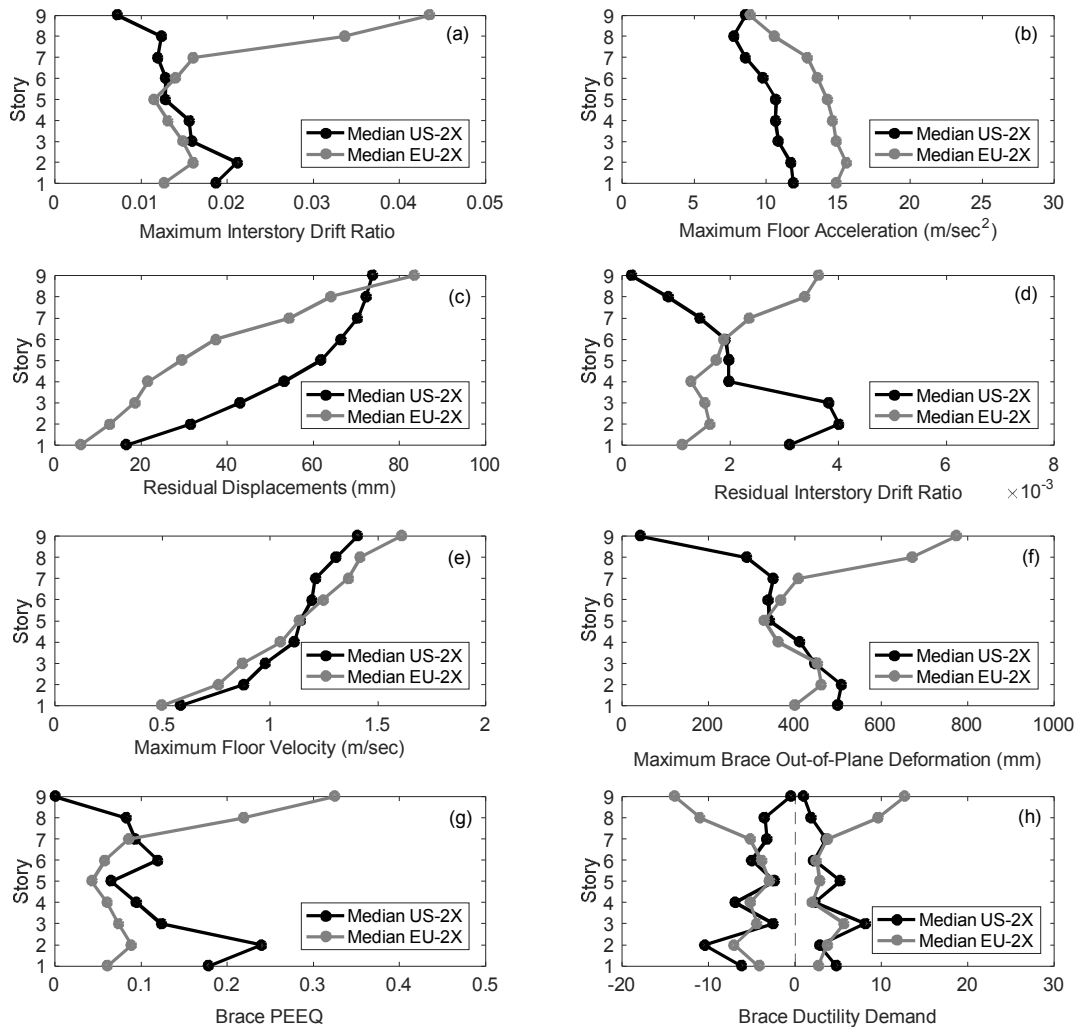


Figure 5.11. Comparison of analysis results for US-2X and EU-2X

Results presented in Figure 5.11f reveal that the braces in both frames have experienced significant out-of-plane deformations due to buckling, sometimes as high as 15% of the brace length. Interestingly, the median values for brace out-of-plane deformations are very similar for US-2X and EU-2X, except for the top two stories which are discussed later.

The medians of brace ductility demands for US-2X and EU-2X are given in Figure 5.11h. The ductility demands are found to be comparable to each other and limited

to ± 10 (except for the top two stories which are discussed later), with the US design exhibiting somewhat higher demands. It is observed in Figure 5.11h that, when the brace ductility demand in compression is relatively high in a story, the ductility demand in tension is relatively low in the same story. Also, the height-wise variation of the ductility demand has a zigzag form with subsequent increases and decreases. Investigation of the analysis results demonstrated that this is due to the deformation of the brace-intersected beams; i.e. those located at the intersection of the split two-story diagonal braces. As thoroughly discussed by Shen et al. [314, 315], the codified seismic design force for these members is zero or very small resulting in the selection of small sections for these beams (e.g. W16 \times 40 sections in Figure 5.8). However, the actual distribution of forces during earthquakes can create large internal forces in these beams and significant deformations at their mid-span, sometimes leading to their yielding [314]. As schematically depicted in Figure 5.12 for a two story CBF with split X-bracings, if the brace-intersected beam does not have sufficient strength or stiffness, the unbalanced loads arising from the buckling of the bottom compression brace (i.e. C_1 in the figure) will deflect the beam downwards, leading to an increase in the ductility demand of the compression brace in the 1st story and an increase in the ductility demand of the tension brace in the 2nd story. If the top compression brace (i.e. C_2 in the figure) buckles sooner, again a similar phenomenon will occur, however, the beam would deflect upwards. Based on the results summarized in Figure 5.11h, it seems that the brace-intersected beams in both US-2X and EU-2X have mostly deflected downwards due to the applied unbalanced forces, increasing the ductility demands of the braces in compression in the 2nd, 4th, 6th, and 8th stories. The height-wise variation of the brace ductility demands is more abrupt in US-2X, suggesting that the deflection of brace-intersected beams might have a more notable effect on the ductility demands of stocky braces, compared to slender brace members. More comprehensive information on the behavior of brace-intersected beams in split X-braced frames can be found in Shen et al. [314, 315].

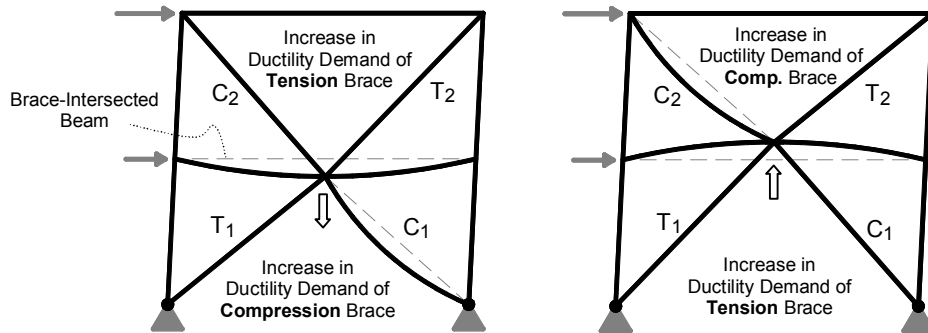


Figure 5.12. Deformation of brace-intersected beam and its effect on brace ductility demands

The most important difference between US-2X and EU-2X was in their interstory drift responses. As summarized in Figure 5.11a, the interstory drifts exhibited by these frames are somewhat similar up to the 7th story, mostly below the design drift limit of 2%. However, the drift ratios tend to increase significantly for EU-2X in the top two stories. The behavior can be considered as a soft-story mechanism developing at the top stories of the EU frame. Simulation results demonstrated that the EU-2X frame experienced the soft-story behavior during most of the earthquakes while no such response was apparent for US-2X. Examining the analysis results revealed that these braces were mostly inadequate in properly restraining the drift at the top stories. During some of the earthquakes, this issue has even led to the development of plastic hinges in the columns of the 8th story (e.g. Figure 5.13). Furthermore, the accumulation of the damage at the top stories of EU-2X might had an effect on reducing the PEEQ (Figure 5.11g) and brace ductility demands (Figure 5.11h) in its lower stories (1 to 7), in which the American design generally experienced higher demands.

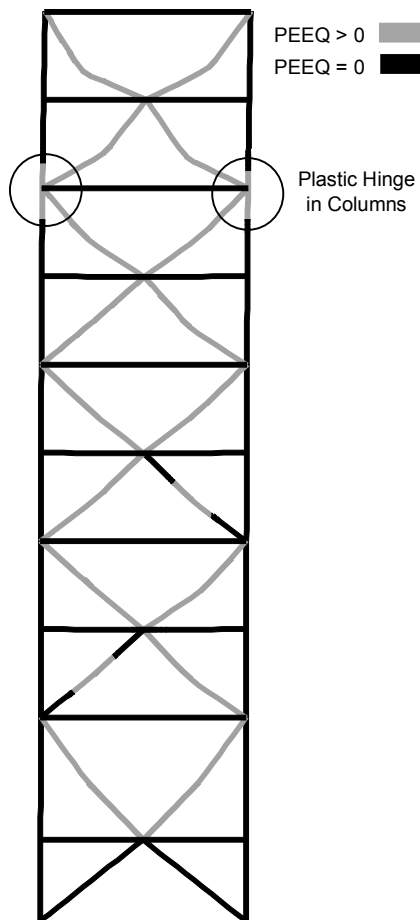


Figure 5.13. Distribution of PEEQ in EU-2X at the end of the analysis for record No. 30

Although a great deal of effort and care was taken in the design phase of all archetypes, it was decided to re-design EU-2X with different approaches to investigate whether the observed soft-story behavior can be resolved or it is an issue related to the core design methodology of the EU provisions. Thus, in addition to the original design (i.e. EU-2X), six alternative design approaches were considered as follows. In the **first alternative** approach, a fully automated design and optimization computer code was programmed considering an evolutionary algorithm developed by Kazemzadeh Azad et al. [334]. As stated in Section 5.3.1, there are many inter-related provisions in the design of CBFs according to EC8, and thus, the aim of this alternative was to check whether an automated routine is capable of providing a

better-performing structure. A total of 15000 designs were checked by the program to reach to the final optimum design (designated as EU-2X-OPT) which satisfied the strength and drift requirements. In the **second alternative** (designated as EU-2X-TOP) an approach proposed by Mazzolani et al. [335] was considered where a portion of the base shear is applied directly to the top floor, to necessitate larger braces at the top stories, and the remaining portion of it is distributed over the building height. This method was in use in older American specifications and is still in use in some codes and tends to resemble higher mode effects in the equivalent lateral load procedure. Considering the fundamental period of the archetype and after examining different seismic specifications, a value of 7% of the base shear was selected as the top load. EC8 states that the lateral stiffness of stories shall not change abruptly over the height unless the structure is designed using modal response spectrum analysis. Although EC8 does not provide a quantifiable criterion for checking this issue, it was decided to also include an split X-braced frame designed using spectrum analysis (i.e. EU-2X-SPC) as the **third alternative**. As mentioned in Section 5.3.2, some researchers suggest that split X-braced frames are in fact a combination of V- and inverted V-braced frames, and thus, should be designed as V-braced frames. Therefore, in the **fourth alternative** (i.e. EU-2X-DSV) the split X-braced frame was designed using the regulations of EC8 for frames with V-bracings. It is worth noting that, although EC8 does not explicitly address the capacity design approach for beams of split X-braced frames which are not intersected by braces (similar to *Beam B* shown in Figure 5.6b), in order to have a fair comparison, these beams are designed by replacing the earthquake loads in standard load combinations of by the case where the tension braces are assumed to reach their nominal tensile capacity (i.e. $F_y A_g$) while the compression braces are assumed to carry $0.3F_y A_g$. As discussed previously and summarized in Table 5.1, the brace overstrengths are rather uniform for EU-2X (because of the Omega Rule) while quite non-uniform for US-2X with drastic increases at the top stories. Since the Omega Rule was employed in the design of the above-mentioned four alternatives, the distribution of overstrengths was also uniform in these alternatives. Therefore, the **fifth alternative** (i.e. EU-2X-

NOM) was designed identical to EU-2X, however, with the Omega Rule being omitted completely. Also, the **sixth alternative** (EU-2X-DSV-NOM) was designed as a V-braced frames (identical to EU-2X-DSV), however, without considering the Omega Rule. The omission of the Omega Rule in the European design process, albeit only for the top braces, was also discussed recently by D’Aniello et al. [336]. The design results for all the above-mentioned alternatives are summarized in Figure 5.14. It is worth noting that the EU-2X-NOM alternative is the lightest design which is 12% lighter than the original EU-2X frame, while EU-2X-DSV is the heaviest one with 15% higher steel weight than the original design.

The height-wise variation of brace overstrengths for all of the designed split X-braced archetypes is presented in Figure 5.15a. As it can be seen, US-2X has generally the highest overstrengths. In order to have a more clear observation, the normalized brace overstrengths (i.e. Ω_i/Ω_i^{min}) are also compared in Figure 5.15b. Because of the Omega Rule, the normalized brace overstrengths for all of the European designs lie between 1.0 and 1.25 (vertical red lines in the figure) except EU-2X-NOM and EU-2X-DSV-NOM, in which the Omega Rule was omitted. The normalized brace overstrengths for the US design also lie inside the bounds defined by EC8 for the first seven stories, however, exceed the upper limit significantly in the top two stories; which are the stories where the soft-story behavior was observed in EU-2X. Interestingly, the European designs which omitted the Omega Rule also followed a similar trend as the US-2X frame by exceeding the EC8 limit at the top two stories.

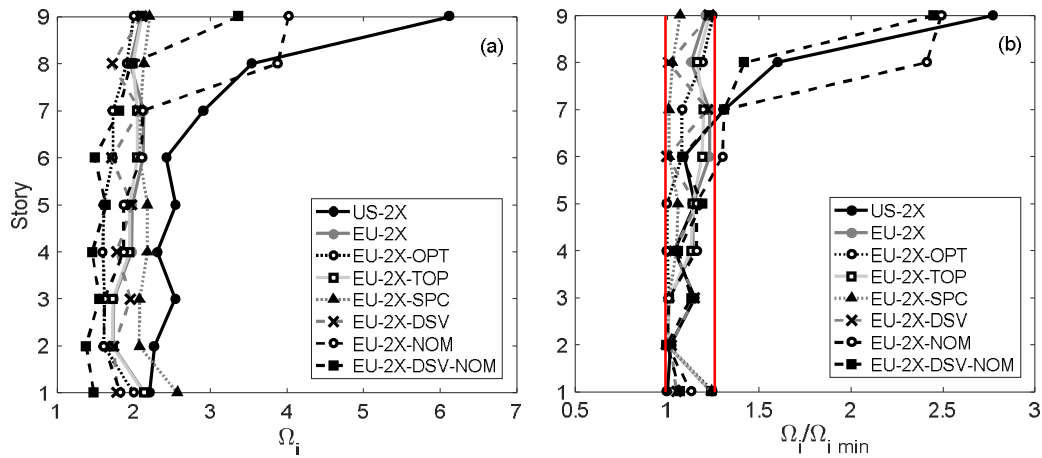


Figure 5.15. Height-wise variation of brace overstrengths for the designed split X-braced archetypes

All six alternatives were subjected to the full set of 44 ground motions, and the results are summarized in Figure 5.16. As expected, the responses are somewhat similar up to the 7th story. However, the soft-story behavior is still observed to some extent in all alternative designs, except EU-2X-NOM, and EU-2X-DSV-NOM, in which the drifts remained mostly below the design limit of 2%. Beside these alternatives, it appears that the most effective approach among the other alternatives is the top load approach (i.e. EU-2X-TOP), proposed by Mazzolani et al. [335], which reduced the top story drift by about 40% compared to the original EU-2X design. More interestingly, the EU-2X-DSV frame which was designed as a V-braced system as per EC8 exhibited the worst performance among the alternatives, experiencing drifts in excess of 6%. On the other hand, the behavior of EU-2X-NOM (which was also the lightest alternative among the EU designs) was almost identical to that observed for US-2X.

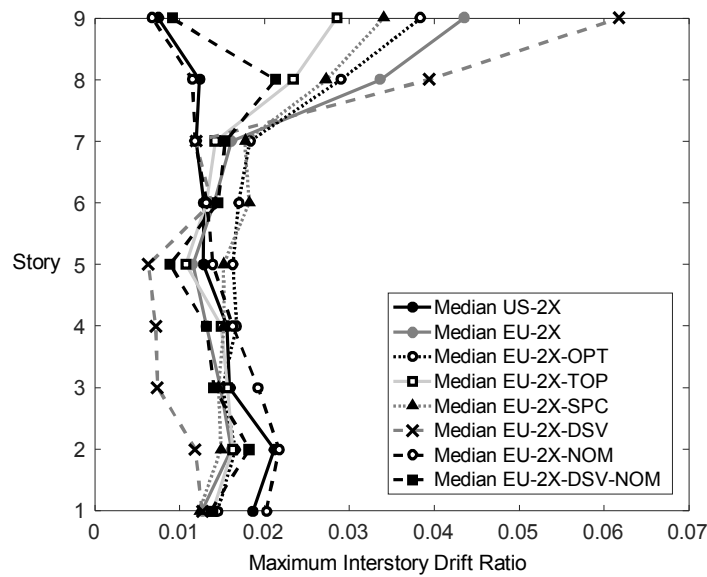


Figure 5.16. Median of drift responses for the designed split X-braced archetypes

The results presented in this section reveals an important fact that split X-braced frames designed according to EC8 can suffer from a soft-story behavior, particularly in top stories, which might be accompanied by plastic hinging in columns due to large interstory drifts. The more important issue is that the designer is usually unable to detect this unless expensive nonlinear time history analyses are conducted. Although convenient approaches such as designing the frame with an additional top load or using spectrum analysis can enhance the behavior, the numerical results for the last alternatives (i.e. EU-2X-NOM and EU-2X-DSV-NOM) demonstrated that the omission of the Omega Rule is a more promising approach for mitigating the soft-story issue.

The yielding behavior of members was also investigated. Table 5.4 presents the median percentage of braces, columns, and beams which experienced yielding or buckling during the earthquakes. Considering the large number of analyses and for the sake of brevity, the members were either categorized as elastic, buckled, or yielded in the preparation of the table and the extent of yielding is not given. To report conservative yielding percentages for beams and columns, the original US-2X and EU-2X frames were re-analyzed considering a material overstrength (γ_{ov} or R_y)

of 1.4 for HSS braces. This approach increased the number of analysis significantly, however, it was required for estimating the maximum probable forces that the braces can exert on other members, causing them to yield. Based on Table 5.4, almost all braces of EU-2X have experienced buckling in compression and yielding in tension during the earthquakes while the numbers are lower for US-2X. In the US design, almost 35% of the braces did not buckle and more than 20% did not yield considering the median of the results. This can be attributed to the design methodology of EC8 which uses slender braces and controls the brace overstrengths (i.e. $\Omega_i^{max} \leq 1.25\Omega_i^{min}$) to guarantee a more uniform distribution of the plastic action over the height. Although the EU design has a better distribution of yielding, the soft-story behavior discussed earlier has caused more yielding in the columns of EU-2X (such as those shown in Figure 5.13) compared to US-2X. The differences that exist between the approaches of AISC341 and EC8 for the capacity design of columns might also have an effect on this issue.

Table 5.4 Percentage of yielded or buckled members of the designed archetypes

Archetype	Median of Results (%)			
	Braces Buckled in Compression	Braces Yielded in Tension	Yielded Columns*	Yielded Beams*
US-2X	66	78	10	10
EU-2X	100	95	25	20
US-X	100	78	20	0
EU-X	100	83	33	0
US-V	83	72	5	25
EU-V	78	39	30	50

* Considering $R_y=1.4$ for HSS braces in the analysis models

Another important concern is the yielding behavior of beams. As discussed earlier, the deflection of brace-intersected beams in both the US and EU designs significantly affected the brace ductility demands. Furthermore, as summarized in Table 5.4, 10%

to 20% of the beams in the split X-braced archetypes experienced yielding, however, all of these beams were brace-intersected ones. Thus, as also discussed by Shen et al. [314, 315], the brace-intersected beams designed to the current requirements do not seem to have the adequate stiffness and strength to act as proper supports for connecting brace members. As a result, developing a convenient approach for overcoming this design shortcoming which is related to both the US and EU provisions seem to be necessary. It is worth noting that although the mentioned beams are almost identical in EU-2X and US-2X, more yielding in these members was observed in the European design, as presented in Table 5.4. This issue requires further investigation and might be related to the use of significantly more slender braces in EU-2X compared to US-2X.

5.4.3 X-Braced System

Summary of the analysis results for the X-braced archetypes is presented in Figure 5.17 and Table 5.3. Based on the table, the median of the maximum column forces recorded for US-X and EU-X are almost identical, however, the European design has experienced somewhat higher base shears (by about 16%) on average. Examining the comparative results of Figure 5.17e, it is observed that the US-X and EU-X frames have exhibited very similar floor velocities. However, as depicted in Figure 5.17b, higher floor accelerations were mostly recorded for the European design, which will in turn increase the seismic demands on its non-structural components. Residual interstory drift ratios (Figure 5.17d) for both frames remained mostly below the permissible limit of 0.5%, except for the top two stories of EU-X, which have experienced the soft-story behavior discussed in the previous section for split X-braced frames designed as per EC8. Similar to the results of split X-braced archetypes, the accumulated plastic strain demands (Figure 5.17g) and brace ductility demands (Figure 5.17h) are generally higher for US-X compared to EU-X, except for the top stories. This might be related to the accumulation of damage at the top stories of EU-X which alleviated the plastic demands in its lower stories. It is

worth noting that, unlike the split X-braced archetypes in which there was significant differences between the compressive and tensile brace ductility demands in a story (Figure 5.11h), in the X-braced frames the positive and negative ductility demands (Figure 5.17h) are very similar and have a more smooth height-wise variation. This is an expected behavior, since the responsible issues for the abrupt changes in the brace ductility demands of split X-braced archetypes (i.e. brace-intersected beams) are not present in the X-braced system.

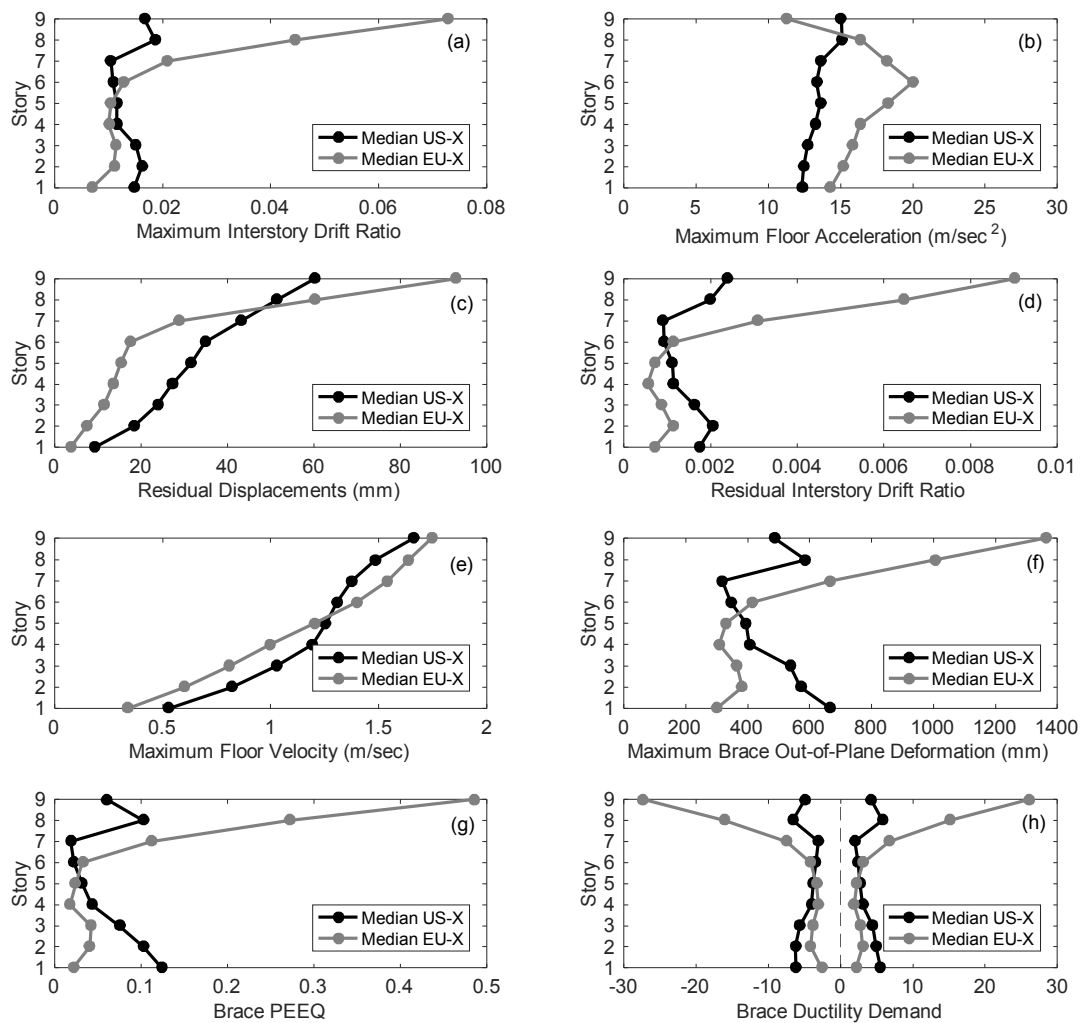


Figure 5.17. Comparison of analysis results for US-X and EU-X

As summarized in Figure 5.17a, the interstory drift ratios for US-X and EU-X are comparable to each other along the first seven stories, mostly below 2%, however, similar to the previous section, the drifts at the top two stories of EU-X suddenly increase to very high values. This behavior has significantly increased the plastic and ductility demands of braces at the top two stories of EU-X. The observed soft-story behavior for EU-X is even more drastic than that of the EU-2X frame. This further confirms the previously discussed issue that the frames with X- or split X-bracings designed as per EC8 are prone to develop soft-story mechanism at their top stories.

Based on the experience gained from the split X-braced case, it was decided to re-design the EU-X frame as per EC8, however, omitting the Omega Rule, to see whether or not this approach can mitigate the observed soft-story behavior. The member sizes for this alternative design (designated as EU-X-NOM) are shown in Figure 5.14. It is worth noting the steel weight for EU-X-NOM was about 30% less than that of both EU-X and US-X which had close weights. The height-wise variation of brace overstrengths (Ω_i) and normalized brace overstrengths (i.e. Ω_i/Ω_i^{min}) for the designed X-braced archetypes are presented in Figure 5.18. Based on Figure 5.18a, it is observed that the American design has significantly higher brace overstrengths, while the overstrengths for EU-X and EU-X-NOM are relatively close to each other. However, when the normalized values of Figure 5.18b are considered, the difference between EU-X and EU-X-NOM is clearly observed, demonstrating that the latter tends to follow a similar normalized brace overstrength distribution to that of US-X. The new design was also subjected to the set of 44 ground motions and the results are summarized in Figure 5.18c. The soft-story behavior is mostly controlled in the EU-X-NOM design, further confirming that the omission of the Omega Rule in EC8 might result in frames which are lighter and perform significantly better.

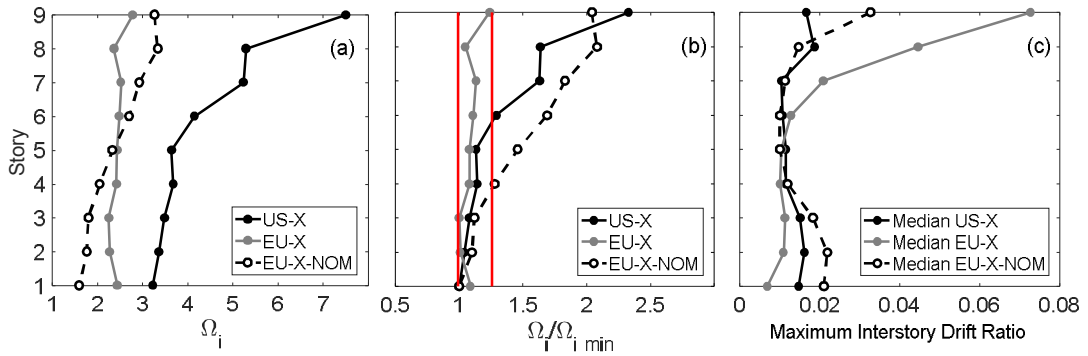


Figure 5.18. (a) and (b) Variation of brace overstrengths and (c) median of drifts for the designed X-braced archetypes

For the original X-braced designs, the percentage of buckled and yielded members is reported in Table 5.4. Similar to the previous section, the percentage of yielded columns and beams is obtained by re-analyzing the models considering a material overstrength (γ_{ov} or R_y) of 1.4 for HSS braces. Based on the table, all of the braces in both US-X and EU-X have experienced buckling, however, the percentage of yielded braces is slightly higher in EU-X, which might be an effect of the Omega Rule. On average, more column yielding is observed in EU-X. This can partly be related to the differences that exist between the capacity design regulations of the provisions and partly to the soft-story behavior observed in the European design which in some cases created plastic hinges at the columns of the top stories. Based on Table 5.4, no beam yielding was observed in X-braced archetypes, unlike the split X-braced frames in which yielding of the brace-intersected beams were common.

5.4.4 V-Braced System

Simulation results for the US-V and EU-V frames are summarized in Figure 5.19. The design base shear for EU-V was about twice that of US-V. On the other hand, the results presented in Table 5.3 demonstrate that the European design has experienced base shear and column forces which are, on average, about 50% higher. Similar to the previous sections, the floor velocities (Figure 5.19e) are very similar

while the floor accelerations (Figure 5.19b) are again higher for the European design. The residual interstory drifts (Figure 5.19d) are below the permissible limit of 0.5%, except for the top two stories of EU-V, which has again exhibited the soft-story behavior. The observed brace out-of-plane deformations (Figure 5.19f), plastic strain demands (Figure 5.19g), and brace ductility demands (Figure 5.19h) reveal that there is a significant accumulation of damage at the top stories of EU-V, while the distribution of damage is more uniform for US-V. The accumulation of damage at the top stories of EU-V has reduced the plastic demands in its lower stories compared to the American design, however, resulted in a significant increase in the interstory drifts (Figure 5.19a) of its top stories. The behavior of EU-V is very similar to the soft-story behavior observed previously for the X- and split X-braced frames designed as per EC8.

To check whether or not the Omega Rule was again responsible for the observed soft-story behavior, an alternative frame (designated as EU-V-NOM in Figure 5.14) was designed as per EC8, however, without considering the Omega Rule, and subjected to the full set of 44 ground motions. It is worth noting that the new design was about 30% lighter than both US-V and EU-V. Based on the results summarized in Figure 5.20a, it can be seen that US-V has significantly higher brace overstrengths than those of EU-V, while the alternative design (i.e. EU-V-NOM) utilized even lower overstrengths. However, the normalized brace overstrengths of EU-V-NOM have a very similar trend to that of US-V, as depicted in Figure 5.20b. The drift responses summarized in Figure 5.20c, revealed that the alternative design was able to fully mitigate the soft-story issue, similar to the X- and split X-braced cases.

Following a similar manner to that of the previous sections, the percentage of buckled and yielded members for the original V-braced archetypes are presented in Table 5.4. The first major difference observed in this table is the higher yielding percentage of columns in EU-V compared to that of US-V. The differences that exist between the capacity design rules of EC8 and AISC341 as well as the soft-story behavior observed in EU-V can be the possible reasons for the issue.

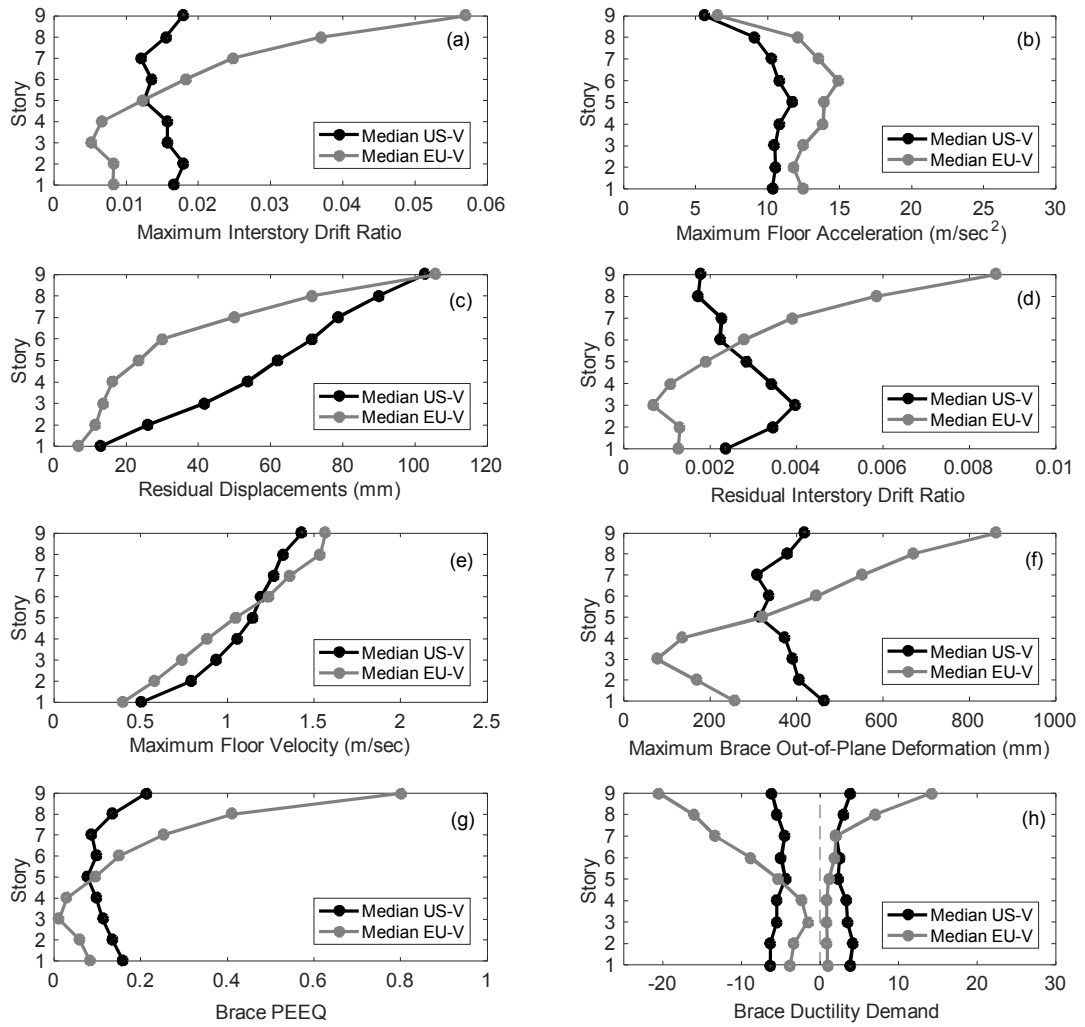


Figure 5.19. Comparison of analysis results for US-V and EU-V

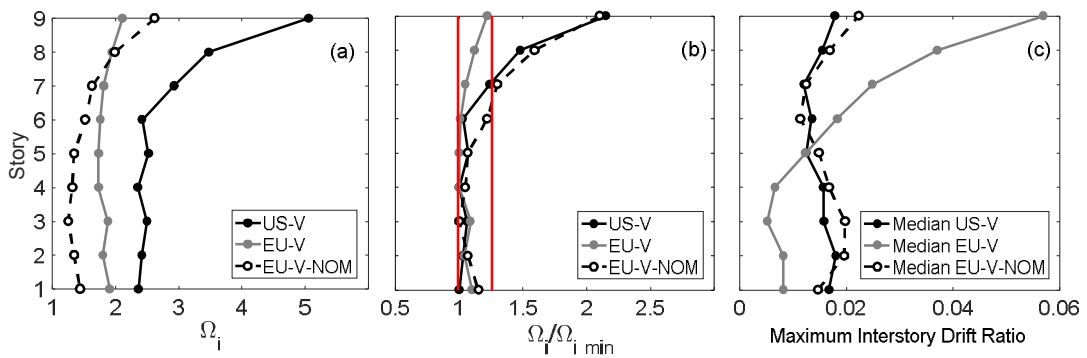


Figure 5.20. (a) and (b) Variation of brace overstrengths and (c) median of drifts for the designed V-braced archetypes

It is a known issue that, in V-braced CBFs, the strength and stiffness of beams can significantly affect the behavior of brace members (e.g. [306, 309, 336]). During earthquakes, beam mid-points act as supports for one end of brace members in these systems. Considering that larger forces are developed when a brace is in tension, the stiffness and strength of beams become a major issue for the yield behavior of braces in V-braced CBFs. When approaching to its tensile capacity, a brace exerts a large tensile force to the mid-point of the supporting beam. If the beam has enough strength and stiffness, the brace can successfully yield in tension. Otherwise, the beam will deflect and the tension in the brace will reduce, preventing the brace from yielding. The data presented in Table 5.4 clearly illustrates how the design requirements of the US and EU provisions are related to the above discussion. On average, about 25% of beams in US-V have experienced yielding, however, to a very limited extent based on the simulation results. Consequently, more than 70% of braces in this frame yielded in tension during the earthquakes, which is similar to the percentage of brace yielding in US-X. Thus, the US design was able to properly estimate the demands on beams and control them to ensure proper tensile behavior of brace members. On the other hand, about 50% of beams in the EU-V frame yielded during the earthquakes, which in turn, resulted in a drastic decrease in the percentage of braces which have yielded in tension. As reported in Table 5.4, only 39% of braces in EU-V have experienced yielding, which is significantly low. It is worth noting that, although the percentages of buckled braces in US-V and EU-V are close, it should be borne in mind that the ductility demands on compression braces will also increase due to the downward deflection of beams, provided that these members not be sufficiently strong and stiff, which is the case for EU-V. This is why there is a significant bias between the positive and negative ductility demands of EU-V (Figure 5.19h). Although the ductility demands in compression are also higher than the tensile ductility demands for braces of US-V, the difference is drastically higher for the EU design, suggesting that the beams were not properly sized for the exerted unbalanced forces. This issue has also been reported in the studies of D'Aniello et al. [336] and Tenchini et al. [337] which have focused on the regulations of EC8. As

discussed by Tenchini et al. [337], the problem can even intensify further if high strength steel is used for the design of beams which will result in more flexible beams.

There are several approaches in the literature for overcoming the issue associated with beams of V-braced CBFs. One of these methods is to use 30% of the buckling load as the expected force in compression braces (somewhat similar to AISC341), during the design of beams, instead of $0.3F_yA_g$ which is currently in use by EC8. This approach is recommended in some National Annexes to EC8, for instance, the UK National Annex [338]. In addition to this, the effect of the material overstrength (γ_{ov}) can also be included in this approach. Another method is the one recently proposed by D'Aniello et al. [336] in which a numerically calibrated formula is given for estimating the unbalanced forces that act on beams of V-braced CBFs. Furthermore, another equation is presented by these researchers which provides the appropriate flexural stiffness of beams, based on the anticipated drift ratio. This equation is used for checking the beam stiffness in addition to the regular strength-based design provisions. Such stiffness checks can be incorporated into the design procedure of V-braced CBFs, regardless of the utilized design provisions.

Although in general yielding of brace members in tension is considered as a desirable energy dissipating mechanism, which requires having strong and stiff beams in V-braced CBFs, an interesting observation was recently reported by Sen et al. [309] based on a number of tests on two-story chevron CBFs, performed at the National Center for Research on Earthquake Engineering in Taiwan. In some of these tests, properly designed chevron SCBFs (according to AISC341), albeit with weaker beams than those required by the code, were subjected to cyclic loading. The results suggested that yielding-beam chevron SCBFs can perform similarly and achieve comparable ductility levels to code-compliant SCBFs, provided that the beam demand-to-capacity ratios not exceed 2.5. It is also worth noting that, there are no substantial differences between the drift responses obtained in the present study and summarized in Figure 5.20c, for US-V and EU-V-NOM, despite the fact that the percentage of yielded beams in the latter (which has been obtained but not reported

in Table 5.4) is almost three times higher than that of the former. Consequently, as emphasized by Sen et al. [309], further research is necessary to fully understand the behavior of V-braced frames with yielding beams and to see if the requirements of AISC341 regarding the design of beams in these frames are too stringent or the requirements of EC8 are inadequate.

5.5 Chapter Summary

The chapter explored in detail the similarities and differences between the design procedures as well as the seismic behaviors of steel CBFs designed to the provisions of AISC341 developed in the United States and EC8 developed in Europe. CBF design as per EC8 was found to be more complicated with many inter-related provisions.

A series of CBF archetypes were designed based on American and European provisions and subjected to a large set of earthquakes in order to investigate and compare their seismic performances. The most notable difference between the behavior of CBFs designed as per EC8 and AISC341 rules was that soft-story behavior occurred in the top stories of the X-, split X-, and V-braced archetypes designed according to the EU provisions. It was observed that the CBFs which satisfied the Omega Rule of EC8 were overly flexible at the top stories. The simulation results revealed that the omission of the Omega Rule would result in structures which are notably lighter and perform substantially better than those designed based on the original methodology of EC8.

All the conclusions drawn based on studies of this chapter are summarized in detail in Chapter 7.

CHAPTER 6

DYNAMIC BUCKLING OF BRACES IN CONCENTRICALLY BRACED FRAMES

Axially loaded members might experience compressive forces above their static buckling capacity as a result of dynamic buckling under rapid shortening. Although the subject is studied in the context of engineering mechanics, it has not been thoroughly investigated in the field of earthquake engineering. Such dynamic overshoots in the compressive capacity can also be observed for braces of concentrically brace frames (CBFs) during earthquakes. Consequently, a comprehensive investigation is conducted in this chapter regarding the effects of dynamic buckling of braces on the seismic behavior of steel CBFs. After providing a theoretical background, recent dynamic experiments on braces and CBFs are simulated and discussed in order to investigate the occurrence of dynamic overshoot during these tests. Eight archetype CBFs are then designed, modeled, and subjected to a large set of ground motions (resulting in over 1600 nonlinear time history analyses) in order to provide a quantified insight on the frequency and anticipated level of dynamic overshoot in the compressive capacity of braces during earthquakes.

6.1 Introduction

Stability of members under *static* and *dynamic* loading conditions has been studied in the past [339-341]. Studies on dynamic stability of compression elements such as columns and rods can be broadly categorized into two main sub-categories [341]: parametric resonance and stability under impulsive actions. A rod might experience parametric resonance when it is subjected to a harmonic axial force with an oscillation frequency which has a certain relation to the natural frequency of the

member [341-345]. The second sub-class is concerned with the stability of compression members under impulsive actions such as the impact of a mass, a rapidly applied axial force, or an imposed boundary velocity [346-358]. A brief summary of these studies, which are mostly conducted prior to the 1980s, can be found in Galambos [341] and Simitzes [359], while more recent studies in this active field of research can be found in [360-366]. The common consensus in the above studies is that, under impulsive actions the axial force of a member can easily exceed its static critical load.

External impulsive actions which can cause axial strain rates of the order of 10^{-1} to 10^2 s^{-1} in a rod are generally considered as *low-velocity excitations* while actions with a resulting axial strain rate of 10^2 to 10^6 s^{-1} as *high-velocity excitations* [341]. Investigation of high-velocity excitations, which are typically encountered under impact or blast conditions, is out of the scope of the current thesis. Previous studies [347, 351, 357, 364, 367-370] have shown that, in low-velocity excitations with low to moderate compression speeds, the expected buckled shape is identical to the fundamental buckling mode observed in a quasi-static case, however, for high compression speeds, higher buckling modes might also be excited.

During strong ground motions, brace members in steel concentrically braced frames (CBFs) exhibit rapid shortenings and elongations leading to repeated cycles of buckling in compression and yielding in tension. When a rod is subjected to rapid shortening, due to the inertia effect of the rod's mass, it will take a certain amount of time for the member to deflect laterally and buckle, and within this time period, the axial force of the rod can exceed its Euler load significantly [347]. Similarly, it is possible for braces of a CBF to exhibit loads above their static buckling load (i.e. to experience *dynamic overshoot*). It should be emphasized that this phenomenon is because of the inertia effect of the mass of the rod (or brace) and is *not* due to the strain rate effect which can increase the material strength. The strain rate effect on material strength is not considered in the present study. Previous experimental and analytical results [347, 363, 364, 366, 370] have shown that, such dynamic overshoots can range from a few percent to hundreds of times the Euler buckling

load. In a brief study by Tada and Suito [371], it was also demonstrated that the buckling and post-buckling behavior of truss structures could notably differ under dynamic and static analysis. It is worth noting that, the study was, however, conducted considering monotonic loads and rather low compressions speeds (< 15 mm/s).

Dynamic buckling behavior of compression members has been mostly studied within the context of engineering mechanics and there has not been any study focusing on the effects of dynamic buckling of braces on the seismic performance of CBFs. Consequently, this chapter investigates in detail the following issues: (i) the frequency that braces of CBFs might experience loads above their static buckling load during strong earthquakes; (ii) the expected level of these dynamic overshoots and their effects on the seismic behavior of CBFs; (iii) possible increases in loads transmitted to other members of the systems as a result of dynamic overshoots and methods for incorporating them in the capacity design procedure; and (iv) appropriate approaches for modeling braces in order to capture their dynamic buckling behavior accurately.

6.2 Theoretical Background

Previous studies have concentrated on the dynamic stability of rods under a suddenly applied constant load or a load with a prescribed regular variation [346, 350, 353, 365, 367, 369, 372-375], the impact of a mass with a predefined initial velocity [348, 351, 354, 355, 358, 361, 362], or an imposed constant velocity to one end of the member [347, 363, 364, 366, 370, 376, 377]. Considering the complexity of the loading history that an earthquake typically applies to a brace member, FE analysis is utilized in this chapter. Nevertheless, in this section, a simple case of dynamic buckling, initially studied by Hoff [347], is considered to present a brief theoretical background.

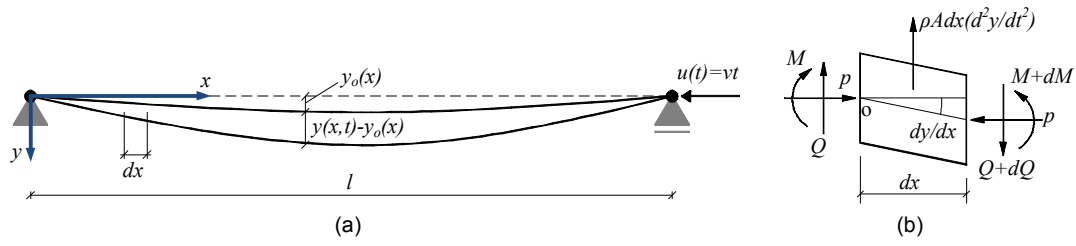


Figure 6.1. Rod under a constant boundary velocity (a) deflected shape (b) an infinitesimal segment of the rod

The investigated case is a low-velocity excitation of a simply supported elastic rod with an *effective buckling length* of l under a prescribed boundary velocity where one end of the member moves towards the other end with a constant velocity of v (Figure 6.1a). Considering the equilibrium of vertical forces in the infinitesimal segment of the rod shown in Figure 6.1b and taking moments about point o and, finally, applying the moment curvature relation, the differential equation for the deflection of the rod can readily be established as follows [352]:

$$EI \frac{\partial^4 (y - y_o)}{\partial x^4} + P \frac{\partial^2 y}{\partial x^2} + \bar{\rho} A \frac{\partial^2 y}{\partial t^2} = 0 \quad (6.1)$$

where E is the elastic modulus of the material, I is the moment of inertia of the rod's cross section, $y(x, t)$ is the total deflection and $y_o(x)$ is the deflection of the rod due to initial imperfections, $P(t)$ is the axial force in the rod, $\bar{\rho}$ is the material density, and A is the cross sectional area of the rod. Pure shortening of the rod due to axial straining, i.e. $u_a(t)$, is in fact equal to the applied total displacement of $u(t) = vt$ minus the axial displacement due to lateral deflection of the rod, i.e. $u_b(t)$. Considering small rotations, $u_b(t)$ can be obtained as follows:

$$u_b(t) = \frac{1}{2} \int_0^l \left[\left(\frac{\partial y}{\partial x} \right)^2 - \left(\frac{\partial y_o}{\partial x} \right)^2 \right] dx \quad (6.2)$$

Consequently, the axial force in the rod can be determined as:

$$P(t) = \frac{EA}{l} u_a \Rightarrow P(t) = \frac{EA}{l} \left(vt - \frac{1}{2} \int_0^l \left[\left(\frac{\partial y}{\partial x} \right)^2 - \left(\frac{\partial y_o}{\partial x} \right)^2 \right] dx \right) \quad (6.3)$$

As mentioned earlier, for low-velocity excitations with low to moderate compression speeds, the expected buckled shape is typically identical to the fundamental buckling mode observed in a quasi-static test. Therefore, Hoff [347] approximated the deflected shape of the rod as a half-sine wave which satisfies the boundary conditions of zero displacement and zero moment at $x = 0$ and $x = l$; i.e. $y(x, \tau) = r y_m \sin(\pi x/l)$, where r is the radius of gyration of the rod's cross section (i.e. $\sqrt{I/A}$), $y_m(\tau)$ is the dimensionless deflection parameter and, thus, $r y_m$ is the maximum lateral deflection of the rod at its mid-span at the investigated time instance, and τ is the dimensionless time defined as $\tau = vt l / \pi^2 r^2$. Similarly, the initial imperfect shape of the rod can be represented as $y_o(x) = r \delta \sin(\pi x/l)$, where δ is the dimensionless imperfection parameter and, therefore, $r \delta$ shows the maximum magnitude of initial imperfection of the rod. Substituting $y(x, \tau)$ and $y_o(x)$ in Equations (6.1) and (6.3) yields:

$$\ddot{y}_m + \hat{\Omega} \left[\frac{1}{4} y_m^3 + \left(1 - \tau - \frac{\delta^2}{4} \right) y_m - \delta \right] = 0, \quad y_m(0) = \delta \quad \text{and} \quad \dot{y}_m(0) = 0 \quad (6.4)$$

as well as

$$P(\tau) = P_{cr} \left[\tau - \frac{1}{4} (y_m^2 - \delta^2) \right] \quad (6.5)$$

where a dot represents the derivative with respect to τ , P_{cr} is the critical Euler buckling load for a quasi-static case which is equal to $\pi^2 EI/l^2$, and $\hat{\Omega}$ is the *dynamic similarity number* introduced by Hoff [347] as:

$$\hat{\Omega} = \frac{\pi^8 c^2}{v^2 \lambda^6} \quad (6.6)$$

where c is the axial velocity of the stress waves in rod's medium (i.e. $\sqrt{E/\rho}$) and λ is the slenderness of the rod (i.e. l/r). First, the ordinary differential equation of (6.4) should be numerically solved to obtain y_m , and then, using Equation (6.5) it is possible to capture the variation of the axial load during a dynamic buckling.

To demonstrate the issue more clearly, consider the hollow structural section HSS 4×4×1/8 with a length of 4805 mm, which corresponds to $\lambda \approx 120$, under an applied constant boundary velocity. The Young's modulus of the elastic medium is considered as 200 GPa and its density as 7850 kg/m³. The maximum magnitude of initial imperfection of the rod is assumed to be $l/1000$. Considering different boundary velocities, Equation (6.4) was solved utilizing a Runge-Kutta approach and the results are summarized in Figure 6.2. The theoretical results depicted in Figure 6.2 clearly show that, increasing the compression speed (rate) can lead to significant dynamic overshoots in the buckling load of an elastic rod. The FE results presented in the figure will be discussed later.

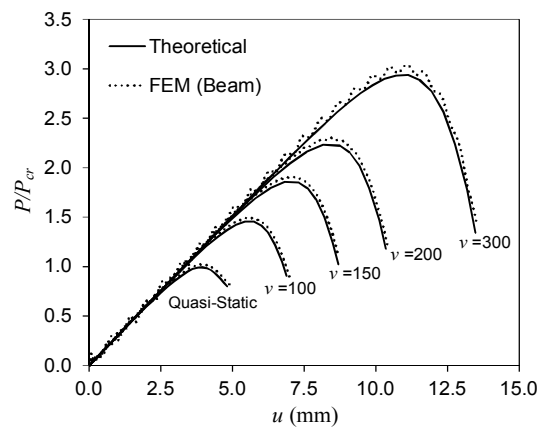


Figure 6.2. Dynamic overshoot in the buckling load of an elastic rod (v in mm/s)

6.3 Investigation of Recent Dynamic Tests

The recent dynamic tests conducted on single brace members and single-story CBFs are investigated in this section by FE analysis to observe whether any sign of dynamic overshoot has been reported in these tests under earthquake-level compression rates. All simulations were conducted using the finite element package ABAQUS 6.12-1 [273]. It is important to note that, in all FE analyses of this chapter, the effect of strain rate on changing the strength of steel material was not incorporated into the models. The reason is to have an isolated investigation on the effects of the mass of CBF braces on their dynamic buckling behavior.

6.3.1 Dynamic Tests of Fell on a Brace Member

The HSS1-3 specimen experimented by Fell [329] is considered here which was an HSS 4×4×1/4 steel brace with an effective buckling length of 2985 mm (i.e. $\lambda \approx 77$) tested under a cyclic protocol. Details of the specimen are schematically depicted in Figure 6.3 along with the developed FE model. Following Fell's [329] modeling approach and in order to reduce the computation time, only a quarter of the specimen was modeled. The boundary conditions depicted in Figure 6.3b were considered and the applied displacement history was accurately extracted from the test data (Figure 6.4) and exerted to the outer nodes of the gusset plate. Eight-node C3D8R brick elements with reduced number of integration points and hourglass control scheme were used for modeling of the brace and gusset plate. Parameters of the utilized von Mises plasticity constitutive model with combined nonlinear isotropic and kinematic hardening were calibrated based on the data provided by Fell [329]. Damping-related information was not reported in [296, 329] and, therefore, a small mass proportional damping corresponding to a damping ratio (ξ) of 2.5% in the first mode of vibration was assigned to the FE model. Since the effect of local imperfections was reported by Fell [329] to be negligible, only global imperfections were incorporated in the FE model using the fundamental buckling mode with a maximum amount of $l/1000$.

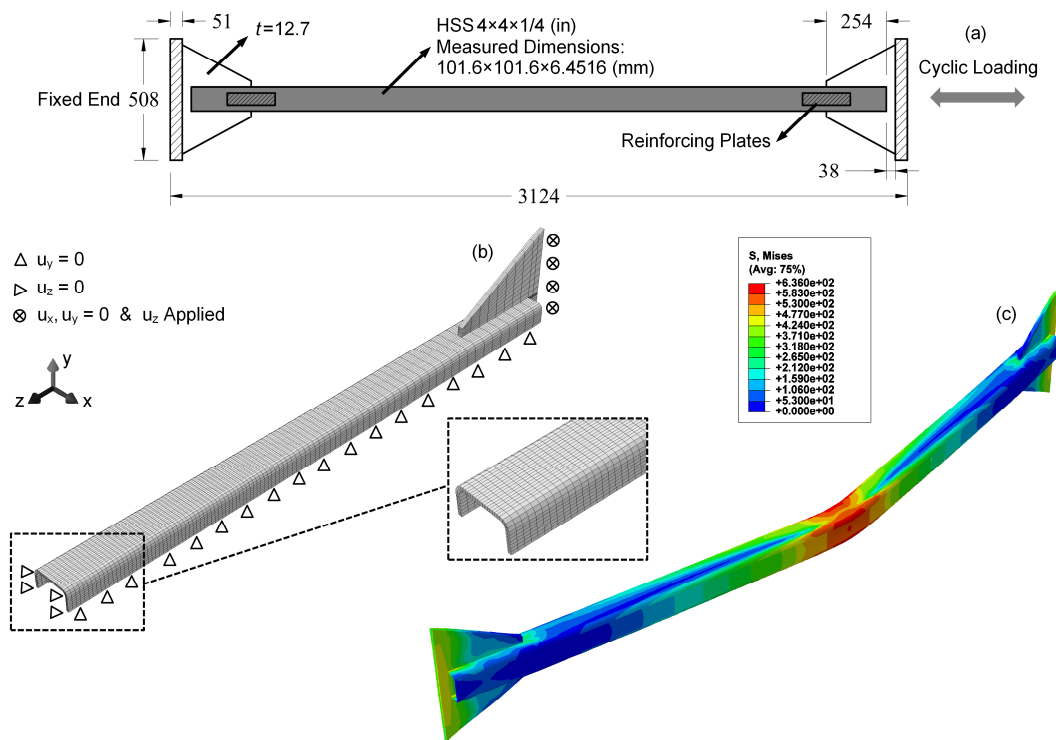


Figure 6.3. FE model of Fell's [329] HSS1-3 test (a) specimen details with dimensions in mm (b) meshed quarter model (c) von Mises stress contour in MPa at the end of the analysis

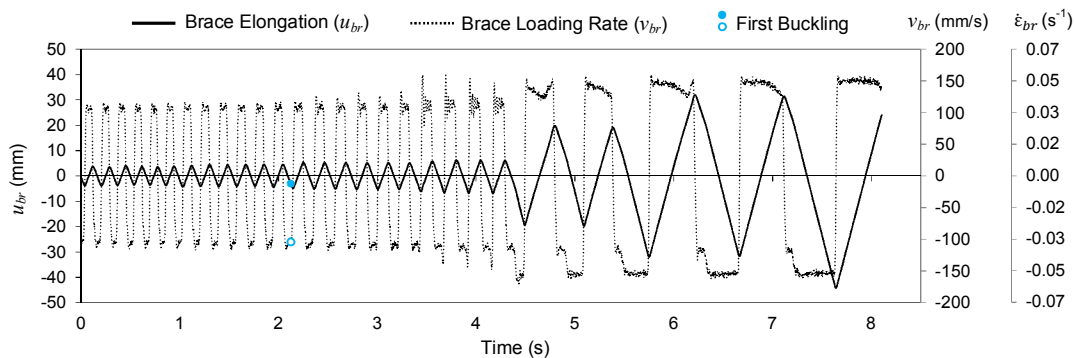


Figure 6.4. Loading history in the HSS1-3 test of Fell [329] (data courtesy of B. V. Fell); Tension (+) Compression (-)

HSS1-3 was experimented dynamically by Fell [329] under a cyclic displacement protocol, with a varying rate, yielding a peak excursion rate (v_{max}) of about 150 mm/s. This rate was selected as a representative speed which a typical CBF brace member

might experience during an earthquake. An identical specimen (HSS1-1) was also tested, however, quasi-statically. The difference between the recorded buckling loads for specimens HSS1-1 and HSS1-3 was reported by Fell [329] to be less than 3%.

It was essential to investigate the reasons for observing no dynamic overshoots in the buckling load of the specimens tested by Fell [329]. The deformed shape of the brace as well as the corresponding von Mises stress contour at the end of the FE analysis are depicted in Figure 6.3c. The brace axial force (P_{br}) versus brace elongation (u_{br}) response of HSS1-3 reported in the experiment and found herein via FE analysis (designated as “FEM (Solid)”) are presented in Figure 6.5a and Figure 6.5b, respectively. It is worth noting that, during the experiment, the brace force was accurately determined from load cell readings of the utilized actuators [329]. A great level of conformity is observed between the results which validates the FE modeling approach. As reported in these figures, the recorded buckling loads are very similar, with the FE results being slightly higher.

As discussed earlier, mass is the essential parameter in dynamic overshoot and analyzing a massless brace model will eliminate the possibility of such behavior. Thus, to quantify the level of dynamic overshoot in the buckling load of the HSS1-3 specimen, the simulation was re-conducted, this time, with a massless brace; i.e. assuming $\bar{\rho} = 0$. Comparison of the buckling loads reported in Figure 6.5b and Figure 6.5c clearly shows that, although the HSS1-3 test was done with a rather high speed, the specimen did not experience any notable dynamic overshoots.

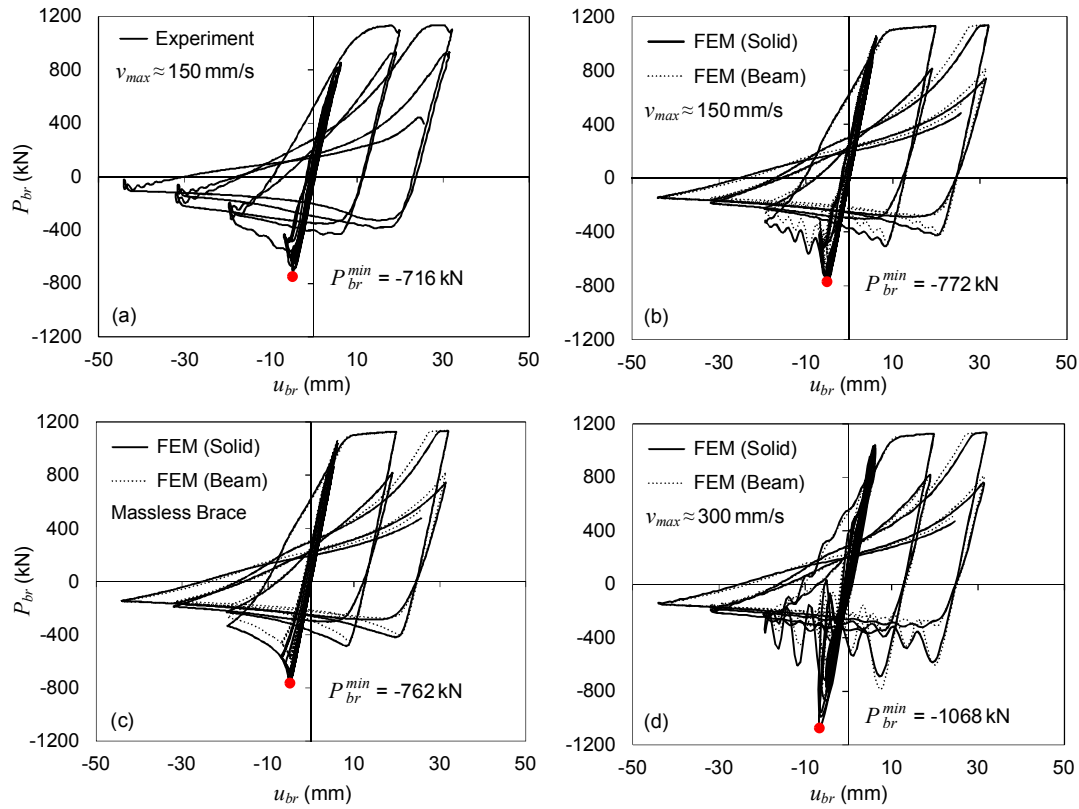


Figure 6.5. Fell's [329] HSS1-3 test results (data courtesy of B. V. Fell) versus FE results of the present study

Variation of *brace loading rate* (v_{br}) for HSS1-3 is depicted in Figure 6.4 by a dotted line. In this figure, the *brace axial strain rate* ($\dot{\epsilon}_{br}$) values corresponding to the brace loading rates are also presented in the right vertical axis by dividing the rates by the brace length. Although the loading rate (v_{br}) has the direct effect on the dynamic buckling behavior, the corresponding strain rate ($\dot{\epsilon}_{br}$) is also reported since it is a normalized quantity which has also been used by others in the context of earthquake engineering [306]. As shown in Figure 6.4, the peak value of brace loading rate for HSS1-3 was about $v_{max} \approx 150$ mm/s. While being a reasonable estimate, the peak rate reported by Okazaki et al. [306] in a recent shake table test for a CBF with comparable brace members demonstrated that such braces might experience significantly higher loading rates. Consequently, it was decided to re-analyze the FE model of the HSS1-3 specimen with twice the previous loading rate (i.e. $v_{max} \approx 300$

mm/s), creating a peak strain rate of about 0.10 s^{-1} . The original displacement history (Figure 6.4) was applied, however, within half of the previous duration. Results for this case, presented in Figure 6.5d, suggest that the HSS1-3 specimen would have exhibited significant dynamic overshoots in its buckling load, provided that it had been tested with a higher speed. An increase of about 40% is observed in the peak buckling load of the specimen, approaching almost to the yield strength of the brace.

As depicted in Figure 6.4, during the HSS1-3 test, the brace experienced its first buckling in an early cycle, during a rather small excursion, with a compression rate of about 100 mm/s (< peak value of 150 mm/s) followed by a series of subsequent bucklings prior to the initiation of larger and faster cycles. In order to further investigate the behavior, the validated FE model was re-analyzed considering a modified displacement protocol which contained a number of small elastic cycles which did not cause buckling in the brace until larger cycles with $u_{br} = \pm 35 \text{ mm}$ and $v_{br} \approx 150 \text{ mm/s}$ initiated. The simulation results, not presented here for brevity, demonstrated that HSS1-3 could have experienced an increase of about 20% in its peak buckling load if it had been experimented with the original loading speed however under such a modified protocol. The results revealed that, the overshoot will be more notable particularly if a brace is tested under displacement histories which guarantee buckling during relatively large and fast excursions rather than during small cycles.

6.3.2 Shake Table Test of Goggins on a Single-Story CBF

A number of shake table tests were conducted by Goggins [378] in 2004 on a single-story one-bay by one-bay CBF to study the cyclic behavior of cold-formed steel tubular braces during seismic events. Results of these tests were also summarized and further discussed by Elghazouli et al. [379] and Broderick et al. [304]. The ST4 test is considered here where the frame was subjected to a sine ramp base acceleration. The input excitation was applied with a constant frequency and an increasing amplitude towards 1.0 g. Details of the specimen as well as the

corresponding FE model, developed in the course of this study, are shown in Figure 6.6. A pair of cold-formed square hollow sections (SHS) with nominal dimensions of 20×20×2.0 (mm) was selected as bracing members. As shown in Figure 6.6b, a sufficient distance was considered between the braces along the z-axis to avoid any contact during the test. The clear length of the brace members between the end stiffeners (Figure 6.6a) is 3050 mm, however, the utilized connection detail created a rigid end condition for these members resulting in an effective buckling length of about 1525 mm (i.e. $\lambda \approx 200$).

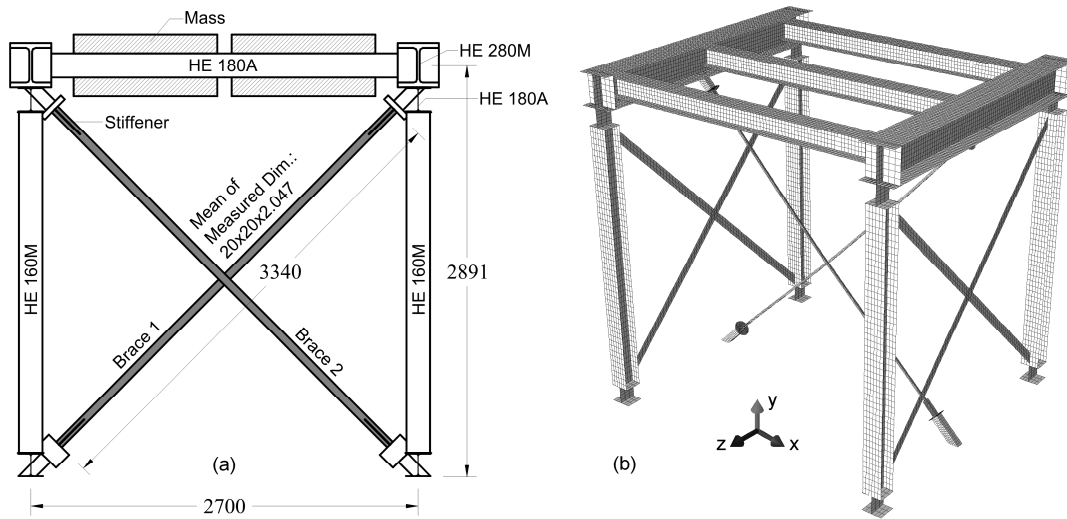


Figure 6.6. FE model of the ST4 test of Goggins [378] (a) specimen details with dimensions in mm (b) meshed model

Four-node S4R shell elements with reduced integration, hourglass control mechanism, and five through-thickness integration points were used for modeling columns, beams, braces, and their connections. A von Mises plasticity constitutive model with combined nonlinear isotropic and kinematic hardening was utilized for braces while elastic material was assigned to all other members. Material parameters for the plasticity model were accurately calibrated using the data reported by Goggins [378]. A mass proportional damping corresponding to $\xi = 3\%$ in the first mode of vibration was assigned to the FE model based on the reported test data [378].

An initial imperfection of 1% of the brace length was considered based on the recommendations of Goggins and his colleagues [380, 381]. During the ST4 test, recording of the axial force of the braces started ahead of the tightening of the connection bolts, and therefore, a pretension of about 5 kN was recorded in these members. To have a more accurate simulation, this pretension was also imposed by applying a temperature load to the braces, prior to the initiation of the main dynamic analysis. The recorded displacement history of the mass was directly applied in the FE model.

A comparison of the test and FE results for Brace 1 is presented in Figure 6.7a, where the time-history of the brace axial force is plotted. During the ST4 test, the axial force of the braces was accurately recorded by connecting their lower ends directly to load cells [378]. Results summarized in Figure 6.7a demonstrate that the brace behavior was well resembled by the FE analysis. The underestimations observed in peak tensile axial forces are considered to be related to the change of material strength under high strain rates that are not incorporated in the FE model and differences that existed between the assumed and actual material properties and section dimensions. The same issue was also noted in the numerical simulations of Broderick et al. [304].

Significant overshoots above the static buckling capacity of the brace were recorded during the test, which were also captured well by the FE analysis (Figure 6.7a). For brace loading rates in the range of 120 mm/s to 210 mm/s (see the buckling instants in Figure 6.7c), increases of the order of 100% to 260% were recorded in the compressive capacity of the brace. It is worth noting that, the history of u_{br} and v_{br} reported in Figure 6.7c is based on the FE results for the case of braces with mass. While not addressing the issue comprehensively, Broderick et al. [304] found the overshoots in the compressive capacity a topic worthy of attention. For further investigation, the FE model was re-analyzed considering massless braces (i.e. assigning $\bar{\rho} = 0$ only to these members). Comparison of results for this case (Figure 6.7b) and the original case (Figure 6.7a) clearly demonstrates that the observed overshoots were solely a consequence of the delaying action of the mass of the brace

during dynamic buckling under high compression rates. Furthermore, the results suggest that, in slender braces, such dynamic overshoots can lead to axial forces which drastically exceed the Euler buckling load.

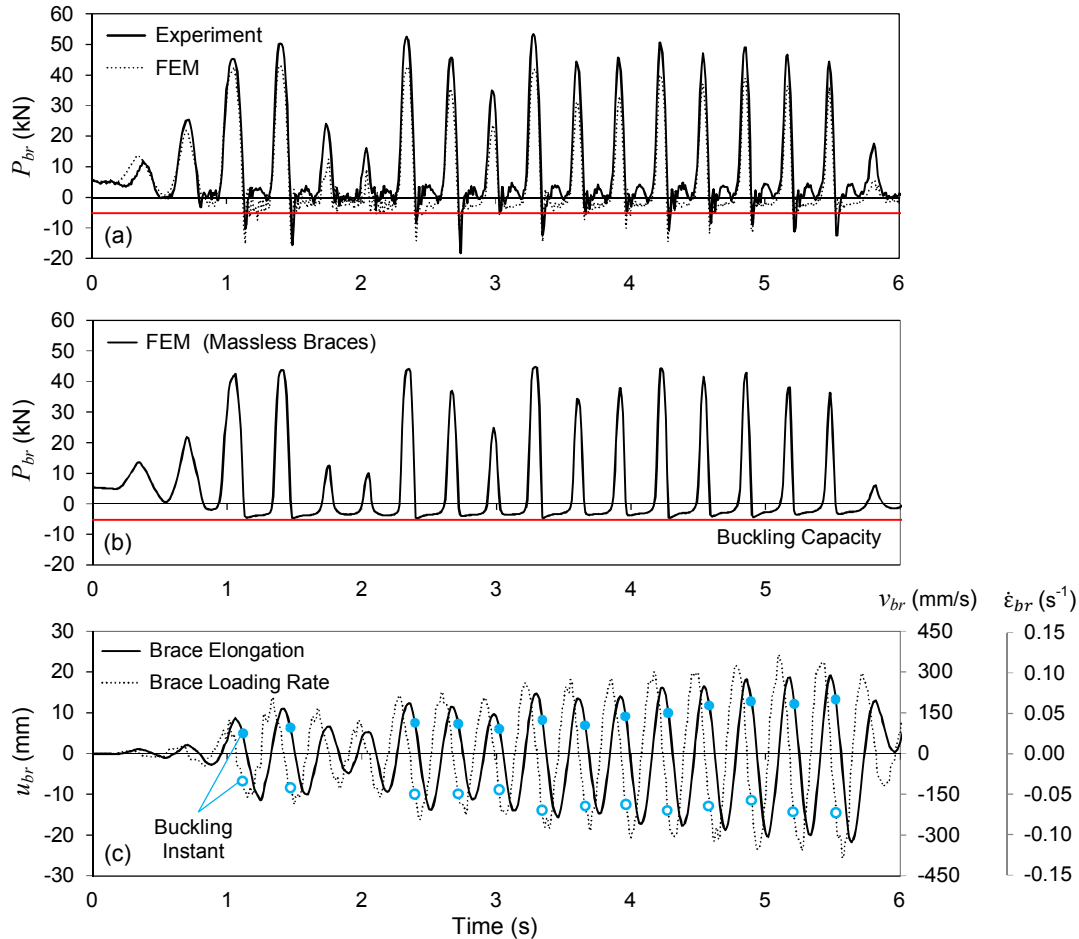


Figure 6.7. Goggins' [378] ST4 test results (data courtesy of S. Salawdeh) versus FE results of the present study

6.3.3 Shake Table Test of Okazaki et al. on a Single-Story CBF

A series of shake table tests conducted by Okazaki et al. [306] on a single-story one-bay CBF with chevron braces is considered in this section. The frame was subjected to consecutive base excitations with different amplification levels. Here, the focus is on the last test which had the highest amplification level. A summary of the specimen

details as well as the developed FE model are presented in Figure 6.8. As shown in Figure 6.8a, the total length of the brace members was 2300 mm, however, the considered elliptic fold lines resulted in an effective buckling length of about 2420 mm (i.e. $\lambda \approx 82.5$).

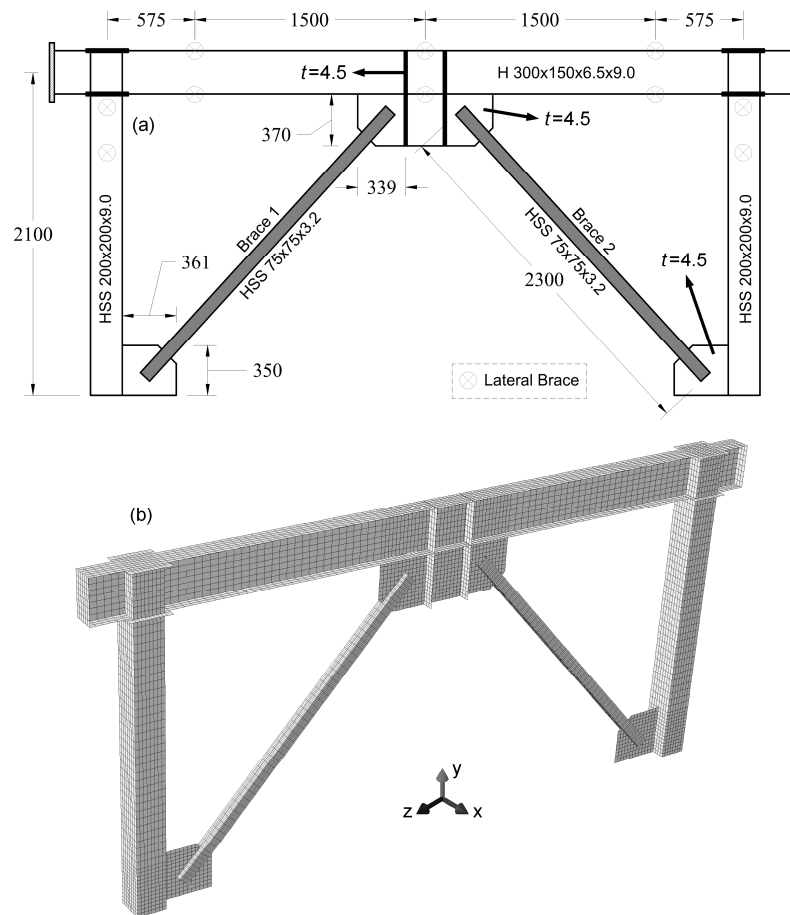


Figure 6.8. FE model of Okazaki et al.'s [306] test (a) specimen details with dimensions in mm (b) meshed model

The specimen was modeled using S4R shell elements (Figure 6.8b). The displacement of the mass recorded during the experiment was directly applied to the FE model. Due to lack of material data, a von Mises plasticity constitutive model with kinematic hardening considering bilinear material behavior was used in the FE analysis which was calibrated based on the yield stress, ultimate stress, and

elongation values reported by Okazaki et al. [306]. Following the recommendation of Okazaki et al. [306], a mass proportional damping corresponding to $\xi = 3\%$ in the first mode of vibration was assigned to the FE model. A residual out-of-plane deformation of 17 mm (i.e. $l/133$) was considered based on the reported value for Brace 1 prior to the last test.

Comparison of the experiment results with those of the FE analysis is presented in Figure 6.9. As shown in Figure 6.9a, the frame response in terms of base shear (V_b) versus interstory drift ratio (Δ) is accurately captured by the simulation. A reasonable level of conformity is also observed in Figure 6.9b which compares the response of Brace 1 during the test and FE analysis. As discussed by Okazaki et al. [306], the brace forces for the experiment were back-calculated using strain gauge readings combined with an assumed equilibrium condition and, thus, high precision should not be expected for these forces. Nevertheless, the utilized technique in this test was also conceptually capable of recording dynamic and inertia-induced effects in brace forces.

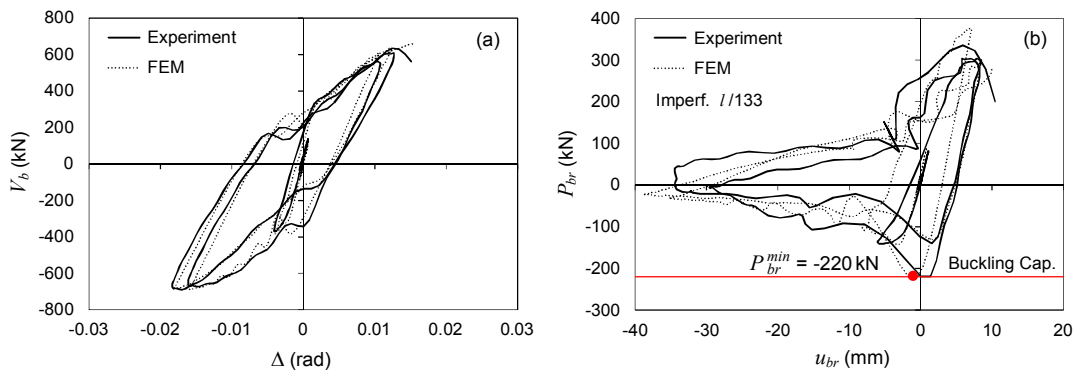


Figure 6.9. Okazaki et al.'s [306] test results (data courtesy of T. Okazaki) versus FE results of the present study

No notable sign of dynamic overshoot was observed in the experiment or FE results. This can be attributed to the considered high level of initial imperfection ($l/133$) for a brace with $\lambda \approx 82.5$. To substantiate this claim, the initial imperfection in the FE model was reduced to a more reasonable level (i.e. $l/1000$) and the analysis was re-

conducted two times: i.e. considering braces with mass and without mass. Comparison of the results presented in Figure 6.10a with those of Figure 6.10b reveals that, if the frame with virgin brace specimens was directly subjected to the highest amplification level, dynamic overshoots of the order of 15% would have been observed in the buckling load of the braces.

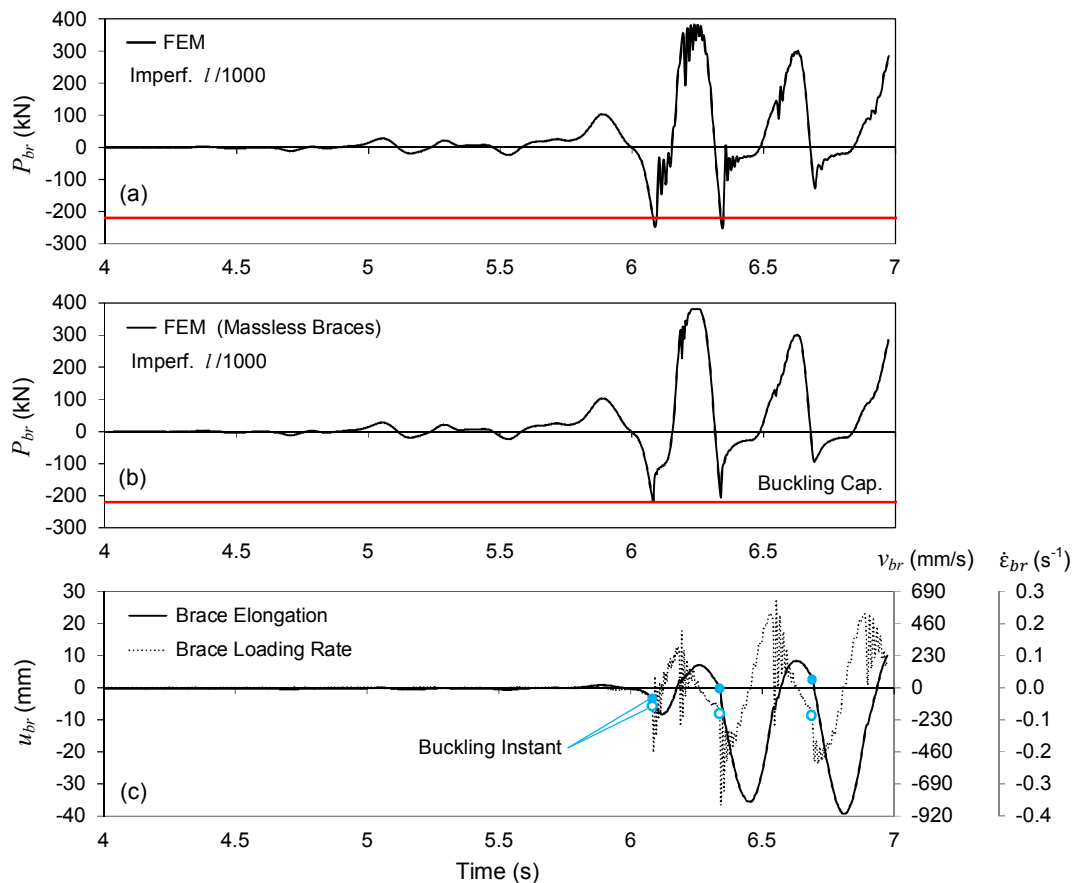


Figure 6.10. FE results of re-analyzing the shake table test of Okazaki et al. [306] with an initial imperfection of $l/1000$

Time history of u_{br} and v_{br} , extracted from the FE results, is reported in Figure 6.10c. Considering the blue symbols in Figure 6.10c, it can be observed that the loading rates corresponding to buckling instants are much lower than the peak values of v_{br} . In other words, although rather high loading rates were recorded, buckling of the brace happened generally at $v_{br} \approx 200$ mm/s. Results of a supplementary FE analysis,

in which the same displacement history was applied within half of the original duration, demonstrated dynamic overshoots as high as 35% above the static buckling load.

6.4 Effect of Dynamic Buckling of Braces on Seismic Behavior of CBFs

The results presented in Section 6.3 demonstrated that dynamic overshoot in the compressive capacity of brace members is either reported in some of the recent experimental studies or, it would have been observed provided that the experiment was conducted with slight modifications. Considering the stochastic nature of earthquakes combined with different possibilities of structural configurations, a comprehensive study is undertaken in this section. The aim is to provide a quantified insight on the frequency of occurrence as well as the anticipated level of dynamic overshoot in the compressive capacity of braces during strong seismic events. Furthermore, the effects of such dynamic overshoots on the behavior of CBF systems and their members are investigated.

6.4.1 Design and Analysis of Archetypes

A total of eight archetype CBF structures were designed considering the plan geometries of the SAC 9-story and SAC 3-story buildings [324]. Plan dimensions and story heights of the buildings as well as the location and designation of the archetype CBFs are summarized in Figure 6.11. As shown in this figure, X-braced and V-braced frames located at the perimeter of the buildings were considered as the archetype CBFs. For V-braced frames, chevron (inverted V) bracings were utilized and for X-braced frames, conventional X-bracings were assumed for the 3-story CBFs whereas two-story split X-bracings were considered for the 9-story CBFs. Each archetype was designed two times, once as per American (AISC 360 [81], AISC 341 [11], and ASCE 7 [145]) and once as per European (Eurocode 3 [252] and Eurocode 8 [142]) provisions in order to cover a wide range of systems with various

brace slenderness values. The American frames were designed as *Special* CBFs whereas the European frames as *Ductility Class High* CBFs. Beams and columns were selected from American wide flange sections made of ASTM A992 steel with a yield stress of $F_y = 345$ MPa while HSS made of ASTM A500 Grade B steel ($F_y = 317$ MPa) were considered for braces. For the US designs, the building was assumed to belong to the seismic design category D_{max} , according to FEMA P695 [250], which represents the highest seismic hazard level with $S_{DS} = 1.0$ g and $S_{DI} = 0.6$ g. Accordingly, $a_g = 0.35$ g with Type C ground was considered as the seismic hazard in the European designs.

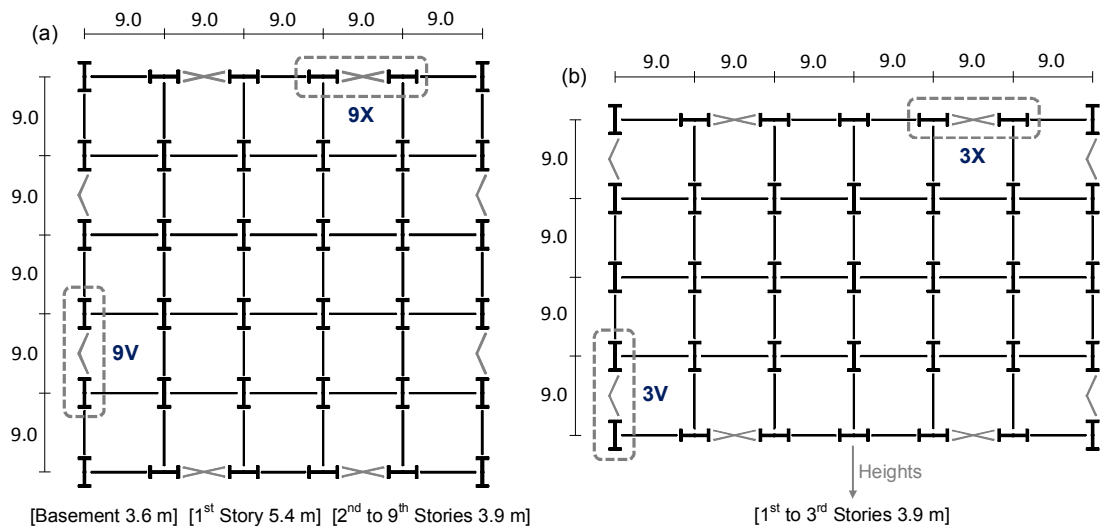


Figure 6.11. Plan dimensions and story heights (in meter) for the archetype buildings (a) 9-story (b) 3-story

Selected member sizes for the designed archetype CBFs are presented in Figure 6.12. The 9-story archetypes were previously designed in Chapter 5 whereas the 3-story archetypes were designed using a similar procedure in the present chapter. The colored and underlined numbers in the figure represent the brace slenderness (λ) at each story which ranges from 40 to 150. It should be noted that, all of the beam-to-column, brace-to-beam, and brace-to-column connections are pinned. Also, X-bracing members are not connected to each other at their mid-points. As shown in

Figure 6.12, each archetype is designated with a two-part name where the first part specifies the number of stories as well as the bracing scheme and the second part shows the utilized design provisions. For instance, “9V-US” is a 9-story CBF with chevron bracings designed as per American provisions.

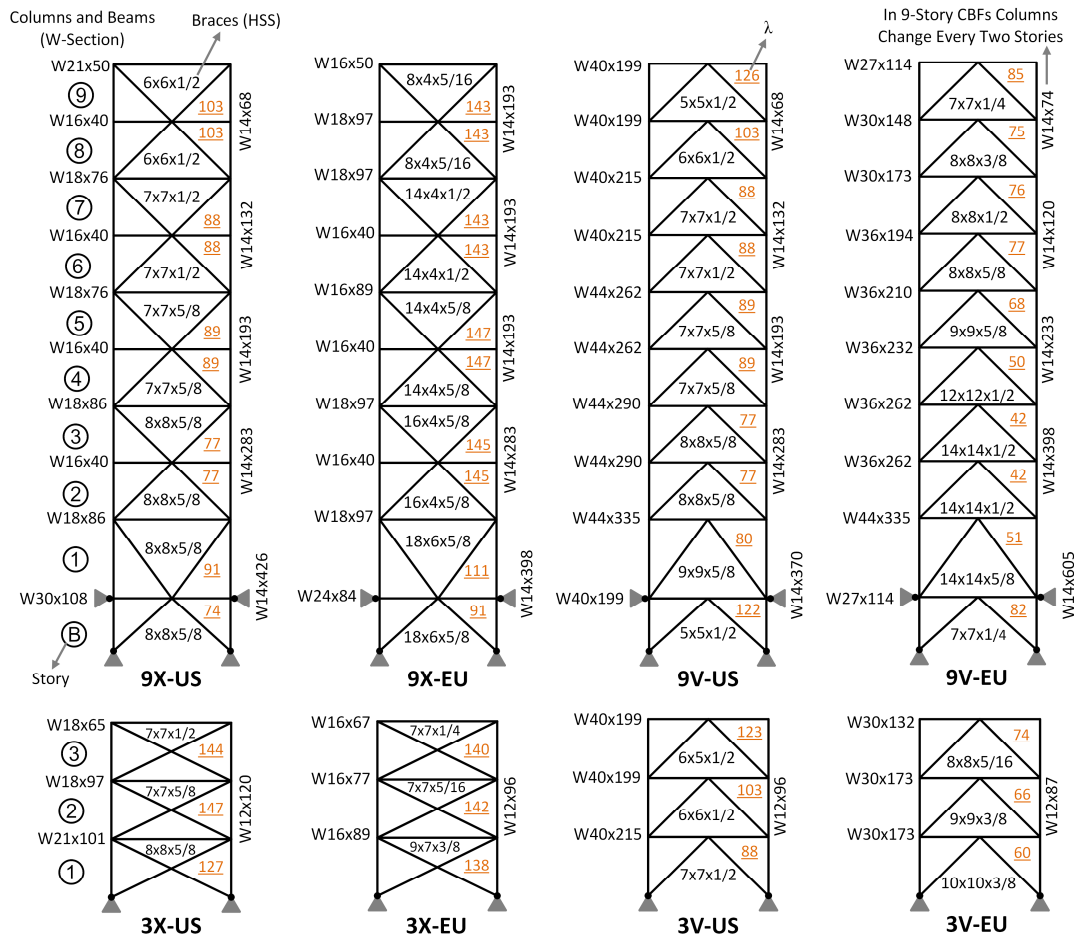


Figure 6.12. Selected member sizes for the designed archetype CBFs

Two-dimensional models of the archetype CBFs were developed in ABAQUS by adopting the same modeling and analysis approaches outlined in Chapter 5. All members of the frame and the leaner column were modeled using B21 two-node beam elements, each having one integration point at the mid-length and five integration points through the height of the section. A rather small mesh size was

employed with 12, 18, and 8 elements in each brace, beam, and column, respectively. For each brace member, an initial imperfection of $l/1000$ was considered. This amount of imperfection has been previously reported as a reasonable estimate by many other studies such as [306, 328, 329].

Another important issue in nonlinear time history analysis is damping. The equivalent viscous damping approach using Rayleigh formulation is commonly adopted where the damping matrix, \mathbf{C} , is determined as follows:

$$\mathbf{C} = \alpha_m \mathbf{M} + \beta_k \mathbf{K} \quad (6.7)$$

where \mathbf{M} and \mathbf{K} are the mass, and stiffness matrices, respectively, and α_m and β_k are proportionality factors which require calibration. As discussed in detail in Section 5.4.1, Deierlein et al. [328] recommend minimizing the stiffness proportional part of damping, and representing damping mostly by the mass proportional component. This approach reflects the fact that the stiffness proportional part of damping is considered to have the major share in producing unrealistic damping forces which are reported in a number of previous studies [326, 330, 331]. Consequently, in the present chapter the mass proportionality factor (α_m) was calibrated such the observed damping in free vibration analyses of the designed archetypes corresponded to $\xi = 5\%$ in the first mode of vibration. The calibrated α_m factors ranged between 0.3/sec and 1.0/sec for the investigated archetypes. It is worth noting that the generated damping forces in the braces were negligible compared to those generated as a result of dynamic overshoots. In order to have a very rough (yet rather conservative) estimate, consider a very heavy brace with a mass of 1000 kg as a dashpot with its full mass lumped at its end, subjected to an extremely rapid shortening of 3000 mm/sec (see Section 6.5). The max axial damping force for such a case considering the highest α_m factor (i.e. 1.0/sec) would be $(1.0/\text{sec} \times 1000 \text{ kg} \times 3 \text{ m/sec}) = 3 \text{ kN}$, which is extremely low compared to the overshoot forces reported in the next section.

The reliability of beam elements is first validated based on the results of two of the previously studied cases. For the first case, the theoretical results obtained in Section

6.2 and presented in Figure 6.2 are considered. The same elastic steel rod with $\lambda \approx 120$ was modeled with 12 beam elements and subjected to different boundary velocities. The FE results, depicted in Figure 6.2 with dotted lines, agree well with the theoretical results. The slight oscillations in the FE results, which are not observed in the theoretical results, are a consequence of the simplifications which were considered in the theoretical solution (e.g. neglect of the effect of axial inertia). For the second case, the FE analyses conducted in Section 6.3 for Fell's [329] HSS1-3 test were repeated, this time using 12 beam elements along the brace length and omitting the gusset plates. The results, presented in Figure 6.5 with dotted lines, demonstrate that beam elements are also capable of capturing the behavior of brace members with a reasonable accuracy.

The FE model of each of the eight archetype CBFs was then subjected to a large set of 44 far-field and 56 near-field ground motion records presented in FEMA P695 [250]. Furthermore, each analysis was conducted two times, considering braces with mass and massless braces, resulting in a total of 1600 nonlinear time history analyses. It should be emphasized that, in models with braces with mass, in addition to the lumped story masses, the mass of all members, i.e. braces, columns, and beams, was included whereas in the models with massless braces only the mass of brace members was set to zero and all other masses were retained. The ground motions discussed above were normalized and scaled using the procedure recommended in FEMA P695 [250] to reach the maximum considered earthquake (MCE) spectral demand of the seismic design category D_{max} .

6.4.2 Discussion of Results

The results are too voluminous to be presented in every detail. Several local and global performance indicators are compared for the cases of braces with mass and massless braces. As representatives, a summary of results for the 3-story CBFs under near-field records and 9-story CBFs under far-field ground motions is presented in Figure 6.13 and Figure 6.14, respectively. In these figures, P_{col} , P_{beam} , P_{br} , μ_{br} , $\delta_{br\theta}$,

and Δ are the *maximum* values of column axial force, beam axial force, brace axial force, brace ductility demand (i.e. brace axial deformation divided by brace axial yield deformation), brace out-of-plane deformation, and interstory drift ratio, respectively, recorded during the analysis. The superscript of “ M ” represents the case of braces with mass and “ ML ” the case with massless braces. Thus, for instance, P_{col}^M/P_{col}^{ML} is the amount of change in the maximum recorded column axial force solely due to dynamic buckling of brace members. In each subplot, thin horizontal grey lines span from the minimum to the maximum value of change, thick grey lines cover the mean \pm one standard deviation of change, and circles represent the median of the amount of change recorded for the earthquake set. For P_{col} , P_{beam} , P_{br} , and μ_{br} two sets of lines are plotted at each story level in order to distinguish the amount of change in tension and compression. In general, the difference in results obtained for far-field and near-field records was not very significant regarding the effects of dynamic buckling of braces on the seismic behavior.

Any change that is recorded in the response due to dynamic buckling of braces is in fact a consequence of two issues: (i) increase in the compressive capacity of brace members due to the delaying effect of the mass, i.e. dynamic overshoot; and (ii) inertia-induced oscillation in the axial response of brace members. These two effects are clearly visible in the results presented previously in Section 6.3 (Figure 6.5d, Figure 6.7a, and Figure 6.10a). According to these results, the oscillation occurs only after the overshoot phase and within a lower load range compared to the peak buckling load. Thus, the overshoot is the dominant factor and the above-mentioned two effects are briefly referred to as “dynamic overshoot” hereafter.

The third row of sub-plots in Figure 6.13 and Figure 6.14 (i.e. P_{br}^M/P_{br}^{ML}) provide an estimate of the expected level of dynamic overshoot for braces of the studied archetypes. In these sub-plots, the black circles which lie on the vertical line of $P_{br}^M/P_{br}^{ML} = 1.0$ indicate that, there is almost no change in the recorded maximum tensile force of brace members, due to the inclusion of their mass in the analysis models. On the other hand, significant dynamic overshoots are observed in the

maximum compressive force of braces, which range from about 10% to very high values of the order of 200%. Investigation of the numerical results revealed that, although the experienced loading rate is also effective, the most dominant parameter regarding the amount of dynamic overshoot is the brace slenderness (λ). The highest levels of overshoots are recorded for 9X-EU, 3X-US, and 3X-EU frames which have the most slender braces (Figure 6.12).

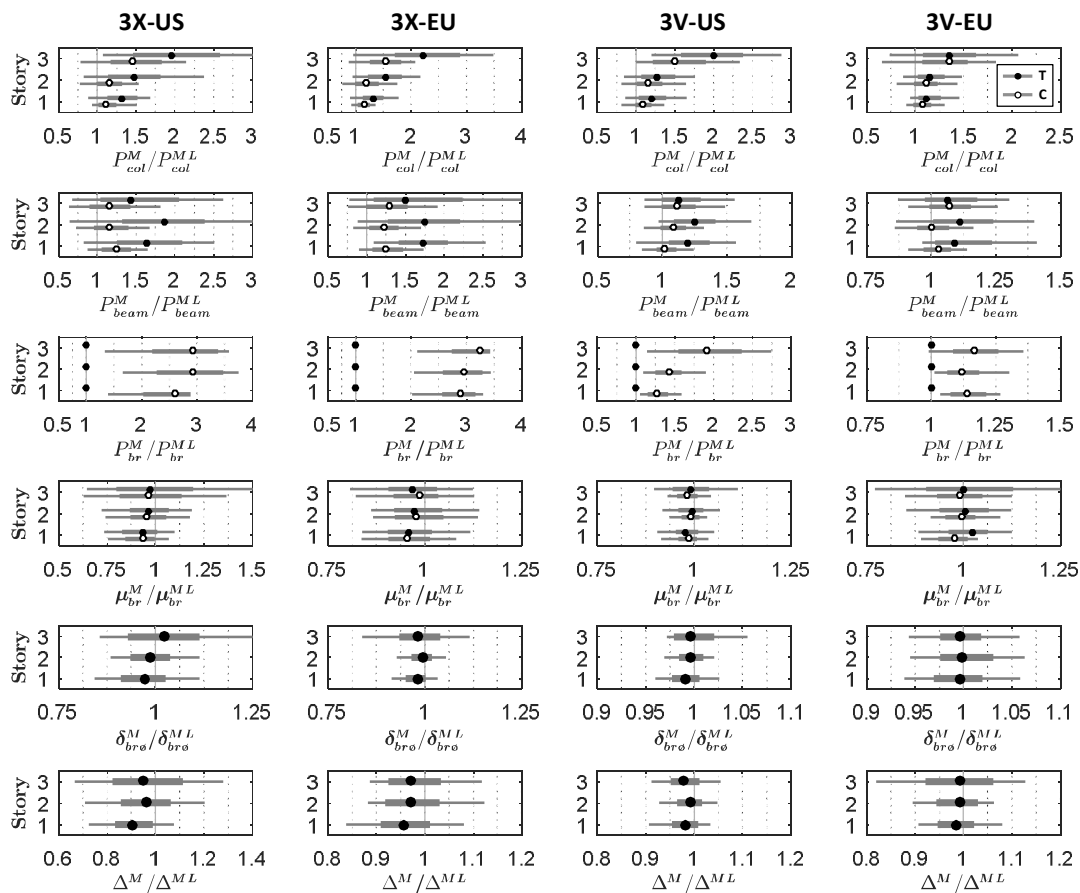


Figure 6.13. Results for 3-story archetype CBFs under near-field ground motions

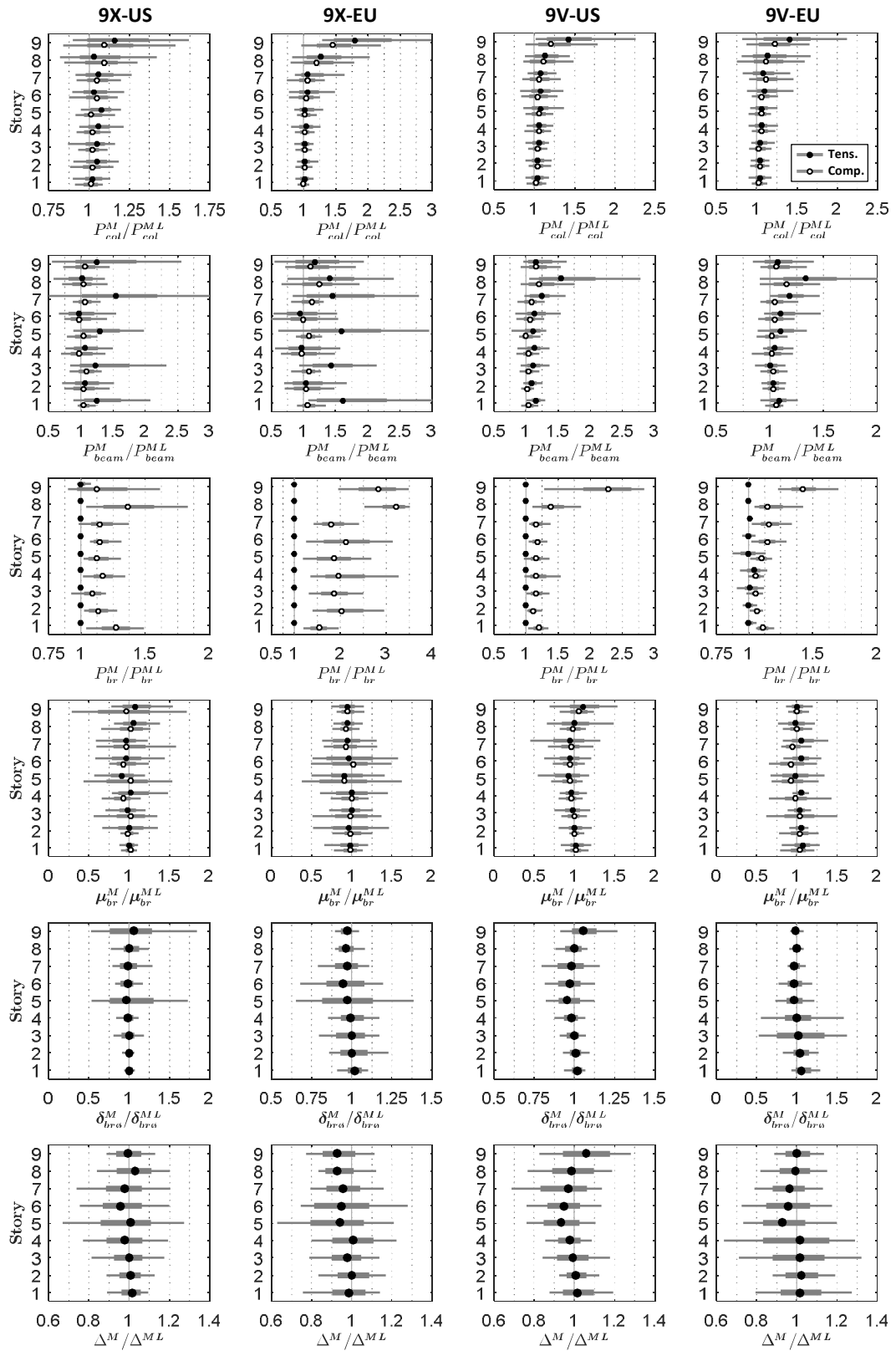


Figure 6.14. Results for 9-story archetype CBFs under far-field ground motions

Although dynamic overshoots do not happen simultaneously for all braces, notable changes in column forces (i.e. P_{col}^M/P_{col}^{ML}) are observed with a general increasing trend towards the upper stories. This is expected since upper columns are less loaded than the lower ones and, thus, dynamic overshoots can result in higher changes in their internal forces. Statistical distribution of the results indicates that, in most cases, column axial forces increased due to dynamic overshoots. The amount of increase varies drastically along the height and among the archetypes, being as high as 20% in lower stories of the 9-story CBFs, ranging to values in excess of 50% in upper stories of these archetypes, and to even higher values in the top story of the 3-story CBFs. The results also indicate that the amount of increase is generally higher for columns connected to more slender braces.

Based on the P_{beam}^M/P_{beam}^{ML} sub-plots, increases in excess of 100% in the tensile axial force and of the order of 25% in the compressive axial force can be observed for beams of 9X-US and 9X-EU frames, located at stories with odd numbers. The reason for the former is that, these beams are typically under compression or small tensile forces due to the utilized brace configuration and any increase in their tensile force results in large P_{beam}^M/P_{beam}^{ML} ratios. Brace-intersected beams of 9X-US and 9X-EU, located at stories with even numbers have mostly experienced similar changes in their tensile and compressive axial forces, within the bounds of $\pm 25\%$, since any change in the exerted unbalanced force will affect the tensile and compressive axial force of these beams somewhat similarly. The abrupt increases in the tensile axial force of beams of 3X-US and 3X-EU are due to the same reason discussed above for beams of 9X-US and 9X-EU located at stories with odd numbers. However, these beams have also mostly experienced significant increases in their compressive axial force which easily reached to values as high as 50%. For the 9- and 3-story V-braced frames more uniform height-wise increases in beam axial force are observed which are mostly bounded by 25% and are found to be higher in tension. The fact that each beam in V-braced archetypes is typically connected to four brace members suggests that the tensile axial force of beams would be more affected when the connecting compression braces exhibit dynamic overshoots.

As shown in Figure 6.13 and Figure 6.14, both increases and reductions are observed in the brace ductility demands (i.e. μ_{br}^M/μ_{br}^{ML}) with a slight tendency towards reduction. The amount of change in μ due to dynamic overshoots is found to be less sensitive to the brace slenderness and mostly bounded by $\pm 25\%$ in the 9-story CBFs and $\pm 10\%$ in the 3-story archetypes. Similarly, the change in brace out-of-plane deformations (i.e. $\delta_{br\theta}^M/\delta_{br\theta}^{ML}$), is also less sensitive to the brace slenderness and mostly stays within the limits of $\pm 10\%$ in the 9-story systems and $\pm 5\%$ in the 3-story CBFs. Furthermore, as a result of overshoots, changes in the range of $\pm 10\%$ are recorded for the maximum interstory drift ratios (i.e. Δ^M/Δ^{ML}) with a notably higher tendency towards reducing the amount of drifts observed during the earthquakes.

Recorded maximum base shears for the cases with braces with mass are compared in Figure 6.15 to those of the cases with massless braces. Considering that the ratios of V_b^M/V_b^{ML} are mostly above 1.0, it can be deduced that the figure is in fact quantifying the level of *structural overstrength* solely due to dynamic overshoots in brace forces. Higher overstrengths are recorded for the low-rise systems and those with more slender brace members. Very high overstrengths of the order of 50% are recorded in some cases, however, majority of the recorded overstrengths are bounded by 12% in the 9-story archetypes and by 25% in the 3-story CBFs.

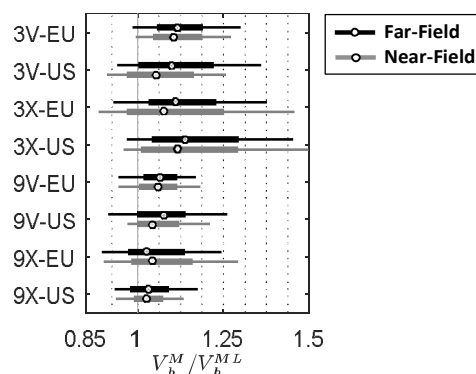


Figure 6.15. Summary of changes recorded for maximum base shears

6.4.3 Further Important Inferences

The effect of dynamic overshoot is not directly accounted for in the typical design procedure of CBFs outlined in most seismic provisions [11, 142]. This indicates that, any additional force that is transmitted to other members as a result of dynamic overshoot in brace forces will be unaccounted for – this being more pronounced for designs which utilize more slender brace members. Such additional forces are in many cases too high to be neglected. Consequently, the development of methods to account for these additional forces in the *capacity design* procedure of members other than braces seems to be necessary. For instance, the design procedures of Eurocode 8 [142] (for all types of CBFs) and AISC 341 [11] (only for *Ordinary* CBFs) utilize an amplified load approach for the capacity design of columns where the seismic forces in column members are amplified with *structural overstrength factors* (Ω_o). Such factors can be reevaluated using data similar to that presented in Figure 6.15. On the other hand, if the capacity design procedure is based on a plastic collapse mechanism type of analysis (e.g. Special CBFs as per AISC 341 [11]) where braces are replaced by their ultimate tensile (T_{ult}) and compressive (C_{ult}) forces, then, measures for including the effect of dynamic overshoot in the ultimate compressive force of braces can be introduced. According to AISC 341 [11], the ultimate brace forces can be determined as follows:

$$T_{ult} = R_y F_y A \quad (6.8)$$

$$C_{ult} = \begin{cases} 1.14 \alpha F_{cre} A \leq T_{ult} \\ or \\ 0.3 \times (1.14 F_{cre} A) \leq 0.3 T_{ult} \end{cases} \quad (6.9)$$

where R_y is the ratio of the expected yield stress to the specified minimum yield stress of the brace material, A is the gross area of the brace, F_{cre} is the critical stress calculated using the column buckling equations of AISC 360 [81] considering the expected yield stress. The factor α , which is discussed below, is equal to 1.0 as per

AISC 341 [11]. The expression which yields the higher demand should be used in Equation (6.9). The ultimate compressive brace force can be altered considering $\alpha \geq 1.0$ to include the dynamic buckling effect. Parameter α is in fact a calibrated *amplification factor* for estimating the expected level of dynamic overshoot. Results of a comprehensive parametric study on α are presented in Section 6.5.

Most seismic provisions require brace end connections to be designed following a capacity design approach. For instance, AISC 341 [11] requires brace end connections of Special CBFs to be designed for a tensile load of T_{ult} and a compressive load of $1.1C_{ult}$. As discussed in the commentary of these provisions [51], a factor of 1.1 has been adopted in order to alleviate the use of conservative column curve equations. Simulation results of the previous section demonstrated that significant dynamic overshoots which can range from 10% to 200% and even more can be observed in the compressive capacity of brace members. The ultimate compressive load for the capacity design of these connections and their elements such as gusset plates, bolts, and welds should also account for the effect of dynamic overshoot. The connections can be designed for a compressive load of $1.1C_{ult}$, however, considering an appropriate $\alpha > 1.0$.

In numerical analyses, removing the mass of a brace will prevent the occurrence of any dynamic overshoot in its compressive capacity. Consequently, it is advisable to include the mass of braces in all time history analyses and avoid using models which only include lumped masses at story levels and do not consider the mass of structural members along their lengths. It is worth reiterating that, the mass of a brace is the dominant factor in observing dynamic overshoot whereas the mass of other members (i.e. beams and columns) does not have a direct effect on this phenomenon. Phenomenological models which simulate the buckling behavior of brace members through special, calibrated axial force versus axial deformation relations should also be avoided as much as possible. These elements do not need to deflect laterally to exhibit buckling behavior and, therefore, are unable to capture dynamic overshoot and its associated issues regardless of the inclusion or neglect of their mass.

6.5 Estimation of Dynamic Overshoot in Brace Compressive Capacity

While P_{br}^M/P_{br}^{ML} ratios are presented in Figure 6.13 and Figure 6.14 the amounts of overshoot with respect to the static buckling capacity (i.e. $\alpha = P_{br}^M/P_{cr}$) are given in Figure 6.16. It should be emphasized that, P_{cr} is determined by conducting separate static FE analyses on single brace members, considering both material and geometric nonlinear effects. The yield limit for each brace member (i.e. $\alpha_y = P_y/P_{cr}$ where $P_y = AF_y$) is also depicted in the figure with a red triangle. As it can be seen, significant overshoots above P_{cr} , have been recorded which, in some cases, even approach to the yield strength of the brace. The values of α presented in Figure 6.16 are those experienced by the brace members and, therefore, can directly be used as a guide during the capacity design of beams and gusset plates. However, since all brace members might not exhibit dynamic overshoots simultaneously, more relaxed values of α can be considered for the capacity design of column members.

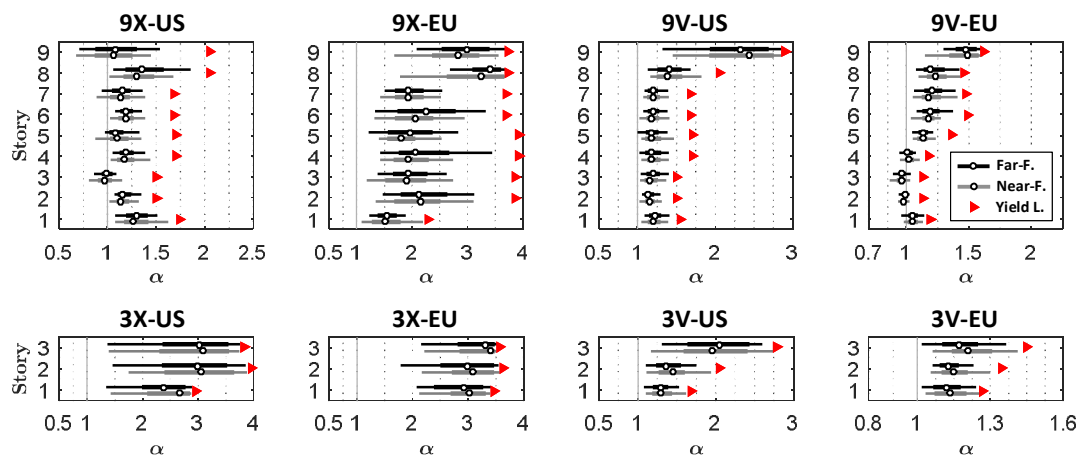


Figure 6.16. Ratio of the recorded maximum compressive brace force divided by the static buckling capacity (i.e. α)

In order to provide a more convenient approach for estimating α , another parametric study is conducted in this section. To this end, length of the HSS $4 \times 4 \times 1/4$ brace in the FE model of Fell's [329] HSS1-3 test was altered to obtain eight different brace models with $\lambda = 40, 60, 80, 100, 120, 150, 170,$ and 200 . Besides the change in

length, the only additional change in the FE model was the omission of gusset plates. Each of the eight FE models was then subjected to a wide range of compressive loading rates (i.e. $v_{br} = 50$ mm/s to 2000 mm/s) where one end of the brace moved towards the other end with a constant speed. Each model was also analyzed once in a quasi-static manner to determine P_{cr} . The applied rates were selected based on the maximum compressive brace loading rates presented in Figure 6.17 which were extracted from the results of the comprehensive study conducted in Section 6.4. The figure demonstrates that a typical CBF brace will mostly experience peak loading rates of the order of 250 mm/s to 1250 mm/s during strong earthquakes. Higher values of v_{br} were also recorded, particularly in 9X-EU and 9V-EU, however, these are considered to be extreme cases which were observed as a result of the development of soft-story behavior at the top two stories of these frames which was discussed in detail in Chapter 5. Based on Figure 6.17, the recorded maximum brace loading rates during the far-field and near-field earthquakes are comparable, which justifies why the results found in Section 6.4.2 regarding the effects of dynamic overshoots on seismic behavior were close to each other for these two ground motion sets.

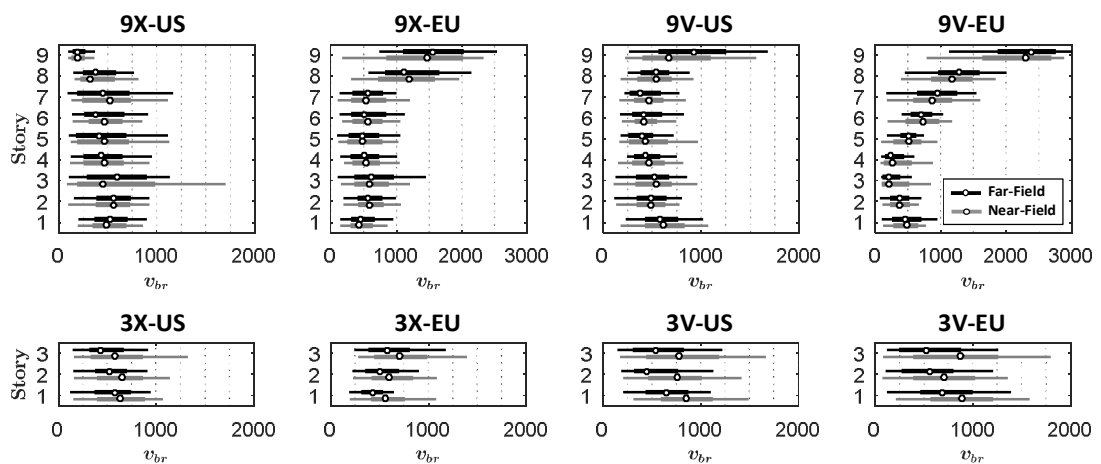


Figure 6.17. Recorded maximum compressive brace loading rates (in mm/s)

A total of 88 refined FE analyses were conducted. As a representative case, results for $\lambda = 60$ are depicted in Figure 6.18 where dynamic overshoot under rapid shortening is clearly visible. Results for α are summarized in Table 6.1. Significant overshoots are recorded for high values of v_{br} and particularly for slender braces. The results of this table suggest that, if the compression rate is high enough, yielding prior to notable buckling-induced lateral deformation (i.e. *saturation*) might also be observed.

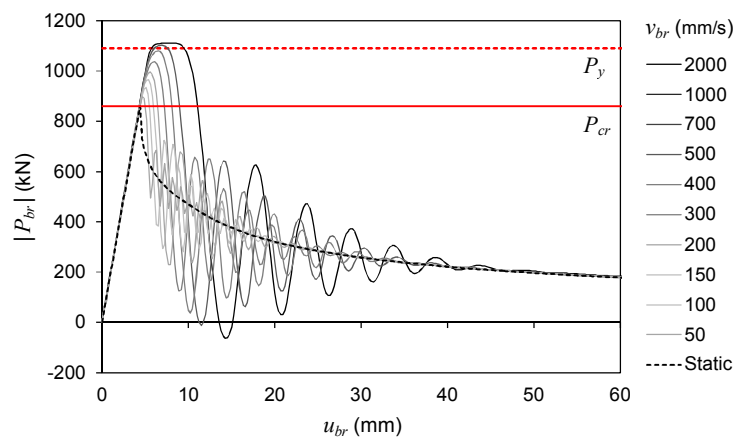


Figure 6.18. FE response of an HSS 4×4×1/4 steel brace with $\lambda = 60$ to different loading rates

Table 6.1 Percentage of yielded or buckled members of the designed archetypes

λ	v_{br} (mm/s)										
	Static	50	100	150	200	300	400	500	700	1000	2000
40	1.00	1.03	1.05	1.07	1.08	Y*	Y	Y	Y	Y	Y
60	1.00	1.04	1.09	1.12	1.16	1.20	1.26	Y	Y	Y	Y
80	1.00	1.06	1.19	1.29	1.40	1.60	1.76	Y	Y	Y	Y
100	1.00	1.08	1.32	1.61	1.87	2.27	2.54	Y	Y	Y	Y
120	1.00	1.21	1.63	2.08	2.49	3.14	3.57	Y	Y	Y	Y
150	1.00	1.50	2.31	3.03	3.69	4.80	5.52	Y	Y	Y	Y
170	1.00	1.82	2.84	3.78	4.63	6.09	7.05	Y	Y	Y	Y
200	1.00	2.30	3.83	4.98	6.14	8.21	9.63	Y	Y	Y	Y

* Indicates that the brace experienced yielding prior to exhibiting notable buckling-induced lateral deformation

The following issues should be borne in mind regarding the data presented in Table 6.1. As discussed in Section 6.3, dynamic overshoot is highly dependent upon the applied displacement history. On the other hand, the results presented in Table 6.1 are obtained by applying one-sided large compressive excursions with different speeds to the brace. Consequently, the results should be considered as upper bound estimates for α . Another important issue is the applicability of the reported data to other cases. Based on the theoretical background presented in Section 6.2, it can readily be shown that the amount of overshoot in the buckling load of a pinned elastic brace, with a predefined imperfection, subjected to a boundary velocity is only dependent upon its material, loading rate, and slenderness. Furthermore, results of additional FE analyses, which are not presented here, demonstrated that if material nonlinearity is also included, the overshoot is again dominantly dependent upon the same parameters. In other words, if two steel braces of similar slenderness (λ) and imperfection (e.g. $l/1000$), one with a section of HSS 4×4×1/4 and the other with a section of HSS 8×8×5/6, are subjected to the same loading rate, they will experience similar levels of dynamic overshoot, regardless of the significant difference that exists between their mass per unit length values. This indicates that the overshoot values presented in Table 6.1 are rather comprehensive and can be used for a variety of steel brace sections with different slenderness values. The main restriction regarding the results is the value of F_y . Based on the material data reported by Fell [329], the results of Table 6.1 are for a brace with $F_y \approx 470$ MPa. However, if the material of a steel brace has a higher yield stress, larger overshoots might be observed prior to the saturation of α by the yield limit (i.e. α_y). Consequently, the results presented in the table are most reliable for steel braces with $F_y \approx 470$ MPa and can be used as an estimate for those with $F_y < 470$ MPa, however, might be erroneous for cases with $F_y \gg 470$ MPa.

The results reported in Table 6.1 can be summarized in form of a simple formula to be used as an aid by design engineers. Based on a curve fitting process, the following power law was found to be a reasonable match for the results:

$$\alpha = 1 + \frac{(v_{br}/c)^{0.85} \lambda^{2.5}}{20} \leq \alpha_y \quad (6.10)$$

Based on the previous discussions, the proposed formula provides an upper bound estimate for the amount of dynamic overshoot that a steel brace ($E = 200$ GPa, $\bar{\rho} = 7850$ kg/m³, and $c = \sqrt{E/\bar{\rho}} \approx 5047$ m/s), with an imperfection of $l/1000$, would experience when subjected to a particular compressive loading rate (v_{br}). The value of overshoot is capped in the formula by the yield limit (α_y). This is in recognition of the saturation of dynamic overshoot and the fact that the increase in the compressive brace force beyond this level was observed to be very limited in the studied FE models and controlled only by the strain hardening behavior of the material. Nevertheless, the threshold of α_y can slightly be altered to also include the strain hardening effect, if required. Other studies such as [364, 366] have also proposed theoretical expressions for estimating α , however, only for elastic members. It is worth noting that, the mean of ratios of overshoot values found via Equation (6.10) to those obtained in the FE analyses of this section is 1.02 with a standard deviation of 0.04.

6.6 Chapter Summary

The dynamic buckling behavior of brace members during strong earthquakes and its effect on the seismic behavior of CBF systems and their members were thoroughly studied in this chapter. A theoretical background on the topic was provided followed by the investigation of recent dynamic tests on brace members and CBFs. A comprehensive parametric study revealed that dynamic overshoots can frequently be observed in brace forces of CBF systems during strong earthquakes. Overshoots of the order of 10% to very high values in excess of 200% were recorded in the FE analyses. The brace slenderness as well as the experienced loading rate were the effective factors in the observed level of overshoot, with the former being the most dominant parameter.

As a consequence of dynamic buckling of braces, notable changes were also recorded in forces transmitted to columns, beams, and brace connections of the studied CBFs. The implications of these extra forces were discussed, and a simple formula was developed which can be used for the estimation of the ultimate brace force (considering the dynamic buckling effect) during the capacity design of CBF systems.

All the conclusions drawn based on studies of this chapter are summarized in detail in Chapter 7.

CHAPTER 7

CONCLUSIONS

A series of topics related to EBF and CBF systems were identified and thoroughly studied in the present thesis. The relevant conclusions related to each topic are presented in the following sections.

7.1 EBF-Related Conclusions

As a part of the present thesis, a comprehensive review of research was conducted in Chapter 2 on EBFs which comprised both component level and system level responses and the relevant experimental and numerical studies. Based on the review study, a total of 22 future research needs were identified and presented in Chapter 2.

A series of shear links were tested in Chapter 3 utilizing a nearly full-scale test setup in order to study their low-cycle fatigue (LCF) behavior. The results of the LCF experiments were then used to develop a generalized damage law to estimate the instant of fracture initiation of EBF shear links. The most important outcomes of the chapter were as follows:

- LCF tests revealed that cycles with higher amplitudes are much more damaging compared to cycles with low amplitudes. As a result, the power of the Coffin-Manson relationship (\bar{c}) was found to be close to 2.0 for both the I-section links studied herein.
- A generalized damage law (Equation (3.10)) for shear links was developed on the basis of results obtained in the current study as well as a comprehensive data compilation of previous tests. According to this law, links are categorized into two groups depending on the cyclic buckling behavior of their webs. For links with webs that exhibit stable cyclic behavior

($\gamma_u \geq 0.11$ rad), the material strength is considered as the most influential factor, whereas for links which exhibit notable web buckling during cyclic loading ($\gamma_u < 0.11$ rad), the web panel aspect ratio (a/h), web slenderness (h/t_w), and material strength are considered as the most influential factors on the LCF life.

- A simple 8-step algorithm was outlined in Section 3.8 which utilizes the generalized damage law for estimating the accumulation of damage as well as the instant of link fracture in nonlinear time history analysis under earthquake-induced loading histories. The algorithm can also contribute significantly to the decision-making process of the post-earthquake replacement of EBF links. Accurate decisions can also be made utilizing simple health monitoring devices where the experienced rotation history of links is recorded during an earthquake. This approach can alleviate the need for post-earthquake nonlinear time history analysis since the link rotation histories will be available after the event. Using these histories and the outlined algorithm, it is possible to estimate the exhausted as well as remaining LCF life of the shear links utilized in the structure after the earthquake.
- The metrics given in the ASCE 41-13 [249] standard as acceptance criteria for EBF shear links were found to be unreliable. The test data reported in Chapter 3 and the evaluations of the Christchurch hospital garage links indicate that assessing failure based on the maximum link rotation can be erroneous, and instead, evaluations should be based on cumulative measures. Future research should also concentrate on dual criteria considering both the maximum link rotation angle and cumulative measures.
- When a properly designed shear link is tested under the current loading protocol of the AISC Seismic Provisions [248], the imposed damage will be negligible until approximately the 25th cycle (i.e. $\gamma = 0.015$ rad) based on the developed generalized damage law. The AISC loading protocol should be re-evaluated in light of the findings presented in the present study. This protocol

was developed based on a linear addition of cycle ranges ($\Sigma(\Delta\gamma)$). Instead, considering the power of 2.0 recommended in the generalized damage law, a more accurate approach would be to determine the target cumulative demand for shear links using time history analysis and considering the sum of square of cycle ranges ($\Sigma(\Delta\gamma)^2$).

In Chapter 4 of the present thesis, the detachable replaceable link concept, which is under development at METU, was numerically investigated. A mid-splice detail is used in the concept which allows for post-earthquake link replacement under residual frame drifts of the order of 0.5% and even higher. Simulations were carried out considering different sophistication levels for investigating different issues from the level of axial force developed in the mid-splice connection to propensity of fracture when the proposed detail is utilized in deeper link sections. The following were concluded from the analyses of the chapter:

- The axial force developed in the mid-splice connection (due to large link deformations and end restraint effects) was determined based on a comprehensive parametric study and a simple design expression (Equation (4.2)) was developed.
- It was concluded that the mid-splice of the detachable replaceable link concept can be safely designed for a shear force of $2R_yV_n$ (where V_n is the nominal shear capacity of the link and R_y is the ratio of the expected to the nominal yield stress of the material) and an axial force of P_{design} determined via Equation (4.2).
- Results of a series of advanced simulations suggested that the proposed detachable replaceable link detail can also be utilized for larger (deeper) EBF shear links. Although this has not been experimentally validated, comparison of modified rapture index (MRI) values in the simulations revealed that the addition of a mid-splice connection has comparable effects on shallow links and deep links in terms of the fracture propensity, further suggesting its potential for practical application.

7.2 CBF-Related Conclusions

Chapter 5 of the present thesis explored in detail the similarities and differences between the design procedures as well as the seismic behaviors of steel CBFs designed to the provisions of AISC341 developed in the United States and EC8 developed in Europe. After reviewing the design philosophies and procedures in these provisions, a series of CBF archetypes were designed based on the American and European provisions and subjected to a large set of earthquakes in order to investigate and compare their seismic performances. The following were concluded from the 880 nonlinear time history analyses of the chapter:

- The most influential differences between the provisions are in the design of brace members. The differences in the design rules are more pronounced for the case of X- and split X-braced frames.
- More inter-related design requirements are given in EC8 compared to AISC341, which makes the design of CBFs according to EC8, relatively harder than AISC341.
- For X- and split X-braced frames, the US design generally results in stocky braces while the EU design results in more slender braces. On the other hand, for V-braced frames, both designs employ stocky brace members.
- AISC341 imposes significantly more stringent width-to-thickness (b/t) limits on HSS braces when compared to EC8. Considering the correlation between the local buckling and low-cycle fatigue with member slenderness, future experimental studies should concentrate on reevaluating the b/t limits for different brace slenderness ratios encountered in American and European practices.
- Although the EU design uses lower response modification coefficients (behavior factors), design base shears and steel weights for the X- and split X-braced archetypes were found to be somewhat comparable to each other, due to other counter-balancing differences that exist between the US and EU provisions. For the case of V-braced archetypes, however, the design base

shear for the EU case was almost twice that of the US frame. Nevertheless, the EU design resulted in a system with only 10% higher steel weight than the US design, mainly due to the differences in the codified b/t limits of HSS braces as well as the lower demands which EC8 estimates for beams.

- Results of the nonlinear time history simulations revealed that floor velocities during earthquakes are not sensitive to the slenderness of brace members in properly designed CBFs. However, floor accelerations were found to be mostly higher for the EU designs, suggesting that higher inertial forces will be exerted on their non-structural components during an earthquake.
- Residual interstory drifts in all of the investigated archetypes remained below the permissible level of 0.5%, except for the top two stories of the EU designs which experienced the soft-story behavior.
- Brace ductility demands were mostly limited to ± 10 , except for the top two stories of the EU designs, in which higher ductilities were recorded, sometimes reaching values as high as ± 20 . Abrupt increases and decreases were observed in brace ductility demands of split X-braced frames, which was attributed to the influence of brace-intersected beams on the behavior of braces located at subsequent stories. On the other hand, more smooth variations were recorded for the ductility demands of X- and V-braced archetypes. Nevertheless, the brace ductility demands in compression were found to be significantly higher than those in tension for the V-braced frame designed according to EC8, due to the inadequate strength and stiffness of its beams.
- Soft-story behavior occurred in the top stories of the X-, split X-, and V-braced archetypes designed according to the EU provisions. Several different alternatives were studied to resolve this issue. Although including an additional lateral load at the top floor has been found to be somewhat effective, it was concluded that the problem cannot be fully mitigated unless the Omega Rule of EC8 is omitted during the design. It was observed that the CBFs which adhere to this rule are overly flexible at the top stories. The

simulation results revealed that the omission of the Omega Rule will result in structures which are notably lighter and perform substantially better than those designed based on the original methodology of EC8. The conclusion was found to be consistent for all three configurations studied in the chapter.

- In all of the investigated archetypes, more column yielding was observed in the EU designs compared to the US designs. The issue can partly be related to the way the demands are calculated for these members in EC8 and partly to the observed soft-story behavior which, in some cases, caused column plastic hinging in the top stories of the EU frames.
- Yielding and large deflection of brace-intersected beams of split X-braced frames occurred in both the US and EU designs, significantly increasing the brace ductility demands. Further research for developing a convenient remedy for this issue is needed. Unlike the US design, yielding of beams in V-braced CBFs designed as per EC8 was frequently recorded, which prevented tensile yielding of the connected braces and increased the brace ductility demands in compression. Nevertheless, further research is necessary to clarify whether the design requirements of AISC341 are too conservative or the requirements of EC8 are unconservative regarding the design of these members in V-braced CBFs.
- It is worth reiterating that the investigation focused on seismic applications of CBFs, and the outcome might be different if wind load applications are considered.

Finally, the dynamic buckling behavior of brace members during strong earthquakes and its effect on the seismic behavior of CBF systems and their members were thoroughly studied in Chapter 6. A theoretical background on the topic was provided followed by the investigation of recent dynamic tests on brace members and CBFs. Eight archetype CBFs were then designed, modeled, and subjected to a large set of ground motions in order to provide a quantified insight on the frequency and anticipated level of dynamic overshoot in the compressive capacity of braces during

earthquakes. Investigation of the results of a total of 1600 nonlinear time history analyses led to the following conclusions:

- Investigation of the recent dynamic experiments conducted by others on braces or CBFs demonstrated that dynamic overshoot in brace forces has been reported, though not discussed thoroughly, in some studies. Furthermore, simulation results revealed that the dynamic overshoot would have been observed in other tests provided that the experiment was conducted with slight modifications such as increasing the applied loading rate or altering the utilized displacement history.
- Detailed FE analyses indicated that dynamic buckling of a steel brace is a rather complex phenomenon which is highly dependent upon many factors such as the brace slenderness, imposed displacement history, magnitude and variation of the loading rate, imperfection of the brace, and the change in its residual out-of-plane deformation.
- Results of a comprehensive study on archetype CBFs revealed that dynamic overshoots can frequently be observed in brace forces during strong earthquakes. Overshoots of the order of 10% to very high values in excess of 200% were recorded in the FE analyses. The brace slenderness as well as the experienced loading rate were found to be the most effective factors in the observed level of overshoot, with the former being the most dominant parameter.
- As a consequence of the dynamic buckling of braces, notable changes were recorded in forces transmitted to other members of the studied CBF systems. Increases as high as 20% to 150% were recorded in column axial forces for different cases. In general, the percentage of increase is expected to be larger in low-rise CBFs and upper columns of mid- and high-rise CBFs, and more particularly, when slender braces are used in the system. Similarly, considerable increases, as high as 25% to 50%, were recorded in beam axial forces of the studied archetypes.

- Dynamic buckling of braces was found to be less influential on altering the deformation demands. Changes in brace ductility demands and the maximum interstory drift ratios were mostly bounded by $\pm 25\%$ and $\pm 10\%$, respectively, with a higher tendency towards reduction, as a result of the overshoots.
- The increase in forces transmitted to members other than braces and to brace end connections necessitates revising the current capacity design procedures to include these effects. To this end, structural overstrength factors can be reevaluated using data similar to that presented in Section 6.4.2, which showed increases as high as 12% to 25% in the recorded maximum base shear, solely due to dynamic overshoots. Furthermore, the presented analysis results and the developed formula (Equation (6.10)) can be used as guides for calibrating amplification factors (α) to be used for a proper estimation of ultimate brace forces (which include the effect of dynamic buckling) during the capacity design of CBFs.
- For the studied archetype CBFs, compressive brace loading rates mostly of the order of 250 mm/s to 1250 mm/s were recorded during strong earthquakes.
- Omitting the mass of a brace in an analysis model will prevent the occurrence of any dynamic overshoot in its compressive capacity. Thus, it is advisable to avoid using analysis models which only include lumped masses at story levels and do not consider the mass of structural members and, more importantly, the mass of braces along their lengths. Phenomenological brace models which are unable to capture dynamic overshoot and its associated issues should also be avoided in nonlinear time history analyses.

REFERENCES

- [1] R. Tremblay, A. Filiatrault, P. Timler, and M. Bruneau, "Performance of steel structures during the 1994 Northridge earthquake," *Canadian Journal of Civil Engineering*, Vol. 22, No. 2, PP. 338-360, 1995.
- [2] M. Nakashima, K. Inoue, and M. Tada, "Classification of damage to steel buildings observed in the 1995 Hyogoken-Nanbu earthquake," *Engineering Structures*, Vol. 20, No. 4, PP. 271-281, 1998.
- [3] M. Fujimoto, T. Aoyagi, K. Ukai, A. Wada, and K. Saito, "Structural Characteristics of Eccentric K-Braced Frames," *Trans. Architectural Institute of Japan*, Vol. 195, PP. 39-49, 1972. (*in Japanese*)
- [4] R. Tanabashi, K. Naneta, and T. Ishida, "On the Rigidity and Ductility of Steel Bracing Assemblage," *Proc. 5th World Conference on Earthquake Engineering*, IAEE, Rome, 1974, PP. 834-840.
- [5] E. P. Popov and M. D. Engelhardt, "Seismic eccentrically braced frames," *Journal of Constructional Steel Research*, Vol. 10, PP. 321-354, 1988.
- [6] C. Clifton, M. Bruneau, G. A. MacRae, R. Leon, and A. Fussell, "Steel structures damage from the Christchurch earthquake series of 2010 and 2011," *Bulletin of the New Zealand Society For Earthquake Engineering*, Vol. 44, No. 4, PP. 297-318, 2011.
- [7] A. M. Kanvinde, K. S. Marshall, D. A. Grilli, and G. Bombia, "Forensic Analysis of Link Fractures in Eccentrically Braced Frames during the February 2011 Christchurch Earthquake: Testing and Simulation," *Journal of Structural Engineering, ASCE*, Vol. 141, No. 5, 2015.

- [8] M. B. Bozkurt and C. Topkaya, "Replaceable links with direct brace attachments for eccentrically braced frames," *Earthquake Engineering & Structural Dynamics*, Vol. 46, No. 13, PP. 2121-2139, 2017.
- [9] M. B. Bozkurt and C. Topkaya, "Replaceable links with gusseted brace joints for eccentrically braced frames," *Soil Dynamics and Earthquake Engineering*, Vol. 115, PP. 305-318, 2018.
- [10] G. Della Corte, M. D'Aniello, and R. Landolfo, "Analytical and numerical study of plastic overstrength of shear links," *Journal of Constructional Steel Research*, Vol. 82, PP. 19-32, 2013.
- [11] AISC, *Seismic Provisions for Structural Steel Buildings, ANSI/AISC 341-10*. American Institute of Steel Construction, Chicago, IL, 2010.
- [12] C. W. Roeder and E. P. Popov, "Inelastic Behavior of Eccentrically Braced Steel Frames Under Cyclic Loading," University of California, Berkeley, UCB/EERC-77/18, 1977.
- [13] C. W. Roeder and E. P. Popov, "Cyclic shear yielding of wide-flange beams," *Journal of the Engineering Mechanics Division*, Vol. 104, No. 4, PP. 763-780, 1978.
- [14] K. D. Hjelmstad and E. P. Popov, "Seismic behavior of active beam link in eccentrically braced frames," Earthquake Engineering Research Center, University of California, Berkeley, CA, Report No. UCB/EERC-83/15, 1983.
- [15] K. D. Hjelmstad and E. P. Popov, "Cyclic Behavior and Design of Link Beams," *Journal of Structural Engineering, ASCE*, Vol. 109, No. 10, PP. 2387-2403, 1983.

- [16] D. N. Manheim and E. P. Popov, "Plastic Shear Hinges in Steel Frames," *Journal of Structural Engineering, ASCE*, Vol. 109, No. 10, PP. 2404-2419, 1983.
- [17] J. O. Malley and E. P. Popov, "Shear Links in Eccentrically Braced Frames," *Journal of Structural Engineering, ASCE*, Vol. 110, No. 9, PP. 2275-2295, 1984.
- [18] K. Kasai and E. P. Popov, "General Behavior of WF Steel Shear Link Beams," *Journal of Structural Engineering, ASCE*, Vol. 112, No. 2, PP. 362-382, 1986.
- [19] M. D. Engelhardt and E. P. Popov, "Behavior of long links in eccentrically braced frames," Earthquake Engineering Research Center, University of California, Berkeley, CA, Report No. UCB/EERC-89/01, 1989.
- [20] SEAOC, *Recommended Lateral Force Requirements and Tentative Commentary*. Structural Engineers Association of California, Sacramento, CA, 1988.
- [21] A. Daneshmand and B. H. Hashemi, "Performance of intermediate and long links in eccentrically braced frames," *Journal of Constructional Steel Research*, Vol. 70, PP. 167-176, 2012.
- [22] X. Ji, Y. Wang, Q. Ma, and T. Okazaki, "Cyclic Behavior of Very Short Steel Shear Links," *Journal of Structural Engineering, ASCE*, 2015. doi:10.1061/(ASCE)ST.1943-541X.0001375
- [23] K. Kasai and E. P. Popov, "A study of seismically resistant eccentrically braced frames," Earthquake Engineering Research Center, University of California, Berkeley, CA, Report No. UCB/EERC-86/01, 1986.

- [24] A. S. Whittaker, C. M. Uang, and V. V. Bertero, "Earthquake simulation tests and associated studies of a 0.3-scale model of a six-story eccentrically braced steel structure," University of California, Berkeley, UCB/EERC-87/02, 1987.
- [25] CSA, *Design of Steel Structures, CAN/CSA S16-14*. Canadian Standards Association, Toronto, ON, 2014.
- [26] J. O. Malley and E. P. Popov, "Design Considerations for Shear Links in Eccentrically Braced Frames," University of California, Berkeley, Report No. UCB/EERC-83/24, 1983.
- [27] J. M. Ricles and E. P. Popov, "Experiments on eccentrically braced frames with composite floors," Earthquake Engineering Research Center, University of California, Berkeley, CA, Report No. UCB/EERC-87/06, 1987.
- [28] A. Ghobarah and T. Ramadan, "Bolted link-column joints in eccentrically braced frames," *Engineering Structures*, Vol. 16, No. 1, PP. 33-41, 1994.
- [29] A. M. Itani, "Cyclic behavior of Richmond-San Rafael tower links," Center for Civil Engineering Earthquake Research, University of Nevada, Reno, NV, Report No. CEER 97-4, 1997.
- [30] B. Chi and C. M. Uang, "Cyclic testing of steel shear links for the San Francisco Moscone Convention Center expansion project," Department of Structural Engineering, University of California, San Diego, La Jolla, CA, Report No. TR-99/06, 2000.
- [31] G. Arce, "Impact of higher strength steels on local buckling and overstrength of links in eccentrically braced frames," M.Sc. Thesis, Department of Civil Engineering, University of Texas at Austin, Austin, TX, 2002.
- [32] C. C. McDaniel, C. M. Uang, and F. Seible, "Cyclic testing of built-up steel shear links for the new bay bridge," *Journal of Structural Engineering, ASCE*, Vol. 129, No. 6, PP. 801-809, 2003.

- [33] P. Galvez, "Investigation of Factors Affecting Web Fractures in Shear Links," M.Sc. Thesis, Department of Civil Engineering, University of Texas at Austin, Austin, TX, 2004.
- [34] T. Okazaki, "Seismic performance of link-to-column connections in steel eccentrically braced frames," Ph.D. Thesis, Department of Civil Engineering, University of Texas at Austin, Austin, TX, 2004.
- [35] A. Stratan and D. Dubina, "Bolted links for eccentrically braced steel frames," *Proc. 5th AISC/ECCS International Workshop: Connections in Steel Structures V. Behaviour, Strength and Design*, Delft, The Netherlands, 2004, PP. 223-332.
- [36] H. C. Ryu, "Effects of loading history on the behavior of links in seismic resistant eccentrically braced frames," M.Sc. Thesis, Department of Civil Engineering, University of Texas at Austin, Austin, TX, 2005.
- [37] T. Okazaki, G. Arce, H. C. Ryu, and M. D. Engelhardt, "Experimental study of local buckling, overstrength, and fracture of links in eccentrically braced frames," *Journal of Structural Engineering, ASCE*, Vol. 131, No. 10, PP. 1526-1535, 2005.
- [38] T. Okazaki, M. D. Engelhardt, M. Nakashima, and K. Suita, "Experimental performance of link-to-column connections in eccentrically braced frames," *Journal of Structural Engineering, ASCE*, Vol. 132, No. 8, PP. 1201-1211, 2006.
- [39] T. Okazaki and M. D. Engelhardt, "Cyclic loading behavior of EBF links constructed of ASTM A992 steel," *Journal of Constructional Steel Research*, Vol. 63, No. 6, PP. 751-765, 2007.

- [40] A. Drolias, "Experiments on link-to-column connections in steel eccentrically braced frames," M.Sc. Thesis, Department of Civil Engineering, University of Texas at Austin, Austin, TX, 2007.
- [41] T. Okazaki, M. D. Engelhardt, A. Drolias, E. Schell, J. K. Hong, and C. M. Uang, "Experimental investigation of link-to-column connections in eccentrically braced frames," *Journal of Constructional Steel Research*, Vol. 65, No. 7, PP. 1401-1412, 2009.
- [42] N. Mansour, "Eccentrically Braced Frames with Replaceable Shear Links," Ph.D. Thesis, Department of Civil Engineering, University of Toronto, Toronto, Ontario, Canada, 2010.
- [43] P. Dusicka and G. Lewis, "Investigation of Replaceable Sacrificial Steel Links," *Proc. 9th US National and 10th Canadian Conference on Earthquake Engineering*, Toronto, Canada, 2010.
- [44] P. Dusicka, A. M. Itani, and I. G. Buckle, "Cyclic Behavior of Shear Links of Various Grades of Plate Steel," *Journal of Structural Engineering*, Vol. 136, No. 4, PP. 370-378, 2010.
- [45] A. Ciutina, D. Dubina, and G. Danku, "Influence of steel-concrete interaction in dissipative zones of frames: I-Experimental study," *Steel and Composite Structures*, Vol. 15, No. 3, PP. 299-322, 2013.
- [46] T. Okazaki, M. D. Engelhardt, J. K. Hong, C. M. Uang, and A. Drolias, "Improved link-to-column connections for steel eccentrically braced frames," *Journal of Structural Engineering, ASCE*, 2014.
- [47] M. Lian, M. Su, and Y. Guo, "Seismic performance of eccentrically braced frames with high strength steel combination," *Steel and Composite Structures*, Vol. 18, No. 6, PP. 1517-1539, 2015.

- [48] P. W. Richards, "Cyclic Stability and Capacity Design of Steel Eccentrically Braced Frames," Ph.D. Thesis, Department of Structural Engineering, University of California, San Diego, CA, 2004.
- [49] N. Mansour, C. Christopoulos, and R. Tremblay, "Experimental validation of replaceable shear links for eccentrically braced steel frames," *Journal of Structural Engineering, ASCE*, Vol. 137, No. 10, PP. 1141-1152, 2011.
- [50] P. Dusicka, A. M. Itani, and I. Buckle, "Cyclic behavior of shear links and tower shaft assembly of San Francisco-Oakland Bay Bridge Tower," Center for Civil Engineering Earthquake Research, University of Nevada, Reno, NV, Report No. CCEER-02-06, 2002.
- [51] K. Kasai, Y. Ooki, P. Suriyamongkol, and Y. Xu, "Fundamental study on inelastic behavior and low-cycle fatigue of a thick shear panel fabricated without welding," *Journal of Structural and Construction Engineering*, Vol. 69, No. 586, PP. 195-202, 2004. (*in Japanese*)
- [52] J. W. Berman and M. Bruneau, "Approaches for the Seismic Retrofit of Braced Steel Bridge Piers and Proof-of-Concept Testing of an Eccentrically Braced Frame with Tubular Link," Multidisciplinary Center for Earthquake Engineering Research, State University of New York at Buffalo, Buffalo, NY, Report No. MCEER-05-0004, 2005.
- [53] J. W. Berman and M. Bruneau, "Further development of tubular eccentrically braced frame links for the seismic retrofit of braced steel truss bridge piers," Multidisciplinary Center for Earthquake Engineering Research, State University of New York at Buffalo, Buffalo, NY, Report No. MCEER-06-0006, 2006.
- [54] J. W. Berman and M. Bruneau, "Experimental and analytical investigation of tubular links for eccentrically braced frames," *Engineering Structures*, Vol. 29, No. 8, PP. 1929-1938, 2007.

- [55] J. W. Berman and M. Bruneau, "Tubular links for eccentrically braced frames. I: Finite element parametric study," *Journal of Structural Engineering, ASCE*, Vol. 134, No. 5, PP. 692-701, 2008.
- [56] J. W. Berman and M. Bruneau, "Tubular links for eccentrically braced frames. II: Experimental verification," *Journal of Structural Engineering, ASCE*, Vol. 134, No. 5, PP. 702-712, 2008.
- [57] M. Bruneau, C. M. Uang, and S. R. Sabelli, *Ductile design of steel structures, 2nd ed.* McGraw Hill Professional, 2011.
- [58] P. W. Richards and C. M. Uang, "Effect of flange width-thickness ratio on eccentrically braced frames link cyclic rotation capacity," *Journal of Structural Engineering, ASCE*, Vol. 131, No. 10, PP. 1546-1552, 2005.
- [59] M. Bulic, M. Causevic, and B. Androic, "Reliability of short seismic links in shear," *Bulletin of earthquake engineering*, Vol. 11, No. 4, PP. 1083-1098, 2013.
- [60] T. Ramadan and A. Ghobarah, "Prediction of the ultimate capacity of wide flange link beams under cyclic loading," *Computers & Structures*, Vol. 40, No. 2, PP. 409-418, 1991.
- [61] A. Ghobarah and T. Ramadan, "Seismic analysis of links of various lengths in eccentrically braced frames," *Canadian Journal of Civil Engineering*, Vol. 18, No. 1, PP. 140-148, 1991.
- [62] A. Mohebbkhah and B. Chegani, "Overstrength and rotation capacity for EBF links made of European IPE sections," *Thin-Walled Structures*, Vol. 74, PP. 255-260, 2014.
- [63] S. Koboevic and S. O. David, "Design and seismic behaviour of taller eccentrically braced frames," *Canadian Journal of Civil Engineering*, Vol. 37, No. 2, PP. 195-208, 2010.

- [64] S. Koboevic, J. Rozon, and R. Tremblay, "Seismic Performance of Low-to-Moderate Height Eccentrically Braced Steel Frames Designed for North American Seismic Conditions," *Journal of Structural Engineering*, Vol. 138, No. 12, PP. 1465-1476, 2012.
- [65] P. W. Richards and B. Thompson, "Estimating inelastic drifts and link rotation demands in EBFs," *AISC Engineering Journal*, No. 3, PP. 123-135, 2009.
- [66] A. Kuşyılmaz and C. Topkaya, "Displacement amplification factors for steel eccentrically braced frames," *Earthquake Engineering & Structural Dynamics*, Vol. 44, No. 2, PP. 167-184, 2015.
- [67] G. J. O'Reilly and T. J. Sullivan, "Direct Displacement-Based Seismic Design of Eccentrically Braced Steel Frames," *Journal of Earthquake Engineering*, Vol. 20, No. 2, PP. 243-278, 2016.
- [68] A. Ghobarah and T. Ramadan, "Effect of axial forces on the performance of links in eccentrically braced frames," *Engineering Structures*, Vol. 12, No. 2, PP. 106-113, 1990.
- [69] S. Dastmalchi, "Numerical study of axial load effect on the seismic behavior of shear links in eccentrically braced frames," M.Sc. Thesis, Department of Civil and Environmental Engineering, The University of Maryland, College Park, MD, 2014.
- [70] J. M. Ricles and E. P. Popov, "Composite Action in Eccentrically Braced Frames," *Journal of Structural Engineering, ASCE*, Vol. 115, No. 8, PP. 2046-2066, 1989.
- [71] M. D. Engelhardt and E. P. Popov, "Experimental performance of long links in eccentrically braced frames," *Journal of Structural Engineering, ASCE*, Vol. 118, No. 11, PP. 3067-3088, 1992.

- [72] K. C. Tsai, Y. F. Yang, and J. L. Lin, "Seismic eccentrically braced frames," *The Structural Design of Tall and Special Buildings*, Vol. 2, No. 1, PP. 53-74, 1993.
- [73] P. W. Richards and C. M. Uang, "Testing protocol for short links in eccentrically braced frames," *Journal of Structural Engineering, ASCE*, Vol. 132, No. 8, PP. 1183-1191, 2006.
- [74] P. W. Richards and C. M. Uang, "Development of testing protocol for short links in eccentrically braced frames," Department of Structural Engineering, University of California at San Diego, San Diego, CA, Report No. SSRP-2003/08, 2003.
- [75] AISC, *Seismic Provisions for Structural Steel Buildings, ANSI/AISC 341-02*. American Institute of Steel Construction, Chicago, IL, 2002.
- [76] AISC, *Seismic Provisions for Structural Steel Buildings, ANSI/AISC 341-05*. American Institute of Steel Construction, Chicago, IL, 2005.
- [77] B. Chegeni and A. Mohebkhah, "Rotation capacity improvement of long link beams in eccentrically braced frames," *Scientia Iranica. Transaction A, Civil Engineering*, Vol. 21, No. 3, PP. 516-524, 2014.
- [78] G. Haaijer, "Plate buckling in the strain-hardening range," *Journal of the Engineering Mechanics Division*, Vol. 83, No. EM2, PP. 1-45, 1957.
- [79] ICBO, *Uniform Building Code*. International Conference of Building Officials, Whittier, CA, 1988.
- [80] AISC, *Load and Resistance Factor Design Specification for Buildings*. American Institute of Steel Construction, Chicago, IL, 1986.
- [81] AISC, *Specification for Structural Steel Buildings, ANSI/AISC 360-10*. American Institute of Steel Construction, Chicago, IL, 2010.

- [82] K. Kasai and E. P. Popov, "Cyclic Web Buckling Control for Shear Link Beams," *Journal of Structural Engineering, ASCE*, Vol. 112, No. 3, PP. 505-523, 1986.
- [83] K. Basler, "Strength of Plate Girders in Shear," *Journal of the Structural Division, ASCE*, Vol. 87, No. ST7, PP. 151-180, 1961.
- [84] F. Bleich, *Buckling Strength of Metal Structures*. McGraw-Hill, New York, 1952.
- [85] Eurocode 0, *Basis of structural design, EN 1990:2002*. European Standard, Comité Européen de Normalisation, Brussels, Belgium, 2002.
- [86] S. Chao, K. Khandelwal, and S. El-Tawil, "Ductile Web Fracture Initiation in Steel Shear Links," *Journal of Structural Engineering*, Vol. 132, No. 8, PP. 1192-1200, 2006.
- [87] H. Bahrampoor and S. Sabouri-Ghomi, "Effect of easy-going steel concept on the behavior of diagonal eccentrically braced frames," *International Journal of Civil Engineering*, Vol. 8, No. 3, PP. 242-255, 2010.
- [88] Y. Yurisman, B. Budiono, M. Moestopo, and M. Suarjana, "Behavior of Shear Link of WF Section with Diagonal Web Stiffener of Eccentrically Braced Frame (EBF) of Steel Structure," *Journal of Engineering and Technological Sciences*, Vol. 42, No. 2, PP. 103-128, 2010.
- [89] M. Ohsaki and T. Nakajima, "Optimization of link member of eccentrically braced frames for maximum energy dissipation," *Journal of Constructional Steel Research*, Vol. 75, PP. 38-44, 2012.
- [90] R. Imani and M. Bruneau, "Effect of Link-Beam Stiffener and Brace Flange Alignment on Inelastic Cyclic Behavior of Eccentrically Braced Frames," *AISC Engineering Journal*, Vol. 52, No. 2, PP. 109-124, 2015.

- [91] D. N. Manheim, "On the Design of Eccentrically Braced Frames," Ph.D. Thesis, Department of Civil and Environmental Engineering, University of California, Berkeley, Berkeley, CA, 1982.
- [92] K. D. Hjelmstad and S. G. Lee, "Lateral buckling of beams in eccentrically-braced frames," *Journal of Constructional Steel Research*, Vol. 14, No. 4, PP. 251-272, 1989.
- [93] M. D. Engelhardt and E. P. Popov, "On Design of Eccentrically Braced Frames," *Earthquake Spectra, EERI*, Vol. 5, No. 3, PP. 495-511, 1989.
- [94] C. W. Roeder, D. A. Foutch, and S. C. Goel, "Seismic Testing of Full-Scale Steel Building - Part II," *Journal of Structural Engineering, ASCE*, Vol. 113, No. 11, PP. 2130-2145, 1987.
- [95] D. A. Foutch, "Seismic Behavior of Eccentrically Braced Steel Building," *Journal of Structural Engineering*, Vol. 115, No. 8, PP. 1857-1876, 1989.
- [96] AISC, *Seismic Provisions for Structural Steel Buildings*. American Institute of Steel Construction, Chicago, IL, 1992.
- [97] T. Ramadan and A. Ghobarah, "Behaviour of bolted link-column joints in eccentrically braced frames," *Canadian Journal of Civil Engineering*, Vol. 22, No. 4, PP. 745-754, 1995.
- [98] A. Pirmoz, P. Ahadi, and V. Farajkhah, "Finite element analysis of extended stiffened end plate link-to-column connections," *Steel Construction*, Vol. 9, No. 1, PP. 46-57, 2016.
- [99] K. C. Tsai, M. D. Engelhardt, and M. Nakashima, "Cyclic performance of link-to-box column connections in steel eccentrically braced frames," *Proc. 1st International Conference on Structural Stability and Dynamics*, Taipei, Taiwan, 2000.

- [100] C. Mao, J. Ricles, L. W. Lu, and J. Fisher, "Effect of local details on ductility of welded moment connections," *Journal of Structural Engineering*, Vol. 127, No. 9, PP. 1036-1044, 2001.
- [101] FEMA, *Recommended seismic design criteria for new steel moment-frame buildings, FEMA-350*. Building Seismic Safety Council for the Federal Emergency Management Agency, Washington, DC, 2000.
- [102] J. Choi, B. Stojadinovic, and S. C. Goel, "Development of free flange moment connection," Department of Civil and Environmental Engineering, University of Michigan, Ann Arbor, MI, Report No. UMCEE 00-15, 2000.
- [103] K. Suita, T. Tamura, S. Morita, M. Nakashima, and M. D. Engelhardt, "Plastic rotation capacity of steel beam-to-column connections using a reduced beam section and no weld access hole design - Full scale tests for improved steel beam-to-column subassemblages - Part 1," *Journal of Structural and Construction Engineering*, Vol. 526, PP. 177-184, 1999. (*in Japanese*)
- [104] J. K. Hong, C. M. Uang, T. Okazaki, and M. D. Engelhardt, "Link-to-column connection with supplemental web doublers in eccentrically braced frames," *Journal of Structural Engineering*, Vol. 141, No. 8, 2015.
- [105] G. S. Prinz and P. W. Richards, "Eccentrically braced frame links with reduced web sections," *Journal of Constructional Steel Research*, Vol. 65, No. 10-11, PP. 1971-1978, 2009.
- [106] J. W. Berman, T. Okazaki, and H. O. Hauksdottir, "Reduced link sections for improving the ductility of eccentrically braced frame link-to-column connections," *Journal of Structural Engineering*, Vol. 136, No. 5, PP. 543-553, 2010.

- [107] P. Dusicka, A. M. Itani, and I. G. Buckle, "Finite element investigation of steel built-up shear links subjected to inelastic deformations," *Earthquake Engineering and Engineering Vibration*, Vol. 3, No. 2, PP. 195-203, 2004.
- [108] G. Yigitsoy, C. Topkaya, and T. Okazaki, "Stability of beams in steel eccentrically braced frames," *Journal of Constructional Steel Research*, Vol. 96, PP. 14-25, 2014.
- [109] M. S. Yang, "Seismic Behavior of an Eccentrically X-Braced Steel Structure," Earthquake Engineering Research Center, University of California, Berkeley, CA, Report No. UCB/EERC-82/14, 1982.
- [110] J. M. Ricles and E. P. Popov, "Dynamic analysis of seismically resistant eccentrically braced frames," Earthquake Engineering Research Center, University of California, Berkeley, CA, Report No. UCB/EERC-87/07, 1987.
- [111] J. M. Ricles and E. P. Popov, "Inelastic link element for EBF seismic analysis," *Journal of Structural Engineering*, Vol. 120, No. 2, PP. 441-463, 1994.
- [112] T. Ramadan and A. Ghobarah, "Analytical model for shear-link behavior," *Journal of Structural Engineering*, Vol. 121, No. 11, PP. 1574-1580, 1995.
- [113] K. Khandelwal, S. El-Tawil, and F. Sadek, "Progressive collapse analysis of seismically designed steel braced frames," *Journal of Constructional Steel Research*, Vol. 65, No. 3, PP. 699-708, 2009.
- [114] P. P. Rossi and A. Lombardo, "Influence of the link overstrength factor on the seismic behaviour of eccentrically braced frames," *Journal of Constructional Steel Research*, Vol. 63, No. 11, PP. 1529-1545, 2007.

- [115] M. Bosco, E. M. Marino, and P. P. Rossi, "Proposal of modifications to the design provisions of Eurocode 8 for buildings with split K eccentric braces," *Engineering Structures*, Vol. 61, PP. 209-223, 2014.
- [116] M. Bosco and P. P. Rossi, "Seismic behaviour of eccentrically braced frames," *Engineering Structures*, Vol. 31, No. 3, PP. 664-674, 2009.
- [117] M. Bosco and P. P. Rossi, "A design procedure for dual eccentrically braced systems: Analytical formulation," *Journal of Constructional Steel Research*, Vol. 80, PP. 440-452, 2013.
- [118] M. Bosco and P. P. Rossi, "A design procedure for dual eccentrically braced systems: Numerical investigation," *Journal of Constructional Steel Research*, Vol. 80, PP. 453-464, 2013.
- [119] M. Bosco, E. M. Marino, and P. P. Rossi, "Modelling of steel link beams of short, intermediate or long length," *Engineering Structures*, Vol. 84, PP. 406-418, 2015.
- [120] A. Zona and A. Dall'Asta, "Elastoplastic model for steel buckling-restrained braces," *Journal of Constructional Steel Research*, Vol. 68, No. 1, PP. 118-125, 2012.
- [121] M. Malakoutian, J. W. Berman, and P. Dusicka, "Seismic response evaluation of the linked column frame system," *Earthquake Engineering & Structural Dynamics*, Vol. 42, No. 6, PP. 795-814, 2013.
- [122] F. McKenna, G. Fenves, F. C. Filippou, and S. Mazzoni. *Open System for Earthquake Engineering Simulation (OpenSees)* [Computer Software]. University of California, Berkeley, CA.
- [123] N. S. Moghaddasi B. and Y. Zhang, "Seismic analysis of diagrid structural frames with shear-link fuse devices," *Earthquake Engineering and Engineering Vibration*, Vol. 12, No. 3, PP. 463-472, 2013.

- [124] M. T. Kazemi and S. Erfani, "Mixed shear-flexural (VM) hinge element and its applications," *Scientia Iranica*, Vol. 14, No. 3, PP. 193-204, 2007.
- [125] M. T. Kazemi and S. Erfani, "Special VM link element for modeling of shear–flexural interaction in frames," *The Structural Design of Tall and Special Buildings*, Vol. 18, No. 2, PP. 119-135, 2009.
- [126] M. T. Kazemi and M. Hoseinzadeh Asl, "Modeling of inelastic mixed hinge and its application in analysis of the frames with reduced beam section," *International Journal of Steel Structures*, Vol. 11, No. 1, PP. 51-63, 2011.
- [127] A. Saritas and F. C. Filippou, "Frame element for metallic shear-yielding members under cyclic loading," *Journal of Structural Engineering*, Vol. 135, No. 9, PP. 1115-1123, 2009.
- [128] A. Papachristidis, M. Fragiadakis, and M. Papadrakakis, "A 3D fibre beam-column element with shear modelling for the inelastic analysis of steel structures," *Computational Mechanics*, Vol. 45, No. 6, PP. 553-572, 2010.
- [129] H. V. Spurr, *Wind bracing: the importance of rigidity in high towers*. McGraw-Hill, New York, 1930.
- [130] C. W. Roeder and E. P. Popov, "Eccentrically Braced Steel Frames for Earthquakes," *Journal of the Structural Division, ASCE*, Vol. 104, No. 3, PP. 391-412, 1978.
- [131] A. S. Whittaker, C. M. Uang, and V. V. Bertero, "Seismic Testing of Eccentrically Braced Dual Steel Frames," *Earthquake Spectra, EERI*, Vol. 5, No. 2, PP. 429-449, 1989.
- [132] A. S. Whittaker, C.-M. Uang, and V. V. Bertero, "Experimental behavior of dual steel system," *Journal of Structural Engineering*, Vol. 115, No. 1, PP. 183-200, 1989.

- [133] T. Balendra, K. Y. Lam, C. Y. Liaw, and S. L. Lee, "Behavior of eccentrically braced frame by pseudo-dynamic test," *Journal of Structural Engineering*, Vol. 113, No. 4, PP. 673-688, 1987.
- [134] K. D. Hjelmstad and E. P. Popov, "Characteristics of Eccentrically Braced Frames," *Journal of Structural Engineering, ASCE*, Vol. 110, No. 2, PP. 340-353, 1984.
- [135] E. P. Popov, M. D. Engelhardt, and J. M. Ricles, "Eccentrically braced frames: US practice," *Engineering Journal*, Vol. 26, No. 2, 1989.
- [136] J. R. Libby, "Eccentrically Braced Frame Construction—A Case History," *Engineering Journal*, Vol. 18, No. 4, 1981.
- [137] A. T. Merovich, J. P. Nicoletti, and E. Hartle, "Eccentric Bracing in Tall Buildings," *Journal of the Structural Division, ASCE*, Vol. 108, No. 9, 1982.
- [138] X. Qi, K. L. Chang, and K. C. Tsai, "Seismic Design of Eccentrically Braced Space Frame," *Journal of Structural Engineering*, Vol. 123, No. 8, PP. 977-985, 1997.
- [139] E. Teal, *Practical Design of Eccentrically Braced Frames to Resist Seismic Forces*. Structural Steel Education Council, El Monte, CA, 1979.
- [140] AISC, *Seismic Design Manual 2nd ed., AISC 327-12A*. American Institute of Steel Construction, Chicago, IL, 2012.
- [141] R. Becker and M. Ishler, *Seismic design practice for eccentrically braced frames based on the 1994 UBC, Steel TIPS*. Structural Steel Education Council, Berkeley, CA, 1996.
- [142] Eurocode 8, *Design of Structures for Earthquake Resistance - Part 1: General Rules, Seismic Actions and Rules for Buildings, EN 1998-1:2004*.

European Standard, Comité Européen de Normalisation, Brussels, Belgium, 2004.

- [143] S. Koboevic and R. Redwood, "Design and seismic response of shear critical eccentrically braced frames," *Canadian Journal of Civil Engineering*, Vol. 24, No. 5, 1997.
- [144] M. D. Engelhardt, K. C. Tsai, and E. P. Popov, "Stability of beams in eccentrically braced frames," In: *Stability and ductility of steel structures*, Y. Fukumoto and G. C. Lee, Eds., 1992, PP. 99-112.
- [145] ASCE, *Minimum Design Loads for Buildings and Other Structures*, ASCE/SEI-7-10. Structural Engineering Institute of the American Society of Civil Engineers, Reston, VA, 2010.
- [146] E. P. Popov, J. M. Ricles, and K. Kasai, "Methodology for optimum EBF link design," *Proc. 10th world conference on earthquake engineering*, Madrid, Spain, 1992, PP. 3983-3988.
- [147] J. M. Ricles and S. Bolin, "Energy Dissipation in Eccentrically Braced Frames," *Proc. 4th U.S. National Conference on Earthquake Engineering*, Palm Springs, CA, 1990.
- [148] J. M. Ricles and S. Bolin, "Seismic performance of eccentrically braced frames," Structural Systems Research Project, Department of Applied Mechanics and Engineering Science, University of California at San Diego, San Diego, CA, Report No. 91-09, 1991.
- [149] A. Jain, S. Koboevic, and R. Redwood, "Design and Behaviour of Eccentrically Braced Frames with Flexural Links," In: *Advances in Steel Structures (ICASS '96)*, S. L. Teng and J. G. Chan, Eds. Pergamon, Oxford, 1996, PP. 233-237.

- [150] K. Kasai and X. Han, "New EBF Design Method and Application: Redesign and Analysis of US-Japan EBF," *Proc. 2nd International Conference on Behaviour of Steel Structures in Seismic Areas (STESSA 1997)*, Kyoto, Japan, 1997, PP. 242-249.
- [151] L. Tirca and V. Gioncu, "Ductility demands for MRFs and LL-EBFs for different earthquake types," *Proc. Stability And Ductility of Steel Structures (SDSS'99)*, 1999, PP. 429-438.
- [152] L. Mastrandrea, R. Montuori, and V. Piluso, "Shear-moment interaction in plastic design: eccentrically braced frames," *Proc. 4th International Conference on Behaviour of Steel Structures in Seismic Areas (STESSA 2003)*, Naples, Italy, 2003, PP. 175-180.
- [153] L. Mastrandrea and V. Piluso, "Plastic design of eccentrically braced frames, I: Moment–shear interaction," *Journal of Constructional Steel Research*, Vol. 65, No. 5, PP. 1007-1014, 2009.
- [154] L. Mastrandrea, R. Montuori, and V. Piluso, "Failure mode control of seismic resistant EB-frames," *Proc. 4th International Conference on Behaviour of Steel Structures in Seismic Areas (STESSA 2003)*, Naples, Italy, 2003, PP. 435-441.
- [155] L. Mastrandrea and V. Piluso, "Plastic design of eccentrically braced frames, II: Failure mode control," *Journal of Constructional Steel Research*, Vol. 65, No. 5, PP. 1015-1028, 2009.
- [156] L. Mastrandrea, E. Nistri, and V. Piluso, "Validation of a design procedure for failure mode control of EB-Frames: Push-over and IDA analyses," *The Open Construction and Building Technology Journal*, Vol. 7, PP. 193-207, 2013.

- [157] R. Montuori, E. Nistri, and V. Piluso, "Theory of Plastic Mechanism Control for MRF–EBF dual systems: Closed form solution," *Engineering Structures*, Vol. 118, PP. 287-306, 2016.
- [158] H. Köber and B. Ștefănescu, "A seismic design of eccentrically braced frames," *Proc. International Conference in Metal Structures (ICMS2006)*, Poiana Brasov, Romania, 2006, PP. 537-544.
- [159] Eurocode 8, *Design of Structures for Earthquake Resistance - EN 1998:2002*. European Standard, Comité Européen de Normalisation, Brussels, Belgium, 2002.
- [160] H. Köber and B. Ștefănescu, "'I' shaped braces in eccentrically braced frames," *Proc. International Conference in Metal Structures (ICMS2006)*, Poiana Brasov, Romania, 2006, PP. 529-535.
- [161] H. Köber and B. Ștefănescu, "Potentially plastic zone details in columns in eccentrically braced frames," *Proc. 6th International Conference on Behaviour of Steel Structures in Seismic Areas (STESSA 2009)*, Philadelphia, PA, 2009, PP. 629-634.
- [162] D. Özhendekci and N. Özhendekci, "Effects of the frame geometry on the weight and inelastic behaviour of eccentrically braced chevron steel frames," *Journal of Constructional Steel Research*, Vol. 64, No. 3, PP. 326-343, 2008.
- [163] S. H. Chao and S. C. Goel, "Performance-based seismic design of EBF using target drift and yield mechanism as performance criteria," Department of Civil and Environmental Engineering, The University of Michigan, Ann Arbor, MI, Report No. UMCEE 05-05, 2005.
- [164] S. H. Chao and S. C. Goel, "Performance-based seismic design of EBF using target drift and yield mechanism as performance criteria," *AISC Engineering Journal*, No. 3, PP. 173-200, 2006.

- [165] T. A. Sabol and D. E. Nishi, "Application of performance-based design to an eccentrically braced frame structure," *The Structural Design of Tall and Special Buildings*, Vol. 20, PP. 76-84, 2011.
- [166] T. J. Sullivan, "Direct displacement-based seismic design of steel eccentrically braced frame structures," *Bulletin of earthquake engineering*, Vol. 11, No. 6, PP. 2197-2231, 2013.
- [167] Eurocode 8, *Design of Structures for Earthquake Resistance - EN 1998:1993*. European Standard, Comité Européen de Normalisation, Brussels, Belgium, 1993.
- [168] M. Bosco, E. M. Marino, and P. P. Rossi, "Critical review of the EC8 design provisions for buildings with eccentric braces," *Earthquakes and Structures*, Vol. 8, No. 6, PP. 1407-1433, 2015.
- [169] P. W. Richards, "Seismic Column Demands in Ductile Braced Frames," *Journal of Structural Engineering*, Vol. 135, No. 1, PP. 33-41, 2009.
- [170] ICC, *International Building Code*. International Code Council, Inc., Whittier, CA, 2006.
- [171] A. Kuşyılmaz and C. Topkaya, "Design overstrength of steel eccentrically braced frames," *International Journal of Steel Structures*, Vol. 13, No. 3, PP. 529-545, 2013.
- [172] A. Kuşyılmaz and C. Topkaya, "Evaluation of Seismic Response Factors for Eccentrically Braced Frames Using FEMA P695 Methodology," *Earthquake Spectra*, Vol. 32, No. 1, PP. 303-321, 2016.
- [173] M. S. Speicher and J. L. Harris, "Collapse Prevention seismic performance assessment of new eccentrically braced frames using ASCE 41," *Engineering Structures*, Vol. 117, PP. 344-357, 2016.

- [174] ICC, *International Building Code*. International Code Council, Inc., Whittier, CA, 2012.
- [175] ASCE, *Seismic rehabilitation of existing buildings, ASCE/SEI 41-06*. Structural Engineering Institute of the American Society of Civil Engineers, Reston, VA, 2006.
- [176] P. W. Richards, "Estimating the Stiffness of Eccentrically Braced Frames," *Practice Periodical on Structural Design and Construction*, Vol. 15, No. 1, PP. 91-95, 2010.
- [177] A. Kuşyılmaz and C. Topkaya, "Fundamental periods of steel eccentrically braced frames," *The Structural Design of Tall and Special Buildings*, Vol. 24, No. 2, PP. 123-140, 2015.
- [178] O. S. Kwon and E. S. Kim, "Evaluation of building period formulas for seismic design," *Earthquake Engineering & Structural Dynamics*, Vol. 39, No. 14, PP. 1569-1583, 2010.
- [179] K. Young and H. Adeli, "Fundamental period of irregular eccentrically braced tall steel frame structures," *Journal of Constructional Steel Research*, Vol. 120, PP. 199-205, 2016.
- [180] R. Tremblay, "Fundamental Periods of Vibration of Braced Steel Frames for Seismic Design," *Earthquake Spectra*, Vol. 21, No. 3, PP. 833-860, 2005.
- [181] M. Badalassi, A. Braconi, S. Caprili, and W. Salvatore, "Influence of steel mechanical properties on EBF seismic behaviour," *Bulletin of earthquake engineering*, Vol. 11, No. 6, PP. 2249-2285, 2013.
- [182] Eurocode 8, *Design of Structures for Earthquake Resistance - EN 1998:2005*. European Standard, Comité Européen de Normalisation, Brussels, Belgium, 2005.

- [183] A. Perretti, "Comportamento sismico di telai in acciaio con controventi eccentrici," Ph.D. Thesis, Department of Civil, Building and Environmental Engineering, University of Naples, Naples, Italy, 1999. (*in Italian*)
- [184] K. C. Lin, C. J. Lin, J. Y. Chen, and H. Y. Chang, "Seismic reliability of steel framed buildings," *Structural Safety*, Vol. 32, No. 3, PP. 174-182, 2010.
- [185] FEMA, *Prestandard and commentary for the seismic rehabilitation of buildings, FEMA-356*. Building Seismic Safety Council for the Federal Emergency Management Agency, Washington, DC, 2000.
- [186] R. Eskandari and D. Vafaei, "Effects of near-fault records characteristics on seismic performance of eccentrically braced frames," *Structural Engineering and Mechanics*, Vol. 56, No. 5, PP. 855-870, 2015.
- [187] M. Naghipour, N. Javadi, and A. Naghipour, "Investigation of RBS Connection Ductility in Eccentrically Braced Frame," *Proc. Twelfth East Asia-Pacific Conference on Structural Engineering and Construction - EASEC12*, Hong Kong, 2011, PP. 743-752.
- [188] Y. Gong, Y. Xue, and L. Xu, "Optimal capacity design of eccentrically braced steel frameworks using nonlinear response history analysis," *Engineering Structures*, Vol. 48, PP. 28-36, 2013.
- [189] R. Karami Mohammadi and A. H. Sharghi, "On the optimum performance-based design of eccentrically braced frames," *Steel and Composite Structures*, Vol. 16, No. 4, PP. 357-374, 2014.
- [190] G. Danku, D. Dubina, and A. Ciutina, "Influence of steel-concrete interaction in dissipative zones of frames: II-Numerical study," *Steel and Composite Structures*, Vol. 15, No. 3, PP. 323-342, 2013.
- [191] G. S. Prinz and A. de Castro-e-Sousa, "Effect of Slab Stiffness on EBF Link Rotation Demands and Implications for Link Ultra Low-Cycle Fatigue

- Susceptibility," *Proc. ASCE Structures Congress 2014*, Boston, MA, 2014, PP. 2664-2674.
- [192] M. Seki, H. Katsumata, H. Uchida, and T. Takeda, "Study on earthquake response of two-storied steel frame with y-shaped braces," *Proc. 9th World Conference on Earthquake Engineering*, Tokyo-Kyoto, Japan, 1988, PP. 65-70.
- [193] M. G. Vetr, "Seismic behavior, analysis and design of eccentrically braced frames with vertical shear links," Ph.D. Thesis, Department of Civil and Environmental Engineering, Technische Universität Darmstadt, Darmstadt, Germany, 1998.
- [194] E. Fehling, W. Pauli, and J. G. Bouwkamp, "Use of vertical shear-links in eccentrically braced frames," *Proc. 10th World Conference on Earthquake Engineering*, Rotterdam, The Netherlands, 1992, PP. 4475-4480.
- [195] J. G. Bouwkamp and M. G. Vetr, "Design of eccentrically braced test frame with vertical shear link," *Proc. 2nd International Conference on Earthquake Resistant Construction and Design*, Berlin, Germany, 1994.
- [196] Y. Shinabe and Y. Takahashi, "The present state of eccentric brace design in Japan," *Proc. 4th Pacific Structural Steel Conference*, Singapore, 1995, PP. 813-820.
- [197] A. Saedi Daryan, H. Bahrampoor, M. Ziaei, A. Golafshar, and M. A. Assareh, "Seismic Behavior of Vertical Shear Links made of Easy-Going Steel," *American Journal of Engineering and Applied Sciences*, Vol. 1, No. 4, PP. 368-377, 2008.
- [198] M. A. Shayanfar, A. R. Rezaeian, and S. Taherkhani, "Assessment of the seismic behavior of eccentrically braced frame with double vertical link (DV-

- EBF)," *Proc. 14th World Conference on Earthquake Engineering*, Beijing, China, 2008.
- [199] M. A. Shayanfar and A. R. Rezaeian, "Assessment of seismic behavior of eccentrically braced frame with double vertical link (DV-EBF)," *Proc. 3rd International Conference on Advances in Experimental Structural Engineering*, San Francisco, CA, 2009.
- [200] M. Dicleli and A. Mehta, "Efficient energy dissipating steel-braced frame to resist seismic loads," *Journal of Structural Engineering*, Vol. 133, No. 7, PP. 969-981, 2007.
- [201] M. Dicleli and A. Mehta, "Seismic Performance of a Special Type of Single-Story Eccentrically Braced Steel Frame," *Advances in Structural Engineering*, Vol. 11, No. 1, PP. 35-51, 2008.
- [202] M. A. Shayanfar, M. A. Barkhordari, and A. R. Rezaeian, "Experimental study of cyclic behavior of composite vertical shear link in eccentrically braced frames," *Steel and Composite Structures*, Vol. 12, No. 1, PP. 13-29, 2012.
- [203] S. M. Zahrai and A. K. Vosooq, "Study of an innovative two-stage control system: Chevron knee bracing & shear panel in series connection," *Structural Engineering and Mechanics*, Vol. 47, No. 6, PP. 881-898, 2013.
- [204] M. A. Shayanfar, A. R. Rezaeian, and A. Zanganeh, "Seismic performance of eccentrically braced frame with vertical link using PBPD method," *The Structural Design of Tall and Special Buildings*, Vol. 23, No. 1, PP. 1-21, 2014.
- [205] R. Montuori, E. Nastri, and V. Piluso, "Rigid-plastic analysis and moment–shear interaction for hierarchy criteria of inverted Y EB-Frames," *Journal of Constructional Steel Research*, Vol. 95, PP. 71-80, 2014.

- [206] R. Montuori, E. Nastri, and V. Piluso, "Theory of plastic mechanism control for eccentrically braced frames with inverted Y-scheme," *Journal of Constructional Steel Research*, Vol. 92, PP. 122-135, 2014.
- [207] S. R. Massah and H. Dorvar, "Design and analysis of eccentrically braced steel frames with vertical links using shape memory alloys," *Smart Materials and Structures*, Vol. 23, No. 11, 2014.
- [208] F. Wang, M. Su, M. Hong, Y. Guo, and S. Li, "Cyclic behaviour of Y-shaped eccentrically braced frames fabricated with high-strength steel composite," *Journal of Constructional Steel Research*, Vol. 120, PP. 176-187, 2016.
- [209] K. Martini, N. Amin, P. L. Lee, and D. Bonowitz, "The Potential Role of Non-Linear Analysis in the Seismic Design of Building Structures," *Proc. 4th National Conference on Earthquake Engineering*, Palm Springs, CA, 1990, PP. 67-76.
- [210] A. Ghersi, S. Pantano, and P. P. Rossi, "On the design of tied braced frames," *Proc. 4th International Conference on Behaviour of Steel Structures in Seismic Areas (STESSA 2003)*, Naples, Italy, 2003.
- [211] P. P. Rossi, "A design procedure for tied braced frames," *Earthquake Engineering & Structural Dynamics*, Vol. 36, No. 14, PP. 2227-2248, 2007.
- [212] S. M. Zahrai, M. Pirdavari, and H. M. Farahani, "Evaluation of hysteretic behavior of eccentrically braced frames with zipper-strut upgrade," *Journal of Constructional Steel Research*, Vol. 83, PP. 10-20, 2013.
- [213] A. Stratan, D. Dubina, and F. Dinu, "Control of global performance of seismic resistant EBF with removable link," *Proc. 4th International Conference on Behaviour of Steel Structures in Seismic Areas (STESSA 2003)*, Naples, Italy, 2003, PP. 175-180.

- [214] D. Dubina, A. Stratan, and F. Dinu, "Dual high-strength steel eccentrically braced frames with removable links," *Earthquake Engineering & Structural Dynamics*, Vol. 37, No. 15, PP. 1703-1720, 2008.
- [215] D. Dubina, A. Stratan, and F. Dinu, "Re-centring capacity of dual-steel frames," *Steel Construction*, Vol. 4, No. 2, PP. 73-84, 2011.
- [216] G. A. Sabau, M. Poljansek, F. Taucer, P. Pegon, F. J. Molina, D. Tirelli, B. Viaccoz, A. Stratan, A. Ioan Chesoi, and D. Dubina, "Seismic Engineering Research Infrastructures For European Synergies: Full-Scale Experimental Validation of a Dual Eccentrically Braced Frame with Removable Links (DUAREM)," Institute for the Protection and Security of the Citizen, Publications Office of the European Union, Luxembourg, Report EUR 27030, 2014.
- [217] A. Ioan, A. Stratan, D. Dubina, M. Poljansek, F. J. Molina, F. Taucer, P. Pegon, and G. Sabau, "Experimental validation of re-centring capability of eccentrically braced frames with removable links," *Engineering Structures*, Vol. 113, PP. 335-346, 2016.
- [218] N. Mago, "Finite Element Analysis of Eccentrically Braced Frames with Replaceable Link," Heavy Engineering Research Association, Manukau, New Zealand, HERA Report R4-145, 2013.
- [219] N. Balut and V. Gioncu, "Suggestion for an improved 'dog-bone' solution," *Proc. 4th International Conference on Behaviour of Steel Structures in Seismic Areas (STESSA 2003)*, Naples, Italy, 2003.
- [220] A. Ashikov, G. C. Clifton, and B. Belev, "Experimental study on eccentrically braced frames with a new type of bolted replaceable active link," *Proc. 6th National Conference on Earthquake Engineering and the 2nd National Conference on Earthquake Engineering and Seismology - 6CNIS & 2CNISS*, Bucharest, Romania, 2017.

- [221] A. Ashikov, G. C. Clifton, and B. Belev, "Finite element analysis of eccentrically braced frames with a new type of bolted replaceable active link," *Proc. New Zealand Society for Earthquake Engineering (NZSEE) Annual Technical Conference*, Christchurch, New Zealand, 2016.
- [222] A. J. Fussell, K. A. Cowie, G. C. Clifton, and N. Mago, "Development and research of eccentrically braced frames with replaceable active links," *Proc. 2014 NZSEE Conference*, Auckland, New Zealand, 2014.
- [223] J. J. Ramsay, A. Fussell, and R. G. Wilkinson, "Design of Replaceable-Link Eccentric Braced Frames in Post-Earthquake Christchurch," *Proc. Steel Innovations Conference 2013*, Christchurch, New Zealand, 2013.
- [224] G. Gardiner, C. Clifton, and G. A. MacRae, "Performance, damage assessment and repair of a multistorey eccentrically braced frame building following the Christchurch earthquake series," *Proc. Steel Innovations Conference 2013*, Christchurch, New Zealand, 2013.
- [225] HERA, *R4-76 Seismic Design Procedures for Steel Structures and P4001 Seismic design of eccentrically braced frames*. Heavy Engineering Research Association, Manukau, New Zealand, 2013.
- [226] A. Bouadi and M. D. Engelhardt, "On Design of EBFs for Seismic Retrofit of Reinforced Concrete Frames," *Proc. 11th World Conference on Earthquake Engineering*, Acapulco, Mexico, 1996.
- [227] A. Ghobarah and H. Abou Elfath, "Rehabilitation of a reinforced concrete frame using eccentric steel bracing," *Engineering Structures*, Vol. 23, No. 7, PP. 745-755, 2001.
- [228] J. G. Bouwkamp, S. Gómez, A. V. Pinto, J. Molina, and H. Varum, "Cyclic tests on RC frame retrofitted with K-bracing and shear-link dissipater," *The*

European Laboratory for Structural Assessment (ELSA), Joint Research Centre (JRC), Ispra, Italy, EUR Report No. 20136 EN, 2001.

- [229] R. Perera, S. Gómez, and E. Alarcón, "Experimental and analytical study of masonry infill reinforced concrete frames retrofitted with steel braces," *Journal of Structural Engineering*, Vol. 130, No. 12, PP. 2032-2039, 2004.
- [230] M. D'Aniello, "Seismic upgrading of RC structure by steel Eccentric Bracing: an experimental and numerical study," *Pollack Periodica*, Vol. 1, No. 2, PP. 17-32, 2006.
- [231] F. M. Mazzolani, G. D. Corte, and M. D'Aniello, "Experimental analysis of steel dissipative bracing systems for seismic upgrading," *Journal of Civil Engineering and Management*, Vol. 15, No. 1, PP. 7-19, 2009.
- [232] F. Pina, G. W. White, G. Taylor, and C. Ventura, "Conventional steel constructions for the performance-based earthquake retrofit of low-rise school buildings," In: *Behaviour of Steel Structures in Seismic Areas*. CRC Press, 2009.
- [233] C. Durucan and M. Dicleli, "Analytical study on seismic retrofitting of reinforced concrete buildings using steel braces with shear link," *Engineering Structures*, Vol. 32, No. 10, PP. 2995-3010, 2010.
- [234] A. E. Özel and E. M. Güneyisi, "Effects of eccentric steel bracing systems on seismic fragility curves of mid-rise R/C buildings: A case study," *Structural Safety*, Vol. 33, No. 1, PP. 82-95, 2011.
- [235] H. Varum, F. Teixeira Dias, P. Marques, A. V. Pinto, and A. Q. Bhatti, "Performance evaluation of retrofitting strategies for non-seismically designed RC buildings using steel braces," *Bulletin of earthquake engineering*, Vol. 11, No. 4, PP. 1129-1156, 2013.

- [236] D. Wang and A. Yu, "Shear Failure Behavior of Y-Eccentrically Brace in RC Frame Structures under Earthquake Action," *Adv. Mat. Res.*, Vol. 639-640, PP. 866-869, 2013.
- [237] S. El-Tawil, K. A. Harries, P. J. Fortney, B. M. Shahrooz, and Y. Kurama, "Seismic design of hybrid coupled wall systems: state of the art," *Journal of Structural Engineering*, Vol. 136, No. 7, PP. 755-769, 2010.
- [238] ASCE, *Minimum Design Loads for Buildings and Other Structures*, ASCE/SEI-7-05. Structural Engineering Institute of the American Society of Civil Engineers, Reston, VA, 2005.
- [239] C. K. Gulec, B. Gibbons, A. Chen, and A. S. Whittaker, "Damage states and fragility functions for link beams in eccentrically braced frames," *Journal of Constructional Steel Research*, Vol. 67, No. 9, PP. 1299-1309, 2011.
- [240] M. Sarraf and M. Bruneau, "Ductile seismic retrofit of steel deck-truss bridges. I: Strategy and modeling," *Journal of Structural Engineering*, Vol. 124, No. 11, PP. 1253-1262, 1998.
- [241] M. Sarraf and M. Bruneau, "Ductile seismic retrofit of steel deck-truss bridges. II: Design applications," *Journal of Structural Engineering*, Vol. 124, No. 11, PP. 1263-1271, 1998.
- [242] S. M. Zahrai and M. Bruneau, "Cyclic testing of ductile end diaphragms for slab-on-girder steel bridges," *Journal of Structural Engineering, ASCE*, Vol. 125, No. 9, PP. 987-996, 1999.
- [243] S. M. Zahrai and M. Bruneau, "Ductile end-diaphragms for seismic retrofit of slab-on-girder steel bridges," *Journal of Structural Engineering*, Vol. 125, No. 1, PP. 71-80, 1999.

- [244] M. Bruneau, M. Sarraf, S. M. Zahrai, and F. Alfawakhiri, "Displacement-based energy dissipation systems for steel bridges diaphragms," *Journal of Constructional Steel Research*, Vol. 58, No. 5–8, PP. 801-817, 2002.
- [245] L. DiSarno, A. S. Elnashai, and D. A. Nethercot, "Seismic response of stainless steel braced frames," *Journal of Constructional Steel Research*, Vol. 64, No. 7–8, PP. 914-925, 2008.
- [246] G. S. Prinz, "Using Buckling-Restrained Braces in Eccentric Configurations," Ph.D. Thesis, Department of Civil and Environmental Engineering, Brigham Young University, Provo, UT, 2010.
- [247] G. S. Prinz and P. W. Richards, "Seismic performance of buckling-restrained braced frames with eccentric configurations," *Journal of Structural Engineering*, Vol. 138, No. 3, PP. 345-353, 2012.
- [248] AISC, *Seismic Provisions for Structural Steel Buildings, ANSI/AISC 341-16*. American Institute of Steel Construction, Chicago, IL, 2016.
- [249] ASCE, *Seismic Evaluation and Retrofit of Existing Buildings, ASCE/SEI 41-13*. Structural Engineering Institute of the American Society of Civil Engineers, Reston, VA, 2013.
- [250] FEMA, *Quantification of Building Seismic Performance Factors, FEMA-P695*. Building Seismic Safety Council for the Federal Emergency Management Agency, Washington, DC, 2009.
- [251] M. B. Bozkurt, "Developing replaceable members for steel lateral load resisting systems," Ph.D. Thesis, Department of Civil Engineering, Middle East Technical University, Ankara, Turkey, 2017.
- [252] Eurocode 3, *Design of steel structures – Part 1-1: general rules and rules for buildings, EN 1993-1:2003*. European Standard, Comité Européen de Normalisation, Brussels, Belgium, 2003.

- [253] EN 10002, *Tensile testing of metallic materials. Method of test at ambient temperature - EN 10002-1:2001*. European Standard, Comité Européen de Normalisation, Brussels, 2001.
- [254] AISC, *Specification for Structural Steel Buildings, ANSI/AISC 360-16*. American Institute of Steel Construction, Chicago, IL, 2016.
- [255] ISO, *Mechanical properties of fasteners made of carbon steel and alloy steel -- Part 1: bolts, screws and studs, ISO 898-1:1999*. International Organization for Standardization, Geneva, Switzerland, 1999.
- [256] ISO, *Preparation of steel substrates before application of paints and related products -- Visual assessment of surface cleanliness -- Part 1: Rust grades and preparation grades of uncoated steel substrates and of steel substrates after overall removal of previous coatings, ISO 8501-1:2007*. International Organization for Standardization, Geneva, Switzerland, 2007.
- [257] M. Veljkovic, C. Heistermann, W. Husson, M. Limam, M. Feldmann, J. Naumes, D. Pak, T. Faber, M. Klose, K.-U. Fruhner, L. Krutshinna, C. Baniotopoulos, I. Lavasas, A. Pontes, E. Ribeiro, M. Hadden, R. Sousa, L. da Silva, C. Rebelo, R. Simoes, J. Henriques, R. Matos, J. Nuutinen, and H. Kinnunen, "High-strength tower in steel for wind turbines (HISTWIN)," European Commission, Directorate-General for Research and Innovation, Research Fund for Coal and Steel Unit, Luxembourg, Final Report, Contract No. RFSR-CT-2006-00031, 2012.
- [258] X. Ji, Y. Wang, Q. Ma, and T. Okazaki, "Cyclic Behavior of Very Short Steel Shear Links," *Journal of Structural Engineering, ASCE*, Vol. 142, No. 2, P. 04015114, 2016.
- [259] H. Krawinkler, M. Zohrei, B. Lashkari-Irvani, N. G. Cofie, and H. Hadidi-Tamjed, "Recommendations for Experimental Studies on the Seismic Behavior of Steel Components and Materials," John A. Blume Earthquake

Engineering Center, Stanford University, Stanford, CA, Report No. 61, NSF Grant CEE-7902616, 1983.

- [260] E. Karamanci and D. G. Lignos, "Computational Approach for Collapse Assessment of Concentrically Braced Frames in Seismic Regions," *Journal of Structural Engineering*, Vol. 140, No. 8, P. A4014019, 2014.
- [261] P. Uriz and S. Mahin, "Towards Earthquake Resistant Design of Concentrically Braced Steel Structures," Pacific Earthquake Engineering Research Center, University of California, Berkeley, CA, Report No. PEER-2008/08, 2008.
- [262] H. Krawinkler, "Cyclic Loading Histories for Seismic Experimentation on Structural Components," *Earthquake Spectra*, Vol. 12, No. 1, PP. 1-12, 1996.
- [263] P. Dusicka, A. M. Itani, and I. G. Buckle, "Cyclic Response and Low Cycle Fatigue Characteristics of Plate Steels," Multidisciplinary Center for Earthquake Engineering Research, State University of New York at Buffalo, Buffalo, NY, Report No. MCEER-06-0013, 2006.
- [264] A. Salem Milani and M. Dicleli, "Low-cycle fatigue performance of solid cylindrical steel components subjected to torsion at very large strains," *Journal of Constructional Steel Research*, Vol. 129, PP. 12-27, 2017.
- [265] X. G. Liu, J. S. Fan, Y. F. Liu, Q. R. Yue, and J. G. Nie, "Experimental research of replaceable Q345GJ steel shear links considering cyclic buckling and plastic overstrength," *Journal of Constructional Steel Research*, Vol. 134, PP. 160-179, 2017.
- [266] ASTM, *Standard Practices for Cycle Counting in Fatigue Analysis, E1049 – 85*. American Society for Testing and Materials, West Conshohocken, PA, 2011.

- [267] K. S. Marshall, "Earthquake Induced Eccentrically Braced Frame Link Fracture in the Christchurch Hospital Parking Garage," M.Sc. Thesis, Department of Civil and Environmental Engineering, University of California Davis, Davis, CA, 2013.
- [268] M. Bruneau and A. Reinhorn, "Overview of the Resilience Concept," *Proc. 8th U.S. National Conference on Earthquake Engineering*, San Francisco, CA, 2006.
- [269] AISC, *Code of Standard Practice for Steel Buildings and Bridges, ANSI/AISC 303-16*. American Institute of Steel Construction, Chicago, IL, 2016.
- [270] EN 1090-2, *Execution of steel structures and aluminium structures — Part 2: Technical requirements for steel structures - EN 1090-2:2008*. European Standard, Comité Européen de Normalisation, Brussels, 2008.
- [271] M. B. Bozkurt and C. Topkaya, "Experimental Validation of Detachable Links for Eccentrically Braced Frames," *Proc. 9th European Conference on Steel and Composite Structures (Eurosteel 2020)*, Sheffield, UK, 2020.
- [272] J. McCormick, H. Aburano, M. Ikenaga, and M. Nakashima, "Permissible residual deformation levels for building structures considering both safety and human elements," *Proc. 14th World Conference on Earthquake Engineering (14 WCEE)*, Beijing, China, 2008.
- [273] *ABAQUS 6.12-1 Documentation*. Dassault Systèmes, Simulia, Providence, RI, 2012.
- [274] E. J. Kaufmann, B. R. Metrovich, and A. W. Pense, "Characterization of cyclic inelastic strain behavior on properties of A572 Gr. 50 and A913 Gr. 50 rolled sections," Lehigh University, Bethlehem, PA, ATLSS Report No. 01-13, 2001.

- [275] A. Korolija, "FE-modeling of bolted joints in structures," M.Sc. Thesis, Department of Mechanical Engineering, Linköping University, Linköping, Sweden, 2012.
- [276] N. Tanlak, F. O. Sonmez, and E. Talay, "Detailed and simplified models of bolted joints under impact loading," *The Journal of Strain Analysis for Engineering Design*, Vol. 46, No. 3, PP. 213-225, 2011.
- [277] M. Baiguera, G. Vasdravellis, and T. L. Karavasilis, "Ultralow Cycle Fatigue Tests and Fracture Prediction Models for Duplex Stainless-Steel Devices of High Seismic Performance Braced Frames," *Journal of Structural Engineering, ASCE*, Vol. 145, No. 1, PP. 04018230-1 - 04018230-18, 2019.
- [278] S. El-Tawil, E. Vidarsson, T. Mikesell, and S. K. Kunnath, "Inelastic behavior and design of steel panel zones," *Journal of Structural Engineering, ASCE*, Vol. 125, No. 2, PP. 183-193, 1999.
- [279] A. M. Kanvinde, "Micromechanical simulation of earthquake induced fracture in steel structures," Ph.D. Thesis, Department of Civil and Environmental Engineering, Stanford University, Stanford, CA, 2004.
- [280] B. V. Fell, A. T. Myers, G. G. Deierlein, and A. M. Kanvinde, "Testing and simulation of ultra-low cycle fatigue and fracture in steel braces," *Proc. 8th US National Conference on Earthquake Engineering*, San Francisco, CA, 2006.
- [281] P. W. Richards and G. S. Prinz, "Nonlinear time-history analysis of refined mesh steel structures," *Proc. 9th Canadian Conference on Earthquake Engineering*, Ottawa, Canada, 2007.
- [282] M. B. Bozkurt, S. Kazemzadeh Azad, and C. Topkaya, "Low-Cycle Fatigue Testing of Shear Links and Calibration of a Damage Law," *Journal of*

Structural Engineering, Vol. 144, No. 10, P. 04018189, 2018. DOI: 10.1061/(ASCE)ST.1943-541X.0002192

- [283] A. K. Jain, R. D. Hanson, and S. C. Goel, "Hysteretic cycles of axially loaded steel members," *Journal of the Structural Division*, Vol. 106, No. 8, PP. 1777-1795, 1980.
- [284] R. G. Black, B. A. Wenger, and E. P. Popov, "Inelastic Buckling of Steel Struts Under Cyclic Load Reversals," Earthquake Engineering Research Center, University of California, Berkeley, CA, Report No. UCB/EERC-80/40, 1980.
- [285] E. P. Popov and R. G. Black, "Steel struts under severe cyclic loadings," *Journal of the Structural Division*, Vol. 107, No. 9, PP. 1857-1881, 1981.
- [286] A. Astaneh-Asl and S. C. Goel, "Cyclic in-plane buckling of double angle bracing," *Journal of Structural Engineering*, Vol. 110, No. 9, PP. 2036-2055, 1984.
- [287] A. Astaneh-Asl, S. C. Goel, and R. D. Hanson, "Cyclic out-of-plane buckling of double-angle bracing," *Journal of Structural Engineering*, Vol. 111, No. 5, PP. 1135-1153, 1985.
- [288] A. M. Remennikov and W. R. Walpole, "A note on compression strength reduction factor for a buckled strut in seismic-resisting braced system," *Engineering Structures*, Vol. 20, No. 8, PP. 779-782, 1998.
- [289] R. Tremblay, "Inelastic seismic response of steel bracing members," *Journal of Constructional Steel Research*, Vol. 58, No. 5-8, PP. 665-701, 2002.
- [290] B. Shaback and T. Brown, "Behaviour of square hollow structural steel braces with end connections under reversed cyclic axial loading," *Canadian Journal of Civil Engineering*, Vol. 30, No. 4, PP. 745-753, 2003.

- [291] K. Lee and M. Bruneau, "Energy Dissipation of Compression Members in Concentrically Braced Frames: Review of Experimental Data," *Journal of Structural Engineering*, Vol. 131, No. 4, PP. 552-559, 2005.
- [292] S. Willibald, J. A. Packer, and G. Martinez-Saucedo, "Behaviour of gusset plate connections to ends of round and elliptical hollow structural section members," *Canadian Journal of Civil Engineering*, Vol. 33, No. 4, PP. 373-383, 2006.
- [293] S. W. Han, W. T. Kim, and D. A. Foutch, "Seismic Behavior of HSS Bracing Members according to Width–Thickness Ratio under Symmetric Cyclic Loading," *Journal of Structural Engineering*, Vol. 133, No. 2, PP. 264-273, 2007.
- [294] R. Tremblay, "Influence of Brace Slenderness on the Fracture Life of Rectangular Tubular Steel Bracing Members Subjected to Seismic Inelastic Loading," *Proc. ASCE 2008 Structures Congress*, Vancouver, Canada, 2008.
- [295] D. E. Lehman, C. W. Roeder, D. Herman, S. Johnson, and B. Kotulka, "Improved Seismic Performance of Gusset Plate Connections," *Journal of Structural Engineering*, Vol. 134, No. 6, PP. 890-901, 2008.
- [296] B. V. Fell, A. M. Kanvinde, G. G. Deierlein, and A. T. Myers, "Experimental Investigation of Inelastic Cyclic Buckling and Fracture of Steel Braces," *Journal of Structural Engineering*, Vol. 135, No. 1, PP. 19-32, 2009.
- [297] K. H. Nip, L. Gardner, and A. Y. Elghazouli, "Cyclic testing and numerical modelling of carbon steel and stainless steel tubular bracing members," *Engineering Structures*, Vol. 32, No. 2, PP. 424-441, 2010.
- [298] S. M. Shaw, A. M. Kanvinde, and B. V. Fell, "Earthquake-induced net section fracture in brace connections — experiments and simulations,"

- Journal of Constructional Steel Research*, Vol. 66, No. 12, PP. 1492-1501, 2010.
- [299] Y. Ghanaat, "Study of X-Braced Steel Frame Structures Under Earthquake Simulation," Earthquake Engineering Research Center, University of California, Berkeley, CA, Report No. UCB/EERC-80/08, 1980.
- [300] S. C. Goel and A. A. El-Tayem, "Cyclic Load Behavior of Angle X-Bracing," *Journal of Structural Engineering*, Vol. 112, No. 11, PP. 2528-2539, 1986.
- [301] G. Ballio and F. Perotti, "Cyclic behaviour of axially loaded members: Numerical simulation and experimental verification," *Journal of Constructional Steel Research*, Vol. 7, No. 1, PP. 3-41, 1987.
- [302] T. Fukuta, I. Nishiyama, H. Yamanouchi, and B. Kato, "Seismic Performance of Steel Frames with Inverted V Braces," *Journal of Structural Engineering*, Vol. 115, No. 8, PP. 2016-2028, 1989.
- [303] R. Tremblay, M. H. Archambault, and A. Filiatrault, "Seismic response of concentrically braced steel frames made with rectangular hollow bracing members," *Journal of Structural Engineering*, Vol. 129, No. 12, PP. 1626-1636, 2003.
- [304] B. M. Broderick, A. Y. Elghazouli, and J. Goggins, "Earthquake testing and response analysis of concentrically-braced sub-frames," *Journal of Constructional Steel Research*, Vol. 64, No. 9, PP. 997-1007, 2008.
- [305] C. W. Roeder, D. E. Lehman, K. Clark, J. Powell, J. H. Yoo, K. C. Tsai, C. H. Lin, and C. Y. Wei, "Influence of gusset plate connections and braces on the seismic performance of X-braced frames," *Earthquake Engineering & Structural Dynamics*, Vol. 40, No. 4, PP. 355-374, 2011.

- [306] T. Okazaki, D. G. Lignos, T. Hikino, and K. Kajiwara, "Dynamic response of a chevron concentrically braced frame," *Journal of Structural Engineering*, Vol. 139, No. 4, PP. 515-525, 2013.
- [307] E. J. Lumpkin, P. C. Hsiao, C. W. Roeder, D. E. Lehman, C. Y. Tsai, A. C. Wu, C. Y. Wei, and K. C. Tsai, "Investigation of the seismic response of three-story special concentrically braced frames," *Journal of Constructional Steel Research*, Vol. 77, PP. 131-144, 2012.
- [308] J. W. Lai and S. Mahin, "Experimental and Analytical Studies on the Seismic Behavior of Conventional and Hybrid Braced Frames," Earthquake Engineering Research Center, University of California, Berkeley, CA, Report No. PEER-2013/20, 2013.
- [309] A. D. Sen, C. W. Roeder, J. W. Berman, D. E. Lehman, C. H. Li, A. C. Wu, and K. C. Tsai, "Experimental Investigation of Chevron Concentrically Braced Frames with Yielding Beams," *Journal of Structural Engineering*, Vol. 142, No. 12, 2016.
- [310] R. Sabelli, "Research on Improving the Design and Analysis of Earthquake Resistant Steel Braced Frames," Federal Emergency Management Agency and Earthquake Engineering Research Institute, Report No. FEMA-EERI PF2000-9, 2001.
- [311] J. Kim and H. Choi, "Response modification factors of chevron-braced frames," *Engineering Structures*, Vol. 27, No. 2, PP. 285-300, 2005.
- [312] Y. Huang and S. Mahin, "Simulating the inelastic seismic behavior of steel braced frames including the effects of low cycle fatigue," Pacific Earthquake Engineering Research Center, University of California, Berkeley, CA, Report No. PEER-2010/104, 2010.

- [313] P. C. Hsiao, D. E. Lehman, and C. W. Roeder, "Evaluation of the response modification coefficient and collapse potential of special concentrically braced frames," *Earthquake Engineering & Structural Dynamics*, Vol. 42, No. 10, PP. 1547-1564, 2013.
- [314] J. Shen, R. Wen, B. Akbas, B. Doran, and E. Uckan, "Seismic demand on brace-intersected beams in two-story X-braced frames," *Engineering Structures*, Vol. 76, PP. 295-312, 2014.
- [315] J. Shen, R. Wen, and B. Akbas, "Mechanisms in two-story X-braced frames," *Journal of Constructional Steel Research*, Vol. 106, PP. 258-277, 2015.
- [316] A. Astaneh-Asl, *Seismic behavior and design of gusset plates, Steel TIPS*. Structural Steel Education Council, Berkeley, CA, 1998.
- [317] S. Majid Zamani, A. Vafaei, C. Desai, and M. Rasouli, "Experimental investigation of behavior of steel frames with y-shaped concentric bracing," *Journal of Constructional Steel Research*, Vol. 70, PP. 12-27, 2012.
- [318] E. Günaydın and C. Topkaya, "Fundamental periods of steel concentrically braced frames designed to Eurocode 8," *Earthquake Engineering & Structural Dynamics*, Vol. 42, No. 10, PP. 1415-1433, 2013.
- [319] F. Mazzolani and V. Piluso, *Theory and design of seismic resistant steel frames*. CRC Press, 1996.
- [320] C. Topkaya and S. Şahin, "A comparative study of AISC-360 and EC3 strength limit states," *International Journal of Steel Structures*, Vol. 11, No. 1, PP. 13-27, 2011.
- [321] M. N. Fardis, E. Carvalho, A. Alnashai, E. Faccioli, P. Pinto, and A. Plumier, *Designers' Guide to EN 1998-1 and 1998-5. Eurocode 8: Design Provisions for Earthquake Resistant Structures*. Thomas Telford, London, 2005.

- [322] M. T. Giugliano, A. Longo, R. Montuori, and V. Piluso, "Seismic reliability of traditional and innovative concentrically braced frames," *Earthquake Engineering & Structural Dynamics*, Vol. 40, No. 13, PP. 1455-1474, 2011.
- [323] A. Y. Elghazouli, "Seismic design of steel structures to Eurocode 8," *The Structural Engineer*, Vol. 85, No. 12, PP. 26-31, 2007.
- [324] FEMA, *State of the Art Report on Systems Performance of Steel Moment Frames Subject to Earthquake Ground Shaking, FEMA-355C*. SAC Joint Venture, Building Seismic Safety Council for the Federal Emergency Management Agency, Washington, DC, 2000.
- [325] A. Y. Elghazouli, *Seismic design of buildings to Eurocode 8*. CRC Press, 2009.
- [326] M. D'Aniello, G. La Manna Ambrosino, F. Portioli, and R. Landolfo, "Modelling aspects of the seismic response of steel concentric braced frames," *Steel and Composite Structures*, Vol. 15, No. 5, PP. 539-566, 2013.
- [327] M. D'Aniello, G. La Manna Ambrosino, F. Portioli, and R. Landolfo, "The influence of out-of-straightness imperfection in physical theory models of bracing members on seismic performance assessment of concentric braced structures," *The Structural Design of Tall and Special Buildings*, Vol. 24, No. 3, PP. 176-197, 2015.
- [328] G. G. Deierlein, A. M. Reinhord, and M. R. Willford, "Nonlinear structural analysis for seismic design: A guide for practicing engineers," National Institute of Standards and Technology, Gaithersburg, MD, NIST GCR 10-917-5, 2010.
- [329] B. V. Fell, "Large-Scale Testing and Simulation of Earthquake-Induced Ultra Low Cycle Fatigue in Bracing Members Subjected to Cyclic Inelastic

Buckling," Ph.D. Thesis, Department of Civil and Environmental Engineering, University of California, Davis, CA, 2008.

- [330] J. F. Hall, "Problems encountered from the use (or misuse) of Rayleigh damping," *Earthquake Engineering & Structural Dynamics*, Vol. 35, No. 5, PP. 525-545, 2006.
- [331] F. A. Charney, "Unintended Consequences of Modeling Damping in Structures," *Journal of Structural Engineering*, Vol. 134, No. 4, PP. 581-592, 2008.
- [332] A. Lepage, J. M. Shoemaker, and A. M. Memari, "Accelerations of Nonstructural Components during Nonlinear Seismic Response of Multistory Structures," *Journal of Architectural Engineering*, Vol. 18, No. 4, PP. 285-297, 2012.
- [333] S. I. Pardalopoulos and S. J. Pantazopoulou, "Seismic response of nonstructural components attached on multistorey buildings," *Earthquake Engineering & Structural Dynamics*, Vol. 44, No. 1, PP. 139-158, 2015.
- [334] S. Kazemzadeh Azad, O. Hasançebi, and S. Kazemzadeh Azad, "Upper bound strategy for metaheuristic based design optimization of steel frames," *Advances in Engineering Software*, Vol. 57, PP. 19-32, 2013.
- [335] F. Mazzolani, R. Landolfo, and G. Della Corte, "Eurocode 8 Provisions for steel and steel-concrete composite structures: Comments, critiques, improvement proposals and research needs," *Proc. Eurocode 8 Perspectives from the Italian Standpoint Workshop*, Napoli, Italy, 2009.
- [336] M. D'Aniello, S. Costanzo, and R. Landolfo, "The influence of beam stiffness on seismic response of chevron concentric bracings," *Journal of Constructional Steel Research*, Vol. 112, PP. 305-324, 2015.

- [337] A. TENCHINI, M. D'ANIELLO, C. REBELO, R. LANDOLFO, L. S. DA SILVA, and L. LIMA, "High strength steel in chevron concentrically braced frames designed according to Eurocode 8," *Engineering Structures*, Vol. 124, PP. 167-185, 2016.
- [338] NA to BS EN 1998-1: 2004, *UK National Annex to Eurocode 8: Design of structures for earthquake resistance - Part 1: General rules, seismic actions and rules for buildings*. British Standards Institution (BSI), London, 2008
- [339] S. P. TIMOSHENKO and J. M. GERE, *Theory of elastic stability*, 2nd ed. McGraw-Hill, New York, 1961.
- [340] Z. P. BAŽANT and L. CEDOLIN, *Stability of structures: elastic, inelastic, fracture, and damage theories*. Oxford University Press, New York, 1991.
- [341] T. V. GALAMBOS, *Guide to stability design criteria for metal structures*, 5th ed. John Wiley, New York, 1998.
- [342] V. V. BOLOTIN, *The dynamic stability of elastic systems*. Holden-Day, San Francisco, 1964.
- [343] R. A. IBRAHIM, *Parametric random vibration*. Research Studies Press, Letchworth, England, 1985.
- [344] G. J. SIMITSIS, *Dynamic stability of suddenly loaded structures*. Springer-Verlag, New York, 1990.
- [345] N. F. MOROZOV and P. E. TOVSTIK, "Dynamic loss of stability of a rod under longitudinal load lower than the Eulerian load," *Doklady Physics*, Vol. 58, No. 11, PP. 510-513, 2013.
- [346] C. KONING and J. TAUB, "Impact buckling of thin bars in the elastic range hinged at both ends," National Advisory Committee for Aeronautics, Washington, DC, NACA-TM-748, 1934.

- [347] N. J. Hoff, "The dynamics of the buckling of elastic columns," *Journal of Applied Mechanics*, Vol. 18, No. 1, PP. 68-74, 1951.
- [348] G. Gerard and H. Becker, "Column behavior under conditions of impact," *Journal of the Aeronautical Sciences*, Vol. 19, No. 1, PP. 58-60, 1952.
- [349] J. F. Davidson, "Buckling of struts under dynamic loading," *Journal of the Mechanics and Physics of Solids*, Vol. 2, No. 1, PP. 54-66, 1953.
- [350] N. J. Huffington, "Response of elastic columns to axial pulse loading," *AIAA Journal*, Vol. 1, No. 9, PP. 2099-2104, 1963.
- [351] H. E. Lindberg, "Impact Buckling of a Thin Bar," *Journal of Applied Mechanics*, Vol. 32, No. 2, PP. 315-322, 1965.
- [352] H. E. Lindberg and A. L. Florence, *Dynamic pulse buckling: theory and experiment*. Springer, Dordrecht, Netherlands, 1987.
- [353] S. M. Holzer, "Stability of columns with transient loads," *Journal of the Engineering Mechanics Division*, Vol. 96, No. 6, PP. 913-930, 1970.
- [354] T. Hayashi and Y. Sano, "Dynamic Buckling of Elastic Bars : 1st Report, The Case of Low Velocity Impact," *Bulletin of JSME*, Vol. 15, No. 88, PP. 1167-1175, 1972.
- [355] T. Hayashi and Y. Sano, "Dynamic Buckling of Elastic Bars : 2nd Report, The Case of High Velocity Impact," *Bulletin of JSME*, Vol. 15, No. 88, PP. 1176-1184, 1972.
- [356] I. Elishakoff, "Axial Impact Buckling of a Column With Random Initial Imperfections," *Journal of Applied Mechanics*, Vol. 45, No. 2, PP. 361-365, 1978.
- [357] L. H. N. Lee, "Dynamic buckling of an inelastic column," *International Journal of Solids and Structures*, Vol. 17, No. 3, PP. 271-279, 1981.

- [358] J. Ari-Gur, T. Weller, and J. Singer, "Experimental and theoretical studies of columns under axial impact," *International Journal of Solids and Structures*, Vol. 18, No. 7, PP. 619-641, 1982.
- [359] G. J. Simitses, "Instability of dynamically loaded structures," *Applied Mechanics Reviews*, Vol. 40, No. 10, PP. 1403-1408, 1987.
- [360] H. Hao, H. K. Cheong, and S. Cui, "Analysis of imperfect column buckling under intermediate velocity impact," *International Journal of Solids and Structures*, Vol. 37, No. 38, PP. 5297-5313, 2000.
- [361] W. Ji and A. M. Waas, "Dynamic bifurcation buckling of an impacted column," *International Journal of Engineering Science*, Vol. 46, No. 10, PP. 958-967, 2008.
- [362] K. Mimura, T. Umeda, M. Yu, Y. Uchida, and H. Yaka, "Effects of Impact Velocity And Slenderness Ratio on Dynamic Buckling Load for Long Columns," *International Journal of Modern Physics B*, Vol. 22, No. 31n32, PP. 5596-5602, 2008.
- [363] K. Mimura, T. Kikui, N. Nishide, T. Umeda, I. Riku, and H. Hashimoto, "Buckling behavior of clamped and intermediately supported long rods in the static-dynamic transition velocity region," *Journal of the Society of Material Science Japan*, Vol. 61, No. 11, PP. 881–887, 2012. (*in Japanese*)
- [364] P. Motamarri and S. Suryanarayan, "Unified analytical solution for dynamic elastic buckling of beams for various boundary conditions and loading rates," *International Journal of Mechanical Sciences*, Vol. 56, No. 1, PP. 60-69, 2012.
- [365] N. F. Morozov, D. N. Il'in, and A. K. Belyaev, "Dynamic buckling of a rod under axial jump loading," *Doklady Physics*, Vol. 58, No. 5, PP. 191-195, 2013.

- [366] V. A. Kuzkin and M. M. Dannert, "Buckling of a column under a constant speed compression: a dynamic correction to the Euler formula," *Acta Mechanica*, Vol. 227, No. 6, PP. 1645-1652, 2016.
- [367] G. W. Housner and W. K. Tso, "Dynamic behavior of supercritically loaded struts," *Journal of the Engineering Mechanics Division*, Vol. 88, No. EM5, PP. 41-65, 1962.
- [368] G. R. Abrahamson and J. N. Goodier, "Dynamic flexural buckling of rods within an axial plastic compression wave," *Journal of Applied Mechanics*, Vol. 33, No. 2, PP. 241-247, 1966.
- [369] I. K. McIvor and J. E. Bernard, "The Dynamic Response of Columns Under Short Duration Axial Loads," *Journal of Applied Mechanics*, Vol. 40, No. 3, PP. 688-692, 1973.
- [370] B. Erickson, S. V. Nardo, S. A. Patel, and N. J. Hoff, "An experimental investigation of the maximum loads supported by elastic columns in rapid compression tests," *Proceedings of the Society for Experimental Stress Analysis*, Vol. 14, No. 1, PP. 13-20, 1956.
- [371] M. Tada and A. Suito, "Static and dynamic post-buckling behavior of truss structures," *Engineering Structures*, Vol. 20, No. 4, PP. 384-389, 1998.
- [372] V. M. Kornev, "Development of dynamic forms of stability loss of elastic systems under intensive loading over a finite time interval," *Journal of Applied Mechanics and Technical Physics*, Vol. 13, No. 4, PP. 536-541, 1972.
- [373] V. M. Kornev, "Asymptotic analysis of the behavior of an elastic bar under aperiodic intensive loading," *Journal of Applied Mechanics and Technical Physics*, Vol. 13, No. 3, PP. 398-406, 1972.

- [374] A. V. Markin, "Buckling in an elastic rod under a time-varying load," *Journal of Applied Mechanics and Technical Physics*, Vol. 18, No. 1, PP. 134-138, 1977.
- [375] N. F. Morozov, A. K. Belyaev, P. E. Tovstik, and T. P. Tovstik, "The Ishlinskii—Lavrent'ev problem at the initial stage of motion," *Doklady Physics*, Vol. 60, No. 8, PP. 368-371, 2015.
- [376] E. Sevin, "On the Elastic Bending of Columns Due to Dynamic Axial Forces Including Effects of Axial Inertia," *Journal of Applied Mechanics*, Vol. 27, No. 1, PP. 125-131, 1960.
- [377] I. Elishakoff, "Hoff's Problem in a Probabilistic Setting," *Journal of Applied Mechanics*, Vol. 47, No. 2, PP. 403-408, 1980.
- [378] J. Goggins, "Earthquake resistant hollow and filled steel braces," Ph.D. Thesis, Department of Civil, Structural and Environmental Engineering, Trinity College, The University of Dublin, Ireland, 2004.
- [379] A. Y. Elghazouli, B. M. Broderick, J. Goggins, H. Mouzakis, P. Carydis, J. Bouwkamp, and A. Plumier, "Shake table testing of tubular steel bracing members," *Structures and Buildings*, Vol. 158, No. 4, PP. 229-241, 2005.
- [380] J. Goggins and S. Salawdeh, "Validation of nonlinear time history analysis models for single-storey concentrically braced frames using full-scale shake table tests," *Earthquake Engineering & Structural Dynamics*, Vol. 42, No. 8, PP. 1151-1170, 2013.
- [381] S. Salawdeh, "Seismic Design of Concentrically Braced Steel Frames," Ph.D. Thesis, Department of Civil Engineering, National University of Ireland, Galway, Ireland, 2012.

CURRICULUM VITAE

PERSONAL INFORMATION

Surname, Name: Kazemzadeh Azad, Sina
Nationality: Iranian
Date and Place of Birth: 16 September 1988, Tabriz, Iran
Marital Status: Married
Email: sina.azad@metu.edu.tr

EDUCATION

Degree	Institution	Year of Graduation
MSc	Amirkabir University of Technology (Structural Engineering)	2012
BSc	The University of Tabriz (Structural Engineering)	2010

EXPERIENCE

Year	Place	Enrollment
2015-2017	METU Department of Civil Engineering	Research Assistant
2012-2015	Pardisan Consulting Engineers	Structural Engineer
2009	Pars-Pol Construction Firm	Intern

LANGUAGES

Azeri (Native), Persian (Native), Turkish (Fluent), English (Fluent)

SELECTED PUBLICATIONS

1. Sina Kazemzadeh Azad, Cem Topkaya, and Milad Bybordiani, “*Dynamic Buckling of Braces in Concentrically Braced Frames*”, *Earthquake Engineering & Structural Dynamics*, 47: 613-633, 2018

2. Mehmet Bakır Bozkurt, Sina Kazemzadeh Azad, and Cem Topkaya, “*Low-Cycle Fatigue Testing of Shear Links and Calibration of a Damage Law*”, ASCE Journal of Structural Engineering, 144(10), 2018
3. Saeid Kazemzadeh Azad, Milad Bybordiani, Sina Kazemzadeh Azad, Farqad KJ Jawad, “*Simultaneous Size and Geometry Optimization of Steel Trusses under Dynamic Excitations*”, Structural and Multidisciplinary Optimization, 58(6): 2545-2563, 2018
4. Sina Kazemzadeh Azad, Cem Topkaya, and Abolhassan Astanteh-Asl, “*Seismic Behavior of Concentrically Braced Frames Designed to AISC341 and EC8 Provisions*”, Journal of Constructional Steel Research, 133: 383-404, 2017
5. Sina Kazemzadeh Azad and Cem Topkaya, “*A Review of Research on Steel Eccentrically Braced Frames*”, Journal of Constructional Steel Research, 128: 53-73, 2017
6. Saeid Kazemzadeh Azad, Oğuzhan Hasançebi, and Sina Kazemzadeh Azad, “*Upper Bound Strategy for Metaheuristic Based Design Optimization of Steel Frames*”, Advances in Engineering Software, 57: 19-32, 2013
7. Sina Kazemzadeh Azad, “*Flexural Failure Mechanisms of Horizontally Curved Steel Girders*”, MSc Thesis, Supervised by Prof. M. M. Alinia, Amirkabir University of Technology, 2012 (in Persian)
8. Sina Kazemzadeh Azad and Saeid Kazemzadeh Azad, “*Optimum Design of Structures Using an Improved Firefly Algorithm*”, International Journal of Optimization in Civil Engineering, 1(2): 327-340, 2011
9. Ali Hadidi, Sina Kazemzadeh Azad, and Saeid Kazemzadeh Azad, “*Structural Optimization Using Artificial Bee Colony Algorithm*”, Proceedings of the 2nd International Conference on Engineering Optimization (EngOpt 2010), Lisbon, Portugal, 2010